

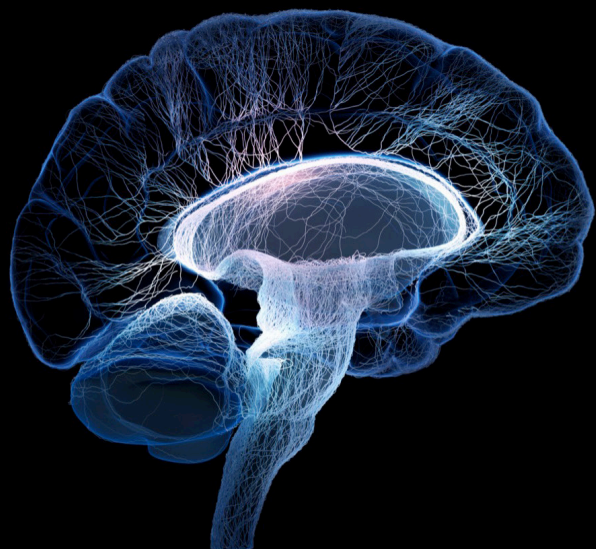
# Methods and applications in neurodegeneration

**Edited by**

Tingyuan Lang, Lei Zhou, Jingming Hou, Nicolas Casadei  
and Eduard Rodriguez-Farre

**Published in**

Frontiers in Neuroscience



## FRONTIERS EBOOK COPYRIGHT STATEMENT

The copyright in the text of individual articles in this ebook is the property of their respective authors or their respective institutions or funders. The copyright in graphics and images within each article may be subject to copyright of other parties. In both cases this is subject to a license granted to Frontiers.

The compilation of articles constituting this ebook is the property of Frontiers.

Each article within this ebook, and the ebook itself, are published under the most recent version of the Creative Commons CC-BY licence. The version current at the date of publication of this ebook is CC-BY 4.0. If the CC-BY licence is updated, the licence granted by Frontiers is automatically updated to the new version.

When exercising any right under the CC-BY licence, Frontiers must be attributed as the original publisher of the article or ebook, as applicable.

Authors have the responsibility of ensuring that any graphics or other materials which are the property of others may be included in the CC-BY licence, but this should be checked before relying on the CC-BY licence to reproduce those materials. Any copyright notices relating to those materials must be complied with.

Copyright and source acknowledgement notices may not be removed and must be displayed in any copy, derivative work or partial copy which includes the elements in question.

All copyright, and all rights therein, are protected by national and international copyright laws. The above represents a summary only. For further information please read Frontiers' Conditions for Website Use and Copyright Statement, and the applicable CC-BY licence.

ISSN 1664-8714  
ISBN 978-2-8325-5450-0  
DOI 10.3389/978-2-8325-5450-0

## About Frontiers

Frontiers is more than just an open access publisher of scholarly articles: it is a pioneering approach to the world of academia, radically improving the way scholarly research is managed. The grand vision of Frontiers is a world where all people have an equal opportunity to seek, share and generate knowledge. Frontiers provides immediate and permanent online open access to all its publications, but this alone is not enough to realize our grand goals.

## Frontiers journal series

The Frontiers journal series is a multi-tier and interdisciplinary set of open-access, online journals, promising a paradigm shift from the current review, selection and dissemination processes in academic publishing. All Frontiers journals are driven by researchers for researchers; therefore, they constitute a service to the scholarly community. At the same time, the *Frontiers journal series* operates on a revolutionary invention, the tiered publishing system, initially addressing specific communities of scholars, and gradually climbing up to broader public understanding, thus serving the interests of the lay society, too.

## Dedication to quality

Each Frontiers article is a landmark of the highest quality, thanks to genuinely collaborative interactions between authors and review editors, who include some of the world's best academicians. Research must be certified by peers before entering a stream of knowledge that may eventually reach the public - and shape society; therefore, Frontiers only applies the most rigorous and unbiased reviews. Frontiers revolutionizes research publishing by freely delivering the most outstanding research, evaluated with no bias from both the academic and social point of view. By applying the most advanced information technologies, Frontiers is catapulting scholarly publishing into a new generation.

## What are Frontiers Research Topics?

Frontiers Research Topics are very popular trademarks of the *Frontiers journals series*: they are collections of at least ten articles, all centered on a particular subject. With their unique mix of varied contributions from Original Research to Review Articles, Frontiers Research Topics unify the most influential researchers, the latest key findings and historical advances in a hot research area.

Find out more on how to host your own Frontiers Research Topic or contribute to one as an author by contacting the Frontiers editorial office: [frontiersin.org/about/contact](https://frontiersin.org/about/contact)

# Methods and applications in neurodegeneration

## Topic editors

Tingyuan Lang — First Affiliated Hospital of Chongqing Medical University, China

Lei Zhou — Hong Kong Polytechnic University, Hong Kong, SAR China

Jingming Hou — Army Medical University, China

Nicolas Casadei — University of Tübingen, Germany

Eduard Rodriguez-Farre — Institute of Biomedical Research of Barcelona, Spanish National Research Council (CSIC), Spain

## Citation

Lang, T., Zhou, L., Hou, J., Casadei, N., Rodriguez-Farre, E., eds. (2024). *Methods and applications in neurodegeneration*. Lausanne: Frontiers Media SA.

doi: 10.3389/978-2-8325-5450-0

## Table of contents

- 05 **Editorial: Methods and applications in neurodegeneration**  
Jiaman Xu and Tingyuan Lang
- 07 **Methods for the isolation and analysis of A $\beta$  from postmortem brain**  
Wei Hong, Wen Liu, Alexandra O. Desousa, Tracy Young-Pearse and Dominic M. Walsh
- 21 **Integrative genetic and single cell RNA sequencing analysis provides new clues to the amyotrophic lateral sclerosis neurodegeneration**  
Hankui Liu, Liping Guan, Min Deng, Lars Bolund, Karsten Kristiansen, Jianguo Zhang, Yonglun Luo and Zhanchi Zhang
- 31 **Solifenacin versus posterior tibial nerve stimulation for overactive bladder in patients with multiple sclerosis**  
Nastaran Majdinasab, Neda Orakifar, Leila Kouti, Gholamreza Shamsaei, Maryam Seyedtabib and Mohammad Jafari
- 38 **Risk factors and nomogram-based prediction of the risk of limb weakness in herpes zoster**  
Shao-jun Li and Dan Feng
- 47 **Protecting RNA quality for spatial transcriptomics while improving immunofluorescent staining quality**  
Nina Hahn, Martin Bens, Marin Kempfer, Christin Reißig, Lars Schmidl and Christian Geis
- 55 **Clinical and cognitive correlates tractography analysis in patients with white matter hyperintensity of vascular origin**  
Qinmei Kuang, Muhua Huang, Yumeng Lei, Lin Wu, Chen Jin, Jiankun Dai and Fuqing Zhou
- 63 **Features of event-related potentials during retrieval of episodic memory in patients with mild cognitive impairment due to Alzheimer's disease**  
Yingying Wang, Xing Ye, Bo Song, Yixin Yan, Wenying Ma and Jingping Shi
- 74 **Not your usual neurodegenerative disease: a case report of neuronal intranuclear inclusion disease with unconventional imaging patterns**  
Luyao Xu, Hongxia Zhang, Hanyue Yuan, Liwen Xie, Junliang Zhang and Zhigang Liang
- 81 **Unraveling the link: exploring the causal relationship between diabetes, multiple sclerosis, migraine, and Alzheimer's disease through Mendelian randomization**  
Hua Xue, Li Zeng and Shuangjuan Liu

- 91 **Parkinson's disease model in zebrafish using intraperitoneal MPTP injection**  
Noor Azzizah Omar, Jaya Kumar and Seong Lin Teoh
- 108 **New insights in animal models of neurotoxicity-induced neurodegeneration**  
Coral Sanfeliu, Clara Bartra, Cristina Suñol and  
Eduard Rodríguez-Farré



## OPEN ACCESS

EDITED AND REVIEWED BY  
Mark P. Burns,  
Georgetown University, United States

\*CORRESPONDENCE  
Tingyuan Lang  
✉ [michaellang2009@163.com](mailto:michaellang2009@163.com)

RECEIVED 26 June 2024  
ACCEPTED 21 August 2024  
PUBLISHED 06 September 2024

CITATION  
Xu J and Lang T (2024) Editorial: Methods and applications in neurodegeneration.  
*Front. Neurosci.* 18:1455063.  
doi: 10.3389/fnins.2024.1455063

COPYRIGHT  
© 2024 Xu and Lang. This is an open-access article distributed under the terms of the [Creative Commons Attribution License \(CC BY\)](https://creativecommons.org/licenses/by/4.0/). The use, distribution or reproduction in other forums is permitted, provided the original author(s) and the copyright owner(s) are credited and that the original publication in this journal is cited, in accordance with accepted academic practice. No use, distribution or reproduction is permitted which does not comply with these terms.

# Editorial: Methods and applications in neurodegeneration

Jiamao Xu<sup>1,2</sup> and Tingyuan Lang<sup>1\*</sup>

<sup>1</sup>Reproductive Medicine Center, The First Affiliated Hospital of Chongqing Medical University, Chongqing, China, <sup>2</sup>Department of Neurology, The First Affiliated Hospital of Chongqing Medical University, Chongqing, China

## KEYWORDS

neurodegeneration, neurodegenerative diseases, method, application, model

Editorial on the Research Topic  
[Methods and applications in neurodegeneration](#)

## 1 New experimental animal models of neurodegeneration

Given that positive results obtained from current animal models are often not replicated in the clinical setting, new experimental animals for neurodegenerative diseases are urgently needed. [Sanfeliu et al.](#) analyzed the known and new neurotoxicity-induced models of neurodegeneration that may complement genetically modified models, including models based on dopaminergic (methyl-4-phenyl-1,2,3,6-tetrahydropyridine (MPTP), rotenone, and 6-hydroxydopamine (6-OHDA) models of Parkinson's disease), cholinergic (scopolamine model of Alzheimer's disease), and neuroinflammation-induced (lipopolysaccharide (LPS), streptozotocin (STZ), monomeric C-reactive protein (mCRP) models of Alzheimer's disease) neurodegeneration. In addition to rodent models, [Omar et al.](#) improved the parameters for the MPTP-induced zebrafish model.

## 2 Technical and mechanistic breakthroughs in molecular research

Single-cell technology provides the opportunity to detect heterogeneity and spatial information among individual cells, but modifying parameters based on the specific specimens remains a challenge. [Hahn et al.](#) developed a novel protocol to protect RNA quality for spatial transcriptomics while improving immunofluorescent staining quality. Also featured in this Research Topic is the work of [Liu et al.](#), who examined new clues to the neurodegeneration of amyotrophic lateral sclerosis (ALS) by employing integrative genetic and single-cell RNA sequencing. Limited protocols have been developed to isolate and analyze amyloid  $\beta$ -protein (A $\beta$ ) from the postmortem brain. [Hong et al.](#) have developed three distinct methods for studying A $\beta$  from human cortical tissue. These innovative protocols and findings will undoubtedly facilitate future neuroscience research.

### 3 Novel clinical features in neurodegenerative diseases

The development of novel clinical features plays a fundamental role in the prevention, diagnosis, treatment, and mechanistic study of diseases. [Xue et al.](#) highlighted the causal link between Alzheimer's disease and type 2 diabetes mellitus. [Wang et al.](#) conducted a neutral image recognition memory task and identified novel features of event-related potentials in patients with Alzheimer's disease. [Kuang et al.](#) investigated the hypertension score, Montreal Cognitive Assessment score, and body mass index as important clinical features in patients with white matter hyperintensity lesions (WMHL). [Li et al.](#) identified potential risk factors for limb weakness in patients with herpes zoster.

### 4 Comparison of therapeutic options

Overactive bladder (OAB) is a serious and most common complication in patients with multiple sclerosis (MS). The study conducted by [Majdinasab et al.](#) showed that both solifenacin (SS) and posterior tibial nerve stimulation (PTNS) were effective in improving symptoms, while patients treated with SS had a better experience, in terms of daytime frequency, urinary, incontinence, and treatment satisfaction.

### 5 Conclusion

These researchers highlighted the latest findings in neurodegeneration, including experimental animal models, technical and mechanistic breakthroughs, clinical features, and therapeutic options. These innovative studies, comprising the Research Topic Methods and Application in Neurodegeneration, represent fundamental and impactful recommendations for future basic, clinical, and translational studies in neurodegeneration-related diseases.

### Author contributions

TL: Conceptualization, Writing – original draft, Writing – review & editing. JX: Writing – review & editing.

### Funding

The author(s) declare that no financial support was received for the research, authorship, and/or publication of this article.

### Acknowledgments

We deeply thank all the authors of the papers published on this Research Topic for their valuable studies and all the referees for their rigorous reviews. We also thank the editorial board of the Methods and Application in Neurodegeneration section.

### Conflict of interest

The authors declare that the research was conducted in the absence of any commercial or financial relationships that could be construed as a potential conflict of interest.

### Publisher's note

All claims expressed in this article are solely those of the authors and do not necessarily represent those of their affiliated organizations, or those of the publisher, the editors and the reviewers. Any product that may be evaluated in this article, or claim that may be made by its manufacturer, is not guaranteed or endorsed by the publisher.



## OPEN ACCESS

## EDITED BY

Tingyuan Lang,  
Chongqing University, China

## REVIEWED BY

Zelan Wei,  
University of Saskatchewan, Canada  
Eric Daniel Hamlett,  
Medical University of South Carolina,  
United States  
Viswanath Das,  
Palacký University Olomouc, Czechia  
Nicolas Sergeant,  
Institut National de la Santé et de la Recherche  
Médicale (INSERM), France  
Ji Yeun Hur,  
Ajou University, Republic of Korea  
Shamseddin Ahmadi,  
University of Kurdistan, Iran

## \*CORRESPONDENCE

Dominic M. Walsh  
✉ dwalsh3@bwh.harvard.edu

## SPECIALTY SECTION

This article was submitted to  
Neurodegeneration,  
a section of the journal  
Frontiers in Neuroscience

RECEIVED 26 November 2022

ACCEPTED 09 January 2023

PUBLISHED 26 January 2023

## CITATION

Hong W, Liu W, Desousa AO, Young-Pearse T  
and Walsh DM (2023) Methods for the isolation  
and analysis of A $\beta$  from postmortem brain.  
*Front. Neurosci.* 17:1108715.  
doi: 10.3389/fnins.2023.1108715

## COPYRIGHT

© 2023 Hong, Liu, Desousa, Young-Pearse and  
Walsh. This is an open-access article distributed  
under the terms of the [Creative Commons  
Attribution License \(CC BY\)](#). The use,  
distribution or reproduction in other forums is  
permitted, provided the original author(s) and  
the copyright owner(s) are credited and that the  
original publication in this journal is cited, in  
accordance with accepted academic practice.  
No use, distribution or reproduction is  
permitted which does not comply with  
these terms.

# Methods for the isolation and analysis of A $\beta$ from postmortem brain

Wei Hong<sup>1,2</sup>, Wen Liu<sup>1</sup>, Alexandra O. Desousa<sup>1</sup>,  
Tracy Young-Pearse<sup>3</sup> and Dominic M. Walsh<sup>1\*</sup>

<sup>1</sup>Laboratory for Neurodegenerative Research, Ann Romney Center for Neurologic Diseases, Brigham and Women's Hospital and Harvard Medical School, Boston, MA, United States, <sup>2</sup>The Brain Cognition and Brain Disease Institute, Shenzhen Institute of Advanced Technology, Chinese Academy of Sciences, Shenzhen, Guangdong, China, <sup>3</sup>Ann Romney Center for Neurologic Diseases, Brigham and Women's Hospital and Harvard Medical School, Boston, MA, United States

Amyloid  $\beta$ -protein (A $\beta$ ) plays an initiating role in Alzheimer's disease (AD), but only a small number of groups have studied A $\beta$  extracted from human brain. Most prior studies have utilized synthetic A $\beta$  peptides, but the relevance of these test tube experiments to the conditions that prevail in AD is uncertain. Here, we describe three distinct methods for studying A $\beta$  from cortical tissue. Each method allows the analysis of different ranges of species thus enabling the examination of different questions. The first method allows the study of readily diffusible A $\beta$  with a relatively high specific activity. The second enables the analysis of readily solubilized forms of A $\beta$  the majority of which are inactive. The third details the isolation of true A $\beta$  dimers which have disease-related activity. We also describe a bioassay to study the effects of A $\beta$  on the neuritic integrity of iPSC-derived human neurons. The combined use of this bioassay and the described extraction procedures provides a platform to investigate the activity of different forms and mixtures of A $\beta$  species, and offers a tractable system to identify strategies to mitigate A $\beta$  mediated neurotoxicity.

## KEYWORDS

amyloid  $\beta$ -protein, soluble aggregates, amyloid plaques, induced neurons, neurotoxicity

## 1. Introduction

Compelling evidences from genetic, neuropathological, biochemical and biomarker studies have shown that the amyloid  $\beta$ -protein (A $\beta$ ) plays a central role in Alzheimer's disease (AD) (Jack et al., 2010; Selkoe and Hardy, 2016; McDade and Bateman, 2017). Recent clinical data suggest that certain monoclonal antibodies (e.g., lecanemab, aducanumab, and donanemab) which facilitate the removal of amyloid plaques can slow cognitive decline in mild AD patients (Sevigny et al., 2017; Mintun et al., 2021; Swanson et al., 2021a,b; Budd Haeberlein et al., 2022; van Dyck et al., 2022). Human A $\beta$  can exist in myriad forms differing in primary structure, conformation and size, and the identity of the most disease-relevant species remains unknown (McDonald et al., 2015; Wildburger et al., 2017; Lau et al., 2021).

Our prior work has shown that the primary structure of A $\beta$  from human brain is highly heterogeneous with a diversity of N- and C-termini (McDonald et al., 2015; Brinkmalm et al., 2019). In contrast, most studies assessing A $\beta$  aggregation, structure and

activity have utilized synthetic peptide of a single sequence (Yankner and Lu, 2009). Only a few groups have studied A $\beta$  extracted from human brain. These studies have been limited to those investigating the structure and composition of A $\beta$  in amyloid plaques (Allsop et al., 1983; Glenner and Wong, 1984; Masters et al., 1985; Roher et al., 1996; Welander et al., 2009), or so-called soluble A $\beta$  (Suzuki et al., 1994; Kuo et al., 1996, 1997; Roher et al., 1996; Shinkai et al., 1997; Enya et al., 1999; McDonald et al., 2015; Brody et al., 2017; Mukherjee et al., 2021). The latter are defined operationally and refer to any form of A $\beta$  released by homogenization in aqueous buffer and which remain in solution following high-speed centrifugation.

Here, we describe three protocols for the preparation of A $\beta$ -containing AD brain extracts and a paradigm to investigate AD relevant bioactivity. The first section of the protocol details two methods to extract aqueous soluble forms of A $\beta$ . Method I involves soaking thin slices of brain in artificial cerebrospinal fluid (aCSF). Method II utilizes a more traditional homogenization procedure. Method III describes a protocol that enables isolation of size exclusion separated pure A $\beta$  dimers and monomers. Finally, we detail the use of human iPSC-derived glutamatergic neurons and live-neuron imaging to measure the neurite disrupting activity of various A $\beta$ -containing extracts.

## 2. Materials and equipment

Here we provide details of vendors and catalog numbers for all chemicals and reagents we used for the experiments described. However, common reagents/chemicals from other sources should work equally well.

### 2.1. Reagents

- Milli-Q water.
- NaCl (Sigma-Aldrich, cat. no. S7653).
- KCl (Sigma-Aldrich, cat. no. P9333).
- NaH<sub>2</sub>PO<sub>4</sub> (Sigma-Aldrich, cat. no. S8282).
- NaHCO<sub>3</sub> (Sigma-Aldrich, cat. no. S5761).
- Leupeptin (Sigma-Aldrich, cat. no. L2884).
- Aprotinin (Sigma-Aldrich, cat. no. A1153).
- Pepstatin A (Sigma-Aldrich, cat. no. P5318).
- EGTA (Sigma-Aldrich, cat. no. E4378).
- Pefabloc (Sigma-Aldrich, cat. no. 76307).
- NaF (Sigma-Aldrich, cat. no. S7920).
- 0.5 M EDTA (Invitrogen, cat. no. 15575-020).
- Protein A sepharose (Sigma-Aldrich, cat. no. P3391).
- Anti-A $\beta$  polyclonal antibody S97 (D. Walsh lab).
- Pre-immune serum (D. Walsh lab).
- Trizma-base (Sigma-Aldrich, cat. no. T6066).
- Hydrochloric Acid (Fisher Scientific, cat. no. A144).
- BSA (Sigma-Aldrich, cat. no. A2153).
- Sodium tetraborate (Sigma-Aldrich, cat. no. S9640).
- Dimethyl pimelimidate (DMP) (Sigma-Aldrich, cat. no. D8388).
- Ethanolamine (Sigma-Aldrich, cat. no. E-9508).
- Glycine (Sigma-Aldrich, cat. no. G7126).
- NaN<sub>3</sub> (Sigma-Aldrich, cat. no. 71289).
- 20% Sodium dodecyl sulfate (Millipore, cat. no. 428018).
- $\beta$ -mercaptoethanol (Sigma-Aldrich, cat. no. 6250).

! CAUTION This reagent is highly caustic. Do not allow its contact with the skin or eyes. Use safety goggles and an 8-inch face shield when handling.

- Sucrose (Sigma-Aldrich, cat. no. 84097).
- Congo red (Sigma-Aldrich, cat. no. C6277).
- 88% formic acid (Fisher Scientific, cat. no. A118P-100).
- ! CAUTION This reagent is highly caustic. Do not allow its contact with the skin or eyes. Use safety goggles and an 8-inch face shield when handling.
- Ammonium bicarbonate (Sigma-Aldrich, cat. no. 09830).
- Blue dextran (Sigma-Aldrich, cat. no. D4772-1VL).
- Gel filtration standard (Bio-Rad, cat. no. 1511901).
- mTeSR Matrix (Corning, cat. no. 354230).
- mTeSR medium-1L kit (Stemcell Tech, cat. no. 85857).
- Penicillin/Streptomycin (Invitrogen, cat. no. 15070063).
- Y-27632 (Stemcell Tech, cat. no. 72304).
- Accutase (Stemcell Tech, cat. no. 07920).
- PBS (Invitrogen, cat. no. 14190250).
- DMSO (Sigma-Aldrich, cat. no. D2650).
- Neurobasal<sup>TM</sup> Medium (Invitrogen, cat. no. 21103-049).
- DMEM/F12 (Invitrogen, cat. no. 11330057).
- GlutaMAX<sup>TM</sup> Supplement (Invitrogen, cat. no. 35050).
- Puromycin (Invitrogen, cat. no. A11138-03).
- Doxycycline Hyclate (Sigma-Aldrich, cat. no. D9891).
- Dextrose (Sigma-Aldrich, cat. no. D9434).
- N2 supplement B (Stemcell Tech, cat. no. 07156).
- MEM non-essential amino acids (Gibco, cat. No. 1140-050).
- KnockOut<sup>TM</sup> DMEM (Gibco, cat. No. 10829018).
- Knockout Replacement Serum (Gibco, cat. No. 10828-028).
- Blocker A (Meso Scale Discovery, cat. no. R93BA).
- 4xMSD Read Buffer P (Meso Scale Discovery, cat. no. R92PC).
- Streptavidin SULFO-TAG Labeled (Meso Scale Discovery, cat. no. R32AD).

### 2.2. Equipment

- Tissue chopper (McIlwain, model no. TC572).
- Bench top centrifuge (Eppendorf, model no. 5810R).
- Ultracentrifuge (Beckman, model no. Optima L-90K).
- Overhead stirrer (Wheaton, model no. 903475).
- 15 mL tissue grinder (Wheaton, model no. 358010).
- Lyophilizer (Labconco, model no. FreeZone).
- FPLC system (GE HealthCare).
- Light microscope with a polarizing filter (Leica).
- Water bath and dry bath.
- Lab vacuum system.
- IncuCyte live-cell video microscopy system (Essen Bioscience).
- Double-Edge Stainless blade (VWR, cat. no. 100491-888).
- Scalpel blade (Aspen Surgical Products, cat. no. 372622).
- Superdex 75 10/300 column (GE HealthCare, cat. no. 17-5174-01).
- HiTrap desalting column (GE HealthCare, cat. no. 17-1408-01).
- Zeba spin 40k MWCO desalting column (Fisher Scientific, cat. no. 87773).
- Slide-A-Lyzer G2 dialysis cassettes, 2000 MWCO (Fisher Scientific, cat. no. 87721).
- Cover slips (Fisher Scientific, cat. no. S17525B).
- 96-well micro plate (Greiner, cat. no. 655096).

- 0.2  $\mu$ m Syringe filters (VWR, cat. no. 28145-501).
- 0.2  $\mu$ m Membrane filters (Sigma-Aldrich, cat. no. 58060-U).
- 1 mL Syringes (BD, cat. no. 309628).
- 10 mL Syringes (BD, cat. no. 309604).
- 50 mL falcon tubes (Fisher Scientific, cat. no. 14-432-22).
- 13.2 and 38.5 mL Ultracentrifuge tubes (Beckman, cat. no. 344059; cat. no. 344058).
- 1.5 mL protein low bind tubes (Eppendorf, cat. no. 13-698-794).
- 2 mL protein low bind tubes (Eppendorf, cat. no. 13-698-795).
- 1.5 mL protein low bind tubes (Eppendorf, cat. no. 13-698-794).
- 40  $\mu$ m Sterile Cell Strainers (Corning, cat. no. 431750).
- 112  $\mu$ m nylon mesh filter (cat. no. U-CMN-112-A).
- 38  $\mu$ m nylon mesh filter (cat. no. U-CMN-38-A).
- 30 mL Syringe (BD, cat. no. 305618).

## 2.3. Recipes for solutions used in protocol

### 2.3.1. 10 $\times$ aCSF based buffer (aCSF-B, pH 7.4)

Dissolve 72.5 g NaCl, 2.1 g KCl, 1.5 g  $\text{NaH}_2\text{PO}_4$ , and 21.8 g  $\text{NaHCO}_3$  in 800 mL distilled water. Bring to 1 L with Milli-Q water and filter sterilize. Store at 4°C.

### 2.3.2. aCSF extraction buffer: aCSF based buffer containing protease inhibitors

Add 10 mL of 10  $\times$  aCSF-B to 80 mL distilled water. Add 1 mL of 0.5 mg/mL leupeptin, 1 mL of 0.5 mg/mL aprotinin, 1 mL of 0.2 mg/mL pepstatin, 1 mL of 12 mg/mL pefabloc, 1 mL of 0.1 M EGTA, 1 mL of 0.5 M EDTA, and 1 mL of 0.5 M sodium fluoride. Bring to 100 mL with Milli-Q water and filter sterilize. Store at 4°C.

### 2.3.3. Resuspension buffer for protein A sepharose beads: 50 mM Tris-HCl, pH 7.6 containing 150 mM NaCl and 2% BSA

Dissolve 3.03 g Trizma-base in 300 mL Milli-Q water and adjust pH to 7.6. Add 4.38 g NaCl and 10 g BSA. When dissolved bring to 500 mL with Milli-Q water and filter sterilize.

### 2.3.4. Antibody coupling buffer: 0.2 M sodium borate, pH 9.0

Dissolve 38.14 g sodium borate in 300 mL Milli-Q water and heat to dissolve. Adjust pH to 9.0 with HCl. Bring to 500 mL with Milli-Q water and filter sterilize.

### 2.3.5. Stop buffer for antibody coupling: 0.2 M ethanolamine

Add 6.035 mL Ethanolamine (density 1.012 g/mL, stock concentration 16.568 M) to 500 mL with Milli-Q water. Adjust pH to 8.0 with approximately 18 mL of 5N HCl and filter sterilize.

### 2.3.6. Wash buffer A for antibody coupling: 100 mM glycine, pH 3.0

Dissolve 3.755 g of glycine in 400 mL Milli-Q water. Adjust pH to 3.0 with HCl. Bring to 500 mL with Milli-Q water and filter sterilize.

### 2.3.7. Wash buffer B for antibody coupling: 100 mM Tris-HCl, pH 8.0

Dissolve 12.11 g Tris-base in 400 mL Milli-Q water. Adjust pH to 8.0 with HCl. Bring to 500 mL with Milli-Q water and filter sterilize.

### 2.3.8. Plaque extraction buffer: 50 mM Tris-HCl containing 2% SDS and 0.1 M $\beta$ -mercaptoethanol, pH 7.6

Dissolve 3.03 g Tris-base in 300 mL Milli-Q water and adjust pH to 7.6. Add 50 mL of 20% SDS and 3.5 mL  $\beta$ -mercaptoethanol. When dissolved bring to 500 mL with Milli-Q water and filter sterilize.

### 2.3.9. 1% Congo red staining solution

Dissolve 1 g Congo red in 90 mL Milli-Q water, bring to 100 mL and filter sterilize.

### 2.3.10. Wash buffer for plaque extraction: 150 mM NaCl, 0.1% SDS

Dissolve 4.38 g NaCl in 300 mL Milli-Q water, add 2.5 mL 20% SDS. When dissolved bring to 500 mL with Milli-Q water and filter sterilize.

### 2.3.11. Sucrose gradient solutions for plaque isolation: 1.2–1.8 M sucrose in 50 mM Tris-HCl, pH 7.6 containing 1% SDS

Dissolve 4.84 g Tris-base in 200 mL Milli-Q water and adjust pH to 7.6, add 40 mL of 20% SDS. Mix thoroughly and split into 4, 50 mL lots placing each in a separate bottle. Add 82.15 g (1.2 M), 95.84 g (1.4 M), 109.54 g (1.6 M), and 123.23 g (1.8 M) sucrose into the four bottles, respectively. When dissolved, bring each solution to 200 mL with Milli-Q water.

### 2.3.12. Blue dextran solution

Dissolve 50 mg blue dextran in 25 mL of Milli-Q water and filter sterilize.

### 2.3.13. Mobile phase of FPLC: 50 mM ammonium bicarbonate, pH 8.5

Dissolve 3.953 g ammonium bicarbonate in 900 mL of Milli-Q water. Adjust pH to 8.5 with ammonium hydroxide. Bring to 1 L with Milli-Q water and filter sterilize.

### 2.3.14. BDNF stock solution (1000 $\times$ ): 10 $\mu$ g/mL in PBS containing 0.1% BSA

Dissolve one vial of 10  $\mu$ g BDNF in 1 mL of PBS containing with 0.1% BSA. Mix thoroughly and aliquot into 100  $\mu$ L vials. Store at  $-20^\circ\text{C}$ .

### 2.3.15. CNTF stock solution (1000 $\times$ ): 10 $\mu$ g/mL in PBS containing 0.1% BSA

Dissolve one vial of 10  $\mu$ g CNTF in 1 mL of PBS containing with 0.1% BSA. Mix thoroughly and aliquot into 100  $\mu$ L vials. Store at  $-20^\circ\text{C}$ .

### 2.3.16. GDNF stock solution (1000 $\times$ ): 10 $\mu$ g/mL in PBS containing 0.1% BSA

Dissolve one vial of 10  $\mu$ g GDNF in 1 mL of PBS containing with 0.1% BSA. Mix thoroughly and aliquot into 100  $\mu$ L vials. Store at  $-20^\circ\text{C}$ .

### 2.3.17. Y-compound (Y-27632): 10 mM in DMSO

Dissolve one vial of 1 mg Y-27632 compound in 312.2  $\mu$ L of DMSO. Filter sterilize and aliquot into 50  $\mu$ L vials. Store at  $-20^\circ\text{C}$ .

### 2.3.18. Doxycycline hyclate stock solution: 20 mg/ml in distilled water

Dissolve 1 g doxycycline hyclate (DOX) in 50 mL Milli-Q water. Filter sterilize and aliquot into 100  $\mu$ L vials. Store at  $-20^{\circ}\text{C}$ .

### 2.3.19. 20% dextrose stock solution

Dissolve 20 g of D-(+)-Glucose in 100 mL of Milli-Q water. Filter sterilize and store at  $4^{\circ}\text{C}$ .

### 2.3.20. mTeSR medium

Add 100 mL of mTeSR<sup>TM</sup> 1 5 $\times$  Supplement and 5 mL of Penicillin/Streptomycin (5,000 U/ml) to 400 mL of mTeSR<sup>TM</sup> 1 Basal Medium. Filter sterilize and store at  $4^{\circ}\text{C}$ .

### 2.3.21. iN induction medium A: KSR medium containing 2 $\mu$ g/mL doxycycline

Add 75 mL of KnockOut Serum Replacement, 5 mL of MEM non-essential amino acids, 5 mL of GlutaMAX<sup>TM</sup> Supplement and 0.5 mL of  $\beta$ -mercaptoethanol to 414.5 mL of KnockOut<sup>TM</sup> DMEM. Filter sterilize, store at  $4^{\circ}\text{C}$ , and shield from light. This medium is designated as KSR base medium. Prior to use, take 10 mL of the KSR base medium and add 1  $\mu$ L of DOX stock solution.

### 2.3.22. iN induction medium B: KSR:N2B medium containing 10 $\mu$ g/mL puromycin and 2 $\mu$ g/mL doxycycline

Add 5 mL of GlutaMAX<sup>TM</sup> Supplement, 7.5 mL of 20% Dextrose stock solution and 5 mL of N2-supplement B to 482.5 mL of DMEM/F-12 Medium. Filter sterilize and store at  $4^{\circ}\text{C}$ . This medium is designated as N2B base medium. Prior to use, add 5 mL of the KSR base medium to 5 mL of the N2B base medium, and then add 10  $\mu$ L of Puromycin and 1  $\mu$ L of DOX stock solution.

### 2.3.23. iN induction medium C: N2B medium containing 1% B27, 10 $\mu$ g/mL puromycin, and 2 $\mu$ g/mL doxycycline

Prior to use, add 100  $\mu$ L of B27 supplement, 10  $\mu$ L of Puromycin and 1  $\mu$ L of DOX stock solution to 10 mL of N2B base medium.

### 2.3.24. Supplemental neurobasal medium

Add 5 mL of GlutaMAX<sup>TM</sup> Supplement, 7.5 mL of 20% Dextrose stock solution and 2.5 mL MEM non-essential amino acids to 485 mL of Neurobasal<sup>TM</sup> Medium. Filter sterilize and store at  $4^{\circ}\text{C}$ .

### 2.3.25. iN cell culture medium

For 50 mL iN cell culture medium, add 1 mL of B27 supplement, 50  $\mu$ L of BDNF, 50  $\mu$ L of CNTF, 50  $\mu$ L of GDNF, 50  $\mu$ L of Puromycin, 5  $\mu$ L of Doxycycline to 49 mL of Supplemental Neurobasal medium. Y-27632 is only required when plating iN cells, but not for iN maintenance.

### 2.3.26. Medium to buffer-exchange brain extracts for application to neurons

For 100 mL buffer exchange medium, add 2 mL of B27 supplement and 1 mL of GlutaMAX<sup>TM</sup> Supplement to 97 mL of Neurobasal<sup>TM</sup> Medium. Filter sterilize and store at  $4^{\circ}\text{C}$ . Note: since buffer-exchanged extracts will be applied to iN cultures all manipulations are done under sterile conditions.

## 3. Stepwise procedure

### 3.1. Isolation of soluble A $\beta$ from human brain tissue

#### 3.1.1. Brain tissue dissection (estimated time: 1 h)

Extreme care should be taken when handling human tissue. Experimenters should wear appropriate personal protective equipment and consumable materials should be disinfected in bleach prior to disposal in hazardous waste. Where possible experimenters should work in an isolated area, and the area should be thoroughly clean at the end of each session.

- 1) Before starting the procedure, set up tissue chopper (thickness = 0.5 mm, force = 50%) and pre-cool the cutting board on ice.
- 2) Remove brain tissue from  $-80^{\circ}\text{C}$  storage and thaw slightly on dry ice. Cut the brain tissue into half gram chunks using a razor blade. Carefully remove blood vessels and white matter, keep gray matter.
- 3) Install pre-cooled cutting board on tissue chopper and chop brain tissue into  $\varnothing$  0.5 mm chunks. Divide chopped tissue in two: one half is used for Method 1 and the other for Method 2.  
Note: We here describe an example procedure appropriate to 20 g of dissected brain tissue. But we recommend adjusting experimental scales optionally for particular purposes. Brain tissue were obtained from four patients who both died with AD at Braak stage VI and temporal cortex used in the current study.

#### 3.1.2. Extraction methods (estimated time: 3 h)

##### 3.1.2.1. Method I

- 1) Prepare two, 5 g lots of chopped brain tissue and transfer each into two separate 50 mL ice-cold falcon tubes. Add 25 mL (20% w/v) of ice-cold extraction buffer (i.e., aCSF-B containing with protease inhibitors) to each tube and incubate with gentle side-to-side shaking at  $4^{\circ}\text{C}$  for 30 min.  
Note: Avoid harsh shaking. Thirty minutes incubation enables soluble proteins, including A $\beta$ , to diffuse out of brain tissue.
- 2) Centrifuge the suspension at  $2,000 \times g$  and  $4^{\circ}\text{C}$  for 10 min, collect the upper 90% supernatant and transfer to clean ice-cold ultracentrifuge tubes.
- 3) Centrifuge at  $200,000 \times g$  and  $4^{\circ}\text{C}$  for 110 min using a SW41 Ti rotor. Carefully collect the upper 90% supernatant. The resulted sample is designated S extract.  
Note: Low speed centrifugation described in step 2 prior to ultracentrifugation is used to minimize physical disruption of plaques.

##### 3.1.2.2. Method II

- 1) Add 50 mL (20% w/v) of ice-cold aCSF-B (pH 7.4) with protease inhibitors to 10 g of chopped brain tissue and homogenize with 25 strokes of a Teflon-glass Dounce homogenizer.
- 2) Centrifuge at  $200,000 \times g$  for 110 min and  $4^{\circ}\text{C}$  in a SW41 Ti rotor. Carefully remove the upper 80% supernatant. The resulted sample is designated H extract.

### 3.1.3. Dialysis to remove low molecular weight compounds from brain extracts (estimated time: 3 days)

- 1) During ultracentrifugation, prepare pre-cooled dialysis buffer (i.e., 1 × aCSF-B, pH 7.4) with a volume of at least 100-fold excess of designated brain extracts.
- 2) Add 50 mL of pre-cooled dialysis buffer to a new dialysis cassette and leave at 4°C for at least 10 min.  
Note: Ensure the cassette is cold prior to adding brain extract and there is no buffer leaking.
- 3) Remove dialysis buffer in the dialysis cassette and then add brain extract using a 10 mL pipette. Place cassette in the 5 L bucket with pre-cooled dialysis buffer and stir slowly for 24 h.
- 4) Replace dialysis buffer. Repeat the above step 3 twice.  
Note: We recommend dialysis against >100-fold excess of aCSF-B at 4°C, with three buffer changes over a 72 h period. The efficiency can be estimated by measuring the amount of glutamate in the final dialyzate vs. the starting extract (Figure 2). Typically, >90% of glutamate is removed by this regimen. Glutamate concentration was measured using the Amplex® Red Glutamic Acid/Glutamate Oxidase Assay Kit (Invitrogen, cat. no. A12221) following manufacturer's instructions.
- 5) Remove sample from the cassette using a 5 mL pipette and aliquot into 1.5 mL protein-low bind tubes. Freeze on dry ice and store at −80°C.  
Note: As Aβ are aggregation prone and sensitive to temperature changes, brain extracts can be thawed once and used. In general, remove samples from −80°C and allow to thaw at room temperature for 20 min.

### 3.1.4. Conjugation of antibody to protein A beads (estimated time: 3 days)

Antibodies are used to deplete brain extracts of Aβ to provide a negative control for bioactivity studies. Polyclonal antibodies are covalently cross-linked to Protein A sepharose (PAS) beads to minimize the potentially confounding effects of free antibody.

- 1) Dissolve 0.25 g of PAS in 10 mL of 50 mM Tris-HCl, pH 7.6 containing 150 mM NaCl and 2% BSA. Incubate the PAS suspension with gentle side-to-side shaking at room temperature for 30 min.
- 2) During incubation, use a Zeba spin desalting column to buffer exchange 3~4 mg of protein A purified anti-Aβ polyclonal antibody (e.g., S97 in our study) or control antibody [e.g., pre-immune serum (PIS)] into 50 mM Tris-HCl, pH 7.6 containing 150 mM NaCl.  
Note: Pre-immune serum is a negative control to anti-Aβ polyclonal antibody and does not recognize Aβ. If polyclonal antibody such as S97 is not available, a commercial antibody 4G8 is optional (Yang et al., 2017).
- 3) Centrifuge PAS suspension at 3,000 rpm for 5 min at room temperature and carefully discard supernatant.
- 4) Keep the PAS pellet (~1 mL from 0.25 g dried PAS) and add 3 mg anti-Aβ polyclonal antibody. Leave stand for 1 h at room temperature and then incubate with gentle side-to-side shaking at room temperature for 1 h.
- 5) Centrifuge at 3,000 rpm for 5 min at room temperature and discard the supernatant. Wash PAS pellet with 10 mL

of antibody coupling buffer (0.2 M sodium borate, pH 9.0). Centrifuge and discard supernatant. Repeat one time.

- 6) Resuspend PAS with 10 mL of antibody coupling buffer and add 50 mg of DMP, then incubate with gentle side-to-side shaking at room temperature for 30 min.  
Note: This coupling reaction requires pH > 8.3, adjust with NaOH if necessary.
- 7) Centrifuge at 3,000 rpm for 5 min at room temperature and discard supernatant. Resuspend PAS pellet with 10 mL of 0.2 M ethanolamine.
- 8) Centrifuge at 3,000 rpm for 5 min at room temperature and discard supernatant. Resuspend PAS pellet with 10 mL of 0.2 M ethanolamine and incubate with gentle side-to-side shaking at room temperature for 2 h.
- 9) Centrifuge at 3,000 rpm for 5 min at room temperature and discard supernatant. Resuspend PAS pellet with 1.75 mL PBS and transfer the suspension into two 2 mL Eppendorf tubes.
- 10) Centrifuge at 3,000 rpm for 5 min at room temperature and discard supernatant. Resuspend PAS pellet with 1.75 mL of 100 mM glycine for a minimal time interval.
- 11) Centrifuge at 10,000 rpm for 30 s at room temperature and discard supernatant. Resuspend PAS pellet with 1.75 mL of 100 mM Tris-HCl, pH 8.0.
- 12) Centrifuge at 3,000 rpm for 5 min at room temperature and discard supernatant. Resuspend each tube of 0.5 mL PAS pellet with 0.5 mL PBS containing 0.02% NaN<sub>3</sub>, yielding a 50% S97-PAS or PIS-PAS slurry.  
Note: Covalently conjugated antibodies can be stored at 4°C for up to 3 months and maintain high immunoreactivity.

### 3.1.5. Aβ immunodepletion (estimated time: 3 days)

- 1) Thaw appropriate aliquots of brain extracts on ice. Add 30 μL S97-PAS [immunodepletion (ID)] or PIS-PAS [mock immunodepletion (mock-ID)] to each 0.5 mL brain extracts, gently mix by hand and then rotate at 4°C overnight.
- 2) Centrifuge at 6,000 rpm for 5 min at 4°C, carefully collect supernatant using gel loading tip and transfer into new 1.5 mL pro-low bind tubes. Keep the pellet as IP'd material.
- 3) Repeat the above step 2 twice. The final supernatant is designated as Aβ-ID'd or mock-ID'd brain extract.
- 4) Analyze the IP'd material from each round by Western Blot if necessary.  
Note: We recommend using a combination of anti-Aβ monoclonal antibodies specific for Aβ40 (e.g., 2G3) and Aβ42 (e.g., 21F12) to probe blots.
- 5) Measure Aβx-42 monomer concentration in Aβ-ID'd or mock-ID'd brain extracts using Aβx-42 immunoassay. Quantitate the efficiency of immunodepletion by comparing Aβ-ID'd and mock-ID'd brain extract. Perform assays using the Meso Scale Discovery (MSD) platform and reagents from Meso Scale (Rockville, MD, USA).  
Note: The Aβx-42 immunoassay preferentially detects Aβ monomers ending at Ala42. It employs m266 (3 μg/mL) for capture and biotinylated 21F12 (0.4 μg/mL) for detection (McDonald et al., 2015).
- 6) Measure aggregated Aβx-42 in Aβ-ID'd or mock-ID'd brain extracts by first dissociating aggregate in chaotrop. Incubate 20 μL of extract with 50 μL of 7 M GuHCl overnight at 4°C. Thereafter dilute samples 1:10 with assay diluent so

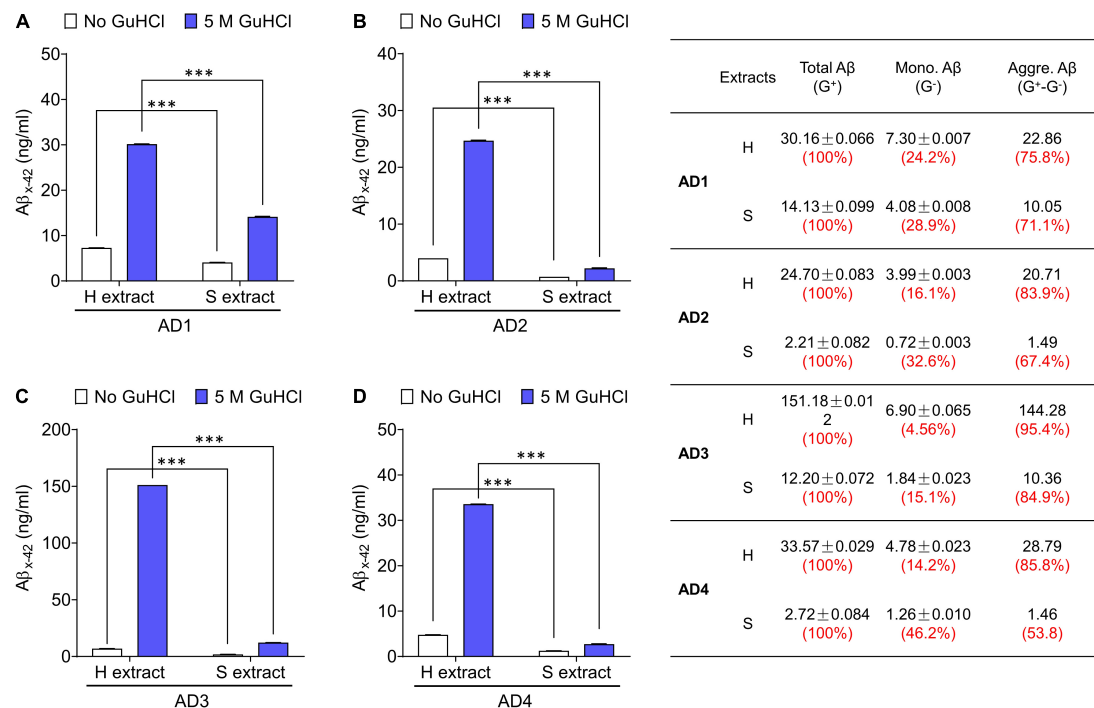


FIGURE 1

Aqueous extracts of AD brains contain a mixture of Aβ monomers and soluble aggregates. (A–D) The MSD-immunoassay preferentially detects monomeric Aβ<sub>x-42</sub>. H extracts and S extracts from four AD brains were assessed for Aβ content with and without pre-incubation in 5 M GuHCl. Aβ measured without incubation in GuHCl is attributed to Aβ monomer, whereas Aβ detected in the homogenate pre-treated with GuHCl is the product of Aβ aggregates dissociated to monomer, plus native monomer. The table indicates the relative amount of Aβ present as native monomer and Aβ in aggregates dissociable with 5 M GuHCl. G<sup>-</sup> and G<sup>+</sup> denote no GuHCl and 5 M GuHCl, respectively. Values were shown as mean ± SD. Treatments were examined by one-way ANOVA and significant differences are denoted as \*\*\**p* < 0.001.

that the final GuHCl concentration is 0.5 M. Quantitate the efficiency of immunodepletion by comparing Aβ-ID'd and mock-ID'd brain extract.

Note: Previously we have shown that Aβ aggregates in AD brain extracts can be dissociated with chaotropes such as GuHCl, and that incubation of aggregate-containing extracts with GuHCl allows their disassembly and quantitation using monomer-preferring immunoassays. To match the buffer composition of standards with samples, prepare monomeric stock of Aβ<sub>1-42</sub> in assay diluent containing 0.5 M GuHCl.

## 3.2. Isolation of amyloid plaques and purification of Aβ from human brain tissue (method III)

### 3.2.1. Pre-screening of plaque-positive brain tissue (estimated time: 1 day)

Amyloid plaque isolation is time-consuming and the distribution and abundance of amyloid plaques in different brains and in different areas of the same brain is highly variable. Therefore, we recommend conducting a less time-consuming preliminary screen which involves randomly selecting a small piece of tissue from different areas, and comparing the abundance of Congo red stained plaques using light microscopy. Thus with this approach we identify regions of brain most likely to give good yields of plaque. Here we show an example of using temporal cortex from an end-stage AD patient.

- 1) Remove brain tissue from -80°C storage place on dry ice and allow to thaw slightly. Dissect frozen cortical tissue with a scalpel blade and selecting ~100 mg aliquots of tissue from the different areas of the available tissue.
- 2) Mince tissue aliquots with a scalpel and transfer to 1 mL homogenizing tube.
- 3) Add 5 volumes of 2% SDS buffer and homogenize 20 strokes with a Teflon-glass Dounce homogenizer.
- 4) Transfer the homogenate to labeled 2 mL low-bind tubes. Heat at 100°C for 5 min and then cool down to room temperature.
- 5) Centrifuge at 10,000 rpm for 10 min at room temperature. Carefully remove supernatant using gel-loading tip attached to vacuum suction unit.
- 6) Vortex pellet in remaining buffer and remove 5 μL using wide-orifice tip and place onto a slide marked with Super Pap Pen.
- 7) Add 100 μL of 1% Congo red staining solution to each slide. Ensure the solution spread over sample.
- 8) Incubate slide at room temperature for 30 min and mount with a coverslip.
- 9) Visualize stained amyloid plaques by using a light microscope fitted with a polarizing filter. Count the number of birefringent cores. Based on this preliminary screen select the tissue that contain the largest number of Congo red positive plaques for plaque isolation.

Note: Amyloid structures can be visualized using polarized light. Amyloid plaques have a characteristic Maltese cross appearance and undergo red/green birefringence when view under polarized light. This birefringence is most apparent when gently rotating the polarizing filter.

### 3.2.2. Isolation of crude plaques from human brain tissue (estimated time: 1 day)

In general, a large amount of cortical tissue (i.e., 100 g of wet tissue) is required for the isolation of amyloid plaques. Here we describe an example procedure appropriate to 100 g of brain tissue.

- 1) Slightly thaw brain tissue on dry ice and dissect tissue away visible blood vessels and white matter. Mince 50 g of gray matter with a scalpel and then transfer to a 500 mL glass beaker.
- 2) Add 250 mL of plaque extraction buffer and incubate at room temperature for 2 h without shaking.  
Note: During the incubation period, set water bath to 100°C and the bench-top centrifuge to 26°C.
- 3) Homogenize the suspension with 20 strokes with a Teflon-glass Dounce homogenizer. Pool homogenates (approximately 300 mL from 50 g of dissected gray matter) from the same subject into a 500 mL glass beaker.
- 4) Place the homogenates in 100°C water bath for 15 min and then cool to room temperature.
- 5) Pass the homogenates through 112  $\mu$ m nylon mesh, transfer the flow through into six 50 mL tubes.
- 6) Centrifuge at  $300 \times g$  for 30 min at 26°C using a Bench top centrifuge.
- 7) Remove the supernatant leaving at least 15 mL liquid above the soft pellet.  
Note: Critical step. Avoid disrupting the soft pellet.
- 8) Combine the material from 6 tubes into 3 tubes. Rinse the emptied tubes three times with 5 mL 0.1% SDS solution and combine all materials together. Bring the content of each tube to 50 mL with 0.1% SDS solution.  
Note: At this stage, samples are quite sticky, thus we recommend rinsing emptied tubes thoroughly and retain all the materials.
- 9) Centrifuge at  $300 \times g$  for 30 min at 26°C using a Bench top centrifuge.  
(10) Remove the supernatant leaving at least 10 mL liquid above the pellet.  
Note: The pellet should be more compact than that in step 7, but still needs to avoid disruption.
- 11) Combine the material from 3 tubes to 2 tubes. Rinse emptied tubes in the same way as described in step 8 and bring each tube to 50 mL with 0.1% SDS solution.
- 12) Centrifuge at  $300 \times g$  for 30 min at 26°C using a benchtop centrifuge.
- 13) Remove the supernatant leaving at least 5 mL liquid above the pellet.
- 14) Combine the material from 2 tubes to 1 tube. Rinse emptied tube in the say way as described in step 8 and bring to 50 mL with 0.1% SDS solution.
- 15) Centrifuge at  $300 \times g$  for 30 min at 26°C using a Bench top centrifuge.
- 16) Remove the supernatant leaving 4 mL liquid above the pellet.
- 17) Resuspend the material by homogenizing with 20 strokes of a Teflon-glass Dounce homogenizer.
- 18) Pass the homogenate through 38  $\mu$ m Nylon mesh, collect flow through into a 50 mL tube. Rinse homogenizer tube with 1 mL 0.1% SDS solution, pass through the same filter and collect flow through. Repeat 2 more times.

- 19) The above procedure typically yields  $\sim 7\text{--}7.5$  mL crude plaque materials from 50 g of gray matter. Store sample at 4°C overnight.

### 3.2.3. Plaque enrichment by gradient centrifugation (estimated time: 4 h)

- 1) Prepare a linear sucrose gradient in a 38.5 mL ultracentrifuge tube. First add 5 mL of 1.8 M sucrose solution to the bottom, then carefully add 8 mL of 1.6 M sucrose solution on top of the 1.8 M sucrose solution. Thereafter, add 8 mL of 1.4 M sucrose solution and 7 mL of 1.2 M sucrose solution on top of the former. Carefully apply 7.5 mL crude plaque suspension to the top of the gradient.
- 2) Centrifuge in an SW28 rotor at  $72,000 \times g$  for 60 min at 26°C.  
Note: Ensure the centrifuge is set at 26°C as SDS will crystallize at lower temperature.
- 3) Beginning at the top collect each layer and transfer to individual 50 mL tubes.  
Note: Typically most amyloid plaque are found in the 1.6 M sucrose layer. Nonetheless, we recommend collecting materials from all layers for further analysis.
- 4) Dilute each layer sample 1:5 with 0.1% SDS in 150 mM NaCl. Centrifuge at  $300 \times g$  for 30 min at 26°C, then transfer each pellet to a 1.5 mL Protein-low bind Eppendorf tube.
- 5) Centrifuge at  $12,000 \times g$  and room temperature for 10 min. Discard supernatant and keep 100  $\mu$ L liquid above the pellet. Add 1 mL filtered MQ water into each tube and vortex thoroughly.
- 6) Repeat step 6 one more time.
- 7) Centrifuge at  $12,000 \times g$  and room temperature for 10 min. Discard supernatant and resuspend pelleted plaques with 100  $\mu$ L of MQ water. Take 10  $\mu$ L of this material, stain with 0.2% Congo red and visualize using polarized microscopy (see section 2.2. Equipment).
- 8) Freeze the remaining material and lyophilize.
- 9) To concentrate lyophilizate at the bottom of the tube centrifuge at  $12,000 \times g$  and room temperature for 10 min.  
Note: The weight of isolated plaques can be estimated by subtracting the weight of pre-weighed empty tubes from the weight of tubes containing plaques.

### 3.2.4. Plaque solubilization and A $\beta$ purification (estimated time: 1 day)

- 1) Add 1.2 mL of 88% formic acid to each vial of lyophilized plaques, vortex and incubate at room temperature overnight, e.g., 12–14 h, with gentle agitation.  
Note: Do not incubate plaques in formic acid longer than 24 h.
- 2) Centrifuge at  $12,000 \times g$  for 15 min at room temperature and carefully transfer the upper 90% of supernatant into a 1.5 mL Protein-low bind Eppendorf tube.
- 3) Equilibrate Superdex 75 10/300 GL size exclusion column (SEC) in 50 mM Ammonium Bicarbonate, pH 8.5 at 0.4 mL/min.
- 4) Inject 1 mL of blue dextran solution and collect 0.5 mL fractions. The peak fraction containing blue dextran is designated as “void volume” and labeled as Fx0. Equilibrate system with 2 column volumes (CV) of Mobile Phase solution.

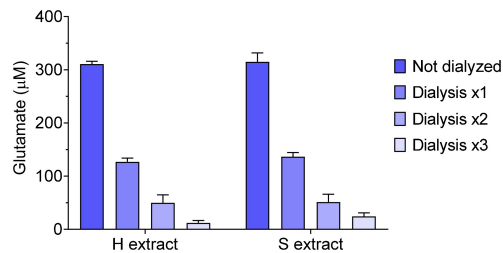


FIGURE 2

Small molecules are effectively removed from samples by dialysis. Glutamate concentration in human brain extracts was measured prior to and after each round of dialysis. The table shows the average values measured and the calculated residual percentage. Values were shown as mean  $\pm$  SD.

- Inject 1 mL of Gel filtration standard (Bio-Rad) and calibrate standards elution by using UV detector. Equilibrate system with 2 CVs of Mobile Phase solution.
- Inject 1 mL solubilized plaque material and collect 0.5 mL fractions from Fx-1 to 17. Take 5  $\mu$ L of each fraction and measure A $\beta$  by Western Blot as described previously (Brinkmalm et al., 2019). Store remainder of the fractions at  $-80^{\circ}\text{C}$  pending further analysis.

### 3.3. Application of human iPSC-derived neurons and live-cell imaging to evaluate neurotoxicity induced by soluble A $\beta$

#### 3.3.1. Generation of induced human neurons (estimated time: 3 weeks)

- Plate human iPS cells on Matrigel coated 12-well plate with  $3.8 \times 10^5$  per well in mTeSR media.
- On the day of viral infection, prepare 1 mL of fresh mTeSR media containing pTet-O-NGN2-puro lentivirus, Tet-O-FUW-eGFP lentivirus and Fudelta GW-rtTA lentivirus. Remove cell culture medium and add lentivirus-containing medium.  
Note: Lentiviruses were prepared using the plasmids from Addgene (#52047, #30130, and #19780) as showed previously (Zhang et al., 2013). The efficiency of lentivirus infection to different iPS cells may be different, thus we recommend testing their infectivity and use the most efficient multiplicity of infection (MOI) in further experiments. Puromycin is used to select infected iPS cells, while the applicable concentration may differ from cell line to cell line. Thus, we recommend conducting a small induction trial (see steps 4–11) to test puromycin selection and neuron differentiation.
- After 24 h, remove lentivirus-containing medium. Dissociate cells with Accutase and resuspend with mTeSR supplemented with Y-27632. Transfer cells to 10 cm dishes and feed with fresh

mTeSR media every day. When cells reach  $>80\%$  confluent, split for expansion or freeze down.

Note: To avoid batch effect of lentivirus infection, we recommend freezing down a large number of cryovials of transduced iPS cells. Transduced iPS cells can be passaged no more than 10 times to maintain high efficiency of neuron differentiation.

- Plate  $4 \times 10^6$  transduced iPS cells using mTeSR with Y-27632 on Matrigel coated 10 cm dish. Feed with 7 mL fresh mTeSR media every day until cells reach 50% confluence.
- On day 1, remove cell culture medium and add 7 mL KSR media containing with 2  $\mu\text{g/mL}$  Doxycycline (iN induction medium A).  
Note: At this stage, Ngn2 and GFP expression are induced.
- On day 2, replace cell culture medium with KSR:N2B (1:1) media containing with 5  $\mu\text{g/mL}$  Puromycin and 2  $\mu\text{g/mL}$  Doxycycline (iN induction medium B).  
Note: At this stage, cells without Ngn2/Puromycin resistance would die off.
- On day 3, replace cell culture medium with N2B media containing with 1% B27, 5  $\mu\text{g/mL}$  Puromycin and 2  $\mu\text{g/mL}$  Doxycycline (iN induction medium C).
- On day 4, split cells for neuron differentiation or freeze down. For freezing down, wash cells with warm PBS and detach with Accutase. Resuspend with freezing medium and store in liquid nitrogen.  
Note: The neuronal differentiation efficiency may differ from batch to batch. To minimize batch effect, we recommend freezing down a large number of cryovials of iN4 (induced neuron at day 4) and using the same batch of cells in one study.
- For neuron differentiation, plate  $1.5 \times 10^4$  iN4 cells/cm<sup>2</sup> using iN culture media with Y-27632 onto Matrigel coated cell culture vessels. Feed cells with iN culture media.  
Note: Select appropriate cell culture vessels according to practical requirements. When changing iN culture medium, we recommend removing half of the medium and add the same volume of fresh medium. Ara-C is optional if divided cells are seen in the iN culture.
- Change iN culture media every 3–4 days. In our preliminary experiments, iN cells mature at iN21, i.e., 17 days after plating, and can be used throughout a time window (approximately a week).

#### 3.3.2. Assessment of neurotoxic activity of A $\beta$ -containing brain extract using live-cell imaging (estimated time: 3–4 days)

- For A $\beta$  toxicity measurement using live-cell imaging system, plate  $5 \times 10^3$  iN4 cells onto Matrigel coated 96-well plate. Feed cells with iN culture medium every 3–4 days.  
Note: To minimize the effect of evaporation cell culture medium from neurons, we recommend plating iN cells into the inner 60 wells of 96-well plate and adding PBS into the outer wells.
- Approximately 7 h prior to treatment, place cell culture plates into IncuCyte live-cell imaging instrument. Set up scanning procedure following manufacturer's instructions. For long-term recording, schedule repeating scans every 2 h for up to 96 h.  
Note: We recommend recording iN cells 7 h prior to treatment. This allows acquisition of three baseline scans which provide

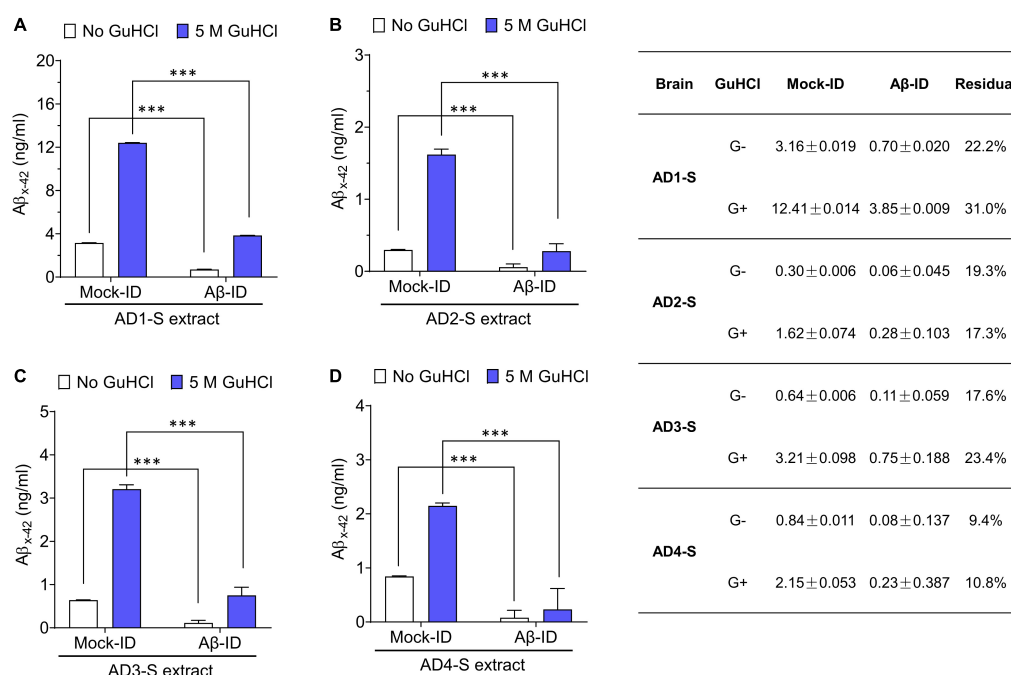


FIGURE 3

Pan anti-Aβ polyclonal antibody S97 readily depletes Aβ from human brain extracts. (A–D) Samples were immunodepleted with S97 (Aβ-ID) or PIS (Mock-ID) conjugated to Protein A Sepharose beads (PAS). Aβ content in Mock-ID and Aβ-ID of S extracts from four AD brains was measured using the Aβx-42 immunoassay ± pre-treatment with 5 M GuHCl. S97 effectively immunodepleted Aβx-42 from S extracts of four AD brains. Table in the right panel indicates the values measured by ELISA. G– and G+ denote no GuHCl and 5 M GuHCl, respectively. Residual Aβ is presented as the ratio of Aβ-ID vs. Mock-ID. Values were shown as mean ± SD. Treatments were examined by one-way ANOVA and significant differences are denoted as \*\*\**p* < 0.001.

a solid reference for time course studies. During this period Aβ-containing human brain extracts are buffer-exchanged into neurobasal medium supplemented with B27/GlutaMAX.

- 3) Buffer exchange is accomplished using a 5 mL HiTrap desalting column and a peristaltic pump. Wash the column with 25 ml of 20% Ethanol and then 25 mL of filtered MQ water. Then equilibrate with 25 mL of neurobasal medium supplemented with B27/GlutaMAX.
- 4) Apply 0.5 mL of human brain extract using a 1 mL syringe at a flow rate of ~1 mL/min. Elute proteins with iN culture medium and collect eight 0.5 mL fractions.
- 5) Remove 50 μL of each fraction and measure Aβ concentration by ELISA. Pool fractions 4 and 5 (total volume 1 mL) and use for further toxicity assays.  
Note: Prior studies indicate that fractions 4 and 5 consistently contain the peak Aβ fractions and exclude low molecular weight brain-derived compounds. Confirmatory ELISA analysis is done on the day after iN cell treatment.
- 6) During the time after the 3rd baseline scan, remove cell culture plates from IncuCyte instrument. Remove approximately half of cell culture medium leaving ~100 μL in each well. Then add 50 μL of fresh iN culture medium and 50 μL of buffer-exchanged human brain extract. This results in a 1:8 dilution of the original brain extract.  
Note: If the scan interval is 2 h, we should be cautious of the time window that allows us to complete the sample application. In fact, the scan interval is optional depending on practical requirements and manipulation feasibility.
- 7) Place treated cells into IncuCyte instrument and continue recording for 3~4 days.

- 8) When experiment is completed, select representative images from different wells to a new NeuroTrack image collection. Launch New Processing Definition and adjust parameters following manufacturer's instructions to define neurite processes and cell bodies based on phase contrast images. Once the training is completed, save the processing definition as a confirmed analysis template.

Note: Typical settings were: Segmentation Mode–Brightness; Segmentation Adjustment–1.2; Cell body cluster filter–minimum 500 μm<sup>2</sup>; Neurite Filtering–Best; Neurite sensitivity–0.4; Neurite Width–2 μm.

- 9) Launch new analysis job to the recorded database of the whole plate using the above confirmed analysis template.

Note: The training of processing definition can be conducted using the baseline scan data. Thus, we can launch real-time analysis job and monitor the scheduled scanning to the whole cell culture plate. Alternatively, an analysis job can be launched when the experiment is completed or even during the scheduled scanning.

- 10) Export Metric Graph/data and quantify neurite length and number of branch points. The neurotoxicity of Aβ is determined to the average value measured during the 6 h period prior to sample addition.

## 4. Data analysis and statistical tests

Figures showing MSD Aβ immunoassay and live-cell IncuCyte imaging data are representative of at least three independent

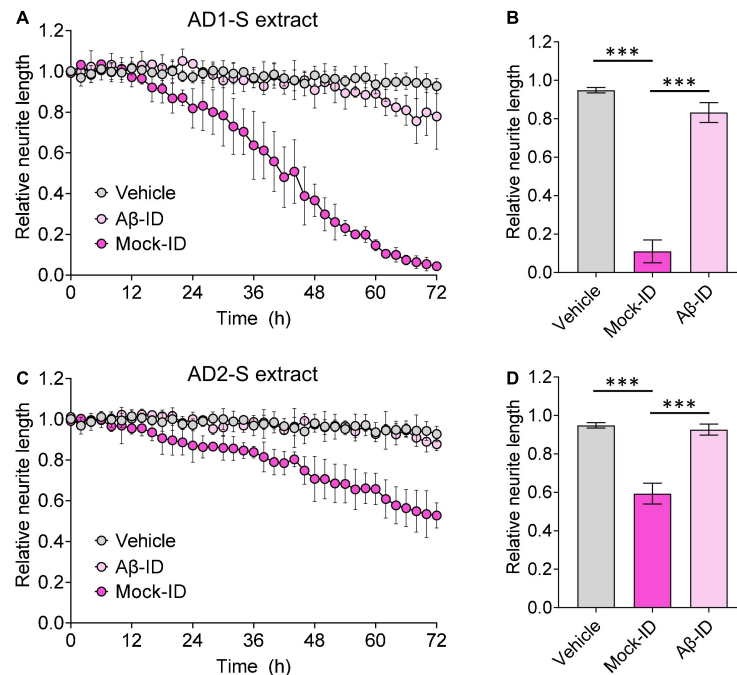


FIGURE 4

Aqueous AD brain extracts impairs neurite integrity of iNs in a manner that requires A $\beta$ . Mock-ID'd and A $\beta$ -ID'd S extracts of two AD brains were used to treat iNs at dilution of 1:4, and cells imaged using IncuCyte live-cell imaging instrument for 72 h. NeuroTrack-identified neurite length was measured and normalized to baseline (6 h recordings prior to sample addition) at each interval after addition of sample. (A,C) Time-course plots show that Mock-ID'd S extracts from 2 AD brains cause neurotoxicity compared to vehicle. (B,D) Histogram plots of normalized neurite length (mean values  $\pm$  SD) are derived from the last 6 h of the traces shown in panels (A,C). Treatments were examined by one-way ANOVA and significant differences are denoted as \*\*\* $p$  < 0.001. Panel (B) is a reproduction of a figure previously published in Brinkmalm et al. (2019).

experiments. Differences between groups were tested with one-way analysis of variance (ANOVA) with Bonferroni *post-hoc* tests or Student's *t*-tests using GraphPad Prism 8.

## 5. Anticipated results

We have used the above protocols to isolate and characterize A $\beta$  from multiple AD brains—but here we show only a few representative cases. The amount of A $\beta$  extracted by Method I (gently soaking minced tissue in aqueous buffer-S extract) and Method II (mechanically homogenizing tissue-H extract) was measured using highly sensitive A $\beta$  immunoassays. Typically, S extracts contain substantially less A $\beta$  than H extracts (Figure 1; Hong et al., 2018). Since A $\beta$  does not distribute equally across brain regions or in different sections from the same brain region, we used large amounts of (~20 g) tissue from each brain. To directly compare H extracts and S extracts, chopped tissue chunks were mixed thoroughly and half of the material was used to prepare H or S extracts. Analysis of at least 10 AD brains revealed that freely diffusible A $\beta$  can be extracted from brain tissue without the need of mechanical disruption.

Human brain extracts may vary in their content of bioactive small molecules such as neurotransmitters and/or pharmacologic agents, thus it is important to take precautions to remove any such material prior to assessing bioactivity. For this reason we dialyzed brain extracts immediately after preparation. For routine analysis we measured glutamate levels in human brain extracts before and after dialysis. We found that both H and S extracts contained ~300  $\mu$ M of glutamate, and that >90% of the starting concentration of glutamate

was removed by three rounds of dialysis (Figure 2). Prior studies revealed that the low level of remaining glutamate did not adversely affect electrophysiological measurement of hippocampal LTP or the morphology of iNs (Wang et al., 2017; Hong et al., 2018). Moreover, further buffer exchange, such as that done prior to addition of extracts to iNs is expected to further deplete glutamate and other low molecular compounds.

To determine whether the neuritotoxicity induced by AD brain extracts was mediated by A $\beta$ , we removed A $\beta$  using a pan anti-A $\beta$  polyclonal antibody, (e.g., S97 conjugated to PAS beads). S97 readily removes >70% of A $\beta$ x-42 from S extracts (Figure 3). Consistent with our previous studies, Mock-ID'd S extracts caused a time-dependent decrease in neurite length, while the A $\beta$ -ID'd S extracts did not (Figures 4A, C). These observations indicate that the neuritotoxicity induced by S extracts is mediated by A $\beta$  (Figures 4B, D).

Using an established method for isolating amyloid plaques from human cortex, we obtained microgram quantities of Congo red-positive plaques (Figure 5A) which were then solubilized in formic acid and fractionated using size exclusion chromatography. Fractions containing dimer (Fx9-11) and monomer (Fx13-16) were identified (Figure 5B) and respective fractions pooled and their effect on iNs assessed using our IncuCyte live cell imaging paradigm. When applied to iNs at a concentration of 100 ng/mL, A $\beta$  dimers potently disrupted neurite, whereas even at higher concentration A $\beta$  monomers had no effect (Figure 6A). Specifically, over the last 12 h of recording A $\beta$  dimers caused a significant decrease in neurite length and branch points both relative to pre-treatment values, and compared to vehicle ( $p$  < 0.001) or monomers ( $p$  < 0.001) (Figures 6B, C). Prior analysis indicates that SEC isolated monomer

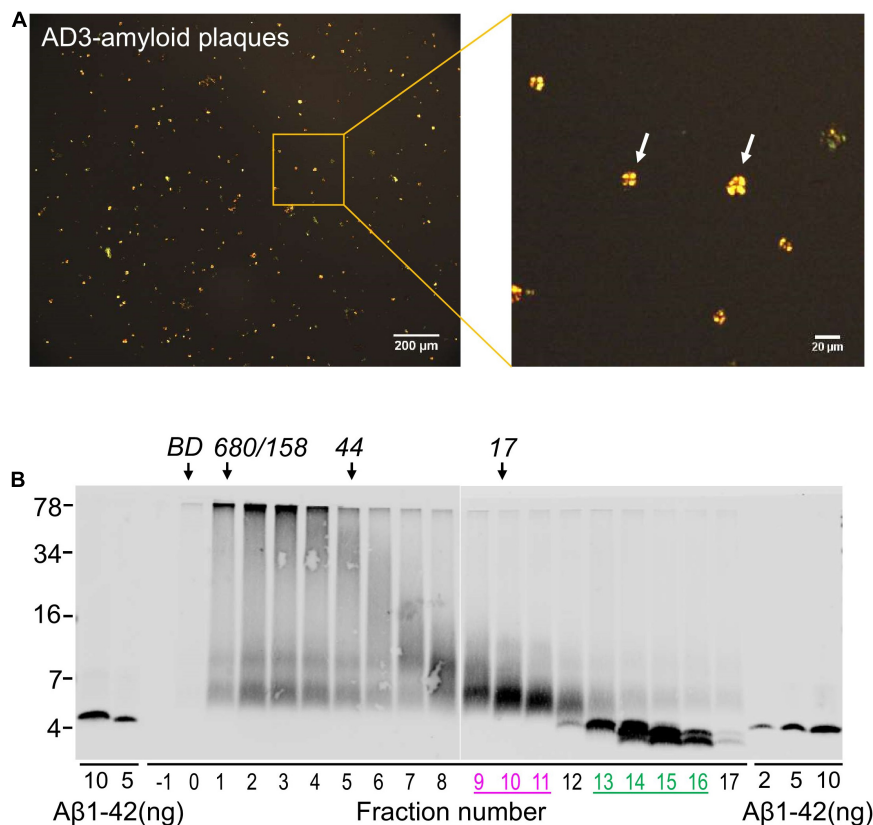


FIGURE 5

Solubilized amyloid plaques contain Aβ dimers and monomers. (A) Amyloid plaques were isolated from AD brain and characterized by Congo red staining. (B) Congo red-positive amyloid plaques were dissolved in formic acid, chromatographed on SEC and used for western blot with 4G8. The elution of Blue dextran (BD) and globular protein standards is indicated by downward arrows and SDS-PAGE molecular weight standards are on the left. Synthetic Aβ1–42 was used as control for Western blotting efficiency.

does not readily form dimers under conditions used to study bioactivity (Brinkmalm et al., 2019).

Although not shown in the current study we have previously used brains from non-Alzheimer subjects as a control (Shankar et al., 2008; Wang et al., 2017, 2022; Hong et al., 2018; Jin et al., 2018) and found they lack bioactivity. We recommend the use of such controls when testing material produced by Method I or Method II, however, since the use of Method III is primarily to compare plaque derived monomer vs. dimer and AD brain is the most abundant and biologically relevant source of plaques the use of difficult to access control brain is not be required.

## 6. Discussion

In contrast to the thousands of studies that have used synthetic Aβ, rodent neurons, or irrelevant cell lines and measures of cell death (Glabe, 2008; Yankner and Lu, 2009; Benilova et al., 2012; Hampel et al., 2021), we pioneered an approach to measure bioactivity utilizing Aβ from human brain applied to human neurons and a readout directly relevant to the human disease. It is well known that Aβ occurs in many forms and there is controversy about which of these mediate disease. Here, we describe protocols to enable the study of different populations of Aβ. Method I involves soaking minced brain tissue in aqueous buffer and allows the isolation of readily diffusible Aβ with high bioactivity. Method II

utilizes homogenization, the product of which contains the same species produced by Method I, plus a large amount of inactive species released by mechanical disruption. Comparison of extracts produced by these methods should allow a greater understanding of the molecular properties of active vs. inactive Aβ. Initial studies comparing Aβ containing extracts prepared using Method I vs. Method II revealed that S extracts contained much lower levels of Aβ than H extracts, while both equivalently block long-term potentiation and impair neuritic integrity (Hong et al., 2018). Moreover, when pellets from S extracts were homogenized and clarified to produce H2 extracts, H2 extracts were found to contain Aβ at levels comparable to H extracts, but H2 extracts were not bioactive. These results demonstrate that Method II enables the isolation of readily solubilized forms of Aβ the majority of which are inactive. Nonetheless, when screening for agents to nullify bioactive Aβ, H extracts provide a stringency tool to assess specificity.

Method III enables isolation of highly pure Aβ dimers and monomers from amyloid plaques. While we have shown dimers to have disease relevant activity (Shankar et al., 2008; Brinkmalm et al., 2019; Zott et al., 2019), certain reports indicate that Aβ monomer has beneficial effects (Plant et al., 2006; Puzzo et al., 2008; Sturchio et al., 2022; Zhou et al., 2022). Utilization of Method III should allow a direct comparison of the activities of monomers and dimers, and the design of agents that would inhibit the adverse effects of dimers without impairing the potentially beneficial effects of monomers. One major advantage of using plaque derived Aβ vs. synthetic Aβ is the

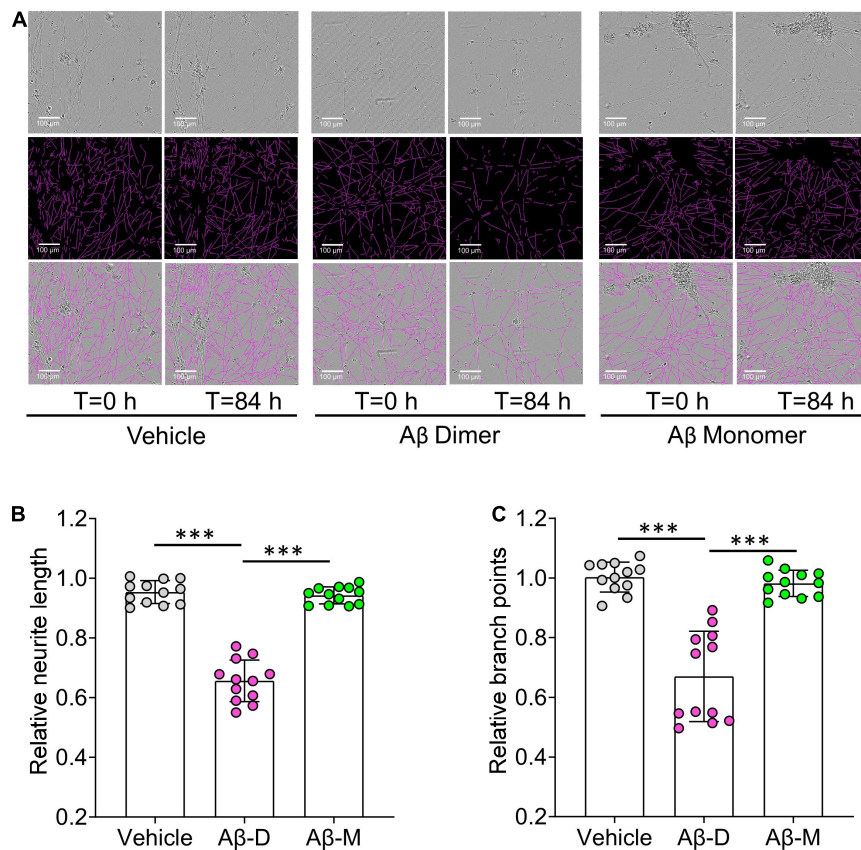


FIGURE 6

Human brain derived Aβ dimers induce neuritic dystrophy when applied to iNs. **(A)** Mature human iPSC-induced neurons (iNs) were treated with vehicle, 22 nM of AD brain derived Aβ dimers (Aβ Dimer) or monomers (Aβ Monomer), and cells imaged using IncuCyte live-cell imaging instrument for 84 h. Phase contrast images (top panel) were used to identify neurites (middle panel) using NeuroTrack software. Identified neurites (purple) are shown on the phase contrast images (bottom panel). Scale bars are 100 μm. **(B,C)** Each well of iNs was imaged for 6 h prior to addition of sample used as baseline. Relative neurite length and branch points at T = 0 and 84 h were normalized to corresponding baselines. Treatments were examined by one-way ANOVA and significant differences are denoted as \*\*\*p < 0.001.

fact that brain derived Aβ is molecularly heterogeneous such that recapitulating this complexity with synthetic peptides is challenging. Specifically, mass spectrometric analysis of plaque derived monomer from six human AD brains, identified 36 different primary Aβ structures (Brinkmalm et al., 2019). Dimers are even more complex, both with regard to the component monomers that contribute to dimers and the linkages that hold dimers together (Brinkmalm et al., 2019). In a separate study we showed that human brain derived Aβ dimers induce neuronal hyperactivation at concentrations estimated to be <50 nM, whereas dimers formed from synthetic Aβ dimer required concentrations of 500 nM to achieve a comparable effect (Zott et al., 2019). It seems reasonable to speculate that the molecular complexity of brain derived dimers contributes to their much higher specific activity relative to synthetic dimers. Although not a focus of this report, we would be remiss, if we did not note that Method III also describes the isolation plaques which without solubilization could prove useful for generation of antibodies and other possible studies.

In future studies, CRISPR-based approaches could be employed to interrogate pathways of both Aβ toxicity and synaptogenic effects. Thus, the combination of the three extraction methods described and the further adaptation of our bioassay should enable a deeper understanding of the positive and negative activities of Aβ and may

facilitate discovery of agents highly specific for the most noxious forms of Aβ.

Limitations of our approach include the requirement for large amounts of postmortem brain tissue, and relatively long duration experiments. Typically, preparation and characterization of brain extracts and/or plaque-derived Aβ takes on the order of 2 weeks. The bioassay is medium throughput and requires data collection periods of 2–4 days. To exclude artifacts arising due to postmortem delays and/or freeze-thawing of tissue, for certain studies it will be important to investigate the use of fresh biopsy tissue. Nonetheless, other investigators have already employed our experimental paradigms (Sideris et al., 2021; Emin et al., 2022; Hsieh et al., 2022; Liu et al., 2022; Stern et al., 2022) and we expect that these protocols will be further exploited. For instance to examine the bioactivity of tau and α-synuclein (Corbett et al., 2020). It is also important to point out that Aβ constitutes only a small fraction of the total protein produced by Method I and Method II and that certain AD brain extracts mediate toxicity independent of Aβ (Ondrejcek et al., 2018; Wang et al., 2022). Here, we focused on brain extracts for which toxicity could be abolished by immunodepletion of Aβ. In contrast, the Aβ species produced by Method III are highly pure and free from other detectable proteins (Hong et al., 2018).

## Data availability statement

The original contributions presented in this study are included in the article, further inquiries can be directed to the corresponding author.

## Ethics statement

This study was reviewed and approved by Partners IRB. Human specimens were obtained from the Massachusetts ADRC Neuropathology Core, Massachusetts General Hospital and used in accordance with the Partners Institutional Review Board (Protocol: Walsh BWH 2011). Written informed consent was obtained from the individual(s) to participate in this study.

## Author contributions

DMW conceived the research. DMW and WH designed the protocols and wrote the manuscript. WH performed the biochemical and IncuCyte experiments, analyzed the data, and prepared the figures. WL cultured iPSC-derived neurons and assisted with biochemical experiments. WL and AD isolated and characterized the amyloid plaques. TY-P provided the viral-infected iPS cells. All authors critically reviewed the manuscript.

## Funding

This work was supported by a grant from the Foundation for Neurologic Diseases and the National Institutes of Health

(AG046275) to DMW, the National Natural Science Foundation of China (32100800), the One Hundred Talents Program of CAS, the Guangdong Basic and Applied Basic Research Foundation (2021A1515010861), and the Shenzhen Science and Technology Program (JCYJ20200109115631248, GJHZ20200731095205016, and KQTD20210811090117032) to WH.

## Acknowledgments

We are grateful to Dr. Matthew P. Frosch for kindly providing human brain tissue. We thank Dr. Frederique Bard for the gift of 266 and 21F12 antibodies.

## Conflict of interest

The authors declare that the research was conducted in the absence of any commercial or financial relationships that could be construed as a potential conflict of interest.

## Publisher's note

All claims expressed in this article are solely those of the authors and do not necessarily represent those of their affiliated organizations, or those of the publisher, the editors and the reviewers. Any product that may be evaluated in this article, or claim that may be made by its manufacturer, is not guaranteed or endorsed by the publisher.

## References

- Allsop, D., Landon, M., and Kidd, M. (1983). The isolation and amino acid composition of senile plaque core protein. *Brain Res.* 259, 348–352. doi: 10.1016/0006-8993(83)91273-8
- Benilova, I., Karran, E., and De Strooper, B. (2012). The toxic Aβ oligomer and Alzheimer's disease: an emperor in need of clothes. *Nat. Neurosci.* 15, 349–357. doi: 10.1038/nn.3028
- Brinkmalm, G., Hong, W., Wang, Z., Liu, W., O'malley, T. T., Sun, X., et al. (2019). Identification of neurotoxic cross-linked amyloid-beta dimers in the Alzheimer's brain. *Brain* 142, 1441–1457. doi: 10.1093/brain/awz066
- Brody, D. L., Jiang, H., Wildburger, N., and Esparza, T. J. (2017). Non-canonical soluble amyloid-beta aggregates and plaque buffering: controversies and future directions for target discovery in Alzheimer's disease. *Alzheimers Res. Ther.* 9:62. doi: 10.1186/s13195-017-0293-3
- Budd Haeberlein, S., Aisen, P. S., Barkhof, F., Chalkias, S., Chen, T., Cohen, S., et al. (2022). Two Randomized Phase 3 Studies of Aducanumab in Early Alzheimer's Disease. *J. Prev. Alzheimers Dis.* 9, 197–210. doi: 10.14283/jpad.2022.30
- Corbett, G. T., Wang, Z., Hong, W., Colom-Cadena, M., Rose, J., Liao, M., et al. (2020). PrP is a central player in toxicity mediated by soluble aggregates of neurodegeneration-causing proteins. *Acta Neuropathol.* 139, 503–526. doi: 10.1007/s00401-019-02114-9
- Emin, D., Zhang, Y. P., Lobanova, E., Miller, A., Li, X., Xia, Z., et al. (2022). Small soluble alpha-synuclein aggregates are the toxic species in Parkinson's disease. *Nat. Commun.* 13:5512. doi: 10.1038/s41467-022-33252-6
- Enya, M., Morishima-Kawashima, M., Yoshimura, M., Shinkai, Y., Kusui, K., Khan, K., et al. (1999). Appearance of sodium dodecyl sulfate-stable amyloid beta-protein (Aβ) dimer in the cortex during aging. *Am. J. Pathol.* 154, 271–279. doi: 10.1016/S0002-9440(10)65273-X
- Glabbe, C. G. (2008). Structural classification of toxic amyloid oligomers. *J. Biol. Chem.* 283, 29639–29643. doi: 10.1074/jbc.R800016200
- Glenner, G. G., and Wong, C. W. (1984). Alzheimer's disease: initial report of the purification and characterization of a novel cerebrovascular amyloid protein. *Biochem. Biophys. Res. Commun.* 120, 885–890. doi: 10.1016/S0006-291X(84)80190-4
- Hampel, H., Hardy, J., Blennow, K., Chen, C., Perry, G., Kim, S. H., et al. (2021). The Amyloid-beta pathway in Alzheimer's disease. *Mol. Psychiatry* 26, 5481–5503. doi: 10.1038/s41380-021-01249-0
- Hong, W., Wang, Z., Liu, W., O'malley, T. T., Jin, M., Willem, M., et al. (2018). Diffusible, highly bioactive oligomers represent a critical minority of soluble Aβ in Alzheimer's disease brain. *Acta Neuropathol.* 136, 19–40. doi: 10.1007/s00401-018-1846-7
- Hsieh, Y. C., Negri, J., He, A., Pearse, R. V. II, Liu, L., Duong, D. M., et al. (2022). Elevated ganglioside GM2 activator (GM2A) in human brain tissue reduces neurite integrity and spontaneous neuronal activity. *Mol. Neurodegener.* 17:61. doi: 10.1186/s13024-022-00558-4
- Jack, C. R. Jr., Wiste, H. J., Vemuri, P., Weigand, S. D., Senjem, M. L., Zeng, G., et al. (2010). Brain beta-amyloid measures and magnetic resonance imaging atrophy both predict time-to-progression from mild cognitive impairment to Alzheimer's disease. *Brain* 133, 3336–3348. doi: 10.1093/brain/awq277
- Jin, M., O'Nuallain, B., Hong, W., Boyd, J., Lagomarsino, V. N., O'Malley, T. T., et al. (2018). An in vitro paradigm to assess potential anti-Aβ antibodies for Alzheimer's disease. *Nat. Commun.* 9:2676. doi: 10.1038/s41467-018-05068-w
- Kuo, Y. M., Emmerling, M. R., Vigo-Pelfrey, C., Kasunic, T. C., Kirkpatrick, J. B., Murdoch, G. H., et al. (1996). Water-soluble Aβ (N-40, N-42) oligomers in normal and Alzheimer disease brains. *J. Biol. Chem.* 271, 4077–4081. doi: 10.1074/jbc.271.8.4077
- Kuo, Y. M., Emmerling, M. R., Woods, A. S., Cotter, R. J., and Roher, A. E. (1997). Isolation, chemical characterization, and quantitation of Aβ 3-pyroglytamy peptide from neuritic plaques and vascular amyloid deposits. *Biochem. Biophys. Res. Commun.* 237, 188–191. doi: 10.1006/bbrc.1997.7083

- Lau, H. H. C., Ingelsson, M., and Watts, J. C. (2021). The existence of Abeta strains and their potential for driving phenotypic heterogeneity in Alzheimer's disease. *Acta Neuropathol.* 142, 17–39. doi: 10.1007/s00401-020-02201-2
- Liu, L., Kwak, H., Lawton, T. L., Jin, S. X., Meunier, A. L., Dang, Y., et al. (2022). An ultra-sensitive immunoassay detects and quantifies soluble Abeta oligomers in human plasma. *Alzheimers Dement.* 18, 1186–1202. doi: 10.1002/alz.12457
- Masters, C. L., Simms, G., Weinman, N. A., Multhaup, G., McDonald, B. L., and Beyreuther, K. (1985). Amyloid plaque core protein in Alzheimer disease and down syndrome. *Proc. Natl. Acad. Sci. U.S.A.* 82, 4245–4249. doi: 10.1073/pnas.82.12.4245
- McDonald, J. M., O'malley, T. T., Liu, W., Mably, A. J., Brinkmalm, G., Portelius, E., et al. (2015). The aqueous phase of Alzheimer's disease brain contains assemblies built from approximately 4 and approximately 7 kDa Abeta species. *Alzheimers Dement.* 11, 1286–1305. doi: 10.1016/j.jalz.2015.01.005
- McDade, E., and Bateman, R. J. (2017). Stop Alzheimer's before it starts. *Nature* 547, 153–155. doi: 10.1038/547153a
- Mintun, M. A., Lo, A. C., Duggan Evans, C., Wessels, A. M., Ardayfio, P. A., Andersen, S. W., et al. (2021). Donanemab in early Alzheimer's Disease. *N. Engl. J. Med.* 384, 1691–1704. doi: 10.1056/NEJMoa2100708
- Mukherjee, S., Perez, K. A., Lago, L. C., Klatt, S., Mclean, C. A., Birchall, I. E., et al. (2021). Quantification of N-terminal amyloid-beta isoforms reveals isomers are the most abundant form of the amyloid-beta peptide in sporadic Alzheimer's disease. *Brain Commun.* 3:fcab028. doi: 10.1093/braincomms/fcab028
- Ondrejcek, T., Klyubin, I., Corbett, G. T., Fraser, G., Hong, W., Mably, A. J., et al. (2018). Cellular Prion Protein Mediates the Disruption of Hippocampal Synaptic Plasticity by Soluble Tau In Vivo. *J. Neurosci.* 38, 10595–10606. doi: 10.1523/JNEUROSCI.1700-18.2018
- Plant, L. D., Webster, N. J., Boyle, J. P., Ramsden, M., Freir, D. B., Peers, C., et al. (2006). Amyloid beta peptide as a physiological modulator of neuronal 'A'-type K<sup>+</sup> current. *Neurobiol. Aging* 27, 1673–1683. doi: 10.1016/j.neurobiolaging.2005.09.038
- Puzzo, D., Privitera, L., Leznik, E., Fa, M., Staniszewski, A., Palmeri, A., et al. (2008). Picomolar amyloid-beta positively modulates synaptic plasticity and memory in hippocampus. *J. Neurosci.* 28, 14537–14545. doi: 10.1523/JNEUROSCI.2692-08.2008
- Rafii, M. S., Sperling, R. A., Donohue, M. C., Zhou, J., Roberts, C., Irizarry, M. C., et al. (2022). The AHEAD 3-45 study: design of a prevention trial for Alzheimer's disease. *Alzheimers Dement.* [Epub ahead of print]. doi: 10.1002/alz.12748
- Roher, A. E., Chaney, M. O., Kuo, Y. M., Webster, S. D., Stine, W. B., Haverkamp, L. J., et al. (1996). Morphology and toxicity of Abeta-(1-42) dimer derived from neuritic and vascular amyloid deposits of Alzheimer's disease. *J. Biol. Chem.* 271, 20631–20635. doi: 10.1074/jbc.271.34.20631
- Selkoe, D. J., and Hardy, J. (2016). The amyloid hypothesis of Alzheimer's disease at 25 years. *EMBO Mol. Med.* 8, 595–608. doi: 10.15252/emmm.201606210
- Sevigny, J., Chiao, P., Bussiere, T., Weinreb, P. H., Williams, L., Maier, M., et al. (2017). Addendum: The antibody aducanumab reduces Abeta plaques in Alzheimer's disease. *Nature* 546:564. doi: 10.1038/nature22809
- Shankar, G. M., Li, S., Mehta, T. H., Garcia-Munoz, A., Shepardson, N. E., Smith, I., et al. (2008). Amyloid-beta protein dimers isolated directly from Alzheimer's brains impair synaptic plasticity and memory. *Nat. Med.* 14, 837–842. doi: 10.1038/nm1782
- Shinkai, Y., Yoshimura, M., Morishima-Kawashima, M., Ito, Y., Shimada, H., Yanagisawa, K., et al. (1997). Amyloid beta-protein deposition in the leptomeninges and cerebral cortex. *Ann. Neurol.* 42, 899–908. doi: 10.1002/ana.410420612
- Sideris, D. I., Danial, J. S. H., Emin, D., Ruggeri, F. S., Xia, Z., Zhang, Y. P., et al. (2021). Soluble amyloid beta-containing aggregates are present throughout the brain at early stages of Alzheimer's disease. *Brain Commun.* 3:fcab147. doi: 10.1093/braincomms/fcab147
- Stern, A. M., Liu, L., Jin, S., Liu, W., Meunier, A. L., Ericsson, M., et al. (2022). A calcium-sensitive antibody isolates soluble amyloid-beta aggregates and fibrils from Alzheimer's disease brain. *Brain* 145, 2528–2540. doi: 10.1093/brain/awac023
- Sturchio, A., Dwivedi, A. K., Malm, T., Wood, M. J. A., Cilia, R., Sharma, J. S., et al. (2022). High soluble amyloid-beta42 predicts normal cognition in amyloid-positive individuals with Alzheimer's disease-causing mutations. *J. Alzheimers Dis.* 90, 333–348. doi: 10.3233/JAD-220808
- Suzuki, N., Iwatsubo, T., Odaka, A., Ishibashi, Y., Kitada, C., and Ihara, Y. (1994). High tissue content of soluble beta 1-40 is linked to cerebral amyloid angiopathy. *Am. J. Pathol.* 145, 452–460.
- Swanson, C., Dhadda, S., Irizarry, M., Kanekiyo, M., Li, D., Koyama, A., et al. (2021a). An assessment of the clinical effects, the correlation of plasma Ab ratio with changes in brain amyloid PET SUVR, and safety from the core and open label extension of the Phase 2 proof-of-concept study, BAN2401-G000-201, in subjects with early Alzheimer's disease. 13. doi: 10.1002/alz.057760
- Swanson, C., Zhang, Y., Dhadda, S., Wang, J., Kaplow, J., Lai, R. Y. K., et al. (2021b). A randomized, double-blind, phase 2b proof-of-concept clinical trial in early Alzheimer's disease with lecanemab, an anti-Abeta protofibril antibody. *Alzheimers Res. Ther.* 13:80. doi: 10.1186/s13195-021-00813-8
- van Dyck, C. H., Swanson, C. J., Aisen, P., Bateman, R. J., Chen, C., Gee, M., et al. (2022). Lecanemab in early Alzheimer's disease. *N. Engl. J. Med.* 88, 9–21. doi: 10.1056/NEJMoa2212948
- Wang, Z., Jackson, R. J., Hong, W., Taylor, W. M., Corbett, G. T., Moreno, A., et al. (2017). Human brain-derived abeta oligomers bind to synapses and disrupt synaptic activity in a manner that requires APP. *J. Neurosci.* 37, 11947–11966. doi: 10.1523/JNEUROSCI.2009-17.2017
- Wang, Z., Jin, M., Hong, W., Liu, W., Reczek, D., Lagomarsino, V. N., et al. (2022). Learnings about Ab from human brain recommend the use of a live-neuron bioassay for the discovery of next generation Alzheimer's disease immunotherapeutics. *Acta Neuropathol. Commun.* (In press).
- Welander, H., Franberg, J., Graff, C., Sundstrom, E., Winblad, B., and Tjernberg, L. O. (2009). Abeta43 is more frequent than Abeta40 in amyloid plaque cores from Alzheimer disease brains. *J. Neurochem.* 110, 697–706. doi: 10.1111/j.1471-4159.2009.06170.x
- Wildburger, N. C., Esparza, T. J., Leduc, R. D., Fellers, R. T., Thomas, P. M., Cairns, N. J., et al. (2017). Diversity of amyloid-beta proteoforms in the Alzheimer's disease brain. *Sci. Rep.* 7:9520. doi: 10.1038/s41598-017-10422-x
- Yang, T., Li, S., Xu, H., Walsh, D. M., and Selkoe, D. J. (2017). Large soluble oligomers of amyloid beta-protein from Alzheimer brain are far less neuroactive than the smaller oligomers to which they dissociate. *J. Neurosci.* 37, 152–163. doi: 10.1523/JNEUROSCI.1698-16.2016
- Yankner, B. A., and Lu, T. (2009). Amyloid beta-protein toxicity and the pathogenesis of Alzheimer disease. *J. Biol. Chem.* 284, 4755–4759. doi: 10.1074/jbc.R800018200
- Zhang, Y., Pak, C., Han, Y., Ahlenius, H., Zhang, Z., Chanda, S., et al. (2013). Rapid single-step induction of functional neurons from human pluripotent stem cells. *Neuron* 78, 785–798. doi: 10.1016/j.neuron.2013.05.029
- Zhou, B., Lu, J. G., Siddu, A., Wernig, M., and Sudhof, T. C. (2022). Synaptogenic effect of APP-Swedish mutation in familial Alzheimer's disease. *Sci. Transl. Med.* 14:eabn9380. doi: 10.1126/scitranslmed.abn9380
- Zott, B., Simon, M. M., Hong, W., Unger, F., Chen-Engerer, H. J., Frosch, M. P., et al. (2019). A vicious cycle of beta amyloid-dependent neuronal hyperactivation. *Science* 365, 559–565. doi: 10.1126/science.aay0198



## OPEN ACCESS

## EDITED BY

Barrington G. Burnett,  
Uniformed Services University of the Health  
Sciences, United States

## REVIEWED BY

Danylo Oliveira,  
Institute of Biosciences, University of São  
Paulo, Brazil  
Margarida Gama-Carvalho,  
University of Lisbon, Portugal

## \*CORRESPONDENCE

Zhanchi Zhang  
✉ zhanchily@126.com  
Yonglun Luo  
✉ alun@biomed.au.dk  
Jianguo Zhang  
✉ zhangjg@genomics.cn

†These authors have contributed equally  
to this work and share first authorship

## SPECIALTY SECTION

This article was submitted to  
Neurodegeneration,  
a section of the journal  
Frontiers in Neuroscience

RECEIVED 05 December 2022

ACCEPTED 02 February 2023

PUBLISHED 17 February 2023

## CITATION

Liu H, Guan L, Deng M, Bolund L,  
Kristiansen K, Zhang J, Luo Y and Zhang Z  
(2023) Integrative genetic and single cell RNA  
sequencing analysis provides new clues to the  
amyotrophic lateral sclerosis  
neurodegeneration.  
*Front. Neurosci.* 17:1116087.  
doi: 10.3389/fnins.2023.1116087

## COPYRIGHT

© 2023 Liu, Guan, Deng, Bolund, Kristiansen,  
Zhang, Luo and Zhang. This is an open-access  
article distributed under the terms of the  
[Creative Commons Attribution License  
\(CC BY\)](https://creativecommons.org/licenses/by/4.0/). The use, distribution or reproduction  
in other forums is permitted, provided the  
original author(s) and the copyright owner(s)  
are credited and that the original publication in  
this journal is cited, in accordance with  
accepted academic practice. No use,  
distribution or reproduction is permitted which  
does not comply with these terms.

# Integrative genetic and single cell RNA sequencing analysis provides new clues to the amyotrophic lateral sclerosis neurodegeneration

Hankui Liu<sup>1,2†</sup>, Liping Guan<sup>1,3†</sup>, Min Deng<sup>4†</sup>, Lars Bolund<sup>5,6</sup>,  
Karsten Kristiansen<sup>3</sup>, Jianguo Zhang<sup>1,2\*</sup>, Yonglun Luo<sup>2,5,6\*</sup> and  
Zhanchi Zhang<sup>7,8\*</sup>

<sup>1</sup>Hebei Industrial Technology Research Institute of Genomics in Maternal and Child Health, BGI-Shijiazhuang Medical Laboratory, Shijiazhuang, China, <sup>2</sup>BGI-Shenzhen, Shenzhen, China, <sup>3</sup>Laboratory of Genomics and Molecular Biomedicine, Department of Biology, University of Copenhagen, Copenhagen, Denmark, <sup>4</sup>Institute of Medical Innovation and Research, Peking University Third Hospital, Beijing, China, <sup>5</sup>Lars Bolund Institute of Regenerative Medicine, BGI-Qingdao, Qingdao, China, <sup>6</sup>Department of Biomedicine, Aarhus University, Aarhus, Denmark, <sup>7</sup>Department of Human Anatomy, Hebei Medical University, Shijiazhuang, Hebei, China, <sup>8</sup>Hebei Key Laboratory of Neurodegenerative Disease Mechanism, Hebei Medical University, Shijiazhuang, China

**Introduction:** The gradual loss of motor neurons (MNs) in the brain and spinal cord is a hallmark of amyotrophic lateral sclerosis (ALS), but the mechanisms underlying neurodegeneration in ALS are still not fully understood.

**Methods:** Based on 75 ALS-pathogenicity/susceptibility genes and large-scale single-cell transcriptomes of human/mouse brain/spinal cord/muscle tissues, we performed an expression enrichment analysis to identify cells involved in ALS pathogenesis. Subsequently, we created a strictness measure to estimate the dosage requirement of ALS-related genes in linked cell types.

**Results:** Remarkably, expression enrichment analysis showed that  $\alpha$ - and  $\gamma$ -MNs, respectively, are associated with ALS-susceptibility genes and ALS-pathogenicity genes, revealing differences in biological processes between sporadic and familial ALS. In MNs, ALS-susceptibility genes exhibited high strictness, as well as the ALS-pathogenicity genes with known loss of function mechanism, indicating the main characteristic of ALS-susceptibility genes is dosage-sensitive and the loss of function mechanism of these genes may involve in sporadic ALS. In contrast, ALS-pathogenicity genes with gain of function mechanism exhibited low strictness. The significant difference of strictness between loss of function genes and gain of function genes provided a priori understanding for the pathogenesis of novel genes without an animal model. Besides MNs, we observed no statistical evidence for an association between muscle cells and ALS-related genes. This result may provide insight into the etiology that ALS is not within the domain of neuromuscular diseases. Moreover, we showed several cell types linked to other neurological diseases [i.e., spinocerebellar ataxia (SA), hereditary motor neuropathies (HMN)] and neuromuscular diseases [i.e. hereditary spastic paraplegia (SPG), spinal muscular atrophy (SMA)], including an association between Purkinje cells in brain and SA, an association between  $\alpha$ -MNs in spinal cord and SA, an association between smooth muscle cells and SA, an association between oligodendrocyte and HMN, a suggestive association

between  $\gamma$ -MNs and HMN, a suggestive association between mature skeletal muscle and HMN, an association between oligodendrocyte in brain and SPG, and no statistical evidence for an association between cell type and SMA.

**Discussion:** These cellular similarities and differences deepened our understanding of the heterogeneous cellular basis of ALS, SA, HMN, SPG, and SMA.

#### KEYWORDS

amyotrophic lateral sclerosis (ALS), motor neurons (MNs), single-cell transcriptome, genome-wide association studies (GWAS), neurological disorder

## Introduction

Amyotrophic lateral sclerosis (ALS) is a neurodegenerative disease characterized by the progressive loss of motor neurons (MNs) in the brain and spinal cord (Kiernan et al., 2011). The incidence of ALS has been estimated to 1.65 per 100,000 people-year in China (Xu et al., 2020), 1.5 in United States (Mehta et al., 2022), and 3.19 in European (Marin et al., 2014). Genetics is a critical factor for ALS. In familial ALS, pathogenic mutations can be identified in about 60–80% of patients, of which *C9orf72* (40%), *SOD1* (20%), *FUS* (1–5%), and *TARDBP* (1–5%) are the most common (Renton et al., 2014). In sporadic ALS, the genetic contribution is estimated to 61% (95% CI: 38–78%) (Graham et al., 1997; Al-Chalabi et al., 2010). Large-scale genome-wide association studies (GWAS) have identified several susceptibility genes, including *C9orf72*, *SOD1*, and *UNC13A*. The ALS-related genes were implicated in altered protein homeostasis (*SOD1*), depositions of intranuclear RNA (*C9orf72*), and altered neuronal cytoskeletal dynamics (*TUBA4A*), leading to the death of upper and/or lower MNs in the brain, brainstem, and spinal cord (Brown and Al-Chalabi, 2017).

Although MN functions have been implicated, the mechanisms of neurodegeneration in ALS are still not fully understood (van Es et al., 2017). Moreover, the roles of two distinct subpopulations— $\alpha$ -MNs and  $\gamma$ -MNs—in ALS pathogenesis are not fully elucidated.  $\alpha$ -MNs located in the spinal cord innervate extrafusal muscle fibers, which create force to move the skeleton. In contrast,  $\gamma$ -MNs innervate intrafusal fibers, which modulate the sensitivity of muscle spindles to stretch (Burke et al., 1977). A comparison of  $\alpha$ - and  $\gamma$ -MNs in the spinal cord showed different behavior in ALS (Ragagnin et al., 2019), indicating that these two MNs subpopulations are not affected equally in ALS pathogenesis, raising the question if genetics contributes to the different roles of MNs subpopulations in ALS. Although several genes were found to be associated with familial and sporadic ALS, few studies have addressed possible genetic differences distinguishing familial and sporadic ALS and the cellular basis governing pathogenicity and susceptibility of ALS.

Recent advances of single-cell RNA-sequencing have provided an accurate and comprehensive depiction of cell types and gene expression. On the basis of cell type identification and diseases-related gene expression, previous studies (Skene et al., 2018; Bryois et al., 2020) have revealed various brain cell types involved in neurological disorders, including associations between monoaminergic neurons and neurodegenerative diseases, associations between embryonic GABAergic neurons and neurodevelopmental diseases, and associations between projecting excitatory neurons and psychotic disorders. Our previous study also showed that serotonergic neurons are involved in the etiology and therapy-genetics of anxiety disorders (Liu et al., 2021).

Here, using the same strategy, we applied an empirical method named expression weighted cell type enrichment (Skene and Grant, 2016) (EWCE) to investigate the cellular basis of ALS and four neurological disorders with phenotypic overlap, including hereditary motor neuropathies (HMN), spinocerebellar ataxia (SA), hereditary spastic paraplegia (SPG), spinal muscular atrophy (SMA). Our results suggested that MNs in the spinal cord play a role in ALS, SA, and HMN; additionally, MNs subpopulations— $\alpha$ - and  $\gamma$ -MNs—are mainly linked to the susceptibility and pathogenicity of ALS.

## Materials and methods

### Pathogenicity genes of ALS, HNM, SA, SPG, and SMA

We scanned the OMIM (Amberger et al., 2015) database (updated till July 14th, 2021) using the phenotypic series “PS105400-Amyotrophic lateral sclerosis” and discovered 37 causal connections between pathogenic mutations in genes and ALS subtypes (e.g., ALS 6, 8, 9, 10, 11, 12, 15, 18, 19, 20, 21, 22, 23, and 26, with or without frontotemporal dementia). We identified 32 unique pathogenicity genes and employed the gene symbols reported in OMIM (Supplementary Table 1). We searched the OMIM (Amberger et al., 2015) database (updated till July 14th, 2021) for the phenotypic series “PS164400-Spinocerebellar ataxia,” “PS303350-Spastic paraplegia,” as well as phenotypic description including of “hereditary motor neuropathies” and “spinal muscular atrophy” that do not belong to a single phenotypic series. Finally,

Abbreviations: ALS, amyotrophic lateral sclerosis; SA, spinocerebellar ataxia; HMN, hereditary motor neuropathies; SPG, hereditary spastic paraplegia; SMA, spinal muscular atrophy; MN, motor neuron; EWCE, expression weighted cell type enrichment; FDR, false discovery rate; HI, haploinsufficient; LoF, loss of function; GoF, gain of function; LoFT, loss of function tolerant; NNN, non-neurodegeneration-or-neurodevelopment.

we discovered 36, 15, 20, 57 genes that are related to HMN, SA, SMA, and SPG, respectively ([Supplementary Table 2](#)).

## Susceptibility genes of ALS

We collected 48 ALS-susceptibility genes from 13 recent large-scale genome-wide association studies ([Laaksovirta et al., 2010](#); [Shatunov et al., 2010](#); [Deng et al., 2013](#); [Fogh et al., 2014](#); [Xie et al., 2014](#); [van Rheenen et al., 2016, 2021](#); [Benyamin et al., 2017](#); [Nicolas et al., 2018](#); [Wei et al., 2019](#); [Iacoangeli et al., 2020](#); [Nakamura et al., 2020](#); [Li et al., 2021](#)). We reviewed these studies carefully and employed the genes that were reported to be significantly associated with ALS ([Supplementary Table 3](#)) in single-variant association and/or gene-level association.

## Single-cell transcriptome datasets

We employed six large-scale single-cell transcriptome datasets from recent studies ([Zeisel et al., 2015](#); [Rosenberg et al., 2018](#); [De Micheli et al., 2020](#); [Supplementary Table 4](#)). The first dataset was generated by [Rosenberg et al. \(2018\)](#). Their study analyzed 156,049 mononuclear transcriptomes in mouse brains and spinal cords and classified these cells into 73 cell types *via* an unsupervised clustering method. The second dataset was generated by [De Micheli et al. \(2020\)](#). The research team integrated 22,058 single-cell transcriptomes in human muscles (e.g., right serratus, left flexor hallucis longus, orbicularis oris, eye lid, left vastus lateralis, left external oblique, left rectus abdominus, trapezius, right external oblique, right flexor hallucis longus) and resolved 16 distinct populations of muscle-resident cells. The third dataset was generated by [Milich et al. \(2021\)](#). Their study generated 66,178 cells from uninjured and injured (Briefly, mice were anesthetized and received a 65-kilodyne mid-thoracic contusion injury) mouse spinal cord. Cluster analysis of these cells resulted in 15 distinct clusters. The fourth dataset was generated by [Sathyamurthy et al. \(2018\)](#). Their study analyzed 17,354 nuclei from adult mouse lumbar spinal cord and founded seven major clusters. The fifth dataset was generated by [Andersen et al. \(2021\)](#). Their study obtained transcriptomes of 112,554 cells and 34,884 nuclei from four samples of human spinal cord and indicated the cellular landscape of the human spinal cord, including  $\alpha$  and  $\gamma$  MNs. The sixth dataset with 9,970 cells was assembled by [Skene et al. \(2018\)](#) from single-cell transcriptome datasets ([Dueck et al., 2015](#); [Saraiva et al., 2015](#); [Usoskin et al., 2015](#); [Zeisel et al., 2015](#)). These cells are distributed in various mouse brain regions and were classified into 24 brain cell types. These datasets were released by the authors and accessed from the Gene Expression Omnibus database.

Datasets 1–2 containing single-cell transcriptomes of mouse brain, mouse spinal cord, and human muscle were used for discovery; Datasets 3–4 were used for replicating the associations that were founded in mouse spinal cord. Dataset 5 is used for validating the associations of mouse in human spinal cord. The reason we did not use it for discovery is that the dataset 5 is provided by a preprint study. Dataset 6 was used for validating the associations that were found in mouse brain. Since no cell

type annotations of MNs and subpopulations were included in the datasets 3–4, we annotated MNs and subpopulations *via* the SingleR ([Aran et al., 2019](#)) R-package<sup>1</sup> with reference to the spinal cord ([Rosenberg et al., 2018](#)) (dataset 1).

## Expression weighted cell type enrichment

The EWCE ([Skene and Grant, 2016](#)) method has been demonstrated to be reliable for studying the expression specificity across various cell types with single-cell transcriptomes. We employed the EWCE R-package<sup>2</sup> to investigate the cell-type expression specificity of ALS-related genes. Firstly, we used the generate-celltype-data function to calculate the specificity of genes in each cell type. Subsequently, we used the bootstrap-enrichment-test function to estimate the *P*-value of specificity of target genes. The bootstrap method randomly samples 10,000 lists of genes with the same number of target genes from all the genes. The specificity of these 10,000 lists of genes was used as background distribution. *P*-values of specificity of target genes were calculated by the cumulative density function of the specificity distribution and adjusted by the false discovery rate (FDR) method. Statistical significances differed by genes number were estimated by randomly selecting the genes number (5–32) from ALS-pathogenicity genes and exhibited in [Supplementary Table 5](#).

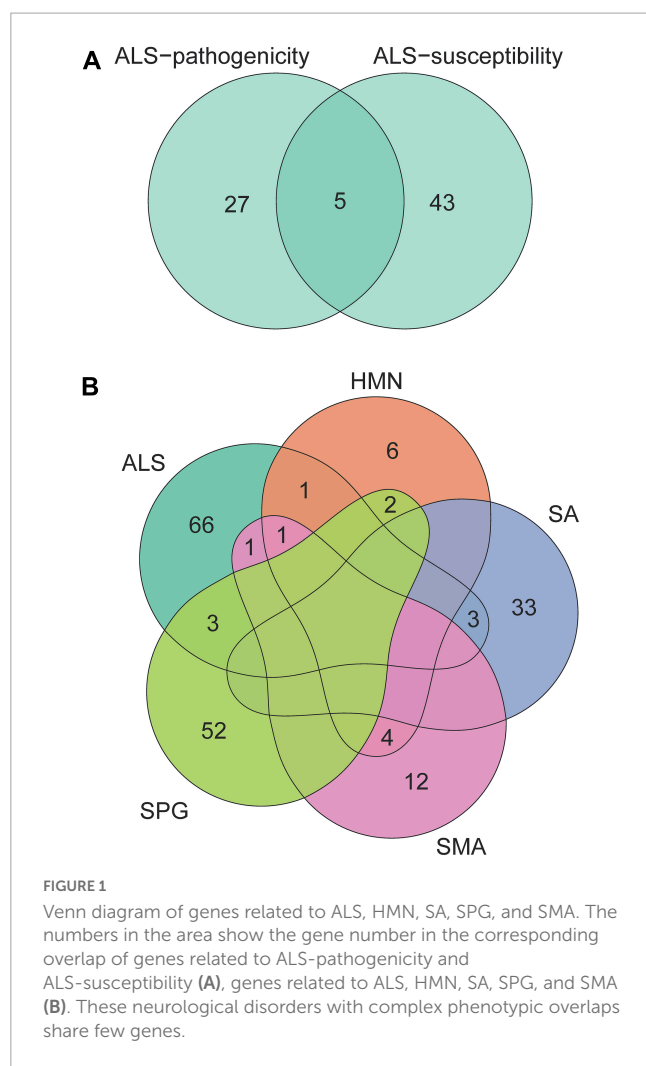
## Dosage requirement in related cells

We developed a strictness measure in this study to estimate the dosage requirement for a given gene. Strictness was calculated by the standard deviation of fold change:  $S = 1/\sqrt{\frac{\sum_i^n (C_i - \bar{C})^2}{n-1}}$ , in which *S* refers to strictness, *C* refers to fold change, *i* refers to the *i*th cell, and *n* refers to the total number of cells. The fold change was calculated by the expression in one cell divided by the mean expression in all cells:  $C_i = E_i/\bar{E}$ , in which *E* refers to the expression in one cell,  $\bar{E}$  refers to the mean expression, *i* refers to the *i*th cell. A high strictness value indicates that a gene is required to have strict expression. A low strictness indicates that the gene expression is tolerant to alterations.

To calculate the significance of strictness for target genes, we developed a method based on the Central Limit Theorem. Central Limit Theorem states that the distribution of the sample means will be approximately normal distribution. Firstly, we have a number (*n*) of target genes that we want to study, and then we calculate the strictness mean for these *n* genes (*x*). Subsequently, we take a sample with *n* genes from all the genes randomly and repeat the sampling 10,000 times *via* a bootstrap method. We calculate the strictness means for each of the 10,000 random samples and then estimate the mean ( $\mu$ ) and the standard deviation ( $\sigma$ ) of the distribution *via* a maximum likelihood estimation. The distribution of sample means should be approximately normal:  $XN(\mu, \sigma^2)$ . Finally, the *P*-value of the target genes mean is calculated

<sup>1</sup> <https://github.com/LTLA/SingleR>

<sup>2</sup> <https://github.com/NathanSkene/EWCE>



as:  $P(x|X) = 1 - \frac{1}{\sigma\sqrt{2\pi}} \int_{-\infty}^x -\exp\left\{-\frac{(x-\mu)^2}{2\sigma^2}\right\} dx$ .  $P$ -values are adjusted by the Bonferroni's method. We employed the three gene sets described below for evaluating the performance of the strictness measure.

## Haploinsufficient genes

We accessed 299 known haploinsufficient (HI) genes from Dang et al. (2008). We retained 49 HI genes that are related to neurodegenerative and/or neurodevelopmental diseases (i.e., Alzheimer's disease, Parkinson's disease, Huntington's disease, SA, multiple system atrophy, epilepsy, autism spectrum disorder, and schizophrenia) (Supplementary Table 6). These 49 genes were used as a positive control for evaluating the strictness measure.

## Loss-of-function tolerant genes

We accessed 330 putative homozygous loss-of-function tolerant (LoFT) genes from Lek et al. (2016) (Supplementary Table 6). These genes contain at least two different high confidence loss-of-function (LoF) variants that were found in a homozygous

state in at least one individual in the ExAC database. These 330 genes were used as a negative control of HI genes.

## Non-neurodegeneration-or-neurodevelopment diseases-related genes

We accessed 1,189 genes related to non-mental-health diseases from Krishnan et al. (2016). These genes were identified from OMIM and used as negative genes for autism spectrum disorder-related genes. We reviewed these 1,189 genes and then excluded the genes related to neurodegenerative and/or neurodevelopmental diseases, including Alzheimer's disease, Parkinson's disease, Huntington's disease, SA, multiple system atrophy, epilepsy, autism spectrum disorder, and schizophrenia. We retained 1,113 genes related to non-neurodegeneration-or-neurodevelopment diseases (NNN) as another negative control of HI genes (Supplementary Table 6).

## Data and code availability

Genes related to ALS, HMN, SA, SPG, and SMA are listed in Supplementary Tables 1–3. Single-cell transcriptome datasets are listed in Supplementary Table 4. HI genes, LoFT genes, and NNN-related genes are listed in Supplementary Table 6.

The code for investigating cell-type specificity and gene expression strictness is written in R-program and is released at GitHub.<sup>3</sup>

## Ethics approval

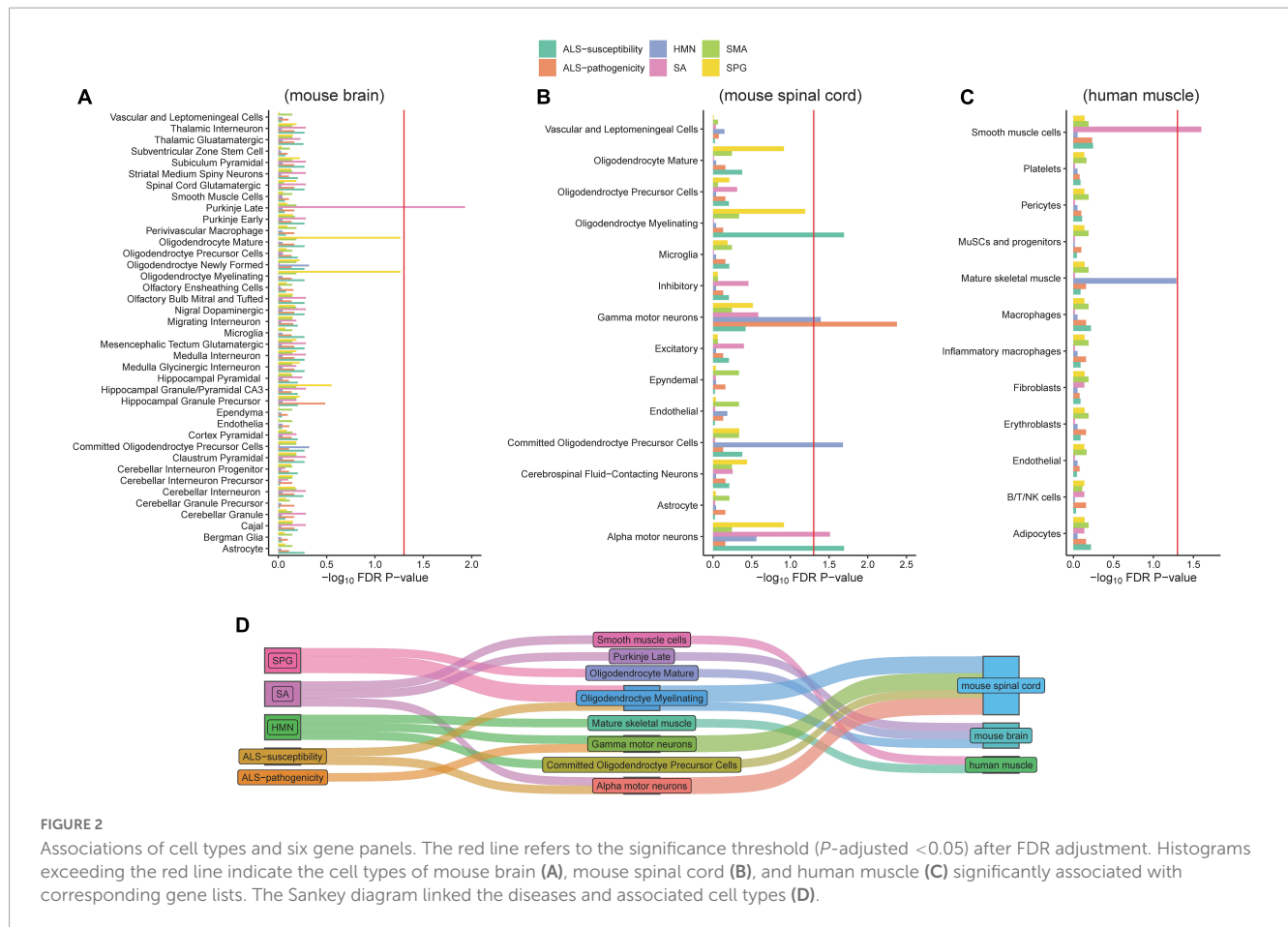
This study was reviewed and approved by the Ethics Review Committee at Hebei Medical University and was performed at Hebei Industrial Technology Research Institute of Genomics. No participant or donor was involved in our study.

## Results

### The involvement of motor neurons in ALS

We collected 32 ALS-pathogenicity genes from the OMIM database and 48 ALS-susceptibility genes from recent large-scale genome-wide association studies. There are five genes (*C9orf72*, *KIF5A*, *NEK1*, *SOD1*, and *TBK1*) related to the pathogenicity and susceptibility of ALS (Figure 1A). To address the cellular basis related to different genetic impacts, we employed the EWCE method developed by Skene and Grant (2016). The EWCE R-package was used to calculate the cell-type specificity of the pathogenicity and susceptibility ALS genes in the single-cell transcriptome data. No neurons in brain were found to

<sup>3</sup> <https://github.com/liuhankui/ALS>



be associated with ALS-pathogenicity genes or ALS-susceptibility genes (Figure 2A). Surprisingly,  $\alpha$ -MNs and  $\gamma$ -MNs in the spinal cord were associated with ALS-susceptibility genes and ALS-pathogenicity genes (Figure 2B), suggesting different involvements of MNs subpopulations in ALS. To confirm our findings, we employed two independent single-cell transcriptome datasets of mouse spinal cord and annotated the cell types using the SingleR package with a reference from Rosenberg et al. (2018). We replicated the specific associations of susceptibility/pathogenicity genes and  $\alpha$ -/ $\gamma$ - MNs (Supplementary Table 7). A significant association ( $P$ -value = 0.05) between susceptibility genes and  $\alpha$ -MNs, as well as a significant association ( $P$ -value = 0.03) between pathogenicity genes and  $\gamma$ -MNs, was observed in the replication data of mouse spinal cord data (Milich's dataset). Suggestive associations ( $P$ -value of susceptibility genes and  $\alpha$ -MNs = 0.08;  $P$ -value of pathogenicity genes and  $\gamma$ -MNs = 0.075) were observed in the replication data of mouse spinal cord data (Sathyamurthy's dataset). We also validated these associations in a single-cell transcriptome dataset of human spinal cord and observed a significant association ( $P$ -value = 0.039) between susceptibility genes and  $\alpha$ -MNs, as well as a significant association ( $P$ -value = 0.015) between pathogenicity genes and  $\gamma$ -MNs. The replications in mouse dataset and validation in human dataset demonstrated the robustness of our findings. We combined the statistical summary of three independent single-cell transcriptome datasets of mouse spinal cord and one single-cell transcriptome dataset of human spinal cord *via* meta-analysis (Willer et al.,

2010) and used the total number of cell types (56) of the four datasets [discovery: 14; replication of mouse spinal cord (Milich's): 14; replication of mouse spinal cord data (Sathyamurthy's): 10; validation of human spinal cord data: 18] for Bonferroni's  $P$ -value correction. The meta-analysis results (Supplementary Table 7) confirmed  $\gamma$ -MNs associated with ALS-pathogenicity ( $P$ -value =  $6.00 \times 10^{-7}$ ) and  $\alpha$ -MNs associated with ALS-susceptibility ( $P$ -value =  $6.86 \times 10^{-6}$ ).

## Cellular differences of ALS, HMN, SA, SPG, and SMA

Besides ALS, we included four neurological disorders—HMN, SA, SPG, and SMA—with phenotypic overlaps and collected their pathogenicity gene sets. Except for five of the HMN-pathogenicity genes shared with SMA, there are few overlaps between each pair among ALS, HMN, SA, SPG, and SMA (Figure 1B). These results showed potential different contributions of cell types to disease pathophysiology. Analysis of cell type-specific expression of genes related to HMN, SA, SPG, and SMA provided insights into their cellular basis: an association between Purkinje cells in brain and SA, an association between  $\alpha$ -MNs in spinal cord and SA, an association between smooth muscle cells and SA, an association between  $\gamma$ -MNs in spinal cord and HMN, an association between oligodendrocyte and HMN, a suggestive association between mature skeletal muscle and HMN

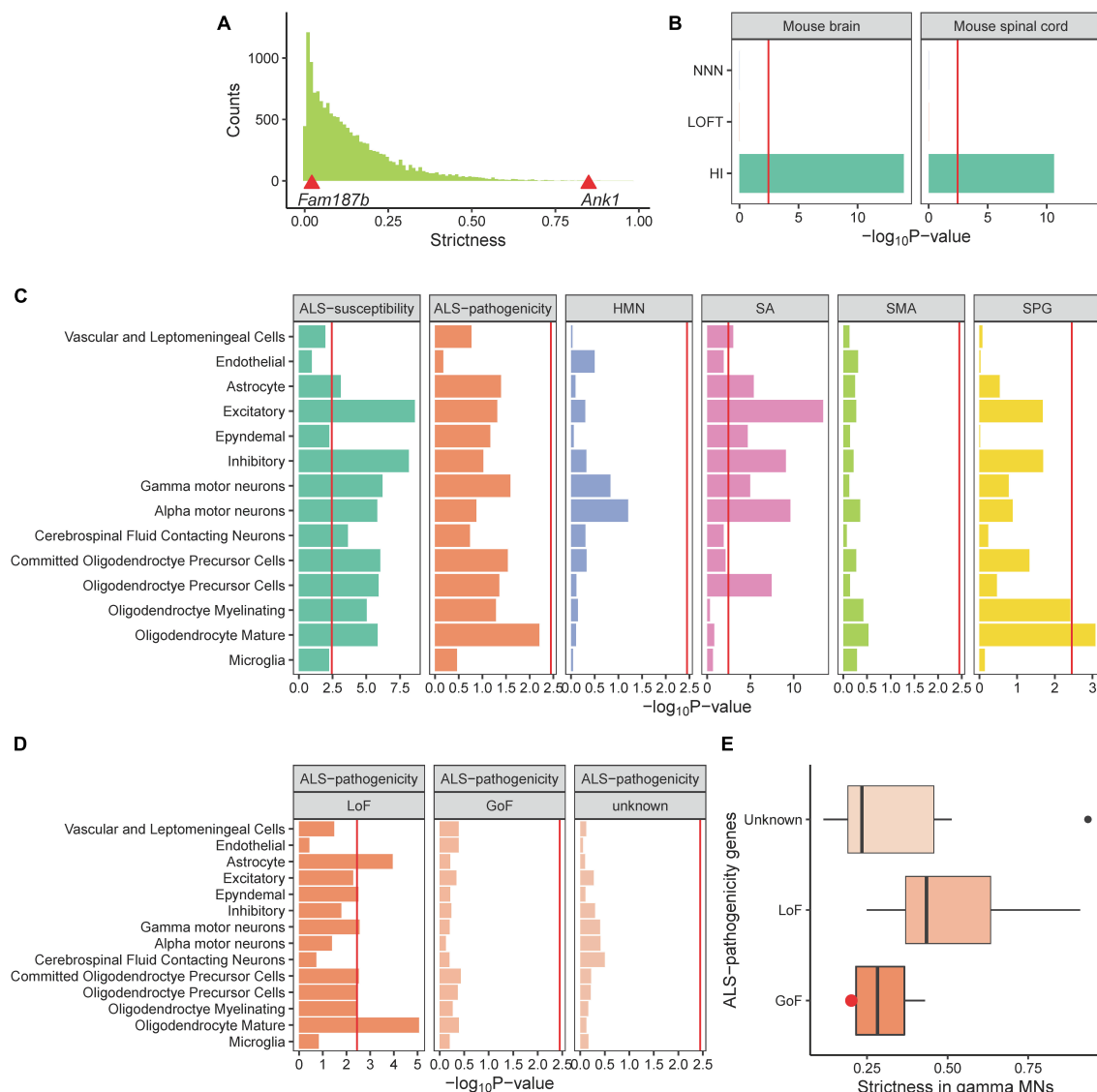


FIGURE 3

The strict dosage requirement of ALS-related genes in MNs. (A) The histogram displays the distribution of strictness value of all genes in brain cells. Strictness values for *Fam187b* and *Ank1* are exhibited by the red triangles. (B) Comparison of three gene panels with known strictness in mouse brain and spinal cord. (C) ALS-susceptibility genes dosage is required strictly in MNs. (D,E) LoF ALS-pathogenicity genes are required strictly in  $\gamma$ -MNs and no evidence are observed for GoF genes or unknown category. Red point refers to the *Sod1* gene.

( $P$ -value = 0.052), associations between oligodendrocyte subtypes and SPG (Figures 2A–C). The associations of MN/oligodendrocyte in spinal cord/brain were confirmed in replicated/validated datasets (Supplementary Table 8). Similar to ALS, MNs were associated with SA and HMN. To our knowledge, SA and HMN both present ALS-like phenotypes (Anand et al., 2014; Garcia-Santibanez et al., 2018) and MNs degeneration (Ikeda et al., 2012; Beijer and Baets, 2020) is involved in their pathogenesis. Oligodendrocyte is also involved in ALS, a cell type that was shown to induce hyperexcitability and death in mutant *SOD1* mouse (Ferrauiolo et al., 2016). Oligodendrocytes in both brain and spinal cord are associated with SPG, consistent with a previous report (Edgar et al., 2004). Oligodendrocytes are associated with HMN. Besides the cellular basis in brain and spinal cord, smooth muscle cells are associated with SA,

skeletal muscle cells are associated with HMN. No evidence was observed for an association of SMA, even though SMA and HMN share five pathogenicity genes. To provide a clear image of the connections, we linked the diseases and cell types via a Sankey diagram (Figure 2D). These similarities and differences may provide insights in the etiology of ALS, HMN, SA, SMA, and SPG.

## The strict dosage requirement of ALS-susceptibility genes in MNs

Here we have revealed that ALS-related genes are specifically expressed in MNs, however, how these genes affect ALS reminds unclear. To provide insight into the mechanism, we developed a

measure called strictness to evaluate the dosage requirement in single-cell populations. We hypothesized that if a gene is dosage-sensitive, it will have a narrow range of expression in normal cells and present a higher strictness measure. For example, *ANK1* was identified as a dosage-sensitive gene (Dang et al., 2008). The LoF variant in *ANK1* causes haploinsufficiency and results in autism spectrum disorder (Yang et al., 2019). The *Ank1* strictness measure in mouse brain cells is in the top strictness decile. In contrast, the *FAM187B* expression is tolerant to be altered because it harbors a common stop-gained variant (MacArthur et al., 2012). There are 43.6% of individuals who have a heterogeneous LoF variant and 34.7% of individuals who have homogeneous LoF variant in the gnomAD (Karczewski et al., 2020) database. The *Fam187b* strictness measure in mouse brain cells is in the bottom strictness decile (Figure 3A). To evaluate the performance of the strictness measure, we employed three gene sets with known expression patterns in the brain. Dosage-sensitive genes involved in brain functions are expected to have high strictness in brain cells. We collected 49 HI genes related to neurodegenerative diseases and/or neurodevelopmental diseases as a positive control, 300 LoFT genes, and 1,113 NNN disease-related genes as negative controls for the absence of dosage-sensitivity or brain functions, respectively. HI genes exhibited significant high strictness in brain and spinal cord. In contrast, LoFT genes and NNN disease-related genes exhibited low strictness (Figure 3B). These results demonstrated that strictness is a robust measure of dosage-sensitive genes.

Subsequently, we calculated the strictness of ALS-related genes in spinal cord cell types and showed that the ALS-susceptibility genes present significant high strictness in  $\alpha$ -MNs (Figure 3C), indicating that the ALS-susceptibility genes are dosage-sensitive and the LoF of genes may be a mechanism of ALS. The *P*-value of the ALS-pathogenicity gene strictness in  $\gamma$ -MNs is close to the significant threshold, indicating that there may be different mechanism among these genes. We reviewed the ALS-pathogenicity genes on the basis of animal model and classified these genes into three categories: LoF, gain of function (GoF), and unknown (Supplementary Table 1). We showed that LoF ALS-pathogenicity genes are strictly required in  $\gamma$ -MNs. In contrast, no statistical evidence for supporting the hypothesis that the GoF genes or the genes in unknown category are dosage-sensitive (Figure 3D). These results are consistent with our hypothesis that LoF genes have high strictness and GoF genes have low strictness.

Besides, ALS-susceptibility genes and LoF pathogenicity genes exhibited high strictness in astrocytes and oligodendrocytes, both these two cell types were shown to play important roles in ALS (Ferraiuolo et al., 2016; Stoklund Dittlau et al., 2023). Excitatory, inhibitory, cerebrospinal fluid contacting neurons also required strict expressions of ALS-susceptibility genes. Abnormal cerebrospinal fluid contacting neurons (Ng Kee Kwong et al., 2020), imbalance between excitatory and inhibitory (Foerster et al., 2013; Cavarsan et al., 2022) were reported to contribute to ALS.

## Discussion

Our study revealed several cell types associated with ALS and three additional neurological disorders, HMN, SA, and SPG. Most

of the related cell types have been demonstrated to be important in the related diseases (Skene et al., 2018; Bryois et al., 2020) [e.g., Purkinje cells (Kasumu and Bezprozvanny, 2012; Xia et al., 2013; Ishida et al., 2016) in SA, oligodendrocyte (Edgar et al., 2004) in SPG]. Notably, MNs are linked to ALS:  $\alpha$ -MNs are associated with ALS-susceptibility genes and  $\gamma$ -MNs are associated with ALS-pathogenicity genes. Although the degeneration of MNs is demonstrated to cause ALS and neuromuscular disorders, the pathogenicity of MNs subpopulations is less known. The different roles of MNs subpopulations are consistent with a previous study (Lalancette-Hebert et al., 2016) that showed different vulnerabilities of MNs subpopulations:  $\alpha$ -MNs are selectively degenerated and  $\gamma$ -MNs are completely spared in an ALS mutant mouse model. These results suggested that  $\alpha$ - and  $\gamma$ -MNs do not play equal roles in ALS. Besides MNs, we found no statistical evidence for an association between muscle cells and ALS-related genes (Figure 2C). To our knowledge, MN death is the core event of ALS pathology (Anakor et al., 2022), however, the disruption of the neuromuscular junction is an early event in ALS pathology (Cappello and Francolini, 2017). Skeletal muscle metabolic dysregulation and atrophy in *SOD1* mutation transgenic mice (Brooks et al., 2004; Marcuzzo et al., 2011) and iPSCs (Badu-Mensah et al., 2020) derived from ALS patients harboring *SOD1* mutation were suggested to play a role in ALS. The muscle atrophy in *SOD1* model doesn't conflict with our result. Our study investigated the most specific cell type expressed ALS-related genes. We cannot exclude the potential connection between specific gene and other cell types. Moreover, we observed *SOD1* is specifically expressed in human muscle (Supplementary Table 9). Limited to the power for detecting minor characteristics of a few genes, the *P*-value of gene expression specificity in muscle did not access the significant threshold after FDR. Taken together, these results deepened our understanding of ALS pathogenesis.

We showed that the ALS-susceptibility genes are dosage-sensitive in MNs, as well as the ALS-pathogenicity genes with known LoF mechanism in  $\gamma$ -MNs. In contrast, the GoF ALS-pathogenicity genes or the genes with unknown mechanism exhibited low strictness (Figures 3D, E). *SOD1* is one of the GoF pathogenicity genes. Transgenic mutant *SOD1* mice and rats develop characteristics that are similar to human ALS. A previous study showed that the complete absence of *SOD1* in mice did not precipitate ALS-related phenotypes (Reaume et al., 1996). A low strictness value of *Sod1* is consistent with the GoF mechanism (Figure 3E). Indeed, which mechanism causes the ALS—gain- or LoF—is still not clear (Kabashi et al., 2010; Saccon et al., 2013; Mizielinska and Isaacs, 2014; Scekic-Zahirovic et al., 2016). Our study suggested the main characteristics of ALS-susceptibility genes is dosage-sensitive, highlighting the need to carefully consider the LoF mechanism in sporadic ALS. For LoF ALS-pathogenicity genes, they were shown to strictly express in  $\gamma$ -MNs but not  $\alpha$ -MNs. This result may suggest  $\gamma$ -MNs are more vulnerable to dosage alteration of the LoF pathogenicity genes. We noticed that there is no significant difference in the vulnerability of  $\alpha$ - and  $\gamma$ -MNs to ALS-susceptibility genes. This result doesn't conflict with the association between ALS-susceptibility genes and  $\alpha$ -MNs. The ALS-susceptibility genes were shown to highly express in  $\alpha$ -MNs. Compared with other cells with lower expression, the  $\alpha$ -MNs were largely affected by the alteration

of ALS-susceptibility genes. In contrast, the strictness of SPG-related genes was shown differences between oligodendrocytes and other un-associated cells, as well as that of ALS-pathogenicity genes and  $\gamma$ -MNs. Indeed, the strictness measure was designed to compare the different expression spectrums in specific cell type between LoF genes and GoF genes as a fellow independent study of cell type expression specificity analysis. This measure was demonstrated by the LoF ALS-pathogenicity genes strictly expressed in related  $\gamma$ -MNs and exhibited the strict expression of SPG-related genes in oligodendrocytes, SA-related genes in  $\alpha$ -MNs, ALS-related genes in oligodendrocytes. HMN-related genes were shown no LoF characteristic in related MNs. Based on these results, strictness analysis may provide *a priori* understanding of the mechanisms of disease-related genes without an animal model.

Similar to ALS, MNs were associated with SA and HMN. To our knowledge, SA and HMN both present ALS-like phenotypes (Anand et al., 2014; Garcia-Santibanez et al., 2018), and MNs degeneration (Ikeda et al., 2012; Beijer and Baets, 2020) are involved in their pathogenesis. Oligodendrocytes are associated with ALS, SPG, and HMN. The links to SPG and ALS are consistent with previous reports (Edgar et al., 2004; Ferraiuolo et al., 2016). Besides, smooth muscle cells are associated with SA, and skeletal muscle cells are associated with HMN. No evidence was observed for an association of SMA, even though SMA and HMN share five pathogenicity genes. These similarities and differences may provide insights into the etiology of ALS, HMN, SA, SMA, and SPG.

Upper MNs should be considered in our further investigation. ALS patients showed loss of pyramidal tract upper MNs, specifically Betz cells (Hammer et al., 1979). The cortical connections of Betz cells are impaired prior to ALS onset (Genç et al., 2017). Betz cells were found below the surface of the cerebral cortex within layer V of the primary motor cortex and make direct connections to spinal MNs (Lemon, 2008). However, the mouse brain single-cell transcriptome datasets employed in our study did not annotate Betz cells. Betz cell specifically expressed *POU3F1* gene (Machado et al., 2014) which can be used as a marker for cell identification in mouse and human. A recent study with more than 450,000 transcriptomes and epigenomes in humans, marmoset monkeys and mice showed a broadly conserved cellular makeup of primary motor cortex, with similarities that mirror evolutionary distance and are consistent between the transcriptome and epigenome. Our discoveries in mouse spinal cord were validated in human spinal cord. These consistent results indicated data from mouse can be used for human disease investigation, providing a reliable pathway for further investigation in Betz cells and other novel cell types.

In summary, our study revealed the cellular basis of ALS, HMN, SA, and SPG and the dosage characteristic of the disease-related genes in specific cell types. Moreover, the methods—cell type enrichment and gene expression variability—are useful for investigating the role of genes in various cell types, which may open the door for valuable mining of public single-cell data and genetic knowledge of human diseases.

## Data availability statement

The original contributions presented in this study are included in the article/**Supplementary material**, further inquiries can be directed to the corresponding authors.

## Author contributions

HL and LG conceived the study. JZ, YL, and ZZ supervised the study. LG and MD collected the disease-related genes. HL performed the investigation and wrote the first draft of the manuscript. MD and ZZ confirmed the study design and research findings for ALS and other neurological disorders. HL, MD, KK, JZ, YL, and ZZ reviewed the manuscript. HL, LG, LB, KK, YL, JZ, and ZZ revised the manuscript. LB, KK, YL, and JZ contributed to a significant improvement of the manuscript. All authors contributed to the article and approved the submitted version.

## Funding

This study was supported by Shenzhen Municipal of Government of China (JCYJ20180507183615145), the National Key R&D Program of China (2017YFC1308400), and Hebei Provincial Natural Science Foundation Precision Medicine Joint Fund Cultivation Project (H2021206414).

## Acknowledgments

We would like to thank the providers of the public databases and software we used in our study.

## Conflict of interest

HL, LG, JZ, LB, and YL were employed by company BGI.

The remaining authors declare that the research was conducted in the absence of any commercial or financial relationships that could be construed as a potential conflict of interest.

## Publisher's note

All claims expressed in this article are solely those of the authors and do not necessarily represent those of their affiliated organizations, or those of the publisher, the editors and the reviewers. Any product that may be evaluated in this article, or claim that may be made by its manufacturer, is not guaranteed or endorsed by the publisher.

## Supplementary material

The Supplementary Material for this article can be found online at: <https://www.frontiersin.org/articles/10.3389/fnins.2023.1116087/full#supplementary-material>

## References

- Al-Chalabi, A., Fang, F., Hanby, M., Leigh, P., Shaw, C., Ye, W., et al. (2010). An estimate of amyotrophic lateral sclerosis heritability using twin data. *J. Neurol. Neurosurg. Psychiatry* 81, 1324–1326.
- Amberger, J. S., Bocchini, C. A., Schiettecatte, F., Scott, A. F., and Hamosh, A. (2015). OMIM.org: Online mendelian inheritance in man (OMIM®), an online catalog of human genes and genetic disorders. *Nucleic Acids Res.* 43, D789–D798. doi: 10.1093/nar/gku1205
- Anakor, E., Duddy, W. J., and Duguez, S. (2022). The cellular and molecular signature of ALS in muscle. *J. Pers. Med.* 12:1868. doi: 10.3390/jpm12111868
- Anand, K. S., Wadhwa, A., Garg, J., and Mahajan, R. K. (2014). Amyotrophic lateral sclerosis-like presentation in a HIV-positive patient. *J. Int. Assoc. Providers AIDS Care (JIAPAC)* 13, 515–518. doi: 10.1177/2325957414535254
- Andersen, J., Thom, N., Shadrach, J., Chen, X., Amin, N., Yoon, S., et al. (2021). Landscape of human spinal cord cell type diversity at midgestation. *bioRxiv* [Preprint]. doi: 10.1101/2021.12.29.473693
- Aran, D., Looney, A., Liu, L., Wu, E., Fong, V., Hsu, A., et al. (2019). Reference-based analysis of lung single-cell sequencing reveals a transitional profibrotic macrophage. *Nat. Immunol.* 20, 163–172. doi: 10.1038/s41590-018-0276-y
- Badu-Mensah, A., Guo, X., McAleer, C. W., Rumsey, J. W., and Hickman, J. J. (2020). Functional skeletal muscle model derived from SOD1-mutant ALS patient iPSCs recapitulates hallmarks of disease progression. *Sci. Rep.* 10:14302. doi: 10.1038/s41598-020-70510-3
- Beijer, D., and Baets, J. (2020). The expanding genetic landscape of hereditary motor neuropathies. *Brain* 143, 3540–3563. doi: 10.1093/brain/awaa311
- Benyamin, B., He, J., Zhao, Q., Gratten, J., Garton, F., Leo, P., et al. (2017). Cross-ethnic meta-analysis identifies association of the GPX3-TNIP1 locus with amyotrophic lateral sclerosis. *Nat. Commun.* 8, 1–7. doi: 10.1038/s41467-017-00471-1
- Brooks, K. J., Hill, M. D. W., Hockings, P. D., and Reid, D. G. (2004). MRI detects early hindlimb muscle atrophy in Gly93Ala superoxide dismutase-1 (G93A SOD1) transgenic mice, an animal model of familial amyotrophic lateral sclerosis. *NMR Biomed.* 17, 28–32. doi: 10.1002/nbm.861
- Brown, R. H., and Al-Chalabi, A. (2017). Amyotrophic lateral sclerosis. *N. Engl. J. Med.* 377, 162–172.
- Broyo, J., Skene, N., Hansen, T., Kogelman, L., Watson, H., Liu, Z., et al. (2020). Genetic identification of cell types underlying brain complex traits yields insights into the etiology of Parkinson's disease. *Nat. Genet.* 52, 482–493. doi: 10.1038/s41588-020-0610-9
- Burke, R. E., Strick, P. L., Kanda, K., Kim, C. C., and Walmsley, B. (1977). Anatomy of medial gastrocnemius and soleus motor nuclei in cat spinal cord. *J. Neurophysiol.* 40, 667–680.
- Cappello, V., and Francolini, M. (2017). Neuromuscular junction dismantling in amyotrophic lateral sclerosis. *Int. J. Mol. Sci.* 18, 2092. doi: 10.3390/ijms18102092
- Cavarsan, C., Steele, P., Genry, L., Reedich, E., McCane, L., LaPre, K., et al. (2022). Inhibitory interneurons show early dysfunction in a SOD1 mouse model of amyotrophic lateral sclerosis. *J. Physiol.* 601, 647–667. doi: 10.1111/JP284192
- Dang, V. T., Kassahn, K. S., Marcos, A. E., and Ragan, M. A. (2008). Identification of human haploinsufficient genes and their genomic proximity to segmental duplications. *Eur. J. Hum. Genet.* 16, 1350–1357. doi: 10.1038/ejhg.2008.111
- De Micheli, A. J., Spector, J. A., Elemento, O., and Cosgrove, B. D. (2020). A reference single-cell transcriptomic atlas of human skeletal muscle tissue reveals bifurcated muscle stem cell populations. *Skeletal Muscle* 10, 1–13. doi: 10.1186/s13395-020-00236-3
- Deng, M., Wei, L., Zuo, X., Tian, Y., Xie, F., Hu, P., et al. (2013). Genome-wide association analyses in Han Chinese identify two new susceptibility loci for amyotrophic lateral sclerosis. *Nat. Genet.* 45, 697–700. doi: 10.1038/ng.2627
- Dueck, H., Khaladkar, M., Kim, T., Spaethling, J., Francis, C., Suresh, S., et al. (2015). Deep sequencing reveals cell-type-specific patterns of single-cell transcriptome variation. *Genome Biol.* 16, 1–17.
- Edgar, J., McLaughlin, M., Yool, D., Zhang, S., Fowler, J., Montague, P., et al. (2004). Oligodendroglial modulation of fast axonal transport in a mouse model of hereditary spastic paraplegia. *J. Cell Biol.* 166, 121–131. doi: 10.1083/jcb.200312012
- Ferraiuolo, L., Meyer, K., Sherwood, T., Vick, J., Likhite, S., Frakes, A., et al. (2016). Oligodendrocytes contribute to motor neuron death in ALS via SOD1-dependent mechanism. *Proc. Natl. Acad. Sci. U.S.A.* 113, E6496–E6505. doi: 10.1073/pnas.1607496113
- Foerster, B., Pomper, M., Callaghan, B., Petrou, M., Edden, R., Mohamed, M., et al. (2013). An imbalance between excitatory and inhibitory neurotransmitters in amyotrophic lateral sclerosis revealed by use of 3-T proton magnetic resonance spectroscopy. *JAMA Neurol.* 70, 1009–1016. doi: 10.1001/jamaneurol.2013.234
- Fogh, I., Ratti, A., Gellera, C., Lin, K., Tiloca, C., Moskvina, V., et al. (2014). A genome-wide association meta-analysis identifies a novel locus at 17q11. 2 associated with sporadic amyotrophic lateral sclerosis. *Hum. Mol. Genet.* 23, 2220–2231. doi: 10.1093/hmg/ddt587
- Garcia-Santibanez, R., Burford, M., and Bucelli, R. C. (2018). Hereditary motor neuropathies and amyotrophic lateral sclerosis: A molecular and clinical update. *Curr. Neurol. Neurosci. Rep.* 18, 1–10.
- Genç, B., Jara, J., Lagrimas, A., Pytel, P., Roos, R., Mesulam, M., et al. (2017). Apical dendrite degeneration, a novel cellular pathology for Betz cells in ALS. *Sci. Rep.* 7:41765.
- Graham, A. J., Macdonald, A. M., and Hawkes, C. H. (1997). British motor neuron disease twin study. *J. Neurol. Neurosurg. Psychiatry* 62, 562–569. doi: 10.1136/jnnp.62.6.562
- Hammer, R. P. J., Tomiyasu, U., and Scheibel, A. B. (1979). Degeneration of the human Betz cell due to amyotrophic lateral sclerosis. *Exp. Neurol.* 63, 336–346.
- Iacoangeli, A., Lin, T., Al Khleifat, A., Jones, A., Opie-Martin, S., Coleman, J., et al. (2020). Genome-wide meta-analysis finds the ACSL5-ZDHHC6 locus is associated with ALS and links weight loss to the disease genetics. *Cell Rep.* 33:108323. doi: 10.1016/j.celrep.2020.108323
- Ikedo, Y., Ohta, Y., Kobayashi, H., Okamoto, M., Takamatsu, K., Ota, T., et al. (2012). Clinical features of SCA36: A novel spinocerebellar ataxia with motor neuron involvement (Asidan). *Neurology* 79, 333–341.
- Ishida, Y., Kawakami, H., Kitajima, H., Nishiyama, A., Sasai, Y., Inoue, H., et al. (2016). Vulnerability of Purkinje cells generated from spinocerebellar ataxia type 6 patient-derived iPSCs. *Cell Rep.* 17, 1482–1490.
- Kabashi, E., Lin, L., Tradewell, M., Dion, P., Bercier, V., Bourgouin, P., et al. (2010). Gain and loss of function of ALS-related mutations of TARDBP (TDP-43) cause motor deficits in vivo. *Hum. Mol. Genet.* 19, 671–683. doi: 10.1093/hmg/ddp534
- Karczewski, K., Francioli, L., Tiao, G., Cummings, B., Alfoldi, J., Wang, Q., et al. (2020). The mutational constraint spectrum quantified from variation in 141,456 humans. *Nature* 581, 434–443.
- Kasumu, A., and Bezprozvanny, I. (2012). Deranged calcium signaling in Purkinje cells and pathogenesis in spinocerebellar ataxia 2 (SCA2) and other ataxias. *Cerebellum* 11, 630–639.
- Kiernan, M., Vucic, S., Cheah, B., Turner, M., Eisen, A., Hardiman, O., et al. (2011). Amyotrophic lateral sclerosis. *Lancet* 377, 942–955.
- Krishnan, A., Zhang, R., Yao, V., Theesfeld, C., Wong, A., Tadych, A., et al. (2016). Genome-wide prediction and functional characterization of the genetic basis of autism spectrum disorder. *Nat. Neurosci.* 19, 1454–1462.
- Laaksovirta, H., Peuralinna, T., Schymick, J., Scholz, S., Lai, S., Myllykangas, L., et al. (2010). Chromosome 9p21 in amyotrophic lateral sclerosis in Finland: A genome-wide association study. *Lancet Neurol.* 9, 978–985.
- Lalancette-Hebert, M., Sharma, A., Lyashchenko, A. K., and Shneider, N. A. (2016). Gamma motor neurons survive and exacerbate alpha motor neuron degeneration in ALS. *Proc. Natl. Acad. Sci. U.S.A.* 113, E8316–E8325. doi: 10.1073/pnas.1605210113
- Lek, M., Karczewski, K., Minikel, E., Samocha, K., Banks, E., Fennell, T., et al. (2016). Analysis of protein-coding genetic variation in 60,706 humans. *Nature* 536, 285–291.
- Lemon, R. N. (2008). Descending pathways in motor control. *Annu. Rev. Neurosci.* 31, 195–218.
- Li, C., Ou, R., Wei, Q., and Shang, H. (2021). Shared genetic links between amyotrophic lateral sclerosis and obesity-related traits: A genome-wide association study. *Neurobiol. Aging* 102, 211.e1–211.e9. doi: 10.1016/j.neurobiolaging.2021.01.023
- Liu, H.-K., He, S.-J., and Zhang, J.-G. (2021). A bioinformatic study revealed serotonergic neurons are involved in the etiology and therapygenetics of anxiety disorders. *Transl. Psychiatry* 11, 1–6. doi: 10.1038/s41398-021-01432-5
- MacArthur, D. G., Balasubramanian, S., Frankish, A., Huang, N., Morris, J., Walter, K., et al. (2012). A systematic survey of loss-of-function variants in human protein-coding genes. *Science* 335, 823–828. doi: 10.1126/science.1215040
- Machado, C. B., Kanning, K., Kreis, P., Stevenson, D., Crossley, M., Nowak, M., et al. (2014). Reconstruction of phrenic neuron identity in embryonic stem cell-derived motor neurons. *Development (Cambridge, England)* 141, 784–794. doi: 10.1242/dev.097188
- Marcuzzo, S., Zucca, I., Mastropietro, A., de Rosbo, N., Cavalcante, P., Tartari, S., et al. (2011). Hind limb muscle atrophy precedes cerebral neuronal degeneration in G93A-SOD1 mouse model of amyotrophic lateral sclerosis: A longitudinal MRI study. *Exp. Neurol.* 231, 30–37. doi: 10.1016/j.expneurol.2011.05.007
- Marin, B., Hamidou, B., Couratier, P., Nicol, M., Delzor, A., Raymondeau, M., et al. (2014). Population-based epidemiology of amyotrophic lateral sclerosis (ALS) in an ageing Europe—the French register of ALS in Limousin (FRAL im register). *Eur. J. Neurol.* 21, 1292–300, e78–79. doi: 10.1111/ene.12474
- Mehta, P., Raymond, J., Punjani, R., Larson, T., Han, M., Bove, F., et al. (2022). Incidence of amyotrophic lateral sclerosis in the United States, 2014–2016. *Amyotroph. Lateral Scler. Frontotemporal Degener.* 23, 378–382. doi: 10.1080/21678421.2021.2023190

- Milich, L., Choi, J., Ryan, C., Cerqueira, S., Benavides, S., Yahn, S., et al. (2021). Single-cell analysis of the cellular heterogeneity and interactions in the injured mouse spinal cord. *J. Exp. Med.* 218:e20210040. doi: 10.1084/jem.20210040
- Mizielinska, S., and Isaacs, A. M. (2014). C9orf72 amyotrophic lateral sclerosis and frontotemporal dementia: Gain or loss of function? *Curr. Opin. Neurol.* 27:515.
- Nakamura, R., Misawa, K., Tohnai, G., Nakatochi, M., Furuhashi, S., Atsuta, N., et al. (2020). A multi-ethnic meta-analysis identifies novel genes, including ACSL5, associated with amyotrophic lateral sclerosis. *Commun. Biol.* 3:526. doi: 10.1038/s42003-020-01251-2
- Ng Kee Kwong, K. C., Mehta, A. R., Nedergaard, M., and Chandran, S. (2020). Defining novel functions for cerebrospinal fluid in ALS pathophysiology. *Acta Neuropathol. Commun.* 8:140. doi: 10.1186/s40478-020-01018-0
- Nicolas, A., Kenna, K., Renton, A., Ticozzi, N., Faghri, F., Chia, R., et al. (2018). Genome-wide analyses identify KIF5A as a novel ALS gene. *Neuron* 97, 1268–1283. doi: 10.1016/j.neuron.2018.02.027
- Ragagnin, A. M. G., Shadfar, S., Vidal, M., Jamali, M. S., and Atkin, J. D. (2019). Motor neuron susceptibility in ALS/FTD. *Front. Neurosci.* 13:532. doi: 10.3389/fnins.2019.00532
- Reaume, A., Elliott, J., Hoffman, E., Kowall, N., Ferrante, R., Siwek, D., et al. (1996). Motor neurons in Cu/Zn superoxide dismutase-deficient mice develop normally but exhibit enhanced cell death after axonal injury. *Nat. Genet.* 13, 43–47. doi: 10.1038/ng0596-43
- Renton, A. E., Chiò, A., and Traynor, B. J. (2014). State of play in amyotrophic lateral sclerosis genetics. *Nat. Neurosci.* 17, 17–23.
- Rosenberg, A., Roco, C., Muscat, R., Kuchina, A., Sample, P., Yao, Z., et al. (2018). Single-cell profiling of the developing mouse brain and spinal cord with split-pool barcoding. *Science* 360, 176–182. doi: 10.1126/science.aam8999
- Saccon, R. A., Bunton-Stasyshyn, R. K. A., Fisher, E. M. C., and Fratta, P. (2013). Is SOD1 loss of function involved in amyotrophic lateral sclerosis? *Brain* 136, 2342–2358.
- Saraiva, L. R., Ibarra-Soria, X., Khan, M., Omura, M., Scialdone, A., Mombaerts, P., et al. (2015). Hierarchical deconstruction of mouse olfactory sensory neurons: From whole mucosa to single-cell RNA-seq. *Sci. Rep.* 5, 1–17. doi: 10.1038/srep18178
- Sathyamurthy, A., Johnson, K., Matson, K., Dobrott, C., Li, L., Ryba, A., et al. (2018). Massively parallel single nucleus transcriptional profiling defines spinal cord neurons and their activity during behavior. *Cell Rep.* 22, 2216–2225. doi: 10.1016/j.celrep.2018.02.003
- Scekic-Zahirovic, J., Sendscheid, O., El Oussini, H., Jambeau, M., Sun, Y., Mersmann, S., et al. (2016). Toxic gain of function from mutant FUS protein is crucial to trigger cell autonomous motor neuron loss. *EMBO J.* 35, 1077–1097. doi: 10.15252/embj.201592559
- Shatunov, A., Mok, K., Newhouse, S., Weale, M., Smith, B., Vance, C., et al. (2010). Chromosome 9p21 in sporadic amyotrophic lateral sclerosis in the UK and seven other countries: A genome-wide association study. *Lancet Neurol.* 9, 986–994. doi: 10.1016/S1474-4422(10)70197-6
- Skene, N. G., and Grant, S. G. N. (2016). Identification of vulnerable cell types in major brain disorders using single cell transcriptomes and expression weighted cell type enrichment. *Front. Neurosci.* 10:16. doi: 10.3389/fnins.2016.00016
- Skene, N., Bryois, J., Bakken, T., Breen, G., Crowley, J., Gaspar, H., et al. (2018). Genetic identification of brain cell types underlying schizophrenia. *Nat. Genet.* 50, 825–833.
- Stoklund Dittlau, K., Terrie, L., Baatsen, P., Kerstens, A., De Swert, L., Janky, R., et al. (2023). FUS-ALS hiPSC-derived astrocytes impair human motor units through both gain-of-toxicity and loss-of-support mechanisms. *Mol. Neurodegener.* 18:5. doi: 10.1186/s13024-022-00591-3
- Usoskin, D., Furlan, A., Islam, S., Abdo, H., Lönnberg, P., Lou, D., et al. (2015). Unbiased classification of sensory neuron types by large-scale single-cell RNA sequencing. *Nat. Neurosci.* 18, 145–153. doi: 10.1038/nn.3881
- van Es, M., Hardiman, O., Chio, A., Al-Chalabi, A., Pasterkamp, R., Veldink, J., et al. (2017). Amyotrophic lateral sclerosis. *Lancet* 390, 2084–2098.
- van Rheenen, W., Shatunov, A., Dekker, A., McLaughlin, R., Diekstra, F., Pulit, S., et al. (2016). Genome-wide association analyses identify new risk variants and the genetic architecture of amyotrophic lateral sclerosis. *Nat. Genet.* 48, 1043–1048.
- van Rheenen, W., van der Spek, R., Bakker, M., van Vugt, J., Hop, P., Zwamborn, R., et al. (2021). Common and rare variant association analyses in amyotrophic lateral sclerosis identify 15 risk loci with distinct genetic architectures and neuron-specific biology. *Nat. Genet.* 53, 1636–1648.
- Wei, L., Tian, Y., Chen, Y., Wei, Q., Chen, F., Cao, B., et al. (2019). Identification of TYW3/CRYZ and FGD4 as susceptibility genes for amyotrophic lateral sclerosis. *Neurol. Genet.* 5:e375. doi: 10.1212/NXG.0000000000000375
- Willer, C. J., Li, Y., and Abecasis, G. R. (2010). METAL: Fast and efficient meta-analysis of genomewide association scans. *Bioinformatics (Oxford, England)* 26, 2190–2191. doi: 10.1093/bioinformatics/btq340
- Xia, G., McFarland, K., Wang, K., Sarkar, P., Yachnis, A., and Ashizawa, T. (2013). Purkinje cell loss is the major brain pathology of spinocerebellar ataxia type 10. *J. Neurol. Neurosurg. Psychiatry* 84, 1409–1411. doi: 10.1136/jnnp-2013-305080
- Xie, T., Deng, L., Mei, P., Zhou, Y., Wang, B., Zhang, J., et al. (2014). A genome-wide association study combining pathway analysis for typical sporadic amyotrophic lateral sclerosis in Chinese Han populations. *Neurobiol. Aging* 35, 1778.e9–1778.e23. doi: 10.1016/j.neurobiolaging.2014.01.014
- Xu, L., Chen, L., Wang, S., Feng, J., Liu, L., Liu, G., et al. (2020). Incidence and prevalence of amyotrophic lateral sclerosis in urban China: A national population-based study. *J. Neurol. Neurosurg. Psychiatry* 91, 520–525. doi: 10.1136/jnnp-2019-322317
- Yang, R., Walder-Christensen, K., Kim, N., Wu, D., Lorenzo, D., Badea, A., et al. (2019). ANK2 autism mutation targeting giant ankyrin-B promotes axon branching and ectopic connectivity. *Proc. Natl. Acad. Sci. U.S.A.* 116, 15262–15271. doi: 10.1073/pnas.1904348116
- Zeisel, A., Muñoz-Manchado, A., Codeluppi, S., Lönnberg, P., La Manno, G., Jureus, A., et al. (2015). Brain structure. Cell types in the mouse cortex and hippocampus revealed by single-cell RNA-seq. *Science* 347, 1138–1142.



## OPEN ACCESS

## EDITED BY

Tingyuan Lang,  
Cancer Hospital, Chongqing University, China

## REVIEWED BY

Janakiraman Udaiyappan,  
Virginia Commonwealth University,  
United States  
Rafieh Alizadeh,  
Iran University of Medical Sciences, Iran  
Kannappan Sriramajayam,  
University of Miami Health System, United States

## \*CORRESPONDENCE

Mohammad Jafari  
✉ dr.mohammadjafari1368@gmail.com

## SPECIALTY SECTION

This article was submitted to  
Neurodegeneration,  
a section of the journal  
Frontiers in Neuroscience

RECEIVED 25 November 2022

ACCEPTED 31 January 2023

PUBLISHED 21 February 2023


## CITATION

Majdinasab N, Orakifar N, Kouti L, Shamsaei G,  
Seyedtabib M and Jafari M (2023) Solifenacin  
versus posterior tibial nerve stimulation  
for overactive bladder in patients with multiple  
sclerosis.  
*Front. Neurosci.* 17:1107886.  
doi: 10.3389/fnins.2023.1107886

## COPYRIGHT

© 2023 Majdinasab, Orakifar, Kouti, Shamsaei,  
Seyedtabib and Jafari. This is an open-access  
article distributed under the terms of the  
[Creative Commons Attribution License \(CC BY\)](https://creativecommons.org/licenses/by/4.0/).  
The use, distribution or reproduction in other  
forums is permitted, provided the original  
author(s) and the copyright owner(s) are  
credited and that the original publication in this  
journal is cited, in accordance with accepted  
academic practice. No use, distribution or  
reproduction is permitted which does not  
comply with these terms.

# Solifenacin versus posterior tibial nerve stimulation for overactive bladder in patients with multiple sclerosis

Nastaran Majdinasab<sup>1</sup>, Neda Orakifar <sup>2,3</sup>, Leila Kouti<sup>4</sup>,  
Gholamreza Shamsaei<sup>5</sup>, Maryam Seyedtabib<sup>6</sup> and  
Mohammad Jafari<sup>7\*</sup>

<sup>1</sup>Member of Musculoskeletal Rehabilitation Research Center, Ahvaz Jundishapur University of Medical Sciences, Ahvaz, Iran, <sup>2</sup>Department of Physiotherapy, School of Rehabilitation Sciences, Ahvaz Jundishapur University of Medical Sciences, Ahvaz, Iran, <sup>3</sup>Musculoskeletal Rehabilitation Research Center, Ahvaz Jundishapur University of Medical Sciences, Ahvaz, Iran, <sup>4</sup>Faculty of Pharmacy, Clinical Pharmacy Department, Ahvaz Jundishapur University of Medical Sciences, Ahvaz, Iran, <sup>5</sup>Department of Neurology, Golestan Hospital, Ahvaz Jundishapur University of Medical Sciences, Ahvaz, Iran, <sup>6</sup>Department of Biostatistics and Epidemiology, School of Public Health, Ahvaz Jundishapur University of Medical Sciences, Ahvaz, Iran, <sup>7</sup>Department of Neurology, Ahvaz Jundishapur University of Medical Sciences, Ahvaz, Iran

**Introduction:** Overactive bladder (OAB) is one of the most common complications in patients with multiple sclerosis (MS). Choosing the effective treatment is very important in improving their quality of life (QOL). Therefore, the aim of this study was to compare solifenacin (SS) and posterior tibial nerve stimulation (PTNS) treatment effects in the MS Patients with OAB.

**Materials and methods:** In total, 70 MS patients suffering from OAB enrolled in this clinical trial study. Patients with a score of at least 3 according to the OAB questionnaire were randomly divided into two groups (35 patients in each group). In one group, patients received SS (5 mg daily for 4 weeks and 10 mg/day for another 8 weeks) and in a second group, patients were treated by PTNS (12 weekly session, 30 min).

**Results:** The mean (SD) age of patients participating in this study was 39.82 (9.088) and 42.41 (9.175) years for the SS group and the PTNS group, respectively. Patients in both groups showed statistically significant improvements in urinary incontinence, micturition, and daytime frequency ( $p < 0.001$ ). Patients in the SS group had a better response for urinary incontinence after 12 weeks compared to the PTNS group. Also, patients in the SS group reported higher satisfaction and less daytime frequency compared to the PTNS group.

**Conclusion:** SS and PTNS were effective for improving the OAB symptoms in patients with MS. However, patients demonstrated a better experience with SS in terms of daytime frequency, urinary incontinence, and treatment satisfaction rate.

## KEYWORDS

multiple sclerosis, overactive bladder, quality of life, electrical nerve stimulation, solifenacin

## Introduction

Multiple sclerosis (MS) is a chronic disease of the nervous system that pathologically characterized by multiple areas of inflammation, demyelination, and glial scarring (sclerosis)

in the white matter of the central nervous system (Harbo et al., 2013; Ghasemi et al., 2017). The clinical course of this disease varies from a benign and asymptomatic disease to a rapidly progressive and debilitating disease. MS commonly occurs at young age, and its peak is around 20–30 years of age.

The symptoms of this disease rarely start before the age of 10 years or after 60 years (Goldenberg, 2012; Harbo et al., 2013; Ghasemi et al., 2017). The main characteristic of this disease is the variability of symptoms; it also tends to change in terms of nature and severity over time (4). The common signs and symptoms of MS include muscle weakness, spasticity, reflex changes, sensory disorders, ataxia, nystagmus, vision disorders, autonomic symptoms (e.g., bladder, intestinal, and sexual disorders), and psychological symptoms. The McDonald diagnostic criteria are the best tool for a definitive diagnosis of this disease (Harbo et al., 2013). According to the McDonald diagnostic criteria, the presence of two or more attacks (dissemination in time), along with the clinical evidence and presence of two or more lesions in different parts of the central nervous system (dissemination in place), is necessary for a definite diagnosis of MS. Therefore, the criteria for the diagnosis of MS are based on the patient's history, clinical examination findings, MRI findings of the brain and spinal cord, and examination of the cerebrospinal fluid.

Bladder and urinary disorders are the common symptoms of MS patients. Bladder care is essential to prevent disabilities, life-threatening infections, and stone formation in these patients. The bladder is probably the only visceral organ with smooth muscles, which is completely controlled by the cerebral cortex. A normal bladder function requires coordination between the sensory and motor components of both autonomic and somatic nervous systems.

Recent advanced studies on neural pathways and neurotransmitters have implicated the presence of neural pathways in the bladder function; therefore, many neurological diseases, including MS, can cause bladder dysfunction (Mahadeva et al., 2014; Khalaf et al., 2015).

The most common bladder dysfunction in MS is excessive bladder contraction. For the treatment of bladder disorders, anticholinergic antimuscarinic agents, such as solifenacin succinate can be used (Ragab et al., 2021). Also, posterior tibial nerve stimulation (PTNS) that involves the stimulation of lower urinary tract nerves often uses to stimulate the nervous pathway of bladder reflex (Staskin et al., 2012). The posterior tibial nerve consists of sensory and motor nerves that directly participates in controlling the sensations and movements of the bladder and pelvic floor muscles (Burks et al., 2010). In PTNS, depolarization of sacral somatic fibers and lumbar afferents indirectly inhibits the activity of the bladder, and can lead to the cessation of bladder contractions (Klingler et al., 2000; Amarenco et al., 2003). Indeed, the PTNS method is based on ancient Chinese acupuncture, which uses acupuncture points on the common peroneal or posterior tibial nerves to inhibit the bladder activity (Geirsson et al., 1993). In spite of available findings, it seems that there is still a need to conduct further research on PTNS. De Gennaro et al. (2011), study highlighted the need for further research on the PTNS. It may be one of the factors which limits the generalizability of previous studies is the selection of samples among patients with a specific disease (Fjorback et al., 2007).

Overall, based on previous studies, urinary dysfunctions strongly affect the patient's mental and psychological health, as well as quality of life (QOL) (Olujide and O'Sullivan, 2005; Mayer and Howard, 2008). According to new reference books, solifenacin succinate is the drug of choice for reducing the symptoms of overactive bladder (OAB). However, due to its side effects and high cost, physiotherapy

has been also suggested. Therefore, the present study aimed to investigate and compare the effects of solifenacin succinate and PTNS on the treatment of OAB and improvement of QOL in patients with MS.

## Patients and methods

This clinical trial was conducted on MS patients with OAB in 2019. It was approved by the ethics committee of Ahvaz Jundishapur University of Medical Sciences (code: IR.AJUMS.HGOLESTAN.REC.1399.127) and registered in the Iranian Registry of Clinical Trials (code: IRCT20210207050277N1). Patients with MS, referred to the MS Association of Khuzestan, Iran, were first examined for OAB after confirming the absence of a urinary tract infection *via* urinalysis. This was achieved using the actionable questionnaire, which is an eight-item tool for screening MS patients with OAB. In this method, MS patients with OAB (with scores  $\geq 3$ ) were screened and diagnosed. Finally, according to the inclusion criteria, 70 patients were examined in this study.

The objectives of the study and the benefits of its results were explained to the patients, and they were ensured that they could withdraw from the study at any time. An informed consent form was obtained from all the patients. The volunteers were randomly divided into two groups (35 patients per group). Randomization was carried out by the random block method, where two patients were randomly assigned to each block, and a random code sequence was generated. For the first group, a drug treatment (solifenacin) was applied, while for the second group, PTNS was performed. The solifenacin group consisted of 28 female and 7 male patients, while the PTNS group consisted of 25 female and 10 male patients.

## Inclusion criteria

The inclusion criteria were as follows: (1) a score  $\geq 3$  on the actionable questionnaire to confirm neurogenic OAB, causing an emergency need to urinate (which may or may not be accompanied by urge incontinence); (2) absence of a urinary tract infection for at least 1 month before the onset of OAB symptoms; (3) the Expanded Disability Status Scale (EDSS) score of 1–5.5; (4) a minimum interval of 1 month from the last MS attack; and (5) age  $\geq 18$  years.

## Exclusion criteria

The exclusion criteria were as follows: (1) pregnancy or planning to conceive in the next 6 months; (2) a history of allergy to solifenacin; (3) cardiac problems (e.g., heart failure); (4) a history of surgery to treat urinary incontinence or other surgeries of the urinary system; (5) stress urinary incontinence or prostatic hyperplasia; (6) diabetes; (7) Parkinson's disease; (8) a history of anticholinergic drug therapy for OAB in the last month; (9) a history of electrotherapy of the lower limbs and the back; (10) performing the pelvic floor muscle exercise in the last month; and (11) having a heart pacemaker and/or leg prosthesis.

## Data collection

First, the standard actionable questionnaire was completed after confirming the absence of a urinary tract infection *via* urinalysis for

screening MS patients with OAB, and MS patients with a minimum score of three on this questionnaire were included in the study.

Subsequently, other questionnaires were completed as scheduled.

### Actionable questionnaire

This questionnaire is a short eight-item tool, whose validity and reliability have been confirmed. It was designed to screen and identify the problems of MS patients with urinary symptoms (possibly caused by neurogenic bladder) and to accurately identify cases of OAB (score  $\geq 3$ ). This questionnaire contains questions which represent the extent to which patients have experienced the symptoms and what effects they have had on their daily life. The Persian version of this questionnaire has excellent internal consistency (Cronbach's  $\alpha = 0.91$ ), with an internal correlation coefficient (ICC) of 0.86. The content validity ratio and content validity index of the questions range from 0.66 to 1. Additionally, the following standard questionnaires were completed by the patients at the beginning of the study and 4, 8, and 12 weeks after implementing the intervention.

### International Consultation on Incontinence Questionnaire in Overactive Bladder (ICIQ-OAB)

This questionnaire was used to determine the severity score of urinary symptoms. Four of the components of this questionnaire were used, that is, the frequency of urination during the day and night and the level of discomfort and the patient's urgency to go to the toilet and the level of discomfort. The translation and localization of the questionnaire, which has acceptable validity and reliability (0.728), were performed by [Sari Motlagh et al. \(2015\)](#). Each question of this questionnaire has five options, scored from 0 to 4, and the total score is calculated for all questions.

### Multiple Sclerosis Quality of Life Questionnaire-54 (MSQOL-54)

The minimum and maximum scores of QOL in this questionnaire were 0 and 100, respectively, with higher scores indicating higher QOL. The 12 dimensions of this questionnaire are divided into two general dimensions: (1) physical health, including the dimensions of role limitations related to physical problems, physical health, physical pain, vitality, perception of health, and sexual performance; and (2) mental health, including the dimensions of role limitations related to mental problems, subjective vitality, social function, health problems, and life satisfaction. This scale was designed for MS patients by Barbara Vickery at the University of California in 1995. Its validity (content and concurrent validity) has been confirmed in different studies outside ([Fjorback et al., 2007](#); [Mayer and Howard, 2008](#)) and inside Iran ([Olujide and O'Sullivan, 2005](#); [Tornic and Panicker, 2018](#)). The reliability of this tool was confirmed with a correlation coefficient of 0.86.

The MSQOL-54 contains 54 questions, 18 of which pertain to 14 areas specific to MS (i.e., physical function, role limitations due to physical problems, role limitations due to mental problems, social function, health stress, sexual function, satisfaction with sexual function, pain, energy, perception of health, overall QOL, health changes, cognitive function, and psychological wellbeing); also, 36 questions are related to general QOL. Each question has two to seven options and is rated on a Likert scale. Finally, the score of QOL is determined by combining the scores of the two areas; these two areas

include "physical health" and "spiritual-psychological health." The scores of all 14 areas and two combined areas are in the range of 0–100, with higher scores indicating a better status.

### International Consultation on Incontinence Questionnaire–Urinary Incontinence Short Form (ICIQ-UI SF)

The validity and reliability of this standard questionnaire were evaluated by [Hajebrahimi et al., 2012](#) in Iran. This questionnaire contains six questions on an individual's status in the last 4 weeks. Questions 1 and 2 are demographic questions; question 3 pertains to the frequency of urinary incontinence; question 4 measures the amount of urinary leakage; and question 5 measures its impact on QOL. The scores of questions 5, 4, and 2 represent the patient's real score; question 6 pertains to the time and type of urinary leakage, which was not considered in this study. The total score of the questionnaire ranges from 0 to 21 (mild, 5–1; moderate, 12–6; severe, 18–13; and very severe, 21–19), with higher scores indicating an increase in the intensity of urinary incontinence. The questionnaire was self-administered; if the respondent was illiterate, it was completed with the researcher's assistance.

### Drug intervention

Oral tablets of solifenacin succinate (5 mg), under the brand name "V-SOL" (Dr. Abidi Pharmaceuticals, Tehran, Iran), were used for drug treatment. This drug, produced in 2004, is one of the antimuscarinic agents, which functions by reducing the bladder contractions. It was initially prescribed at a dose of 5 mg daily for 4 weeks. Its dose was then increased to 10 mg per day (5 mg twice a day) and continued for 12 weeks.

### Posterior tibial nerve stimulation

Electrical stimulation of the posterior tibial nerve was performed using a two-channel TENS 710 device (model 1395, Iran). The characteristics of the current were as follows: intensity, 0.5–10 mA; frequency, 20 Hz; and pulse length, 200  $\mu$ m. The current intensity increased up to the threshold of motor nerve stimulation, which was determined by the big toe flexion. So far, no studies have reported any side effects for the surface electrical stimulation of the posterior tibial nerve. To perform electrical stimulation, a negative electrode (cathode) was placed behind the inner ankle of the body, and a positive electrode (anode) was placed 10 cm above the cathode. Twelve posterior tibial nerve stimulation sessions (30 min per session) were held over 12 weeks (one session per week).

### Sample size calculation and sampling methods

After entering the study, the patients were randomly divided into two groups. Considering the longitudinal design of the study, the sample size was based on previous studies ([Tornic and Panicker, 2018](#)). Considering a type I error of 0.05 and statistical power of 0.95, the correlation coefficient between responses in three measurements was equal to 0.50, the difference in the average

response of the two groups was equal to one, and the standard deviation (SD) was equal to one. A sample size of 35 patients per group and a total sample size of 70 patients were finally estimated.

## Statistical methods

To describe the data, mean and SD were measured for quantitative variables, and frequency (percentage) was measured for qualitative variables. The normal distribution of data was evaluated using Kolmogorov–Smirnov test. Moreover, statistical analysis was performed using Chi-square and independent samples *t*-test to examine the distribution of demographic variables in the two groups. Additionally, a generalized estimating equation (GEE) method with an unstructured correlation matrix was used to analyze longitudinal data. Four factors, including group, gender, time, and interaction of time and group, were included in each model. All analyses were performed in SPSS version 25 at a significance level of 0.05.

## Results

The mean age of the patients was  $39.82 \pm 9.088$  years in the solifenacin group and  $42.41 \pm 9.175$  years in the PTNS group;

however, there was no significant difference between the two groups ( $p = 0.249$ ). Two patients from the solifenacin group were excluded due to severe constipation. Also, one patient from the PTNS group was excluded due to death because of coronavirus disease. In the solifenacin group, 7 patients (21.2%) were male, and 26 patients (78.8%) were female, while in the PTNS group, 10 patients (29.4%) were male, and 24 patients (70.6%) were female; nevertheless, there was no significant difference regarding the distribution of patients in terms of gender ( $p = 0.441$ ). Urinary incontinence due to solifenacin treatment increased from  $2.97 \pm 16.33$  on the first day to  $3.06 \pm 5.97$  in the 12th week; other findings are presented in [Table 1](#).

Based on the results of GEE models, there was no significant difference between males and females for any dependent variables ( $p > 0.05$ ). The findings showed that the trend of changes during the follow-up was not statistically significant for “physical health” and “Mental health” between the two groups ( $p > 0.05$ ). Also, this result was established for other variables except for “urinary incontinence” and “Suffering from micturition during the day” ([Table 1](#)). The results showed that there were significant interactions between time and group for two factors, including “urinary incontinence” ( $p \leq 0.001$ ) and “suffering from micturition during the day” ( $p \leq 0.001$ ). In other words, there was a statistically significant difference in the urinary incontinence variable between the two groups over time ([Figure 1](#)). Based on the findings, the mean of urinary incontinence in the Solifenacin group was 1.41 units less than another group ( $\beta = -1.406$ ,  $p < 0.001$ ).

TABLE 1 The result of generalized equation estimation (GEE) model for trend of changes in each factor over 3 months follow-up.

Dependent variable	Group	Mean $\pm$ SD				GEE model	
		Day 1	Week 4	Week 8	Week 12	$\beta$	<i>p</i> -Value
Urinary incontinence	S	16.33 $\pm$ 2.97	12.3 $\pm$ 3.44	8.90 $\pm$ 3.51	5.97 $\pm$ 3.06	−1.406	< 0.001*
	P	14.35 $\pm$ 3.77	11.41 $\pm$ 3.89	9.47 $\pm$ 3.70	8.21 $\pm$ 3.66		
Physical health	S	53.22 $\pm$ 20.04	53.68 $\pm$ 19.81	56.21 $\pm$ 18.35	59.78 $\pm$ 17.60	−0.666	0.163
	P	48.22 $\pm$ 15.24	50.08 $\pm$ 14.92	52.56 $\pm$ 15.07	56.53 $\pm$ 15.07		
Mental health	S	45.84 $\pm$ 20.65	46.98 $\pm$ 19.77	49.06 $\pm$ 19.50	52.18 $\pm$ 19.75	−0.625	0.344
	P	44.69 $\pm$ 18.71	47.03 $\pm$ 17.86	49.64 $\pm$ 16.68	52.31 $\pm$ 16.45		
Micturition frequency during the day	S	2.88 $\pm$ 0.89	2.58 $\pm$ 0.97	1.88 $\pm$ 0.96	1.09 $\pm$ 0.91	−0.029	0.612
	P	2.68 $\pm$ 1.04	2.41 $\pm$ 1.05	1.68 $\pm$ 0.98	1.06 $\pm$ 1.01		
Suffering from micturition during the day	S	8.85 $\pm$ 1.50	6.79 $\pm$ 1.84	4.91 $\pm$ 1.84	3.42 $\pm$ 2.60	−0.884	< 0.001*
	P	8.50 $\pm$ 1.60	6.24 $\pm$ 1.94	6.88 $\pm$ 2.09	5.18 $\pm$ 2.32		
Micturition frequency during the night	S	3.00 $\pm$ 0.87	2.58 $\pm$ 0.83	1.67 $\pm$ 0.89	1.33 $\pm$ 0.89	−0.095	0.338
	P	2.69 $\pm$ 0.84	2.41 $\pm$ 0.82	1.76 $\pm$ 0.99	1.53 $\pm$ 0.99		
Suffering from micturition during the night	S	9.03 $\pm$ 1.72	7.21 $\pm$ 2.22	5.21 $\pm$ 2.64	3.91 $\pm$ 3.21	−0.106	0.818
	P	7.76 $\pm$ 2.19	6.68 $\pm$ 2.37	5.97 $\pm$ 2.74	4.74 $\pm$ 3.22		
Urgency	S	2.91 $\pm$ 0.95	2.55 $\pm$ 0.97	1.85 $\pm$ 0.87	1.36 $\pm$ 0.78	−0.082	0.441
	P	2.97 $\pm$ 0.90	2.68 $\pm$ 0.95	2.03 $\pm$ 0.90	1.68 $\pm$ 0.94		
Suffering from urgency	S	8.33 $\pm$ 2.13	7.88 $\pm$ 2.19	4.70 $\pm$ 2.88	4.03 $\pm$ 3.22	0.315	0.465
	P	8.35 $\pm$ 2.10	7.76 $\pm$ 2.32	5.68 $\pm$ 2.97	4.74 $\pm$ 3.08		
Incontinence	S	2.24 $\pm$ 0.97	1.91 $\pm$ 0.63	1.12 $\pm$ 0.78	0.70 $\pm$ 0.85	−0.031	0.748
	P	2.41 $\pm$ 0.89	2.12 $\pm$ 0.69	1.44 $\pm$ 0.89	1.03 $\pm$ 1.03		
Suffering from incontinence	S	7.97 $\pm$ 2.38	6.82 $\pm$ 2.27	4.45 $\pm$ 3.27	3.06 $\pm$ 3.71	−0.241	0.496
	P	8.53 $\pm$ 1.21	6.91 $\pm$ 2.21	5.38 $\pm$ 3.17	4.06 $\pm$ 3.89		

S, solifenacin; P, PTNS; SD, standard deviation;  $\beta$ , coefficient of interaction between time and group in GEE model adjusted for group, time, and gender variables; \**p*-value, significant level at 0.001.

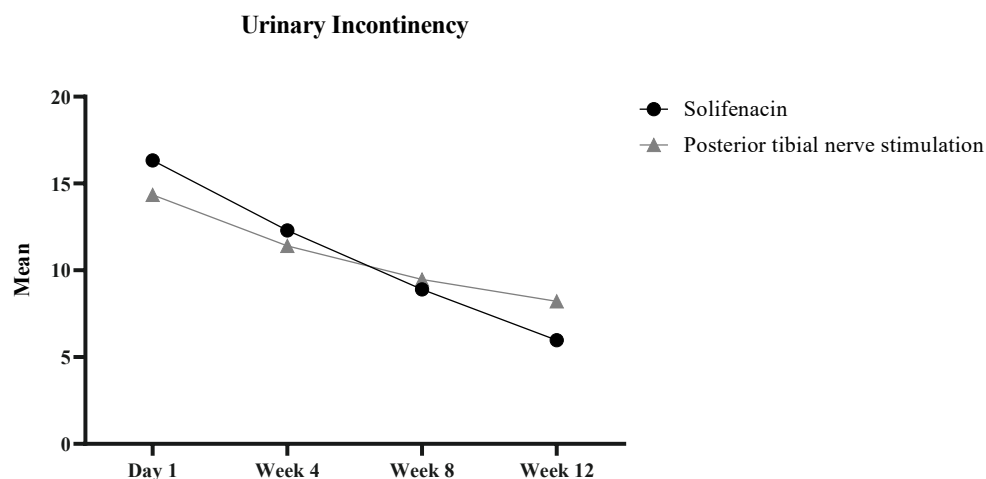


FIGURE 1

The trend of changes in urinary incontinence during the 3-month follow-up.

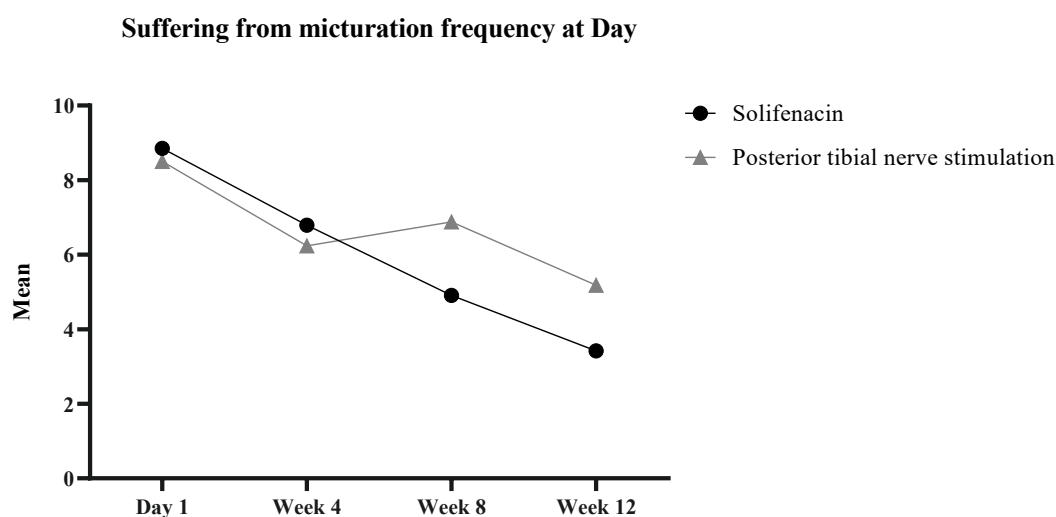


FIGURE 2

The trend of changes in the micturition frequency during the 3-month follow-up.

Also, the trend of changes in the variable suffering from micturition frequency during the day in the two groups over time was accompanied by a statistically significant difference ( $\beta = 0.884$ ,  $p < 0.001$ ). Based on the results, the patients in the Solifenacin group expressed less dissatisfaction with the number of urinations during the day compared to the patients in the PTNS group (Figure 2).

## Discussion

In the present study, the effect of surface electrical stimulation of the posterior tibial nerve and drug therapy (solifenacin) on the treatment of OAB and improvement of the QOL of patients with MS was investigated. To the best of our knowledge, comparison of solifenacin and PTNS therapeutic effects has not been performed on the MS patients in previous studies. The results showed significant between-group differences in the severity of urinary incontinence

and the level of inconvenience due to the decrease in frequency of urination at night (for 12 weeks), while there were no significant differences regarding other variables. Also, the findings demonstrated no significant difference in the treatment effects between males and females in this study.

The present results are consistent with some previous studies examining the effects of drug therapy (solifenacin) and PTNS (Al-Danakh et al., 2022). In a study by van Rey and Heesakkers (2011), using 8.8 mg of solifenacin for 8 weeks led to a significant decrease in the number of pads used per day in the MS patients with OAB. Also, the intensity of urinary urgency decreased significantly.

Twenty out of 30 patients chose to continue solifenacin treatment after completing the study. The majority of the patients reported improved QOL. They concluded that solifenacin is effective in the treatment of patients with OAB symptoms (van Rey and Heesakkers, 2011). Besides, Chapple et al. (2006) studied the effects of solifenacin in 2,800 patients with symptoms of OAB, and the findings of this clinical trial showed that a solifenacin dose of 5 mg can be increased

to 10 mg once a day. Compared to the placebo, it was effective in reducing incontinence, anxiety, and frequency of urination and increasing the volume of bladder emptying each time; the results of this clinical trial confirmed the use of solifenacin in the treatment of OAB (Chapple et al., 2006).

Additionally, Olujide and O'Sullivan (2005) evaluated the effect of internal stimulation of the posterior tibial nerve by passing a needle through the skin in 37 patients with OAB symptoms and 12 patients with non-obstructive urinary retention problems in 12 weeks. The QOL questionnaire and daily urinary excretion registration forms were used to evaluate the patients. The symptoms improved in 60% of the patients, although QOL improved more significantly in patients with OAB, which is consistent with the results of the present study. The findings of a study by Amarenco et al. (2003) also showed the positive effect of PTNS, which is in line with the current results. In their study, 44 patients with urgent and frequent urinary incontinence and emergencies, caused by an overworked bladder, were selected among patients without any specific neurological diseases, as well as patients with MS, spinal cord injuries, and Parkinson's disease. Their bladder capacity was compared before and after electrical PTNS. The bladder capacity of 22 patients increased by about 100 ml, which indicates the immediate effect of this intervention; however, in their study, no control group was included to determine the effect of stimulation more precisely, and the participants included both neurological and non-neurological patients. Also, the final results of these two groups were not compared to determine the effect of this intervention more accurately.

Also, Finazzi Agrò et al. (2005) investigated the effect of PTNS over 4 weeks (three sessions every week, 30 min per session) in women with OAB and incontinence. In their study, PTNS was the only intervention used for the treatment group. For the control group, placebo stimulation was performed, and no other intervention with proven effectiveness was used to treat these patients. The results showed that in 71% of the patients in the treatment group, PTNS was an effective intervention. Therefore, similar to the results of the current study, the QOL score increased, and the frequency of urination decreased, whereas in the control group with placebo stimulation, no therapeutic effects were observed.

## Limitations

Although the sample size of this study was sufficient to draw valid conclusions, patients with confounding factors, such as diabetes or Parkinson's disease, needed to be excluded, and OAB was merely assessed as a complication of MS.

For a better patient response, some physicians may add PTNS to drug therapy. It can be concluded that solifenacin plus PTNS is superior to each intervention used independently (Al-Danakh et al., 2022). Therefore, we only evaluated and compared the efficacy and safety of PTNS versus drug therapy, which is easier to access and less costly.

## Conclusion

The results of the current study showed that both drug therapy with solifenacin and PTNS for OAB reduced the severity of urinary

symptoms (e.g., urinary incontinence) and improved the QOL of patients with MS.

## Data availability statement

The original contributions presented in this study are included in this article/supplementary material, further inquiries can be directed to the corresponding author.

## Ethics statement

The studies involving human participants were reviewed and approved by the Ahvaz Jundishapur University of Medical Sciences, Ahvaz, Iran. The patients/participants provided their written informed consent to participate in this study. Written informed consent was obtained from the individual(s) for the publication of any potentially identifiable images or data included in this article.

## Author contributions

NM and NO wrote the manuscript and contributed in conceptualization of the work. LK, GS, and MS collected the samples. MJ provided the ideas and critically edited the entire composition of the manuscript. All authors contributed to the article and approved the submitted version.

## Funding

Funding was provided by the Research Deputy of AJUMS (grant number: IR.AJUMS.HGOLESTAN.REC.1399.127).

## Acknowledgments

This study was based on the results of a thesis by MJ, who is a neurology resident at Ahvaz Jundishapur University of Medical Sciences (AJUMS). We appreciate the reviewers' constructive feedback. We would also like to thank all the patients for their contributions to this research.

## Conflict of interest

The authors declare that the research was conducted in the absence of any commercial or financial relationships that could be construed as a potential conflict of interest.

## Publisher's note

All claims expressed in this article are solely those of the authors and do not necessarily represent those of their affiliated organizations, or those of the publisher, the editors and the reviewers. Any product that may be evaluated in this article, or claim that may be made by its manufacturer, is not guaranteed or endorsed by the publisher.

## References

- Al-Danakh, A., Safi, M., Alradhi, M., Almoiliqy, M., Chen, Q., Al-Nusaif, M., et al. (2022). Posterior tibial nerve stimulation for overactive bladder: Mechanism, classification, and management outlines. *Parkinsons Dis.* 2022:2700227. doi: 10.1155/2022/2700227
- Amarenco, G., Ismael, S. S., Even-Schneider, A., Raibaut, P., Demaille-Wlodyka, S., Parratte, B., et al. (2003). Urodynamic effect of acute transcutaneous posterior tibial nerve stimulation in overactive bladder. *J. Urol.* 169:22102215. doi: 10.1097/01.ju.0000067446.17576.bd
- Amato, M. P., Portaccio, E., Goretti, B., Zipoli, V., Hakiki, B., Giannini, M., et al. (2010). Cognitive impairment in early stages of multiple sclerosis. *Neurol. Sci.* 31, 211–214. doi: 10.1007/s10072-010-0376-4
- Burks, F. N., Bui, D. T., and Peters, K. M. (2010). Neuromodulation and the neurogenic bladder. *Urol. Clin.* 37, 559–565. doi: 10.1016/j.ucl.2010.06.007
- Chapple, C. R., Cardozo, L., Steers, W. D., and Govier, F. E. (2006). Solifenacin significantly improves all symptoms of overactive bladder syndrome. *Int. J. Clin. Pract.* 60, 959–966. doi: 10.1111/j.1742-1241.2006.01067.x
- De Gennaro, M., Capitanucci, M. L., Mosiello, G., and Zaccara, A. (2011). Current state of nerve stimulation technique for lower urinary tract dysfunction in children. *J. Urol.* 185, 1571–1577. doi: 10.1016/j.juro.2010.12.067
- Finazzi Agrò, E., Campagna, A., Sciobica, F., Petta, F., Germani, S., Zuccalà, A., et al. (2005). Posterior tibial nerve stimulation: is the once-a-week protocol the best option?. *Minerva Urol. Nefrol.* 57, 119–123.
- Fjorback, M. V., Rey, F. S., Pal, F. v., Rijkhoff, N. J., Petersen, T., and Heesakkers, J. P. (2007). Acute urodynamic effects of posterior tibial nerve stimulation on neurogenic detrusor overactivity in patients with MS. *Eur. Urol.* 51, 464–472. doi: 10.1016/j.eururo.2006.07.024
- Geirsson, G., Wang, Y. H., Lindström, S., and Fall, M. (1993). Traditional acupuncture and electrical stimulation of the posterior tibial nerve: A trial in chronic interstitial cystitis. *Scand. J. Urol. Nephrol.* 27, 67–70. doi: 10.3109/00365599309180416
- Ghasemi, N., Razavi, S., and Nikzad, E. (2017). Multiple sclerosis: Pathogenesis, symptoms, diagnoses and cell-based therapy. *Cell J.* 19:1.
- Goldenberg, M. M. (2012). Multiple sclerosis review. *Pharm. Ther.* 37:175.
- Hajebrahimi, S., Nourizadeh, D., Hamedani, R., and Pezeshki, M. Z. (2012). Validity and reliability of the international consultation on incontinence questionnaire-urinary incontinence short form and its correlation with urodynamic findings. *Urol. J.* 9, 685–690.
- Harbo, H. F., Gold, R., and Tintoré, M. (2013). Sex and gender issues in multiple sclerosis. *Ther. Adv. Neurol. Disorder.* 6, 237–248. doi: 10.1177/1756285613488434
- Khalaf, K. M., Coyne, K. S., Globe, D. R., Armstrong, E. P., Malone, D. C., and Burks, J. (2015). Lower urinary tract symptom prevalence and management among patients with multiple sclerosis. *Int. J. MS Care* 17, 14–25. doi: 10.7224/1537-2073.2013-040
- Klingler, H. C., Pycha, A., Schmidbauer, J., and Marberger, M. (2000). Use of peripheral neuromodulation of the S3 region for treatment of detrusor overactivity: A urodynamic-based study. *Urology* 56, 766–771. doi: 10.1016/S0090-4295(00)00727-5
- Mahadeva, A., Tanasescu, R., and Gran, B. (2014). Urinary tract infections in multiple sclerosis: Under-diagnosed and under-treated? A clinical audit at a large University hospital. *Am. J. Clin. Exp. Immunol.* 3:57.
- Mayer, R. D., and Howard, F. M. (2008). Sacral nerve stimulation: Neuromodulation for voiding dysfunction and pain. *Neurotherapeutics* 5, 107–113. doi: 10.1016/j.nurt.2007.10.063
- Olujide, L. O., and O'Sullivan, S. M. (2005). Female voiding dysfunction. *Best Pract. Res. Clin. Obstet. Gynaecol.* 19, 807–828. doi: 10.1016/j.bpobgyn.2005.08.001
- Ragab, A., Ibrahim, A., Helal, R., Elsaid, A., Younis, H., Elsherbiny, M., et al. (2021). Pharmacotherapy of multiple sclerosis and treatment strategies. *Front. Clin. Drug Res. CNS Neurol. Disord.* 9:206. doi: 10.2174/9781681089041121090009
- Sari Motlagh, R., Hajebrahimi, S., Sadeghi-Bazargani, H., and Joodi Tutunsaz, J. (2015). Reliability and validation of the international consultation on incontinence questionnaire in over active bladder to persian language. *Low. Urin. Tract Symptoms* 7, 99–101. doi: 10.1111/luts.12059
- Staskin, D. R., Peters, K. M., MacDiarmid, S., Shore, N., and de Groat, W. C. (2012). Percutaneous tibial nerve stimulation: A clinically and cost effective addition to the overactive bladder algorithm of care. *Curr. Urol. Rep.* 13, 327–334. doi: 10.1007/s11934-012-0274-9
- Tornic, J., and Panicker, J. N. (2018). The management of lower urinary tract dysfunction in multiple sclerosis. *Curr. Neurol. Neurosci. Rep.* 18, 1–11. doi: 10.1007/s11910-018-0857-z
- van Rey, F., and Heesakkers, J. (2011). Solifenacin in multiple sclerosis patients with overactive bladder: A prospective study. *Adv. Urol.* 2011:834753. doi: 10.1155/2011/834753



## OPEN ACCESS

## EDITED BY

Eduard Rodríguez-Farre,  
Institute of Biomedical Research of Barcelona  
(CSIC), Spain

## REVIEWED BY

Anuska V. Andjelkovic,  
University of Michigan, United States  
Riccardo Pascuzzo,  
IRCCS Carlo Besta Neurological Institute  
Foundation, Italy

## \*CORRESPONDENCE

Dan Feng  
✉ 13995621216@163.com

## SPECIALTY SECTION

This article was submitted to  
Neurodegeneration,  
a section of the journal  
Frontiers in Neuroscience

RECEIVED 28 November 2022

ACCEPTED 27 February 2023

PUBLISHED 13 March 2023

## CITATION

Li SJ and Feng D (2023) Risk factors  
and nomogram-based prediction of the risk  
of limb weakness in herpes zoster.  
*Front. Neurosci.* 17:1109927.  
doi: 10.3389/fnins.2023.1109927

## COPYRIGHT

© 2023 Li and Feng. This is an open-access  
article distributed under the terms of the  
[Creative Commons Attribution License](#)  
(CC BY). The use, distribution or reproduction  
in other forums is permitted, provided the  
original author(s) and the copyright owner(s)  
are credited and that the original publication in  
this journal is cited, in accordance with  
accepted academic practice. No use,  
distribution or reproduction is permitted which  
does not comply with these terms.

# Risk factors and nomogram-based prediction of the risk of limb weakness in herpes zoster

Shao-jun Li and Dan Feng\*

Department of Pain Management, Wuhan No.1 Hospital, Wuhan, Hubei, China

**Background:** Limb weakness is a less common complication of herpes zoster (HZ). There has been comparatively little study of limb weakness. The aim of this study is to develop a risk nomogram for limb weakness in HZ patients.

**Methods:** Limb weakness was diagnosed using the Medical Research Council (MRC) muscle power scale. The entire cohort was assigned to a training set (from January 1, 2018 to December 30, 2019,  $n = 169$ ) and a validation set (from October 1, 2020 to December 30, 2021,  $n = 145$ ). The least absolute shrinkage and selection operator (LASSO) regression analysis method and multivariable logistic regression analysis were used to identify the risk factors of limb weakness. A nomogram was established based on the training set. The discriminative ability and calibration of the nomogram to predict limb weakness were tested using the receiver operating characteristic (ROC) curve, calibration plots, and decision curve analysis (DCA). A validation set was used to further assess the model by external validation.

**Results:** Three hundred and fourteen patients with HZ of the extremities were included in the study. Three significant risk factors: age (OR = 1.058, 95% CI: 1.021–1.100,  $P = 0.003$ ), VAS (OR = 2.013, 95% CI: 1.101–3.790,  $P = 0.024$ ), involving C6 or C7 nerve roots (OR = 3.218, 95% CI: 1.180–9.450,  $P = 0.027$ ) were selected by the LASSO regression analysis and the multivariable logistic regression analysis. The nomogram to predict limb weakness was constructed based on the three predictors. The area under the ROC was 0.751 (95% CI: 0.673–0.829) in the training set and 0.705 (95% CI: 0.619–0.791) in the validation set. The DCA indicated that using the nomogram to predict the risk of limb weakness would be more accurate when the risk threshold probability was 10–68% in the training set and 15–57% in the validation set.

**Conclusion:** Age, VAS, and involving C6 or C7 nerve roots are potential risk factors for limb weakness in patients with HZ. Based on these three indicators, our model predicted the probability of limb weakness in patients with HZ with good accuracy.

## KEYWORDS

risk factors, nomogram, limb weakness, herpes zoster, treatment

## Introduction

Herpes zoster (HZ) is a painful skin disease caused by the reactivation of the latent varicella-zoster virus (VZV). It appears as a vesicular rash with a dermatomal distribution (Pan et al., 2022). Postherpetic neuralgia is a common complication of HZ. Persistent pain can have a negative impact on daily life and increase the financial burden. Limb weakness is a less common complication of HZ. The VZA damages nerve in the upper or lower limbs, causing myotomal motor weakness or paralysis. HZ-related limb weakness is distinguished by focal, asymmetrical dyskinesia in the myotome corresponding to the rash's dermatome (Ruppert et al., 2010). This disease is much more prevalent in the elderly, diabetes mellitus, and immunodeficient patients. Weakness does not occur in all patients with limb HZ. In the early stages of HZ, as the pain is controlled, limb weakness can be self-limited. With time, limb weakness may become difficult to treat. Even if the pain is relieved, the strength of the limbs cannot be restored to normal levels. Long-term persistent limb weakness can lead to physical disability, reduce the quality of life, and raise the economic burden.

Early diagnosis of limb weakness in HZ is difficult. The majority of HZ patients have no specific clinical manifestations. Previous research has found that magnetic resonance imaging (MRI) and electrophysiologic diagnosis have a high sensitivity for detecting motor impairments (Santiago-Pérez et al., 2012). Reda et al. (2012) reviewed eight HZ patients who had segmental paresis. Four patients had MRI scans and all affected nerves in the MRI were enlarged. Affected nerves had abnormalities that extended longitudinally along the length of the nerve. All the patients had electrophysiologic changes of mononeuropathies. Jones et al. (2014) reviewed 49 HZ patients with zoster-associated limb paresis. Twenty-six patients underwent MRI examination. Nerve imaging abnormalities were found in 19 patients. An electrodiagnostic examination revealed that 47 of the 49 patients had fibrillation potentials. Electrophysiologic changes were present in all of the patients. However, although imaging and electrophysiologic examinations are helpful in diagnosing limb weakness in HZ, they are not specific. A retrospective analysis of 10 patients with zoster-associated limb paresis found that imaging abnormalities were found in 7 patients. 50% of patients presented with secondary denervation changes in shoulder girdle muscles and nerve T2 signal hyperintensity. 20% of patients had nerve enlargement (Zubair et al., 2017). Mondelli et al. (2002) have reported a prospective case series with 158 HZ patients. 36% of patients had electromyographic signs of abnormal spontaneous activity. Motor fiber damage was evident clinically in 19% (segmental zoster paresis) and was subclinical and detectable only by electromyography in 17%. MRI and electrophysiologic examination may be normal in the early stages of the disease. Once limb weakness appears, treatment can be extremely difficult. Furthermore, previous studies have had relatively small sample sizes and have focused on describing clinical characteristics, electrophysiologic, and imaging features. In this study, we retrospectively analyzed 314 limb HZ patients and identified risk factors for limb weakness in HZ patients. In particular, we sought to create a prediction model that can quickly identify patients at risk of limb weakness in the HZ.

## Materials and methods

### Patient selection

This retrospective study was approved by the Medical Ethics Committee of the Wuhan No 1 Hospital. All patients provided written informed consent. The records of 330 patients with limbs HZ were reviewed for the study. The entire cohort was assigned to a training set (from January 1, 2018 to December 30, 2019,  $n = 169$ ) and a validation set (from October 1, 2020 to December 30, 2021).

### Inclusion and exclusion

The inclusion criteria were as follows: (1) limbs HZ pain; (2) inpatient treatment (i.e., when VAS  $\geq 4$  and disease course  $\geq 1$  week); (3) age  $\geq 18$  years or  $\leq 85$  years; (4) having a good understanding of Chinese.

The exclusion criteria were as follows: (1) HZ located in the head, neck, trunk, and perineum area; (2) tumor-induced limb weakness; (3) nervous system-related diseases; (4) musculoskeletal system-related diseases; (5) incomplete data; (6) refusing to participate in the study (Figure 1).

### Data collection and follow-up

This is a retrospective study conducted with the aid of an electronic medical record system. Data were gathered using an electronic medical record system, the telephone, letters, and e-mail. We created a dedicated database in which we recorded demographic data (such as age, and gender), individual disease history, VAS, rash site, course of HZ, history of the HZ episode, location of skin lesions, disease stage and severity, immune status, and clinical treatments. All patients had electrophysiologic evidence of nerve injury in the study. Limb weakness was diagnosed using the Medical Research Council (MRC) muscle power scale, which ranks muscle power from 0 to 5 (0: no muscle contraction; (1): muscle contraction but no joint activity; (2): full range movement of joint under no gravity; (3): full range movement of joint under anti-gravity state; (4): joint can resist partial resistance activity, but worse than normal; (5): normal muscle strength, that is, joint can achieve full range movement under maximum resistance). Muscle weakness is defined as muscle strength below grade 5 and lower than that of the contralateral limb (normal side). Muscle strength equal to or less than grade 5, but the same as the contralateral limb, was not recognized as muscle weakness (Medical Research Council, 1981). The intensity of pain was measured using a VAS scale ranging from 0 to 10 (0 represents no pain, and 10 represent the most severe pain). Questionnaires for muscle weakness and pain scores were completed by a physician at admission and 3 months after discharge.

### Statistical analyses

R software (version 4.2.1; R Foundation for Statistical Computing, Vienna, Austria) was used for statistical analyses.

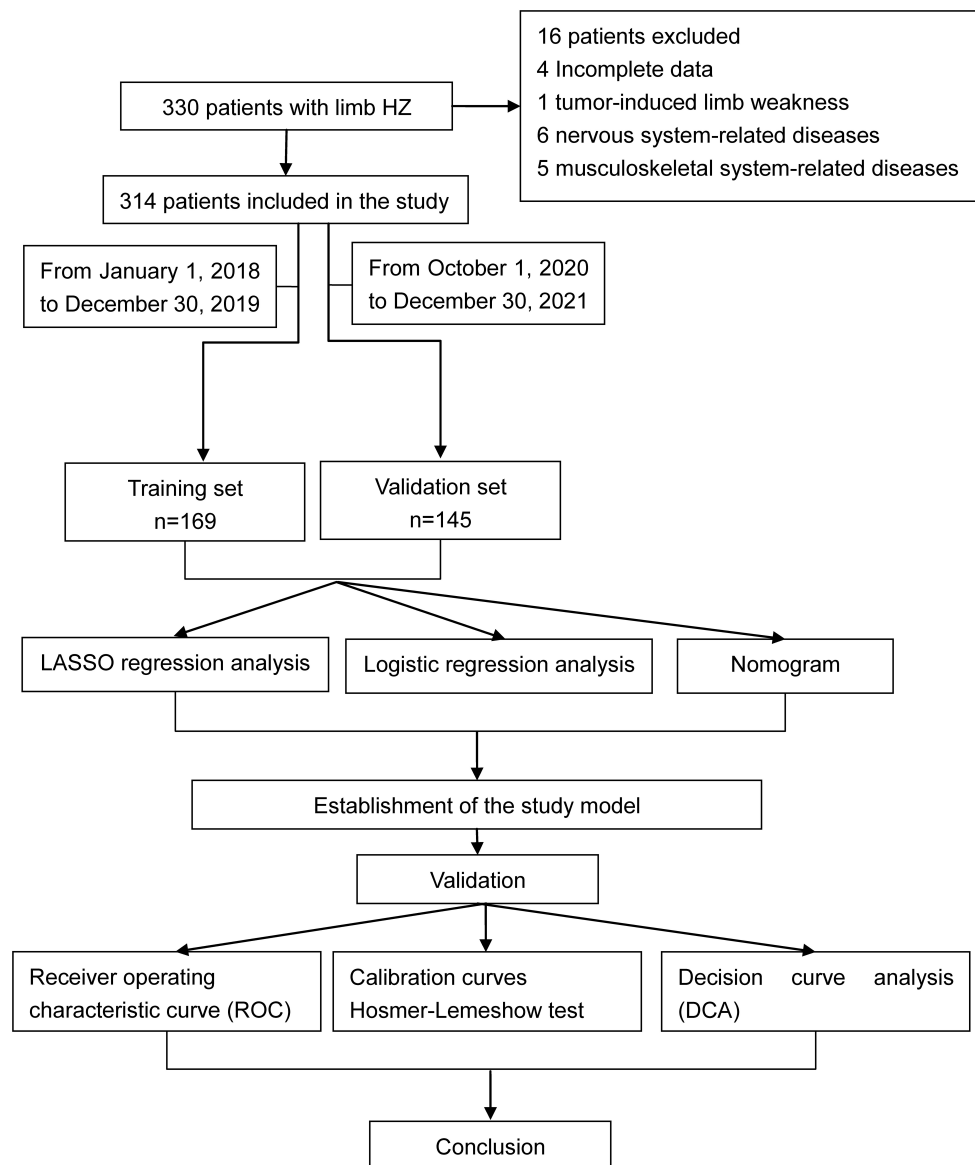


FIGURE 1  
Flowchart of the study.

Demographic and clinical data for patients with limbs HZ were characterized using mean  $\pm$  SD and count (percentage), respectively, to represent continuous and categorical factors. The least absolute shrinkage and selection operator (LASSO) regression analysis was performed to analyze the data in the training set in order to identify the best predictors among the candidate risk variables. The “glmnet” package of R was used to run LASSO regression analysis. The optimal hyper-parameter lambda of the LASSO model was determined through a K-fold cross-validation procedure repeated 10 times by identifying the largest lambda value that obtained an error within one standard deviation from the minimum binomial deviance (“lambda.1se”). The number K of folds used for the cross-validation was 10. “Lambda.1se” provides a model with good performance and a minimal set of independent variables. The multivariable logistic regression analysis was used to determine the risk factors of limb weakness in HZ patients.

The predicting model was formulated based on the results of the multivariable logistic regression analysis.

A nomogram was created based on the results of multivariate analysis using the “rms” R software package. The nomogram maps the predicted probabilities as points on a scale from 0 to 100. The total score accumulated by the various covariates corresponds to the predicted probability of the patient. The pROC package was used to plot the receiver operating characteristic (ROC) curve and to compute the area under the curve (AUC) of the predictive model. Hosmer–Lemeshow goodness-of-fit test and a calibration curve were used to calibrate the model. A 45-degree diagonal line indicates the perfect calibration line. The calibration line, and deviations above or below this line reflect under-prediction or over-prediction. The decision curve analysis (DCA) was performed to quantify the clinical practicability of nomograms based on the net benefit under different threshold probabilities. By using the data

of the validation set, ROC, calibration curve, DCA were used to estimate the accuracy of the risk prediction model.

## Results

### Baseline characteristics

The entire cohort was assigned to a training set (from January 1, 2018 to December 30, 2019,  $n = 169$ ) and a validation set (from October 1, 2020 to December 30, 2021,  $n = 145$ ).

Ninety-six (30.6%) HZ patients presented with limb weakness (53 out of 169 in the training set; 43 out of 145 in the validation set). The proportion of male and female patients with HZ was similar in

the two sets. Forty-four (14.0%) HZ patients had more than twice hospitalizations. The vast majority of the patients (69.1%) had a course of disease longer than 14 days. **Table 1** shows the baseline characteristics of participants in the training set and validation set.

### Variables selection

All the variables (including age, gender, and times of hospitalization, course, side, VAS, diabetes, comorbidity, malignant tumor, rash site, and HZ involving C6 or C7 nerve roots) were evaluated by the LASSO regression analysis. The variables selected by optimal lambda ( $\lambda$ ) are the simplest model with the highest performance. The optimal penalty parameter  $\lambda$  was 0.05527638. Five significant risk factors (including age, VAS, involving C6 or C7 nerve roots, diabetes, and course) were selected by the LASSO regression analysis (**Figures 2A, B**). Then the selected factors were analyzed by multivariable logistic regression. The results showed that age (OR = 1.058, 95% CI: 1.021–1.100,  $P = 0.003$ ), VAS (OR = 2.013, 95% CI: 1.101–3.790,  $P = 0.024$ ), involving C6 or C7 nerve roots (OR = 3.218, 95% CI: 1.180–9.450,  $P = 0.027$ ) were independent predictors for limbs weakness in patients with HZ (**Table 2**).

**TABLE 1** Baseline characteristics of participants in the training set and validation set.

Items	Whole cohort ( $n = 314$ )	Training set ( $n = 169$ )	Validation set ( $n = 145$ )
Age, year, Mean $\pm$ SD	66.8 $\pm$ 10.6	66.5 $\pm$ 10.6	67.2 $\pm$ 10.7
<b>Gender, n (%)</b>			
Men	149(47.5)	77(45.6)	72(49.7)
Women	165(52.5)	92(54.4)	73(50.3)
<b>Times of hospitalization</b>			
Once	270(86.0)	147(87.0)	123(84.8)
More than twice	44(14.0)	22(13.0)	22(15.2)
Course, day, Mean $\pm$ SD	45.1 $\pm$ 110.6	37.3 $\pm$ 102.4	54.2 $\pm$ 119.2
<b>Side, n (%)</b>			
Left	159(50.6)	85(50.3)	74(51.0)
Right	155(49.4)	84(49.7)	71(49.0)
VAS, Mean $\pm$ SD	6.17 $\pm$ 0.67	6.08 $\pm$ 0.61	6.26 $\pm$ 0.73
<b>Diabetes, n (%)</b>			
Yes	64(20.4)	35(20.7)	29(20.0)
No	250(79.6)	134(79.3)	116(80.0)
<b>Comorbidity<sup>a</sup>, n (%)</b>			
<3	273(86.9)	146(86.4)	127(87.6)
$\geq 3$	41(13.1)	23(13.6)	18(12.4)
<b>Malignant tumor, n (%)</b>			
Yes	16(5.1)	12(7.1)	4(2.8)
No	298(94.9)	157(92.9)	141(97.2)
<b>Rash site, n (%)</b>			
Upper limbs	163(51.9)	87(51.5)	76(52.4)
Lower limbs	151(48.1)	82(48.5)	69(47.6)
<b>C6 or C7 level*, n (%)</b>			
Yes	97(30.9)	56(33.1)	41(28.3)
No	217(69.1)	113(66.9)	104(71.7)

<sup>a</sup>Conditions other than diabetes, such as hypertension, coronary heart disease, pulmonary disease, etc.

\*Involving C6 or C7 nerve roots.

### Predictive model construction

**Figure 3A** showed a nomogram to predict limb weakness of HZ patients. The nomogram to predict limb weakness was constructed based on the three predictors: age, VAS, and HZ involving C6 or C7 nerve roots. Total points were calculated by adding the number of points allocated to each factor in the nomogram. A high total score indicated a high probability of limb weakness. For example, an HZ patient with 64 years, a VAS of 7, and HZ involving C6 or C7 nerve roots has an estimated probability of limb weakness of 62.9% (**Figure 3B**).

### Predictive model validation

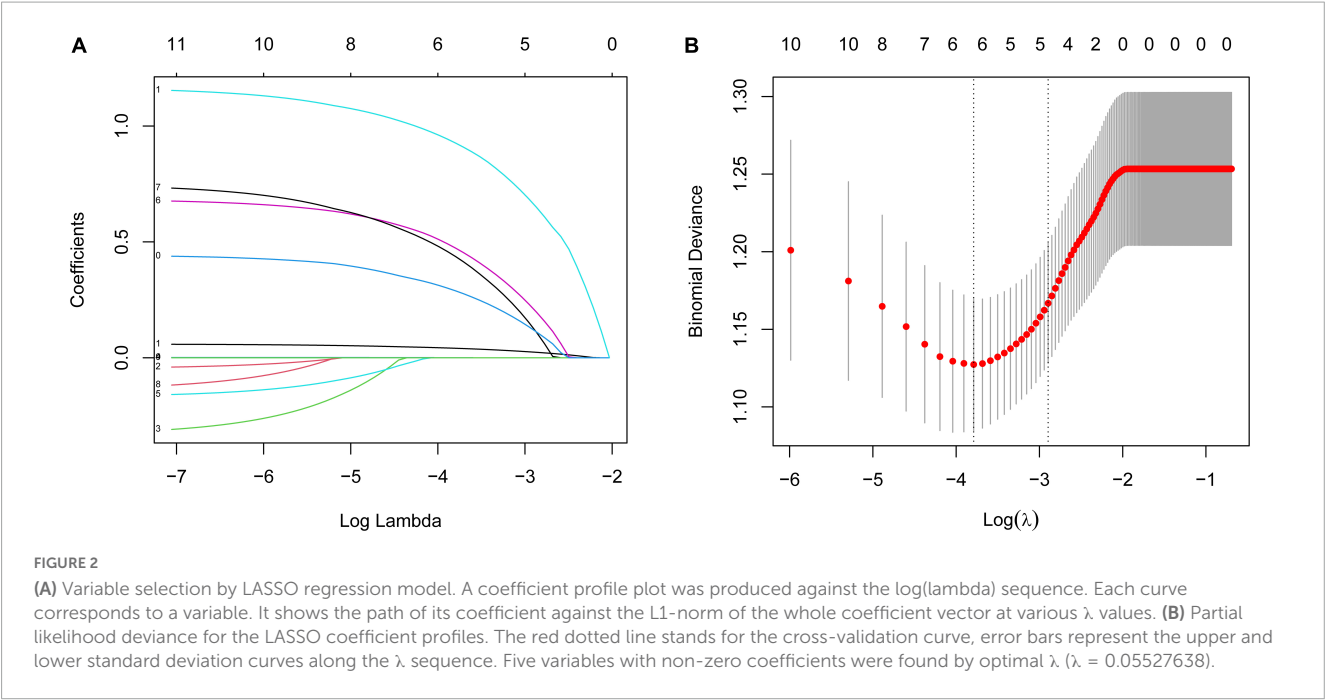
For the training set, the area under the ROC was 0.751 (95% CI: 0.673–0.829), indicating good discrimination. While the area under the ROC of the validation set was 0.705 (95% CI: 0.619–0.791) indicating acceptable discriminative power (**Figures 4A, B**).

The calibration curve showed that there was good agreement between the predicted and observed probabilities in both the training set and the validation set (**Figures 5A, B**). Hosmer–Lemeshow test was also used to calibrate the model. The results showed good agreement in the training sets ( $P = 0.783$ ).

The DCA indicated that using the nomogram to predict the risk of limb weakness would be more accurate when the risk threshold probability was 10–68% in the training set and 15–57% in the validation set (**Figures 6A, B**).

## Discussion

Limb weakness is a relatively rare neurological complication of HZ. The rate of limb weakness ranged from 0.3 to 5%



(Gupta et al., 1969; Thomas and Howard, 1972). The true incidence of this neurological complication was underestimated due to the atypical clinical symptoms and difficulty in clinical diagnosing. Anterior spinal roots, anterior horn cells, the brachial or lumbar plexus, and peripheral nerves may be the injury sites. MRI and electrophysiologic examinations help to correctly diagnose and assess the extent of the lesion.

The mechanisms of limb weakness in patients with HZ are not completely understood. In the past, the sites of motor injury were believed to occur at the level of the root or anterior horn cell. Studies have found that viral spread from the dorsal root ganglion to the adjacent nerve tissue, including the anterior horn cells and motor roots (Ismail et al., 2009; Ayoub et al., 2010). More recent studies have reported that axonal pathology may be the responsible mechanism for limb weakness. Reda et al. (2012) reported 8 patients with zoster-associated limb paresis. Electrophysiologic examination revealed that all the patients had fibrillation potentials in affected muscles. This suggested that motor injury was associated with axonal loss, resulting in nerve conduction block. While Worrell and Cockerell (1997) have reported that VZV infected the peripheral and central nervous systems cells, leading to peri- and intraneural inflammation as well as mononuclear or leukocytoclastic vasculitis. In addition, the pathological injury at the anterior root, anterior horn cells, brachial plexus, lumbar plexus, and peripheral nerves was related to zoster-associated limb paresis (Dobrev et al., 2008; Tashiro et al., 2010). These mechanisms are mainly speculative, with conflicting opinions and a lack of histological basis. Therefore, further studies are needed.

The present study established a nomogram for the prediction of the risk of limb weakness in patients with HZ. Age, VAS, and involving C6 or C7 nerve roots are independent risk factors for limb weakness in patients with HZ.

Age is risk factors for limb weakness in patients with HZ. Age is significantly associated with the incidence of limb weakness.

**TABLE 2** Multivariable logistic regression analysis of limb weakness in HZ patients.

Items	OR	95% CI	P-value
Age, years	1.058	1.021–1.100	0.003
VAS	2.013	1.101–3.790	0.024
C6 or C7 level* (yes or no)	3.218	1.180–9.450	0.027

\*Involving C6 or C7 nerve roots.

Studies have found that the mean age of segmental zoster paresis was 69 years old. The highest incidence was 60–70 years old (Liu et al., 2018; Meng et al., 2021). The elderly are more vulnerable to VZV and higher motor complications than children and young adults. A 6-year population-based analysis of HZ has found that postherpetic neuralgia risk was increased with age. The cumulative risk of developing postherpetic neuralgia between ages 50–90 years was 6.9 (95% CI: 6.7–7.1) (Muñoz-Quiles et al., 2018). Reda et al. (2012) believed that segmental zoster paresis was associated with a high rate of postherpetic neuralgia. Therefore, physicians should be alert to the need for early intervention of HZ in the extremities in the elderly.

Pain intensity is also related to the occurrence of limb weakness. Pain is the main clinical manifestation of HZ and postherpetic neuralgia. One study reported the relationship between pain and limb weakness. They concluded that the numerical rating scale (NRS) score was not related to motor dysfunction of limb HZ (Tang et al., 2022). Our study reported, on the contrary, the opposite. A higher VAS at onset is a risk factor for developing zoster paresis of limbs. Numerous studies have demonstrated that serious pain has been found to correlate with poor quality of life (Bowsher, 1997; Pickering and Leplege, 2011; Van Wijck and Aerssens, 2017). Pain occurring in the extremities may prevent the patient from moving the upper or lower extremities. Long-term inactivity of the limbs can aggravate limb weakness, even

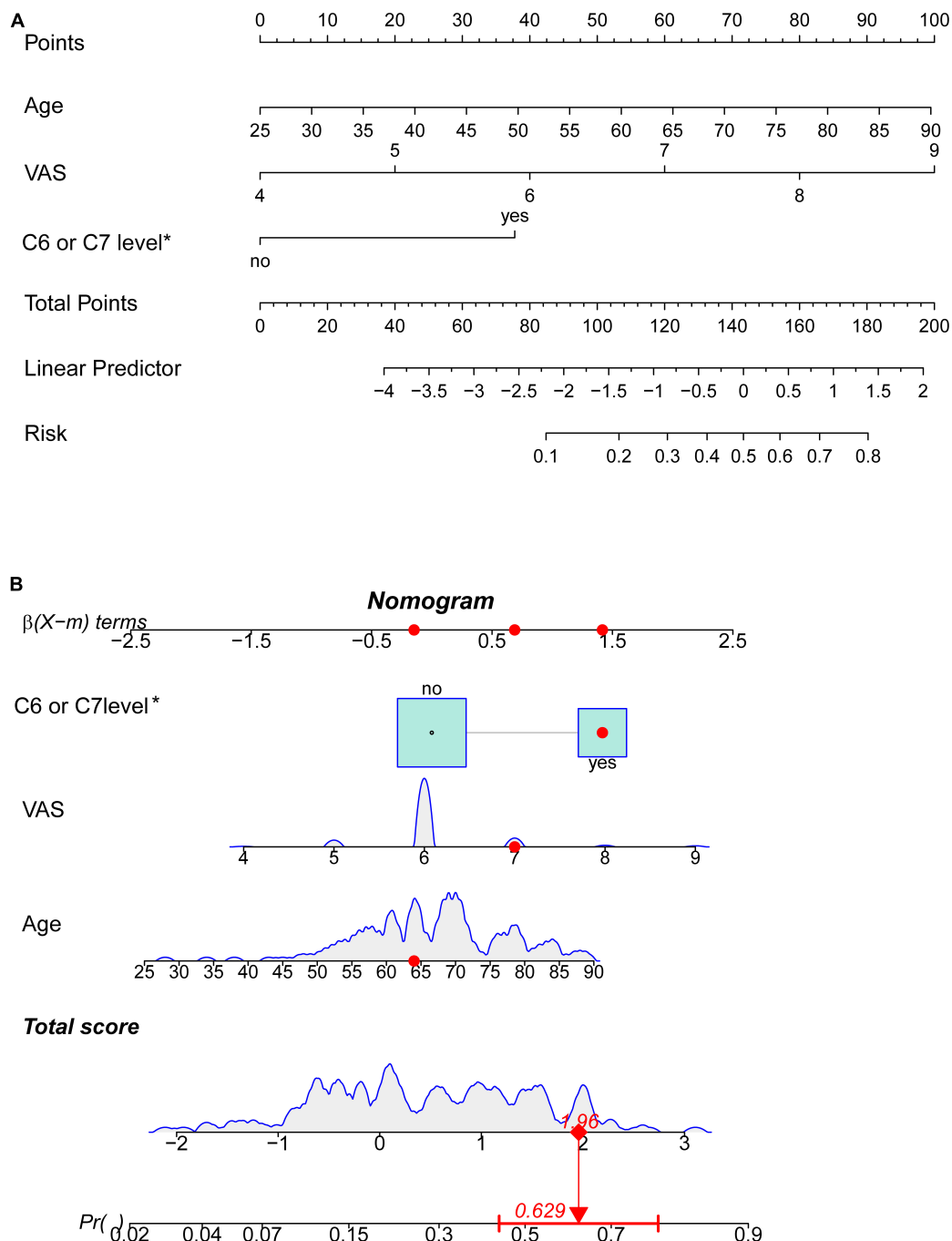


FIGURE 3

Nomogram prediction model (\*involving C6 or C7 nerve roots). **(A)** Nomogram based on three risk factors to predict limb weakness probabilities of HZ patients. **(B)** The dynamic nomogram for an example. An HZ patient with less than 64 years, a VAS of 7, and involving C6 or C7 nerve roots has an estimated probability of limb weakness of 62.9%.

leading to muscle atrophy. It should be noted that severe pain can cause temporary paralysis in patients who are reluctant to move their limbs. Some patients had a full return of limb function after pain relief. Therefore, reducing pain helps in limb effective rehabilitation.

The upper limb HZ, particularly involving C6 or C7 segments, was strongly connected with the incidence of limb weakness. Segmental zoster paresis occurrence on the upper extremities seemed to be higher than lower extremities in several case reports

in the literature (Yoleri et al., 2005; Rastegar et al., 2015; Teo et al., 2016; Chen et al., 2020; Patel et al., 2022). Liu et al. (2018) found that limb weakness occurred in 6 out of 8 patients with upper limbs HZ. A previous study has revealed that under half (22/49) of the paresis affected the upper limb (Jones et al., 2014). There have been reports of both upper and lower extremities being the same incidence (Thomas and Howard, 1972; Molloy and Goodwill, 1979). However, the results of these studies were not statistically significant. Tang et al. (2022) found that motor

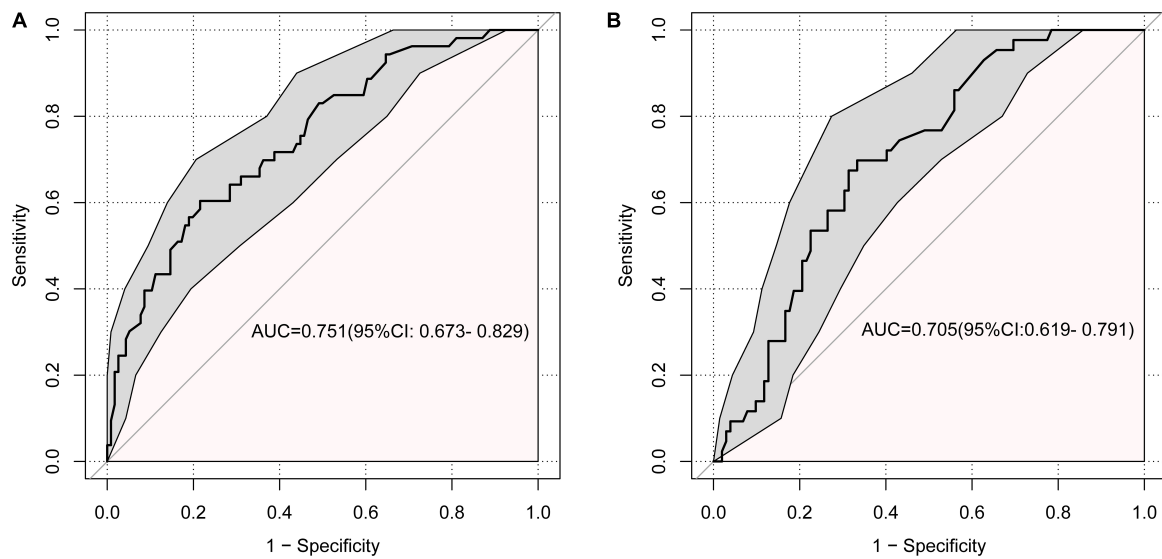


FIGURE 4

Receiver operating characteristic curve (ROC) for the discrimination of the model. (A) The training set, 0.751 (95% CI: 0.673–0.829). (B) The validation set, 0.705 (95% CI: 0.619–0.791).

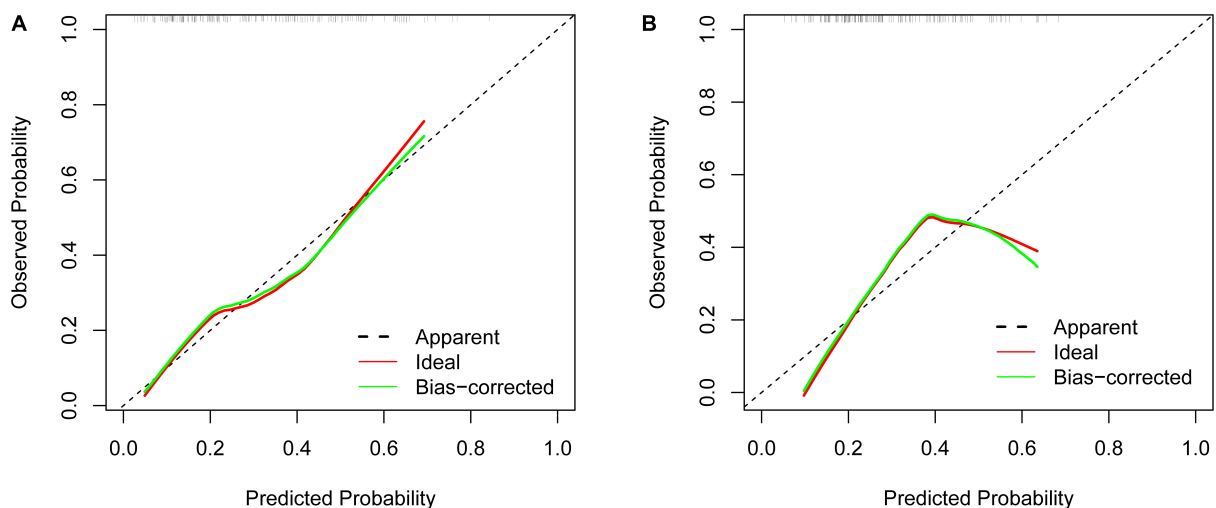


FIGURE 5

Calibration curves of the predictive limb weakness risk nomogram. (A) The training set. (B) The validation set.

dysfunction was more likely to occur in HZ patients with upper limb involvement (95% CI: 1.829–8.387,  $P = 0.001$ ). Our study supports this conclusion. The HZ involving C6 or C7 segments is more likely to develop motor weakness. A study retrospectively analyzing 87 cases of upper extremity weakness from 1961– to 2007 showed that weakness was most frequent in the proximal muscles or C5–C7 segments (Kawajiri et al., 2007). Therefore, physicians should pay high attention to the upper limbs HZ, especially involving C6 or C7 segments patients.

The DCA is used to determine the clinical practicability of nomograms based on the net benefit under different threshold probability in patients with HZ on the extremities. According to the DCA in the training set, clinicians can use the following methods when they make decisions using predictive models: (1) A specific

threshold probability was set for all patients (e.g., 10%). If the model predicts a value greater than this probability, treatment of limb weakness is performed, and if less, no treatment is performed; (2) All patients with herpes zoster of the extremities were divided into low- and medium-risk and high-risk groups; the high-risk group was treated for limb weakness, the low-risk group was not, and the medium-risk group was specifically analyzed according to age, systemic condition, and patient wishes. It should be noted that the thresholds used for identifying the three proposed risk groups have to be decided by the clinicians that want to use the nomogram; (3) An individualized threshold is determined based on communication with the patient, and this threshold is then compared with the model predicted value. If the predicted value is greater than the threshold, treatment of limb weakness

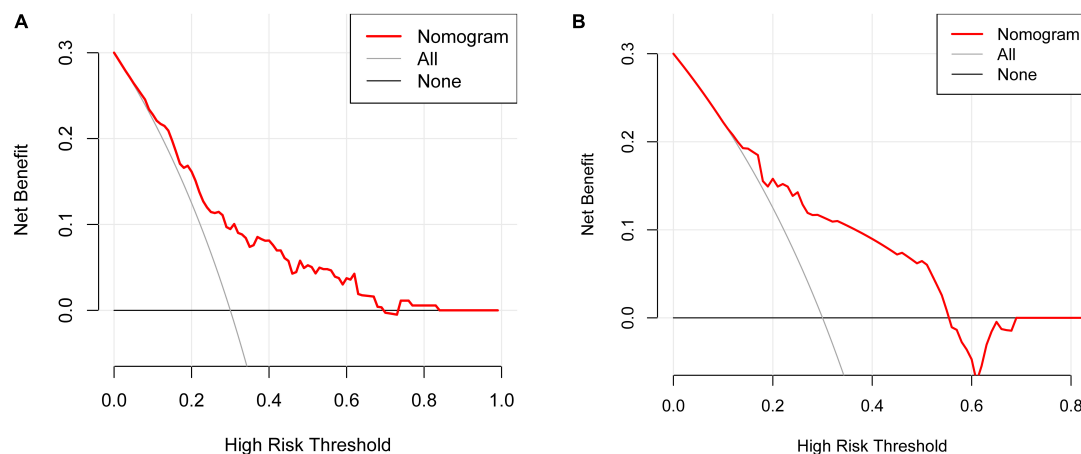


FIGURE 6

Decision curve analysis (DCA) for the limb weakness risk nomogram. The thick solid line indicated the assumption that no limb weakness existed in any of the patients. The thin solid line denoted the idea that all patients suffered from limb weakness. The risk nomogram was represented by the red line. (A) The training set. (B) The validation set.

is performed, and vice versa. In short, this model can provide an idea and a therapeutic direction for clinicians to treat limb weakness early. Early detection and early intervention can alleviate the decline in quality of life caused by limb weakness. However, application of the model in clinical practice should pay attention to individualized treatment because of the proposed predictive model obtaining modest accuracy.

Nomogram is widely used in both oncologic and non-oncologic diseases (Huang et al., 2022; Zan et al., 2022; Zhang et al., 2022). Nomograms can create a simple graphical representation of a statistical predictive model that generates a numerical probability of a clinical event (Iasonos et al., 2008). The ability of nomograms to combine multiple important prognostic factors to quantify individual risk enables it more acceptable to physicians and patients. We construct a model to predict the risk of upper limb weakness in HZ patients. The LASSO regression analysis was used to resolve the problem of multicollinearity in the variables. According to the time of enrollment in the study, we divided patients into two groups for external verification. The results of ROC, calibration and DCA curves for the training set and validation set verified the accuracy and stability of the model.

Our study has several limitations. First, the number of limb weakness factors and the sample size are relatively small. We mainly focused on clinical characteristics and lacked laboratory data. Second, we did not assess the MRI and electrophysiological abnormalities in the HZ patients. Third, the Medical Research Council (MRC) muscle power system and VAS are subjective measurements for the assessment of muscle power and pain intensity.

## Conclusion

Age, VAS, and involving C6 or C7 nerve roots are potential risk factors for limb weakness in patients with HZ. Based on these three indicators, our model predicted the probability of limb weakness in patients with HZ with good accuracy.

## Data availability statement

The raw data supporting the conclusions of this article will be made available by the authors, without undue reservation.

## Ethics statement

The studies involving human participants were reviewed and approved by the Wuhan No.1 Hospital. The patients/participants provided their written informed consent to participate in this study.

## Author contributions

DF: conceptualization, methodology, supervision, software, and validation. S-JL: data curation, writing—original draft preparation, visualization, investigation, and writing—review and editing. Both authors contributed to the article and approved the submitted version.

## Conflict of interest

The authors declare that the research was conducted in the absence of any commercial or financial relationships that could be construed as a potential conflict of interest.

## Publisher's note

All claims expressed in this article are solely those of the authors and do not necessarily represent those of their affiliated organizations, or those of the publisher, the editors and the reviewers. Any product that may be evaluated in this article, or claim that may be made by its manufacturer, is not guaranteed or endorsed by the publisher.

## References

- Ayoub, T., Raman, V., and Chowdhury, M. (2010). Brachial neuritis caused by varicella-zoster diagnosed by changes in brachial plexus on MRI. *J. Neurol.* 257, 1–4. doi: 10.1007/s00415-009-5266-4
- Bowsher, D. (1997). The management of postherpetic neuralgia. *Postgrad. Med. J.* 73, 623–629.
- Chen, G., Tuan, S., Liou, I., Huang, H., Hu, Y., and Wu, S. (2020). Segmental zoster paresis of unilateral upper extremity: A case report and literature review. *Medicine (Baltimore)* 99:e20466.
- Dobrev, H., Atanassova, P., and Sirakov, V. (2008). Postherpetic abdominal-wall pseudohernia. *Clin. Exp. Dermatol.* 33, 677–678.
- Gupta, S., Helal, B., and Kiely, P. (1969). The prognosis in zoster paralysis. *J. Bone Joint Surg. Br.* 51, 593–603.
- Huang, X., Luo, Z., Liang, W., Xie, G., Lang, X., Gou, J., et al. (2022). Survival nomogram for young breast cancer patients based on the seer database and an external validation cohort. *Ann. Surg. Oncol.* 29, 5772–5781. doi: 10.1245/s10434-022-11911-8
- Iasonos, A., Schrag, D., Raj, G., and Panageas, K. (2008). How to build and interpret a nomogram for cancer prognosis. *J. Clin. Oncol.* 26, 1364–1370.
- Ismail, A., Rao, D., and Sharrack, B. (2009). Pure motor herpes zoster induced brachial plexopathy. *J. Neurol.* 256, 1343–1345. doi: 10.1007/s00415-009-5149-8
- Jones, L. Jr., Reda, H., and Watson, J. (2014). Clinical, electrophysiologic, and imaging features of zoster-associated limb paresis. *Muscle Nerve*. 50, 177–185.
- Kawajiri, S., Tani, M., Noda, K., Fujishima, K., Hattori, N., and Okuma, Y. (2007). Segmental zoster paresis of limbs: Report of three cases and review of literature. *Neurologist* 13, 313–317. doi: 10.1097/NRL.0b013e31811e9d6d
- Liu, Y., Wu, B., Ma, Z., Xu, J., Yang, B., Li, H., et al. (2018). A retrospective case series of segmental zoster paresis of limbs: Clinical, electrophysiological and imaging characteristics. *BMC Neurol.* 18:121. doi: 10.1186/s12883-018-1130-4
- Medical Research Council (1981). *Aids to the examination of the peripheral nervous system, Memorandum no. 45*. London: Her Majesty's Stationery Office.
- Meng, Y., Zhuang, L., Jiang, W., Zheng, B., and Yu, B. (2021). Segmental zoster paresis: A literature review. *Pain Phys.* 24, 253–261.
- Molloy, M., and Goodwill, C. (1979). Herpes zoster and lower motor neurone paresis. *Rheumatol. Rehabil.* 18, 170–173.
- Mondelli, M., Romano, C., Rossi, S., and Cioni, R. (2002). Herpes zoster of the head and limbs: Electroneuromyographic and clinical findings in 158 consecutive cases. *Arch. Phys. Med. Rehabil.* 83, 1215–1221. doi: 10.1053/apmr.2002.33989
- Muñoz-Quiles, C., López-Lacort, M., Orrico-Sánchez, A., and Díez-Domingo, J. (2018). Impact of postherpetic neuralgia: A six years population-based analysis on people aged 50 years or older. *J. Infect.* 77, 131–136.
- Pan, C., Lee, M., and Nambudiri, V. (2022). Global herpes zoster incidence, burden of disease, and vaccine availability: A narrative review. *Ther. Adv. Vaccines Immunother.* 10:25151355221084535.
- Patel, K., Darweesh, S., Lund, D., and Vanderkolk, K. (2022). A rare complication of herpes zoster: Segmental zoster paresis. *Cureus* 14:e27261.
- Pickering, G., and Leplege, A. (2011). Herpes zoster pain, postherpetic neuralgia, and quality of life in the elderly. *Pain Pract.* 11, 397–402.
- Rastegar, S., Mahdavi, S., Mahmoudi, F., and Basiri, K. (2015). Herpes zoster segmental paresis in an immunocompromised breast cancer woman. *Adv. Biomed. Res.* 4:170. doi: 10.4103/2277-9175.162547
- Reda, H., Watson, J., and Jones, L. Jr. (2012). Zoster-associated mononeuropathies (ZAMs): A retrospective series. *Muscle Nerve* 45, 734–739. doi: 10.1002/mus.23342
- Ruppert, L., Freeland, M., and Stubblefield, M. (2010). Segmental zoster paresis of the left upper limb in a pediatric patient. *Am. J. Phys. Med. Rehabil.* 89, 1024–1029. doi: 10.1097/PHM.0b013e3181e7204b
- Santiago-Pérez, S., Nevado-Estévez, R., and Pérez-Conde, M. (2012). Herpes zoster induced abdominal wall paresis: Neurophysiological examination in this unusual complication. *J. Neurol. Sci.* 312, 177–179. doi: 10.1016/j.jns.2011.08.035
- Tang, J., Tao, J., Luo, G., Zhu, J., and Yao, M. (2022). Analysis of risk factors and construction of a prediction model of motor dysfunction caused by limb herpes zoster. *J. Pain Res.* 15, 367–375. doi: 10.2147/JPR.S346564
- Tashiro, S., Akaboshi, K., Kobayashi, Y., Mori, T., Nagata, M., and Liu, M. (2010). Herpes zoster-induced trunk muscle paresis presenting with abdominal wall pseudohernia, scoliosis, and gait disturbance and its rehabilitation: A case report. *Arch. Phys. Med. Rehabil.* 91, 321–332. doi: 10.1016/j.apmr.2009.10.011
- Teo, H., Chawla, M., and Kaushik, M. (2016). A rare complication of herpes zoster: Segmental zoster paresis. *Case Rep. Med.* 2016, 7827140.
- Thomas, J., and Howard, F. Jr. (1972). Segmental zoster paresis—A disease profile. *Neurology* 22, 459–466. doi: 10.1212/wnl.22.5.459
- Van Wijck, A., and Aerssens, Y. (2017). Pain, itch, quality of life, and costs after herpes zoster. *Pain Pract.* 17, 738–746.
- Worrell, J., and Cockerell, C. (1997). Histopathology of peripheral nerves in cutaneous herpesvirus infection. *Am. J. Dermatopathol.* 19, 133–137.
- Yoleri, O., Olmez, N., Oztura, I., Sengül, I., Günaydin, R., and Memiş, A. (2005). Segmental zoster paresis of the upper extremity: A case report. *Arch. Phys. Med. Rehabil.* 86, 1492–1494.
- Zan, Y., Song, W., Wang, Y., Shao, J., Wang, Z., Zhao, W., et al. (2022). Nomogram for predicting in-hospital mortality of nonagenarians with community-acquired pneumonia. *Geriatr. Gerontol. Int.* 22, 635–641. doi: 10.1111/ggi.14430
- Zhang, W., Ji, L., Wang, X., Zhu, S., Luo, J., Zhang, Y., et al. (2022). Nomogram predicts risk and prognostic factors for bone metastasis of pancreatic cancer: A population-based analysis. *Front. Endocrinol. (Lausanne)* 12:752176. doi: 10.3389/fendo.2021.752176
- Zubair, A., Hunt, C., Watson, J., Nelson, A., and Jones, L. (2017). Imaging findings in patients with zoster-associated plexopathy. *AJNR Am. J. Neuroradiol.* 38, 1248–1251.



## OPEN ACCESS

## EDITED BY

Tingyuan Lang,  
Chongqing University, China

## REVIEWED BY

Carmen Rubio,  
Manuel Velasco Suárez National Institute of  
Neurology and Neurosurgery, Mexico  
Jiangfeng Qiu,  
Shanghai Jiao Tong University, China

## \*CORRESPONDENCE

Nina Hahn

✉ [nina.hahn@med.uni-jena.de](mailto:nina.hahn@med.uni-jena.de)

RECEIVED 31 March 2023

ACCEPTED 03 May 2023

PUBLISHED 18 May 2023

## CITATION

Hahn N, Bens M, Kempfer M, Reißig C,  
Schmidl L and Geis C (2023)  
Protecting RNA quality for spatial  
transcriptomics while improving  
immunofluorescent staining quality.  
*Front. Neurosci.* 17:1198154.  
doi: 10.3389/fnins.2023.1198154

## COPYRIGHT

© 2023 Hahn, Bens, Kempfer, Reißig, Schmidl  
and Geis. This is an open-access article  
distributed under the terms of the [Creative Commons Attribution License \(CC BY\)](https://creativecommons.org/licenses/by/4.0/). The  
use, distribution or reproduction in other  
forums is permitted, provided the original  
author(s) and the copyright owner(s) are  
credited and that the original publication in this  
journal is cited, in accordance with accepted  
academic practice. No use, distribution or  
reproduction is permitted which does not  
comply with these terms.

# Protecting RNA quality for spatial transcriptomics while improving immunofluorescent staining quality

Nina Hahn<sup>1,2\*</sup>, Martin Bens<sup>3</sup>, Marin Kempfer<sup>1</sup>, Christin Reißig<sup>1</sup>,  
Lars Schmidl<sup>1</sup> and Christian Geis<sup>1,2</sup>

<sup>1</sup>Section of Translational Neuroimmunology, Department of Neurology, Jena University Hospital, Jena, Germany, <sup>2</sup>Center for Sepsis Control and Care, Jena University Hospital, Jena, Germany, <sup>3</sup>Leibniz Institute on Aging – Fritz Lipmann Institute (FLI), Jena, Germany

In comparison to bulk sequencing or single cell sequencing, spatial transcriptomics preserves the spatial information in tissue slices and can even be mapped to immunofluorescent stainings, allowing translation of gene expression information into their spatial context. This enables to unravel complex interactions of neighboring cells or to link cell morphology to transcriptome data. The 10x Genomics Visium platform offers to combine spatial transcriptomics with immunofluorescent staining of cryo-sectioned tissue slices. We applied this technique to fresh frozen mouse brain slices and developed a protocol that still protects RNA quality while improving buffers for immunofluorescent staining. We investigated the impact of various parameters, including fixation time and buffer composition, on RNA quality and antibody binding. Here, we propose an improved version of the manufacturer protocol, which does not alter RNA quality and facilitates the use of multiple additional antibodies that were not compatible with the manufacturer protocol before. Finally, we discuss the influence of various staining parameters, which contribute to the development of application specific staining protocols.

## KEYWORDS

spatial transcriptomics, Visium spatial, mouse brain transcriptome, RNA quality, RNA protection, immunofluorescent staining, methanol fixation

## 1. Introduction

The understanding of mechanisms underlying neurodegenerative diseases has been fueled by the development of new methods unraveling pathological alteration in the transcriptome. Starting from bulk ribonucleic acid (RNA) sequencing, which identifies the average expression across cell populations, RNA sequencing developed to single cell resolution. This enables the discrimination between individual cell types within a population and even between cell states. However, single cell RNA sequencing loses any information about spatial relationships or cell morphology, which are often necessary for in-depth investigation of complex interactions between cells.

Spatial information on gene expression can be precisely obtained by fluorescent *in situ* hybridization (FISH) based techniques (Itzkovitz and van Oudenaarden, 2011; Shakoory, 2017). There, tissue slices or whole mount preparations are incubated with fluorescently labeled probes to detect transcripts of interest. This approach offers a high sensitivity with the ability to resolve

single transcripts (Femino et al., 1998; Itzkovitz and van Oudenaarden, 2011). However, FISH has a substantial drawback. The selection of probes limits insights to a pre-defined set of marker genes and thereby does not represent the whole transcriptome. Recently developed spatial transcriptomic platforms with spatial barcode technologies can preserve tissue architecture information while enabling whole transcriptome sequencing. So far, various platforms have been developed, each with certain limitations. Stereo-Seq provides excellent spatial resolution (spot size 220 nm) and is applicable to large tissue samples (capture area 200 mm<sup>2</sup>) such as an entire macaque brain (Chen et al., 2022). Nevertheless, drawbacks of such high-resolution include a high effort for sequencing, proper restriction of messenger RNA diffusion and decreased sensitivity. In contrast, the 10× Genomics Visium platform allows the investigation of 10 µm thick tissue sections with a size of 6.5 × 6.5 mm (Stahl et al., 2016). Tissue sections are placed on a microscope slide that is equipped with 5,000 barcoded spots (diameter 55 µm) which capture polyadenylated transcripts after tissue permeabilization. This approach leads to a lower spatial resolution of 1–10 cells per spot but offers the great opportunity to perform immunostaining and transcriptome analysis within the same tissue section. Thus, not only information about tissue architecture is preserved but also cell morphology. To improve the spatial resolution of 1–10 cells per spot, the Visium platform can be combined with single nuclei sequencing using an adjacent tissue slice. High-resolution single nuclei data can then be mapped back to the spatial transcriptome data using deconvolution algorithms (Elosua-Bayes et al., 2021; Cable et al., 2022; Kleshchevnikov et al., 2022; Lopez et al., 2022) to infer the cell composition of each spot.

Here, we tested various parameters including tissue fixation, staining buffer composition and RNA protecting agents that influence RNA quality and antibody binding, thus providing a toolbox to optimize immunofluorescent staining protocols for spatial transcriptomics. We applied our optimized protocol to fresh frozen mouse brain slices and used the 10× Genomics Visium platform to analyze the transcriptome.

## 2. Materials and methods

### 2.1. Animals and tissue dissection

All animal experiments have been approved by the Thuringian state authorities (authorization twz08-2020 and UKJ-18-026). We used male C57BL/6J mice of our own breeding facility (service center for small rodents, Jena, University Hospital) at the age of 10–16 weeks. Animals were housed under controlled day/night (12 h/12 h) conditions at room temperature (23 ± 1°C, 30%–60% environmental humidity) and received a standard diet and water *ad libitum*.

For tissue collection, mice were deeply anesthetized with isoflurane, transcardially perfused with 25 mL of phosphate buffered saline (PBS) for 5 min. The brain was dissected and snap frozen for 1 min in isopentane placed in a nitrogen bath prior to OCT embedding and storage at –80°C. Tissue was sliced to 10 µm thick sections using a cryostat (Leica CM3050 S, Nussloch, Germany) and stored up to 4 weeks in a sealed container with a moisture absorbing pad at –80°C. To measure RNA integrity, 10 brain tissue sections were collected in a tube for RNA extraction with QIAzol lysis reagent (Qiagen, #79306) according to the user manual. The RNA integrity

was measured with an Agilent 2100 Bioanalyzer (Santa Clara, United States) and the calculated RIN value was 9.4.

### 2.2. Immunostaining and imaging

Microscope slides were removed from –80°C, placed on carbon dioxide snow and processed quickly to protect RNA quality. Slides were dried at 37°C for 1 minute using a thermocycler (TOne 96 G, Biometra, Jena, Germany) equipped with the 10× Genomics thermocycler adaptor and subsequently placed into ice-cold methanol or other organic solvent (compare Table 1). Fixation duration ranged from dipping up to 30 min at –20°C, as indicated. In addition, fixation with ethanol and acetone was tested (compare Table 1). After fixation, OCT was removed with the aid of forceps and the microscope slide was placed into the slide cassette. The reference stainings are performed according to the protocol demonstrated by 10× Genomics for methanol fixation and immunofluorescent staining, Rev. B (#CG000312). In our modified protocol, slices were washed twice prior to 20 min blocking and 30 min primary antibody incubation at room temperature. Then, slices were washed three times with wash buffer, 15 min incubated with the secondary antibodies and DAPI, washed four times and finally 20 times rinsed in 3× saline-sodium citrate (SSC) buffer. We tested various blocking, wash and antibody binding buffers that are summarized in Table 2. The mounting medium consisted of 170 µL sterile glycerol, 20 µL RNase inhibitor (RNasin, New England Biolabs, #M0314L) and 10 µL water.

Slides were imaged with a LSM900 (Carl Zeiss Microscopy GmbH, Oberkochen, Germany) equipped with an EC “Plan-Neofluar” 10×/0.30 M27 objective (Carl Zeiss Microscopy GmbH, Oberkochen, Germany) and Zen Blue Software (Version 3.1, Carl Zeiss Microscopy GmbH, Oberkochen, Germany). Tissue optimization slides were imaged as one tile region to ensure comparison. The overlap between tiles was set to 10% and stitching was performed with standard settings without shading correction and saved as tiff files. Fluorescently labeled cDNA on tissue optimization slides was imaged with the texas red filter (Zeiss #45; 40 ms exposure) while immunostainings on gene expression slides were imaged with a DAPI (Zeiss #49; 5 ms exposure), texas red (Zeiss #45; 150 ms exposure), green fluorescent protein (Zeiss #38; 80 ms exposure) and a Cy5 filter (Zeiss #50; 300 ms exposure).

TABLE 1 Evaluation of tissue fixation with organic solvents.

Fixative	Fixation time	Staining quality
Methanol	Dipping	–
Methanol	5 min	++
Methanol	10 min	+
Methanol	20 min	No staining
Methanol	30 min	No staining
Ethanol	5 min	–
Ethanol	30 min	No staining
Acetone	5 min	No staining
Acetone	10 min	No staining
Acetone:Methanol 1:1	5 min	No staining

The staining quality was exemplary assessed on the basis of TMEM119 and DAPI staining. –, very poor staining; +, good staining; ++, very good staining.

## 2.3. Antibodies

Used antibodies are listed in [Table 3](#).

## 2.4. Tissue permeabilization and fluorescently labeled cDNA synthesis

Tissue permeabilization was conducted according to the user manual of the tissue optimization kit (#000193, 10× Genomics, Pleasanton, CA, United States). First, several permeabilization times were tested ranging from 30 min to 6 min, selecting 8 min as the most appropriate permeabilization time for following experiments ([Supplementary Figure S1](#)). In order to test the RNA preserving capability of various staining and washing buffers, slides from the tissue optimization kit were used and fluorescently labeled complementary deoxyribonucleic acid (cDNA) was synthesized according to the user manual. The fluorescence intensity indicates the quality of RNA used for cDNA synthesis and was assessed qualitatively.

**TABLE 2** Summary of tested washing, blocking and antibody binding buffers.

Solution	pH value
1× PBS	pH 7.4
1× PBS	pH 7 Adjusted from pH 7.4
3× SSC	pH 7
3× SSC	pH 7.4 Adjusted from pH 7
BSA Merck 10%	pH 6.5
BSA MACS 10%	pH 7.2

Comparisons between tissues were performed between with adjacent tissue slices on the identical microscope slide.

## 2.5. Visium spatial transcriptomics library preparation and sequencing

cDNA synthesis, second strand synthesis and cDNA amplification were performed according to the Visium spatial gene expression user guide CG000239, Rev. D (#1000187, 10× Genomics, Pleasanton, CA, United States). The cycle number for cDNA amplification was determined by qPCR using a Corbett Rotor-Gene 6000 thermocycler. Finally, cDNA was cleaned up by SPRIselect (#B23317, BeckmannCoulter, Krefeld, Germany) and checked for quality and quantity using an Agilent 2100 Bioanalyzer instrument and a high sensitivity DNA kit. The library was constructed using 10 µL of total cDNA following the user manual. Quantification and quality check of libraries was performed using the Agilent 2100 Bioanalyzer instrument and DNA 7500 kit. Libraries from each slide were pooled and each pool sequenced on NovaSeq 6000 using 100 cycle SP Reagent Kit v1.5 (Read1 = 28, Read2 = 90, Index1 and Index2 = 10). Base calling was performed using bcl2fastq (v2.20.0.422).

## 2.6. Visium data procession and quality control

Manual fiducial alignment and tissue outlining was performed using Loupe Browser (v6.1.0). Samples were processed with spaceranger (1.3.1) based on mouse reference genome mm10 (reference package refdata-gex-mm10-2020-A). Spaceranger data was

**TABLE 3** Result summary of tested antibodies in our optimized protocol.

Target	Cell type marker	Host	Supplier	Product ID	RRID	Dilution; concentration	Usability
Bassoon	Presynapse	gp	Synaptic systems	141 004	AB_2290619	1:500 from antiserum	Yes
Gephyrin	Inhibitory postsynapse	ms	Synaptic systems	147 011	AB_887717	1:100; 10 µg/mL	No
GFAP	Astrocyte	ms	Biotium	BNUM0789-50	Clone ASTRO/789	1:100; 10 µg/mL	Yes
Homer1	Excitatory postsynapse	ch	Synaptic systems	160 006	AB_2631222	1:400; 2.5 µg/mL	Yes
HopE	Neural stem cells	ms	Santa Cruz	sc-398703	AB_2687966	1:50; 4 µg/mL	No
Mannose (CD206)	Border associated macrophages	rb	Abcam	ab64693	AB_1523910	1:250; 4 µg/mL	Yes
Map2	Neurons	ch	Synaptic systems	188 006	AB_2619881	1:500; 2 µg/mL	Yes
PSD95	Excitatory postsynapse	ms	StressMarq	SMC-122D	AB_2300386	1:500; 2 µg/mL	No
PU.1	Mikroglia	rb	Cell Signaling Technology	2258S	AB_2186909	1:25; 6 µg/mL	Yes
Sox2	Neural stem cells	rb	Abcam	ab97959	AB_2341193	1:100; 10 µg/mL	No
Sox2	Neural stem cells	ms	Abcam	ab79351	AB_10710406	1:100; 10 µg/mL	No
TMEM119	Mikroglia	gp	Synaptic systems	400 004	AB_2744645	1:100 from antiserum	Yes
VGAT	Inhibitory presynapse	gp	Synaptic systems	131 004	AB_887873	1:500 from antiserum	Yes
VGlut1	Excitatory presynapse	gp	Synaptic systems	135 304	AB_887878	1:750 from antiserum	Yes
VGlut1	Excitatory presynapse	rb	Synaptic systems	135 303	AB_887875	1:500; 2 µg/mL	Yes

Lyophilized antibodies were reconstituted according to the data sheet. ch, chicken; gp, guinea pig; ms, mouse; rb rabbit.

further analyzed with R (version 4.2.2) and R Studio (version 2022.02.2) using the Seurat package (Hao et al., 2021). For visualization, dplyr, ggplot2, patchwork, hdf5r and viridis packages were used (Wickham, 2016; Garnier et al., 2021; Hoefling and Annau, 2022; Pedersen, 2022; Wickham et al., 2022). As reference, two mouse brain datasets from 10× Genomics were integrated. Similar to our samples, both are from adult mice, coronal 10 µm thick coronal cryosection. The dataset “10×\_HE” was retrieved from <https://www.10xgenomics.com/resources/datasets/mouse-brain-section-coronal-1-standard> and collected from hematoxylin and eosin stained tissue. The dataset “10×\_IF” was retrieved from <https://www.10xgenomics.com/resources/datasets/adult-mouse-brain-section-2-coronal-stains-dapi-anti-gfap-anti-neu-n-1-standard-1-1-0> and collected from DAPI, anti-GFAP and anti-NeuN stained tissue. Statistical analysis using a pairwise permutation test was performed with the aid of the coin and rcompanion packages (Hothorn et al., 2006, 2008; Mangiafico, 2023).

## 3. Results and discussion

### 3.1. Tissue fixation with organic solvents

Along with tissue collection, tissue fixation is one of the main critical steps for immunostainings and transcriptome analysis since it helps to preserve both, protein and RNA quality. The protocol demonstrated by 10× Genomics suggests 30 min fixation with ice-cold methanol, however, this does not lead to successful staining with all our tested antibodies. We found that reducing the fixation time to 5 min leads to optimal staining results on 10 µm thick mouse brain cryosections (Table 1) while preserving RNA quality properly. In addition, reducing the fixation time has the benefit of reducing the risk of RNA leakage (Esser et al., 1995). Besides methanol, we tested ethanol and acetone as organic solvents. However, methanol fixation outperformed both. We could further improve the immunostaining by introducing two additional washing steps after methanol fixation to rehydrate the sample, which markedly recovers specific antibody binding.

Most antibodies validated for immunostainings were tested on native or paraformaldehyde (PFA) fixed tissue and hence do not recognize epitopes after fixation with organic solvents. For spatial transcriptomics, PFA fixation is less suited, since PFA leads to RNA degradation as well as RNA modification (Ben-Ezra et al., 1991; Evers et al., 2011). Organic solvents such as methanol dehydrate the sample leading to precipitation of proteins and affecting RNA quality to a lesser extent compared to PFA (Ben-Ezra et al., 1991; Su et al., 2004). Due to precipitation, epitopes change their conformation and are often not recognized by antibodies that have been validated on PFA fixed tissue. However, we found that antibodies validated for flow cytometry applications are often better suited for the Visium platform in combination with immunofluorescence staining. Cells for flow cytometric assays are typically fixed with ice-cold ethanol, which may explain this phenomenon.

### 3.2. Blocking and antibody binding buffer composition

The blocking buffer introduced by the manufacturer protocol is composed of 3× SSC buffer, 2% bovine serum albumin (BSA), 0.1%

Triton X-100, 1 U/µL RNase inhibitor, 20 mM Ribonucleoside Vanadyl complex (RVC) and 14 µg/mL TruStain FcX (#101319, BioLegend, San Diego, United States). For the primary antibody binding solution, 270 U RNase inhibitor are added to the blocking buffer. With all tested antibodies this protocol leads to no or very weak staining, high background and blurred unspecific fluorescent signals (Figures 1A,B; middle right). Hence, we started to decipher the respective characteristics of each component to control for its advantages as well as disadvantages during blocking and antibody binding.

First, we focused on components that are not involved in RNA protection but can interfere with immunostaining. Triton X-100 permeabilizes the cell membrane but is also known to interfere with immunostaining of membrane-bound proteins (Oliver and Jamur, 1984; Hobro and Smith, 2017). Additional permeabilization with Triton X-100 was not necessary for staining for intracellular antigens, as methanol already permeabilises membranes (Oliver and Jamur, 1984; Hobro and Smith, 2017), so we left it out. In addition, we excluded TruStain FcX which blocks unwanted Fc receptor binding. Furthermore, we increased the BSA concentration from 2% to 10% and thereby noticeably improved the stainings and reduced background.

### 3.3. RVC interferes with immunostaining and is inactivated by SSC buffer

It is crucial to protect the RNA for downstream transcriptome analysis during the course of immunostaining and imaging which last approximately 4 h in total and is performed at room temperature. To avoid RNA degradation by ribonucleases, 10× Genomics recommends adding 20 mM RVC in blocking, wash and antibody binding buffer. RVC is an efficient and inexpensive inhibitor of RNase (Shieh et al., 2018). However, we found that RVC leads to blurred, unspecific fluorescent signals and prevents antibodies from specific binding, when applied according to the manufacturer protocol (Figures 1A,B; middle right). Even reducing the RVC concentration from 20 mM to 10 mM as recommended by the RVC product manual, does not improve immunofluorescent staining. We needed to reduce the concentration of RVC further to 1 mM to exclude interference with antibody binding (Figures 1A,B; middle left). In line with previous results that showed RNA protective behaviour of RVC at 0.2 mM (Shieh et al., 2018), we observe RNA protection using 1 U/mL RNasin and 1 mM RVC, however markedly less than 20 mM RVC (Figure 1C; middle left).

RVC is very sensitive to oxidation and dissociation. After reconstitution, it should have a brilliant forest green color. When dissociated, it turns black and loses its capability as an inhibitor of RNases (Shankar and Ramasarma, 1993). Figure 2A shows that addition of RVC to SSC buffer leads to a change of color from forest green to black after 10 min, even if the SSC buffer is diluted to a concentration of 0.5X. In addition, a black precipitate was noticed. According to the user manual, RVC should not be used in the presence of ethylenediaminetetraacetic acid (EDTA), which leads to dissociation of the complex. EDTA and citrate are both chelating agents. Thus, sodium citrate in SSC buffer will lead to dissociation and inactivation of RVC as well. This is in line with previous reports that 2× SSC buffer reduces the effective lifetime of RVC in MERFISH stainings (Moffitt et al., 2016). Altogether, this indicates that RVC is inactivated by SSC buffer and should not provide substantial RNA protection in the

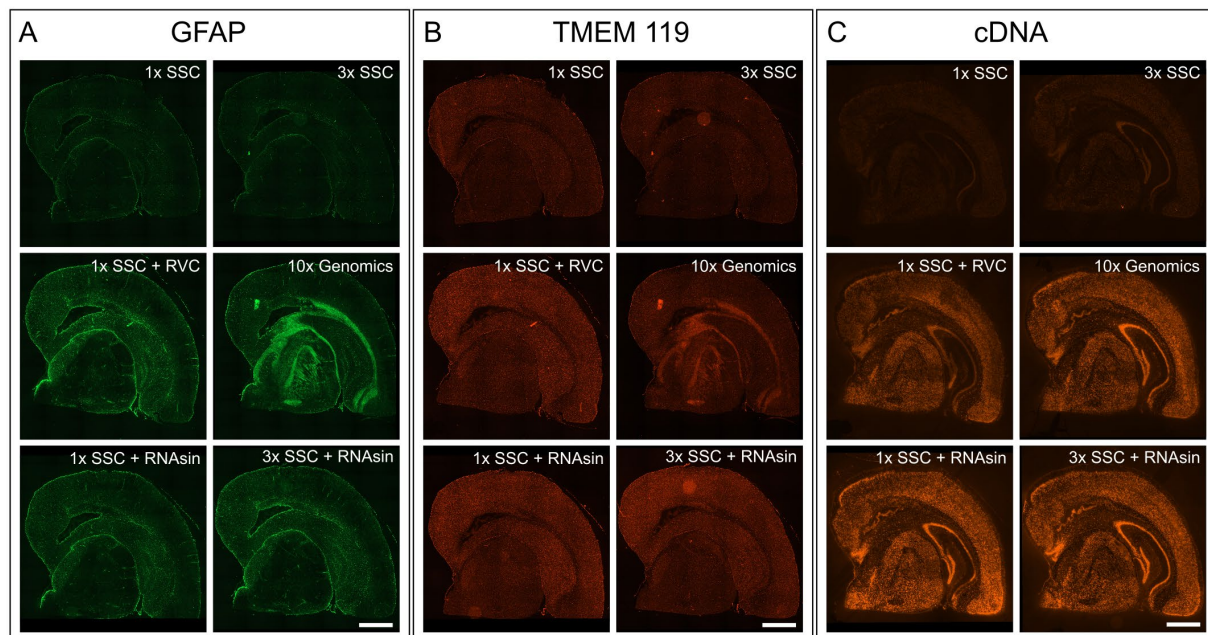


FIGURE 1

Impact of RVC, SSC buffer and RNase inhibitor (RNAsin) on GFAP astrocyte marker staining (A), TMEM119 microglia marker staining (B) and RNA quality protection based on fluorescently labeled cDNA (C). The demonstrated 10x Genomics protocol was used as a reference (middle right). Scale bar 1mm.

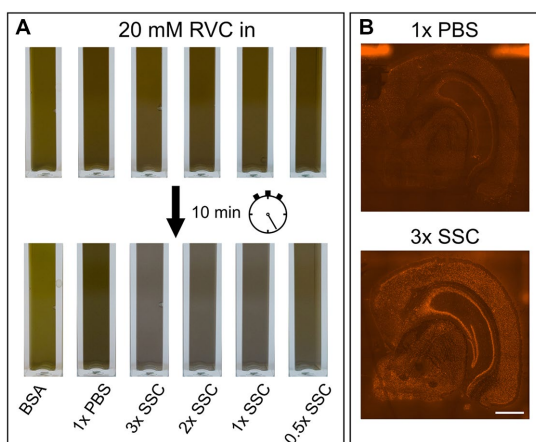


FIGURE 2

Influence of PBS, SSC and RVC in wash buffer. (A) Color change of RVC after 10min diluted in BSA, PBS and various SSC buffer concentrations. Forest green indicates active RVC, black color inactive RVC. (B) Effect of 1x PBS and 3x SSC on RNA quality measured on the basis of fluorescently labeled cDNA. 3x SSC protects RNA better against degradation than 1x PBS. Scale bar 1mm.

buffers used for immunostaining suggested by the manufacturer. Interfering with the immunostaining whilst providing only limited protection of RNA quality, we excluded RVC from our staining buffers. Instead, we included RNase inhibitor in all of our buffers with a final concentration of 1,000 U/mL. Indeed, replacement of RVC with RNase inhibitor does not interfere with antibody binding while reliably protecting RNA quality (Figures 1A–C; bottom row). In addition, the

used RNase inhibitor is stable at room temperature providing a robust protection during immunostaining as well as during imaging steps. However, in comparison to RVC, RNase inhibitor is more expensive and increases the cost for each microliter of wash buffer 80–90 times.

### 3.4. Increasing antibody binding without harming RNA quality

The main component of the wash buffer for immunostaining is 3x SSC. We found that increasing concentration of SSC in the antibody binding buffer decreases antibody binding (Figures 1A,B; upper row). Substituting 3x SSC by 1x PBS, which is the most common buffer for immunostainings, remarkably increased specific antibody binding. However, this dramatically decreased RNA quality (Figure 2B).

Lowering the pH value and increasing the ionic strength are common approaches to adjust binding properties in affinity chromatography or co-immunoprecipitation (Roberts et al., 2015). 3x SSC (pH 7.0 at room temperature) and PBS (pH 7.4 at room temperature) buffer differ in both, pH and ionic strength. Decreasing the pH of PBS to 7 as present in SSC buffer, prevented antibody binding. In contrast, increasing the pH to 7.4 in 3x SSC buffer did not promote antibody binding. Thus, a lower pH value decreases antibody binding but is not the only reason why 3x SSC interferes with proper immunostaining. 3x SSC buffer is typically used in FISH or northern blotting protocols, since its higher salt concentration supports RNA integrity. The salt concentration in 3x SSC buffer is higher than in 1x PBS buffer, hence, we tested as well 1x SSC buffer (Figures 1A–C; left column) to evaluate the effect of ionic strength.

Usually, antibodies for immunostainings are selected with antibody binding buffers based on PBS (pH 7.4) and TBS (pH 7.6).

Thus, antibodies for immunostaining might be selected for complement-determining regions (CDRs) that form strong bounds at pH 7.4–7.6 but only weak bounds at pH 7. Depending on the CDR composition, antibodies are susceptible to pH change. Specifically, CDRs composed of aspartic acid are vulnerable to variation in pH (Psimadas et al., 2012). In addition, protein–protein interaction of immunoglobulins is more attractive with an increasing pH (Roberts et al., 2015). This effect might be particularly substantial since epitopes might suffer from slight conformational changes due to methanol fixation challenging antibody to antigen binding anyway.

Due to the effect of pH on antibody binding, we carefully tested the pH of BSA solutions suggested in the demonstrated protocols. BSA from Merck (pH 6.9; #126615-25ML) prevents antibody binding, while BSA MACS (pH 7.4; Miltenyi Biotec, #130-091-376) leads to specific staining with low background. This is in line, with our previous results, showing pH 7 as inappropriate for antibody binding.

We tested whether a lower pH and a higher salt concentration only affects antibody binding itself or even the binding persistence of an already bound antibody. While 3× SSC in the antibody binding buffer prevents antibody binding, 3× SSC in the washing buffer does not affect immunostaining quality. Consequently, we diluted the antibodies in 10% BSA blocking buffer, not using SSC buffer during the binding phase, but keeping it in the wash buffer to protect RNA. Wash buffer composed of 3× SSC (Figure 1C; upper right) shows a stronger protective effect on RNA quality compared to wash buffer with 1× SSC (Figure 1C; upper left).

In summary, our optimized protocol reduces methanol fixation time to 5 min, omits TruStain FcX, Triton X-100 and RVC but adds RNase inhibitor to all buffers with a concentration of 1,000 U/mL. In addition, we inserted an additional washing step after methanol fixation to rehydrate the tissue samples and replaced 3× SSC containing blocking and antibody binding buffer by 10%

BSA. Antibodies targeting various cell types and that are usable with our protocol are shown in Table 3 and Supplementary Figure S4. Further stainings with antibodies that were not compatible are shown in Supplementary Figure S5.

### 3.5. Staining protocol optimization does not affect the quality of spatial transcriptome data

Improving immunostaining must not worsen RNA integrity and consequently spatial transcriptome data quality. We sequenced libraries using the Visium platform from four samples and compared their quality to 10× Genomics mouse brain datasets (10×\_HE and 10×\_IF) as reference. While the dataset “10×\_HE” was derived from hematoxylin and eosin (HE) stained tissue, the data set “10×\_IF” was derived from tissue after immunofluorescent (IF) staining with DAPI, anti-GFAP and anti-NeuN according to the manufacturer demonstrated protocol for methanol fixation and IF staining. Figure 3A and Table 4 shows a similar number of log10 transcript counts per spot using our optimized protocol (minimum 2.18–2.91; median 3.90–4.09) compared to 10×\_IF (minimum 1.84; median 4.04). Using HE stained tissue leads to higher log10 transcript counts in comparison to IF stained tissue (minimum 2.76, median 4.46). Figure 4 shows that the number of transcript counts (nCount) and number of detected genes (nFeature) per spot correlate well with another (Pearson coefficient: 0.9) and that IF stained samples are highly similar.

The number of detected log10 features per spot in our samples (median 3.52–3.63, Figure 3B) is similar compared to the 10×\_IF stained sample (median 3.63). In both, log10 transcript counts and log10 feature, the maximum variation between the 10×\_IF reference

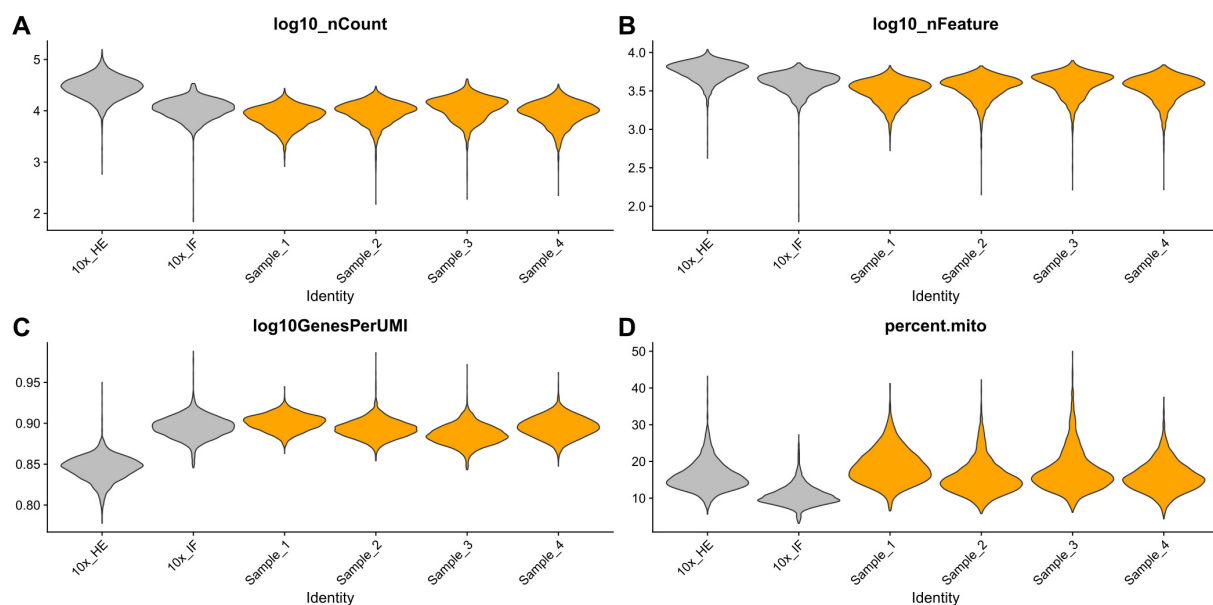
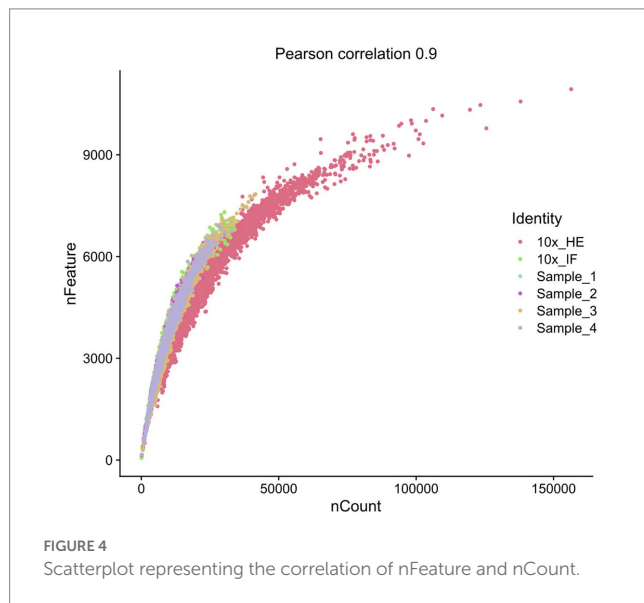


FIGURE 3

Comparison of four samples stained with our optimized IF staining protocol (orange) to 10× Genomics reference data sets (HE stained and IF stained, grey). Violin plots summarize the respective transcript counts (A), features (B), the complexity (log10 genes per UMI) (C) and mitochondrial related transcript counts (D).

TABLE 4 Summary of main sequencing metrics.

Sample IDs	Minimum Log10Counts	Median Log10Counts	Minimum Log10Features	Median Log10Features	Minimum complexity	Median complexity
10x_HE	2.76	4.46	2.63	3.78	0.78	0.85
10x_IF	1.84	4.04	1.80	3.63	0.85	0.90
Sample_1	2.91	3.90	2.72	3.52	0.86	0.90
Sample_2	2.18	4.00	2.15	3.58	0.85	0.89
Sample_3	2.28	4.09	2.21	3.63	0.84	0.89
Sample_4	2.35	3.98	2.21	3.57	0.85	0.90



sample and our samples is lower than the variation between 10x\_HE stained and 10x\_IF stained tissue. Comparing the minimum and median using a pairwise permutation test, does not detect any significant difference ( $p > 0.05$ ). The number of total detected genes in IF stained tissue is similar and varies between 19,812 and 20,933 genes (Supplementary Table S1). The complexity (log10genesPerUMI) is lowest in the 10x\_HE sample (minimum 0.78, median 0.85) and higher in IF stained samples (minimum 0.84, median 0.89–0.90) (Figure 3C; Table 4) with an even distribution throughout the tissue (Supplementary Figure S2). Overall, our staining protocol, which improves antibody binding, does not negatively affect RNA quality and sequencing thereby presenting an optimized alternative. Deviations between 10x\_IF and our samples are lower than the deviation between 10x\_HE and 10x\_IF samples. A better performance of 10x\_HE samples might be due to a markedly lower tissue staining time (approx. 30 min) compared to IF stained tissue (approx. 3 h). Mitochondrial counts are slightly higher in our samples (median 14.71–18.09) compared to 10x samples (median 15.33 and 10.25; Figure 3D). Supplementary Figure S3 shows that spots with higher mitochondrial counts are distributed along the tissue border indicating damage during tissue dissection and being independent from the staining protocol.

In summary, we systematically investigated the manufacturer immunostaining protocol for the Visium platform. The detailed knowledge, which characteristics of the buffer components affect

antibody binding and RNA quality, helped to optimize the staining protocol that we propose for 10  $\mu$ m mouse brain section. Our protocol preserves epitopes better and enhances antibody binding while it still protects RNA quality for downstream transcriptome analysis. In addition, we present suitable antibodies for often-used markers for several brain cell types and synaptic structures (Table 3). Overall, the findings presented here regarding the impact of fixatives and immunostaining buffers on RNA quality are as well crucial for optimizing protocols for other spatial transcriptomic platforms independent from the Visium platform.

## Data availability statement

The datasets presented in this study can be found in online repositories. The names of the repository/repositories and accession number(s) can be found at: <https://www.ncbi.nlm.nih.gov/geo/>, GSE228891.

## Ethics statement

The animal study was reviewed and approved by Thueringer Landesamt fuer Lebensmittelsicherheit und Verbraucherschutz.

## Author contributions

NH and CG: conceptualization and funding acquisition. NH, MB, and CR: methodology. NH, MB, MK, CR, and LS: investigation. CG: resources. NH and MB: data curation. NH: writing—original draft, supervision, and project administration. NH, MB, and CG: writing—review and editing. NH and MK: visualization. All authors contributed to the article and approved the submitted version.

## Funding

The study was funded by the Friedrich-Schiller-University program IMPULSEproject (IP2021-06 to NH), the Center for Sepsis Control and Care (CSCC; to NH and CG), and the Hermann and Lilly Schilling foundation (to CG). We acknowledge support by the German Research Foundation Project-No. 512648189 and the Open Access Publication Fund of the Thueringer Universitaets- und Landesbibliothek Jena.

## Acknowledgments

The authors thank Claudia Sommer for excellent technical assistance and Ha-Yeun Chung as well as Jonathan Wickel for scientific advice and discussion. In addition, the authors thank Ivonne Görlich and Marco Groth from the Core Facility Next Generation Sequencing of the Leibniz Institute on Aging—Fritz Lipmann Institute in Jena for their help with library preparation and sequencing.

## Conflict of interest

The authors declare that the research was conducted in the absence of any commercial or financial relationships that could be construed as a potential conflict of interest.

## References

- Ben-Ezra, J., Johnson, D. A., Rossi, J., Cook, N., and Wu, A. (1991). Effect of fixation on the amplification of nucleic acids from paraffin-embedded material by the polymerase chain reaction. *J. Histochem. Cytochem.* 39, 351–354. doi: 10.1177/39.3.1704393
- Cable, D. M., Murray, E., Zou, L. S., Goeva, A., Macosko, E. Z., Chen, F., et al. (2022). Robust decomposition of cell type mixtures in spatial transcriptomics. *Nat. Biotechnol.* 40, 517–526. doi: 10.1038/s41587-021-00830-w
- Chen, A., Sun, Y., Lei, Y., Li, C., Liao, S., Liang, Z., et al. (2022). Global spatial transcriptome of macaque brain at single-cell resolution. *bioRxiv*. 2022.03.23.485448. [Epub ahead of print]. doi: 10.1101/2022.03.23.485448v1
- Elosua-Bayes, M., Nieto, P., Mereu, E., Gut, I., and Heyn, H. (2021). SPOTlight: seeded NMF regression to deconvolute spatial transcriptomics spots with single-cell transcriptomes. *Nucleic Acids Res.* 49:E50. doi: 10.1093/nar/gkab043
- Esser, C., Güttlinger, C., Kremer, J., and Hündel, C. (1995). Isolation of full-size mRNA from ethanol-fixed cells after cellular immunofluorescence staining and fluorescence-activated cell sorting (FACS). *Cytometry* 21, 382–386. doi: 10.1002/cyto.990210411
- Evers, D. L., Fowler, C. B., Cunningham, B. R., Mason, J. T., and O'Leary, T. J. (2011). The effect of formaldehyde fixation on RNA: optimization of formaldehyde adduct removal. *J. Mol. Diagn.* 13, 282–288. doi: 10.1016/j.jmoldx.2011.01.010
- Femino, A. M., Fay, F. S., Fogarty, K., and Singer, R. H. (1998). Visualization of single RNA transcripts in situ. *Science* 280, 585–590. doi: 10.1126/science.280.5363.585
- Garnier, S., Ross, N., Rudis, R., Camargo, A. P., Sciaini, M., and Scherer, C. (2021). Viridis: colorblind-friendly color maps for R. Available at: <https://sjmgarnier.github.io/viridis/>.
- Hao, Y., Hao, S., Andersen-Nissen, E., Mauck, W. M., Zheng, S., Butler, A., et al. (2021). Integrated analysis of multimodal single-cell data. *Cells* 184, 3573–3587.e29. doi: 10.1016/j.cell.2021.04.048
- Hobro, A. J., and Smith, N. I. (2017). An evaluation of fixation methods: spatial and compositional cellular changes observed by Raman imaging. *Vib. Spectrosc.* 91, 31–45. doi: 10.1016/j.vibspec.2016.10.012
- Hoefling, H., and Annau, M. (2022). hdf5r: Interface to the HDF5 binary data format. Available at: <https://cran.r-project.org/package=hdf5r>.
- Hothorn, T., Hornik, K., van de Wiel, M. A., and Zeileis, A. (2006). A Lego system for conditional inference. *Am. Stat.* 60, 257–263. doi: 10.1198/000313006X118430
- Hothorn, T., Hornik, K., van de Wiel, M. A., and Zeileis, A. (2008). Implementing a class of permutation tests: the coin package. *J. Stat. Softw.* 28, 1–23. doi: 10.18637/jss.v028.i08
- Itzkovitz, S., and van Oudenaarden, A. (2011). Validating transcripts with probes and imaging technology. *Nat. Methods* 8, S12–S19. doi: 10.1038/nmeth.1573
- Kleshchevnikov, V., Shmatko, A., Dann, E., Aivazidis, A., King, H. W., Li, T., et al. (2022). Cell2location maps fine-grained cell types in spatial transcriptomics. *Nat. Biotechnol.* 40, 661–671. doi: 10.1038/s41587-021-01139-4
- Lopez, R., Li, B., Keren-Shaul, H., Boyeau, P., Kedmi, M., Pilzer, D., et al. (2022). DestVI identifies continuums of cell types in spatial transcriptomics data. *Nat. Biotechnol.* 40, 1360–1369. doi: 10.1038/s41587-022-01272-8
- Mangiafico, S. (2023). Rcompanion: functions to support extension education program evaluation. Available at: <https://cran.r-project.org/package=rcompanion>.
- Moffitt, J. R., Hao, J., Bambach-Mukku, D., Lu, T., Dulac, C., and Zhuang, X. (2016). High-performance multiplexed fluorescence in situ hybridization in culture and tissue with matrix imprinting and clearing. *Proc. Natl. Acad. Sci. U. S. A.* 113, 14456–14461. doi: 10.1073/pnas.1617699113
- Oliver, C., and Jamur, M. C. (1984). *Immunocytochemical methods and protocols*. 3rd ed. Totowa, NJ: Humana
- Pedersen, T. L. (2022). Patchwork: the composer of plots. Available at: <https://cran.r-project.org/package=patchwork>.
- Psimadas, D., Georgoulas, P., Valotassiou, V., and Loudos, G. (2012). Molecular nanomedicine towards Cancer. *J. Pharm. Sci.* 101, 2271–2280. doi: 10.1002/jps
- Roberts, D., Keeling, R., Tracka, M., Van Der Walle, C. F., Uddin, S., Warwicker, J., et al. (2015). Specific ion and buffer effects on protein – protein interactions of a monoclonal antibody. *Mol. Pharm.* 12, 179–193. doi: 10.1021/mp500533c
- Shakoori, A. R. (2017). “Fluorescence in situ hybridization (FISH) and its applications” in *Chromosome structure and aberrations*. eds. T. Bhat and A. Wani (India: Springer), 343–367.
- Shankar, H. N. R., and Ramasarma, T. (1993). Multiple reactions in vanadyl-V(IV) oxidation by H<sub>2</sub>O<sub>2</sub>. *Mol. Cell. Biochem.* 129, 9–29. doi: 10.1007/BF00926572
- Shieh, T. M., Chen, C. Y., Hsueh, C., Yu, C. C., Chen, C. C., and Wang, T. H. (2018). Application of ribonucleoside vanadyl complex (RVC) for developing a multifunctional tissue preservative solution. *PLoS One* 13, e0194393–e0194314. doi: 10.1371/journal.pone.0194393
- Stahl, P. L., Salmén, F., Vickovic, S., Lundmark, A., Navarro, J. F., Magnusson, J., et al. (2016). Visualization and analysis of gene expression in tissue sections by spatial transcriptomics. *Science* 353, 78–82. doi: 10.1126/science.aaf2403
- Su, J. M. F., Perlaky, L., Li, X. N., Leung, H. C. E., Antalffy, B., Armstrong, D., et al. (2004). Comparison of ethanol versus formalin fixation on preservation of histology and RNA in laser capture microdissected brain tissues. *Brain Pathol.* 14, 175–182. doi: 10.1111/j.1750-3639.2004.tb00050.x
- Wickham, H. (2016). *ggplot2: Elegant graphics for data analysis*. New York: Springer-Verlag
- Wickham, H., François, R., Henry, L., and Müller, K. (2022). Dplyr: a grammar of data manipulation. Available at: <https://cran.r-project.org/package=dplyr>.

## Publisher's note

All claims expressed in this article are solely those of the authors and do not necessarily represent those of their affiliated organizations, or those of the publisher, the editors and the reviewers. Any product that may be evaluated in this article, or claim that may be made by its manufacturer, is not guaranteed or endorsed by the publisher.

## Supplementary material

The Supplementary material for this article can be found online at: <https://www.frontiersin.org/articles/10.3389/fnins.2023.1198154/full#supplementary-material>



## OPEN ACCESS

## EDITED BY

Eduard Rodriguez-Farre,  
Spanish National Research Council (CSIC),  
Spain

## REVIEWED BY

Diana L. Giraldo,  
University of Antwerp, Belgium  
Maryam Haghsomar,  
Northwestern Medicine, United States

## \*CORRESPONDENCE

Fuqing Zhou  
✉ ndyfy02301@ncu.edu.cn

<sup>†</sup>These authors have contributed equally to this work

RECEIVED 16 March 2023

ACCEPTED 30 May 2023

PUBLISHED 16 June 2023

## CITATION

Kuang Q, Huang M, Lei Y, Wu L, Jin C, Dai J and Zhou F (2023) Clinical and cognitive correlates tractography analysis in patients with white matter hyperintensity of vascular origin. *Front. Neurosci.* 17:1187979. doi: 10.3389/fnins.2023.1187979

## COPYRIGHT

© 2023 Kuang, Huang, Lei, Wu, Jin, Dai and Zhou. This is an open-access article distributed under the terms of the [Creative Commons Attribution License \(CC BY\)](#). The use, distribution or reproduction in other forums is permitted, provided the original author(s) and the copyright owner(s) are credited and that the original publication in this journal is cited, in accordance with accepted academic practice. No use, distribution or reproduction is permitted which does not comply with these terms.

# Clinical and cognitive correlates tractography analysis in patients with white matter hyperintensity of vascular origin

Qinmei Kuang<sup>1,2†</sup>, Muhua Huang<sup>1,2†</sup>, Yumeng Lei<sup>3</sup>, Lin Wu<sup>1,2</sup>, Chen Jin<sup>1,2</sup>, Jiankun Dai<sup>4</sup> and Fuqing Zhou<sup>1,2\*</sup>

<sup>1</sup>Department of Radiology, First Affiliated Hospital of Nanchang University, Nanchang, Jiangxi, China, <sup>2</sup>Clinical Research Center for Medical Imaging in Jiangxi Province, Nanchang, China, <sup>3</sup>Department of Radiology, Nanchang First Hospital, Nanchang, Jiangxi, China, <sup>4</sup>GE Healthcare, MR Research China, Beijing, China

**Purpose:** White matter hyperintensity lesions (WMHL) in the brain are a consequence of cerebral small vessel disease and microstructural damage. Patients with WMHL have diverse clinical features, and hypertension, advanced age, obesity, and cognitive decline are often observed. However, whether these clinical features are linked to interrupted structural connectivity in the brain requires further investigation. This study therefore explores the white matter pathways associated with WMHL, with the objective of identifying neural correlates for clinical features in patients with WMHL.

**Methods:** Diffusion magnetic resonance imaging (MRI) and several clinical features (MoCA scores, hypertension scores, body mass index (BMI), duration of hypertension, total white matter lesion loads, and education.) highly related to WMHL were obtained in 16 patients with WMHL and 20 health controls. We used diffusion MRI connectometry to explore the relationship between clinical features and specific white matter tracts using DSI software.

**Results:** The results showed that the anterior splenium of the corpus callosum, the inferior longitudinal fasciculus, the anterior corpus callosum and the middle cerebellar peduncle were significantly correlated with hypertension scores (false discovery rate (FDR)=0.044). The anterior splenium of the corpus callosum, the left thalamoparietal tract, the inferior longitudinal fasciculus, and the left cerebellar were significantly correlated with MoCA scores (FDR=0.016). The anterior splenium of corpus callosum, inferior fronto-occipital fasciculus, cingulum fasciculus, and fornix/fimbria were significantly correlated with body mass index (FDR=0.001).

**Conclusion:** Our findings show that hypertension score, MoCA score, and BMI are important clinical features in patients with WMHL, hypertension degree and higher BMI are associated with whiter matter local disconnection in patients with WMHL, and may contribute to understanding the cognitive impairments observed in patients with WMHL.

## KEYWORDS

white matter hyperintensity, diffusion magnetic resonance imaging, hypertension, cognition, body mass index, tractography

## Introduction

White matter hyperintensities lesions (WMHL) are characterized by multiple punctate, patchy, or confluent hyperintensities in the bilateral periventricular or subcortical white matter on T2-weighted images or T2-weighted fluid-attenuated inversion recovery images (T2-Flair) and are one of the common imaging markers of cerebral small vessel disease (CSVD) (Wardlaw et al., 2013). Various factors contribute to WMHL formation, including age, female sex, hypertension, hyperlipidemia, apolipoprotein Eε4 allele, diabetes, smoking, and alcohol consumption (Alber et al., 2019; Frey et al., 2019). Previous studies have demonstrated that WMHL are associated with an increased risk of stroke, cognitive decline, dementia, and death (Debetto and Markus, 2010). Even in healthy aging, higher whole-brain lesion volume and regional WMHL load are consistently associated with poorer cognitive performance in processing speed, memory, and executive functioning (van Rooden et al., 2018).

Previous studies have shown anomalies not only within T2-WMHL but also in apparently “normal appearing white matter (NAWM)” (Maillard et al., 2011). Over time, abnormal changes in NAWM precede WMHL progression, known as WMHL penumbra (Wu et al., 2019). Cognitive impairment in patients with WMHL is correlated with microstructural destruction of various white matter fibers, which may include “disconnection” of cortical–subcortical pathways (Yuan et al., 2017; Lu et al., 2021), and the relationship between overall cognitive function and white matter integrity may be closer than that with blood supply (Zhong et al., 2017).

Serious vascular diseases can lead to cortical and subcortical infarction, affect brain functional areas, and result in vascular cognitive impairment (Frantellizzi et al., 2020; Meng et al., 2022). Compared to all other regions, the front permanent WMHL has more pronounced diffusion tensor imaging metrics changes with the same Fazekas grades, which may represent the effects of severe demyelination within the frontal periventricular WMHL (Min et al., 2021). The results also indicate an increased WMHL burden selectively in deep white matter in obese subjects with high visceral fat accumulation. Independent of common obesity comorbidities such as hypertension, it may be that the visceral obesity contributes to deep white matter lesions through increases in proinflammatory cytokines (Min et al., 2021). In fact, most patients with WMHL may not lead to typical clinical symptoms because of collateral circulation development in these ischemic regions.

However, consensus is lacking as to regarding which etiology or clinical characteristic and corresponding white matter tract provide the most accurate reflection of patients with WMHL and may be used as neural correlates (white matter fiber bundle segments correlated with study variables) to assist clinical diagnosis. We hypothesized that even asymptomatic patients with WMHL may have microstructural impairment. This study intends to use the diffusion MRI connectome analysis method to identify neural correlates that reflect the underlying deficits in WMHL and to identify the most representative neural correlates for WMHL.

## Materials and methods

### Subjects

All subjects provided signed, informed consent prior to inclusion in the study in accordance with the local institutional review board. From

May 2020 to December 2021, patients with WHM ( $n = 16$ ) from inpatient were recruited to the first affiliated hospital of Nanchang University. The inclusion criteria for WMHL subjects were as follows: (1) presence of grade 2 or 3 WMHL according to Fazekas scale on FLAIR; (2) no contraindications to MRI. Exclusion criteria were as follows: (1) history of ischemic stroke with infarct size greater than 1.5 cm in diameter or cardiogenic cerebral embolism, (2) cerebral hemorrhage, (3) internal carotid artery or vertebral artery stenosis ( $>50\%$ ) or coronary atherosclerosis heart disease, (4) WMHL due to immune-mediated inflammatory demyelinating disease (multiple sclerosis, neuromyelitis optica, acute disseminated encephalomyelitis), metabolic leukodystrophy and genetic leukoencephalopathy, and (5) other neurological disorders.

Healthy controls (HC,  $n = 20$ ) were randomly recruited, who had no history of hypertensive disease, traumatic brain injury, neurologic diseases, or brain abnormalities based on conventional MRI (T1 weight image, T2 weight image, T2 fluid attenuated inversion recovery).

### Image acquisition

A total of 36 diffusion MRI scans were included in the connectometry database. The diffusion images were obtained on a 3 T MR system (Premier, GE Healthcare, Madison, Wisconsin) using a 2D EPI diffusion sequence. Foam padding was used to position subjects on the coil so that the cervical spine was straight but comfortable to minimize head motion. The spatial resolution was  $0.875\text{ mm} \times 0.875\text{ mm} \times 2.5\text{ mm}$  isotropic.  $TR = 5,500\text{ ms}$ ,  $TE = 71\text{ ms}$ .  $FOV = 224\text{ mm} \times 224\text{ mm}$ . The diffusion data was acquired with 100 directions with  $b$ -values ( $3,000\text{ s/mm}^2$ ). Thickness of the slice was 2 mm. Axial conventional T1WI, T2WI, T2-FLAIR (fluid-attenuated inversion recovery) were acquired in the brain for each patient's diagnosis. The following scan parameters were used: axial T1WI:  $TR = 250\text{ msec}$ ,  $TE = 2.46\text{ msec}$ , slice number = 19, slice thickness = 5.0 mm,  $FOV = 24 \times 24\text{ cm}$ , matrix size =  $256 \times 256$ ; axial T2WI: repetition time ( $TR$ ) = 4,000 msec, echo time ( $TE$ ) = 113 msec, slice number = 19, slice thickness = 5.0 mm, field of view ( $FOV$ ) =  $24 \times 24\text{ cm}$ , matrix size =  $256 \times 256$ ; axial T2-FLAIR:  $TR = 7,000\text{ msec}$ ,  $TE = 162\text{ msec}$ , slice number = 19, slice thickness = 5.0 mm,  $FOV = 24 \times 24\text{ cm}$ , and matrix size =  $256 \times 256$ .

### Lesion load, hypertension scores assessments

A binary lesion mask was manually drawn from T2WI to identify all visible lesions by an experienced neuroradiologist (F.Z.) using MRICron. The T2WI was coregistered with the T1-weighted structural image. After co-registration with the T1WI-based individual brain according to the Montreal Neurological Institute (MNI) standard brain dimensions, and this information was used to warp the lesion mask [as the normalized total white matter lesion load (TWMLL)] reflected the TWMLL relative to the standard MNI brain volume rather than the individual brain volume so that the effects of differences in brain volume were controlled (Pelletier et al., 2004).

According to the diagnosis of hypertension and the cardiovascular risk factors stratification standard (Williams et al., 2018), hypertension is divided into Grade I, Grade II, and Grade III, and we give corresponding scores of 1, 2 and 3; the degree of danger includes low risk, medium risk, high risk and very high risk, and the corresponding scores are 1, 2, 3, and 4. Total hypertension score is equal to hypertension

level score plus hypertension risk score. Based on patient admission diagnosis, the score of the WMHL patient is 2–5, as shown in Table 1.

## Demographic, BMI, clinical, and neuropsychological assessments

Demographic, clinical, and neuropsychological characteristics, including age, sex, disease duration (From the first diagnosis of the disease to enrollment), height (m) and weight (kg), Montreal Cognitive Assessment (MoCA), body mass index (BMI) is a person's weight in kilograms divided by the square of height in meters ( $\text{kg}/\text{m}^2$ ).

## Diffusion MRI connectometry analysis

The diffusion data were reconstructed in the MNI space using q-space diffeomorphic reconstruction (Yeh and Tseng, 2011) to obtain the spin distribution function (SDF) (Yeh et al., 2010) using DSI Studio.<sup>1</sup> With the default settings, a diffusion sampling length ratio of 1.25 was used. The sdf values were used in the connectometry analysis.

Diffusion MRI connectometry analysis enabled us to further investigate the specific pathways associated with study variable (Yeh et al., 2016). In this study, our study variables included hypertension scores, MoCA scores, BMI, TWMLL, duration of hypertension, and education. Because most study variable were highly correlated with each other, we first conducted a principal component analysis (PCA) to isolate the principal components that explained overall score variability. This avoided overfitting in the regression model. A multiple regression model was used to adjust for sex and age, and the following default parameters were used. At the group level, we used concatenated HC and WMHL data to create a connectometry database. Considering of higher length thresholds provide more specific results for identifying affected tracks, while lower length thresholds are more sensitive to potentially affected tracks. In our study, different length thresholds (30 mm, 40 mm, and 50 mm) were used to study the correlation at different significance levels between the two groups. To further analyze the study variables associated with tracks, we only used WMHL group data to create a connectometry database, a 40 mm length threshold was used to select tracks. The seeding density was 20 seeds per  $\text{mm}^3$ . Local connectomes were tracked using a deterministic fiber tracking algorithm. Track trimming was performed with 2 iterations. All tracks generated from bootstrap resampling were included. To estimate the false discovery rate (FDR), 2000 random permutations were applied to the group label to obtain the null distribution of the track length. An FDR lower than 0.05 can be considered as significant.

## Results

### Demographic and clinical data

Sixteen patients with WMHL and 20 HC were included in this study. Population and clinical characteristics are summarized in

**TABLE 1** Demographic and clinical characteristics of the study population.

	Patients with WMHL ( $n=16$ )	HC ( $n=20$ )	$p$ value
Age (years)	$57.06 \pm 6.85$	$55.90 \pm 5.39$	0.31 <sup>a</sup>
Sex (female: male)	8:8	12:8	0.46 <sup>b</sup>
Education level (years)	8.43(5–16)	9.4(5–14)	0.57 <sup>a</sup>
Duration (years)	8 (2–20)	–	–
MoCA scores	$20.44 \pm 4.40$	$24.60 \pm 2.01$	0.000 <sup>a</sup>
TWMLL( $\text{cm}^3$ )	67.62(19.56–285.69)	–	–
Hypertension scores	$3.06 \pm 1.29$	–	–
BMI( $\text{kg}/\text{m}^2$ )	$23.43 \pm 3.47$	$21.31 \pm 3.16$	0.003 <sup>a</sup>

MoCA, Montreal Cognitive Assessment; BMI, body mass index; WMHL, White matter hyperintensity lesions; HC, Healthy controls; TWMLL, total white matter lesion loads in the normalized standard brain. a: Two-sample  $t$  test; b: Chi square test.

**TABLE 2** Principle component analysis of the study variables.

	First component (IC1)	Second component (IC2)	Third component (IC3)
Variance explained(%)	32.939	26.542	27.718
	Component coefficient	Component coefficient	Component coefficient
Hypertension scores	0.712	0.511	−0.236
MoCA scores	0.466	0.812	0.439
BMI	0.374	−0.231	0.825
nTWMLL	−0.613	0.468	0.165
Duration	0.027	−0.774	0.153
Education	−0.645	0.292	0.289

Table 1. The WMHL has significantly lower MOCA scores and higher BMI than HC (respective  $p=0.000$  and  $p=0.003$ ).

## Principle component analysis

The PCA indicated that only three components were sufficient to explain 87.196% of the score variance. The first component was hypertension scores, with a coefficient of 0.712, which explained 32.936% of the behavioral data. The second component was MoCA, with a coefficient of 0.812, which explained 26.542% of the behavioral data. The third component was BMI, with a coefficient of 0.825, which explained the other 27.718%. The results are shown in Table 2.

## Tracks correlated with group

We use different length thresholds (30 mm, 40 mm, and 50 mm) to study the correlation at different significance levels between the two groups. Figure 1 shows the WMHL group had decreased fiber connectivity in the brain network compared with the HC. The FDR was 0.023, 0.013, 0.020 when the length was 30 mm, 40 mm, 50 mm,

<sup>1</sup> <http://dsi-studio.labsolver.org/>

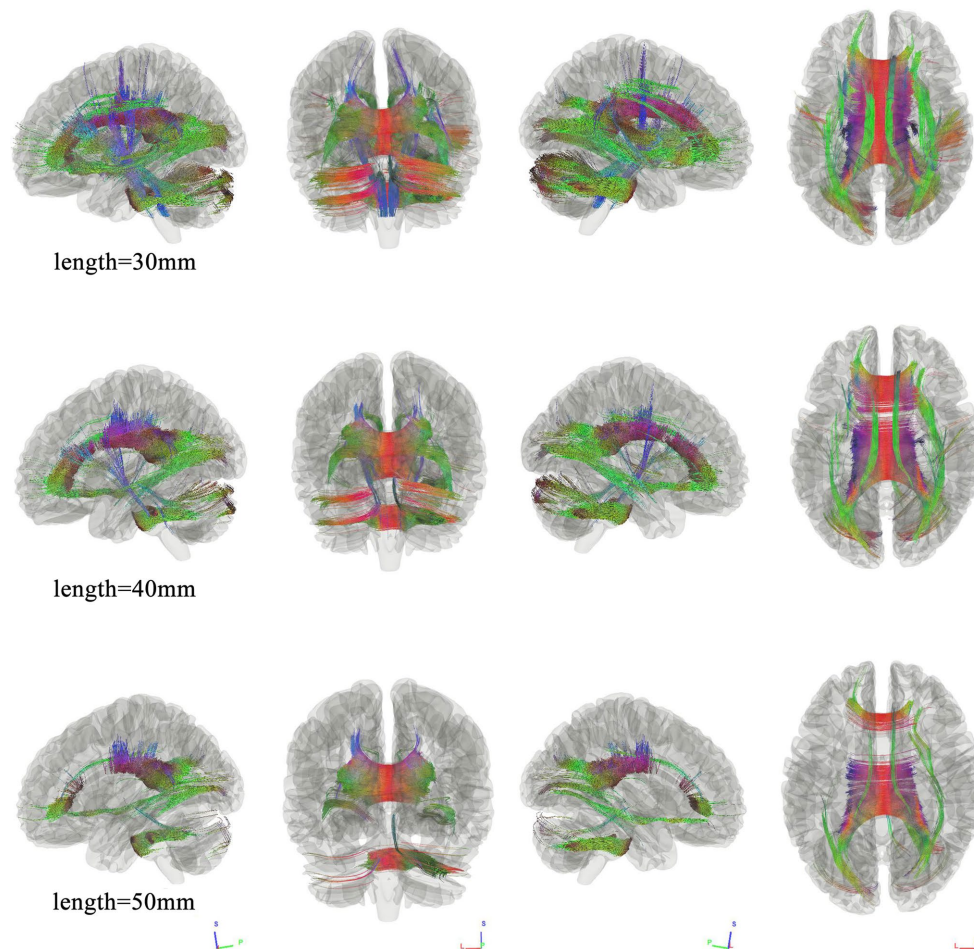


FIGURE 1

Connectometry results under different length thresholds between the two groups. Connectometry analysis identified connectivity differences that appeared and wide-spread the whole brain, involving bilateral association bundles, corpus callosum, projection bundles, and cerebellar peduncle. (FDR was 0.023, 0.013, 0.020 when the length was 30 mm, 40 mm, 50 mm, respectively).

respectively. The analysis showed that the differential tractography involving bilateral association bundles, corpus callosum, projection bundles and cerebellar peduncle.

## Tracks correlated with hypertension scores

We first used connectometry analysis to map the fiber pathways correlated with the first component of PCA, which was predominantly weighted by the hypertension score. Figure 2 shows the tracks negatively correlated with hypertension scores. The FDR was 0.044. The analysis indicated that the pathways correlated with hypertension cores were anterior splenium of corpus callosum (ASCC), bilateral inferior longitudinal fasciculus (ILF), anterior corpus callosum (ACC), middle cerebellar peduncle.

## Tracks correlated with MoCA

We used connectometry analysis to map fiber pathways correlated with the second PCA component, which was predominantly weighted by the MoCA scores. Figure 3 shows the tracks negatively correlated

with MoCA scores. The FDR was 0.016. The analysis indicated that the pathways correlated with MoCA scores were ASCC, left thalamoparietal pathways, right inferior longitudinal fasciculus ILF, and left cerebellar.

## Tracks correlated with BMI

We used connectometry analysis to map the fiber pathways correlated with the third PCA component, which was predominantly weighted by the BMI. Figure 4 shows the tracks negatively correlated with BMI. The FDR was 0.001. The analysis indicated that the pathways correlated with BMI were ASCC, bilateral inferior fronto-occipital fasciculus (IFOF), bilateral cingulum fasciculus, fornix/fimbria.

## Discussion

This study provides evidence for the association between white matter fibers and hypertension scores, MoCA scores, and BMI in patients with WMHL. Anatomically, ASCC, bilateral ILF, ACC, and middle cerebellar peduncle were significantly correlated with

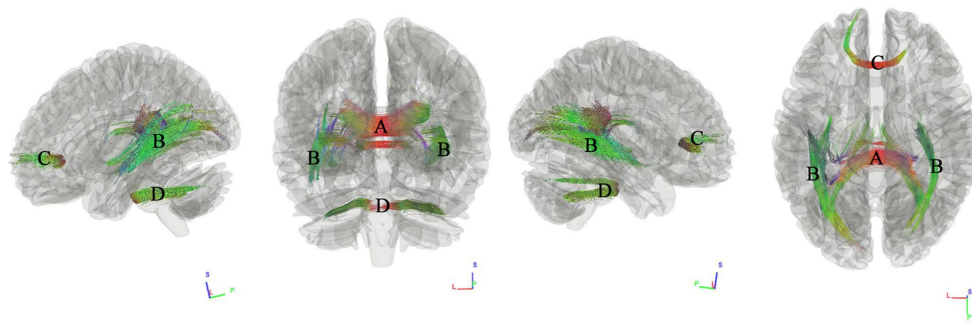


FIGURE 2

Tracks negatively correlated with hypertension scores in patients with WMHL. Connectometry analysis identified (A) anterior splenium of corpus callosum, (B) inferior longitudinal fasciculus, (C) anterior corpus callosum, (D) middle cerebellar peduncle with decreased connectivity to hypertension cores (FDR=0.044).

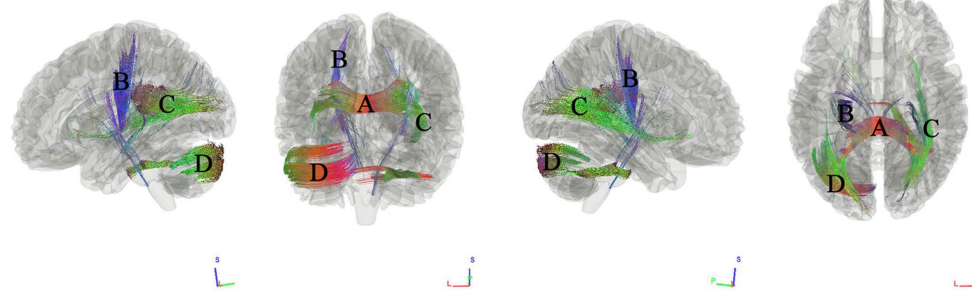


FIGURE 3

Tracks negatively correlated with MoCA scores in patients with WMHL. Connectometry analysis identified (A) anterior splenium of the corpus callosum, (B) left thalamoparietal pathways, (C) right inferior longitudinal fasciculus, and (D) left cerebellar with decreased connectivity to MoCA scores (FDR=0.016).

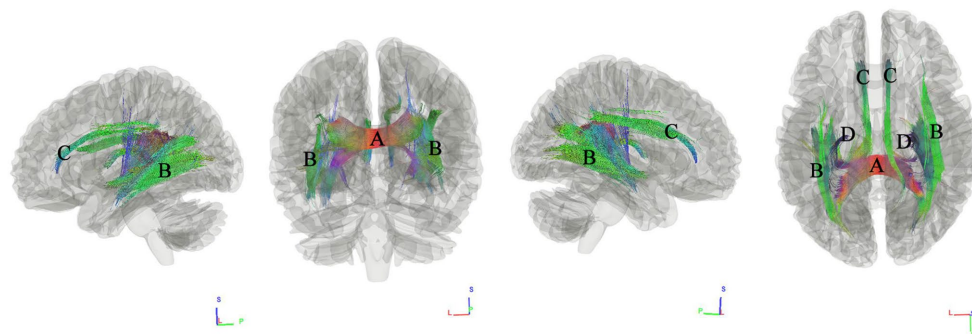


FIGURE 4

Tracks negatively correlated with BMI in patients with WMHL. Connectometry analysis identified (A) the anterior splenium of the corpus callosum, (B) inferior fronto-occipital fasciculus, (C) cingulum fasciculus, and (D) fornix/fimbria with decreased connectivity to BMI (FDR=0.001).

hypertension scores. ASCC, left thalamoparietal pathways, right ILF, and left cerebellar were significantly correlated with MoCA scores. ASCC, IFOF, cingulum fasciculus, fornix/fimbria were significantly correlated with BMI.

Hypertension is a well-known significant risk factor for WMHL, which is closely related to WMHL progression. Among hypertensive individuals, the prevalence of WMHL may rise to 40–44% (Liao et al.,

1996; Verhaaren et al., 2013; Gebeily et al., 2014; Sargurupremraj et al., 2020). In addition, hypertension is highly relevant to the annual progression of WMHL. People with uncontrolled untreated hypertension had significantly more WMHL progression than regular treatment (Verhaaren et al., 2013; Shen et al., 2022). In our study, we found that decreased connectivity in ASCC, bilateral ILF, ACC, and middle cerebellar peduncle were significantly negatively correlated

with hypertension scores. Previous studies have reported the relationship between hypertension and lower microstructural fiber density, macrostructural fiber bundle cross-section, and a combination of both, such as corpus callosum, ILF, and middle cerebellar peduncle (Gons et al., 2012; Li et al., 2015; Wong et al., 2017; Andica et al., 2022). Studies have also found impaired microstructural integrity of the corpus callosum in hypertensive patients compared to normotensive patients in individuals with cerebral small vessel disease (Gons et al., 2012). This may be related to the vulnerability of posterior brain regions to vascular risk factors (Artero et al., 2004). The fibers in splenium are projections from the occipital-parietal and temporal cortex. It has been shown to be involved in language, reading, and calculation skills, IQ, conduct, and consciousness (Blaauw and Meiners, 2020). The ILF is a long-range white matter pathway that primarily connects the occipital lobe of the brain with the anterior temporal lobe. It may involve a wide range of brain functions concerning the visual modality, including object, face and place processing, reading, lexical and semantic processing, emotion processing, and visual memory (Herbet et al., 2018). Previous studies have mostly found that hypertension shows significantly reduced white matter integrity in the bilateral superior longitudinal fasciculus (Li et al., 2015). In patients with WMHL with higher FA values, the integrity of the ILF moderates the association between higher WMHL and slower gait speed (Rosario et al., 2016). The middle cerebellar peduncles are the main afferent pathway to the cerebellum and are composed of white matter fibers originating from the contralateral pontine nuclei. The pontine nuclei are intermediate gray matter scattered in the basis pons and part of the corticopontocerebellar pathway that controls not only the action of motor tasks but also the planning and initiation of movements. Thus, difficulty walking (cerebellar ataxia), difficulty speaking (scanning speech), and in some cases vertigo and facial weakness are common clinical manifestations of middle cerebellar peduncles lesion (Morales and Tomsick, 2015).

Compared to HC, patients with WMHL has been associated with an increased risk of cognitive impairment and a significantly greater burden (Hu et al., 2021; Dadar et al., 2022). Our study found that hypertension scores and MoCA scores show a significant correlation with decreased connectivity in corpus callosum and ILF. Previous studies have reported that disruption of the corpus callosum microstructure especially the WMHL penumbra of the corpus callosum body may contribute to cognitive deficits associated with subcortical ischemic vascular disease (Qiu et al., 2021). Microstructural disruption of the right IFOF and ILF contributes to WMHL-related cognitive impairment (Chen et al., 2020) which is basically consistent with our research results, the effect of WMHL on the microstructural integrity of WM tracts may propagate along tracts to distal regions beyond the penumbra (Liu et al., 2021). In addition, in our study, decreased connectivity in left thalamoparietal pathways and left cerebellar were negatively correlated with MoCA scores. The thalamus is a crucial node in networks supporting cognitive functions known to deteriorate with normal aging, including component processes of memory and executive functions of attention and information processing (Fama and Sullivan, 2015). The cerebellum has both sensorimotor and cognitive effects. The lesions of the anterior lobe lead to dyskinesia, and the lesions of the posterior lobe result in cerebellar cognitive affective syndrome, which may explain WMHL susceptibility to motor and emotional disorders or other symptoms (Schmahmann, 2019).

In our study, patients with WMHL had higher BMI. Interestingly, previous studies have reported that higher BMI contributed to an

increased deep-periventricular WMHL ratio (Lampe et al., 2019), which may be due to obesity leading to higher white matter burden through inflammatory processes, as indexed by elevated IL-6. Negative BMI associations are widely distributed across white matter pathways in a largely bilateral pattern primarily in corpus callosum, which is consistent with our findings (Karlsson et al., 2013; Verstynen et al., 2013). In particular, we found that BMI was negatively correlated with cingulum fasciculus, fornix/fimbria, which are the most prominent tracts within the limbic system. The fornix is a C-shaped fiber bundle that provides strong connections from the hippocampus to other brain regions. The cingulum is another C-shaped structure of WM fiber wrapped around the frontal and temporal lobe above the corpus callosum. The anterior part is important for emotion processing, while the posterior region is involved in cognition. This result may show BMI's heterogeneous association with white matter pathways across the brain (Verstynen et al., 2013).

Our research still has several limitations. First, the age range of patients and sample sizes were small, a larger sample should be used in future studies. Secondly, the lack of longitudinal traces cannot provide evidence for progressive changes between white matter hyperintensities and the main clinical features, in future, research based on longitudinal data may make the correlations we observe more specific. In addition to the clinical features discussed in this paper, other factors such as smoking, alcohol consumption, diabetes, and hyperlipemia are risk factors for WMHL. Further research is needed to include hypertensive patients with different accompanying symptoms (eg. cerebrovascular disease, cardiovascular disease, kidney disease, etc.) in the future. Especially longitudinal studies may better describe this characteristic in patients with WMHL.

In conclusion, this study employed a novel approach to diffusion connectometry to identify hypertension related clinical features and corresponding white matter structures. This preliminary study results support hypertension degree and higher BMI are associated with white matter local disconnection in patients with WMHL, and may contribute to understanding the cognitive impairments observed in patients with WMHL.

## Data availability statement

The raw data supporting the conclusions of this article will be made available by the authors, without undue reservation.

## Ethics statement

The studies involving human participants were reviewed and approved by Medical Research Ethics Committee of the First Affiliated Hospital of Nanchang University. The patients/participants provided their written informed consent to participate in this study.

## Author contributions

FZ, QK, MH, YL, and LW: conceptualization. YL, QK, and MH: data collection. FZ, MH, QK, and LW: data analysis. FZ: funding analysis. MH, QK, FZ, LW, JD, and YL: investigation, writing—original draft, and writing—review and editing. FZ, LW, and YL:

supervision. All authors contributed to the article and approved the submitted version.

## Funding

This study was supported by the National Science Foundation of China (Grant no 82160331).

## Acknowledgments

The authors thank their patients and volunteers for participating in this study. The funders had no role in the study design, data collection and analysis, decision to publish, or preparation of the manuscript.

## References

- Alber, J., Alladi, S., Bae, H. J., Barton, D. A., Beckett, L. A., Bell, J. M., et al. (2019). White matter hyperintensities in vascular contributions to cognitive impairment and dementia (VCID): knowledge gaps and opportunities. *Alzheimers Dement (N Y)* 5, 107–117. doi: 10.1016/j.trci.2019.02.001
- Andica, C., Kamagata, K., Uchida, W., Takabayashi, K., Shimoji, K., Kaga, H., et al. (2022). White matter fiber-specific degeneration in older adults with metabolic syndrome. *Mol Metab* 62:101527. doi: 10.1016/j.molmet.2022.101527
- Artero, S., Tiemeier, H., Prins, N. D., Sabatier, R., Breteler, M. M., and Ritchie, K. (2004). Neuroanatomical localisation and clinical correlates of white matter lesions in the elderly. *J. Neurol. Neurosurg. Psychiatry* 75, 1304–1308. doi: 10.1136/jnnp.2003.023713
- Blaauw, J., and Meiners, L. C. (2020). The splenium of the corpus callosum: embryology, anatomy, function and imaging with pathophysiological hypothesis. *Neuroradiology* 62, 563–585. doi: 10.1007/s00234-019-02357-z
- Chen, H. F., Huang, L. L., Li, H. Y., Qian, Y., Yang, D., Qing, Z., et al. (2020). Microstructural disruption of the right inferior fronto-occipital and inferior longitudinal fasciculus contributes to WMHL-related cognitive impairment. *CNS Neurosci. Ther.* 26, 576–588. doi: 10.1111/cns.13283
- Dadar, M., Mahmoud, S., Zhernovaia, M., Camicioli, R., Maranzano, J., and Duchesne, S. (2022). White matter hyperintensity distribution differences in aging and neurodegenerative disease cohorts. *Neuroimage Clin.* 36:103204. doi: 10.1016/j.nicl.2022.103204
- Debette, S., and Markus, H. S. (2010). The clinical importance of white matter hyperintensities on brain magnetic resonance imaging: systematic review and meta-analysis. *BMJ* 341:c3666. doi: 10.1136/bmj.c3666
- Fama, R., and Sullivan, E. V. (2015). Thalamic structures and associated cognitive functions: relations with age and aging. *Neurosci. Biobehav. Rev.* 54, 29–37. doi: 10.1016/j.neubiorev.2015.03.008
- Frantellizzi, V., Pani, A., Ricci, M., Locuratolo, N., Fattapposta, F., and De Vincentis, G. (2020). Neuroimaging in vascular cognitive impairment and dementia: a systematic review. *J. Alzheimers Dis.* 73, 1279–1294. doi: 10.3233/jad-191046
- Frey, B. M., Petersen, M., Mayer, C., Schulz, M., Cheng, B., and Thomalla, G. (2019). Characterization of white matter Hyperintensities in large-scale MRI-studies. *Front. Neurol.* 10:238. doi: 10.3389/fneur.2019.00238
- Gebeily, S., Fares, Y., Kordahi, M., Khodeir, P., Labaki, G., and Fazekas, F. (2014). Cerebral white matter hyperintensities (WMHL): an analysis of cerebrovascular risk factors in Lebanon. *Int. J. Neurosci.* 124, 799–805. doi: 10.3109/00207454.2014.884087
- Gons, R. A., van Oudheusden, L. J., de Laat, K. F., van Norden, A. G., van Uden, I. W., Norris, D. G., et al. (2012). Hypertension is related to the microstructure of the corpus callosum: the RUN DMC study. *J. Alzheimers Dis.* 32, 623–631. doi: 10.3233/jad-2012-121006
- Herbet, G., Zemmoura, I., and Duffau, H. (2018). Functional anatomy of the inferior longitudinal fasciculus: from historical reports to current hypotheses. *Front. Neuroanat.* 12:77. doi: 10.3389/fnana.2018.00077
- Hu, H. Y., Ou, Y. N., Shen, X. N., Qu, Y., Ma, Y. H., Wang, Z. T., et al. (2021). White matter hyperintensities and risks of cognitive impairment and dementia: a systematic review and meta-analysis of 36 prospective studies. *Neurosci. Biobehav. Rev.* 120, 16–27. doi: 10.1016/j.neubiorev.2020.11.007
- Karlsson, H. K., Tuuluri, J. J., Hirvonen, J., Lepomäki, V., Parkkola, R., Hiltunen, J., et al. (2013). Obesity is associated with white matter atrophy: a combined diffusion

## Conflict of interest

The authors declare that the research was conducted in the absence of any commercial or financial relationships that could be construed as a potential conflict of interest.

## Publisher's note

All claims expressed in this article are solely those of the authors and do not necessarily represent those of their affiliated organizations, or those of the publisher, the editors and the reviewers. Any product that may be evaluated in this article, or claim that may be made by its manufacturer, is not guaranteed or endorsed by the publisher.

- tensor imaging and voxel-based morphometric study. *Obesity (Silver Spring)* 21, 2530–2537. doi: 10.1002/oby.20386
- Lampe, L., Zhang, R., Beyer, F., Huhn, S., Kharabian Masouleh, S., Preusser, S., et al. (2019). Visceral obesity relates to deep white matter hyperintensities via inflammation. *Ann. Neurol.* 85, 194–203. doi: 10.1002/ana.25396
- Li, X., Liang, Y., Chen, Y., Zhang, J., Wei, D., Chen, K., et al. (2015). Disrupted Frontoparietal network mediates white matter structure dysfunction associated with cognitive decline in hypertension patients. *J. Neurosci.* 35, 10015–10024. doi: 10.1523/jneurosci.5113-14.2015
- Liao, D., Cooper, L., Cai, J., Toole, J. F., Bryan, N. R., Hutchinson, R. G., et al. (1996). Presence and severity of cerebral white matter lesions and hypertension, its treatment, and its control. The ARIC study. Atherosclerosis risk in communities study. *Stroke* 27, 2262–2270. doi: 10.1161/01.str.27.12.2262
- Liu, Y., Xia, Y., Wang, X., Wang, Y., Zhang, D., Nguchu, B. A., et al. (2021). White matter hyperintensities induce distal deficits in the connected fibers. *Hum. Brain Mapp.* 42, 1910–1919. doi: 10.1002/hbm.25338
- Lu, T., Wang, Z., Cui, Y., Zhou, J., Wang, Y., and Ju, S. (2021). Disrupted structural brain connectome is related to cognitive impairment in patients with ischemic Leukoaraisosis. *Front. Hum. Neurosci.* 15:654750. doi: 10.3389/fnhum.2021.654750
- Maillard, P., Fletcher, E., Harvey, D., Carmichael, O., Reed, B., Mungas, D., et al. (2011). White matter hyperintensity penumbra. *Stroke* 42, 1917–1922. doi: 10.1161/strokeaha.110.609768
- Meng, F., Yang, Y., and Jin, G. (2022). Research Progress on MRI for white matter Hyperintensity of presumed vascular origin and cognitive impairment. *Front. Neurol.* 13:865920. doi: 10.3389/fneur.2022.865920
- Min, Z. G., Shan, H. R., Xu, L., Yuan, D. H., Sheng, X. X., Xie, W. C., et al. (2021). Diffusion tensor imaging revealed different pathological processes of white matter hyperintensities. *BMC Neurol.* 21:128. doi: 10.1186/s12883-021-02140-9
- Morales, H., and Tomsick, T. (2015). Middle cerebellar peduncles: magnetic resonance imaging and pathophysiologic correlate. *World J. Radiol.* 7, 438–447. doi: 10.4329/wjr.v7.i12.438
- Pelletier, D., Garrison, K., and Henry, R. (2004). Measurement of whole-brain atrophy in multiple sclerosis. *J. Neuroimaging* 14, 11S–19S. doi: 10.1111/j.1552-6569.2004.tb00274.x
- Qiu, X., Yu, L., Ge, X., Sun, Y., Wang, Y., Wu, X., et al. (2021). Loss of integrity of Corpus callosum white matter Hyperintensity penumbra predicts cognitive decline in patients with subcortical vascular mild cognitive impairment. *Front. Aging Neurosci.* 13:605900. doi: 10.3389/fnagi.2021.605900
- Rosario, B. L., Rosso, A. L., Aizenstein, H. J., Harris, T., Newman, A. B., Satterfield, S., et al. (2016). Cerebral white matter and slow gait: contribution of Hyperintensities and Normal-appearing parenchyma. *J. Gerontol. A Biol. Sci. Med. Sci.* 71, 968–973. doi: 10.1093/gerona/glv224
- Sargurupremraj, M., Suzuki, H., Jian, X., Sarnowski, C., Evans, T. E., Bis, J. C., et al. (2020). Cerebral small vessel disease genomics and its implications across the lifespan. *Nat. Commun.* 11:6285. doi: 10.1038/s41467-020-19111-2
- Schmahmann, J. D. (2019). The cerebellum and cognition. *Neurosci. Lett.* 688, 62–75. doi: 10.1016/j.neulet.2018.07.005
- Shen, X., Raghavan, S., Przybelski, S. A., Lesnick, T. G., Ma, S., Reid, R. I., et al. (2022). Causal structure discovery identifies risk factors and early brain markers related to evolution of white matter hyperintensities. *Neuroimage Clin.* 35:103077. doi: 10.1016/j.nicl.2022.103077

- van Rooden, S., van den Berg-Huysmans, A. A., Croll, P. H., Labadie, G., Hayes, J. M., Viviano, R., et al. (2018). Subjective cognitive decline is associated with greater white matter Hyperintensity volume. *J. Alzheimers Dis.* 66, 1283–1294. doi: 10.3233/jad-180285
- Verhaaren, B. F., Vernooij, M. W., de Boer, R., Hofman, A., Niessen, W. J., van der Lugt, A., et al. (2013). High blood pressure and cerebral white matter lesion progression in the general population. *Hypertension* 61, 1354–1359. doi: 10.1161/hypertensionaha.111.00430
- Verstynen, T. D., Weinstein, A., Erickson, K. I., Sheu, L. K., Marsland, A. L., and Gianaros, P. J. (2013). Competing physiological pathways link individual differences in weight and abdominal adiposity to white matter microstructure. *NeuroImage* 79, 129–137. doi: 10.1016/j.neuroimage.2013.04.075
- Wardlaw, J. M., Smith, E. E., Biessels, G. J., Cordonnier, C., Fazekas, F., Frayne, R., et al. (2013). Neuroimaging standards for research into small vessel disease and its contribution to ageing and neurodegeneration. *Lancet Neurol.* 12, 822–838. doi: 10.1016/s1474-4422(13)70124-8
- Williams, B., Mancia, G., Spiering, W., Agabiti Rosei, E., Azizi, M., Burnier, M., et al. (2018). 2018 ESC/ESH guidelines for the management of arterial hypertension: the task force for the management of arterial hypertension of the European Society of Cardiology and the European Society of Hypertension: the task force for the management of arterial hypertension of the European Society of Cardiology and the European Society of Hypertension. *J. Hypertens.* 36, 1953–2041. doi: 10.1097/hjh.0000000000001940
- Wong, N. M. L., Ma, E. P., and Lee, T. M. C. (2017). The integrity of the Corpus callosum mitigates the impact of blood pressure on the ventral attention network and information processing speed in healthy adults. *Front. Aging Neurosci.* 9:108. doi: 10.3389/fnagi.2017.00108
- Wu, X., Ge, X., Du, J., Wang, Y., Sun, Y., Han, X., et al. (2019). Characterizing the penumbras of white matter Hyperintensities and their associations with cognitive function in patients with subcortical vascular mild cognitive impairment. *Front. Neurol.* 10:348. doi: 10.3389/fneur.2019.00348
- Yeh, F. C., Badre, D., and Verstynen, T. (2016). Connectometry: a statistical approach harnessing the analytical potential of the local connectome. *NeuroImage* 125, 162–171. doi: 10.1016/j.neuroimage.2015.10.053
- Yeh, F. C., and Tseng, W. Y. (2011). NTU-90: a high angular resolution brain atlas constructed by q-space diffeomorphic reconstruction. *NeuroImage* 58, 91–99. doi: 10.1016/j.neuroimage.2011.06.021
- Yeh, F. C., Wedeen, V. J., and Tseng, W. Y. (2010). Generalized q-sampling imaging. *IEEE Trans. Med. Imaging* 29, 1626–1635. doi: 10.1109/tmi.2010.2045126
- Yuan, J. L., Wang, S. K., Guo, X. J., Teng, L. L., Jiang, H., Gu, H., et al. (2017). Disconnections of Cortico-subcortical pathways related to cognitive impairment in patients with Leukoaraiosis: a preliminary diffusion tensor imaging study. *Eur. Neurol.* 78, 41–47. doi: 10.1159/000477899
- Zhong, G., Zhang, R., Jiaerken, Y., Yu, X., Zhou, Y., Liu, C., et al. (2017). Better correlation of cognitive function to white matter integrity than to blood supply in subjects with Leukoaraiosis. *Front. Aging Neurosci.* 9:185. doi: 10.3389/fnagi.2017.00185



## OPEN ACCESS

## EDITED BY

Tingyuan Lang,  
Chongqing University, China

## REVIEWED BY

Arianna Polverino,  
Università degli Studi di Napoli Parthenope,  
Italy  
Cinzia Coppola,  
Università Della Campania Luigi Vanvitelli, Italy

## \*CORRESPONDENCE

Jingping Shi  
✉ profshijp@163.com

†These authors have contributed equally to this work

RECEIVED 13 March 2023

ACCEPTED 20 June 2023

PUBLISHED 04 July 2023

## CITATION

Wang Y, Ye X, Song B, Yan Y, Ma W and Shi J (2023) Features of event-related potentials during retrieval of episodic memory in patients with mild cognitive impairment due to Alzheimer's disease. *Front. Neurosci.* 17:1185228. doi: 10.3389/fnins.2023.1185228

## COPYRIGHT

© 2023 Wang, Ye, Song, Yan, Ma and Shi. This is an open-access article distributed under the terms of the [Creative Commons Attribution License \(CC BY\)](https://creativecommons.org/licenses/by/4.0/). The use, distribution or reproduction in other forums is permitted, provided the original author(s) and the copyright owner(s) are credited and that the original publication in this journal is cited, in accordance with accepted academic practice. No use, distribution or reproduction is permitted which does not comply with these terms.

# Features of event-related potentials during retrieval of episodic memory in patients with mild cognitive impairment due to Alzheimer's disease

Yingying Wang<sup>†</sup>, Xing Ye<sup>†</sup>, Bo Song, Yixin Yan, Wenyan Ma and Jingping Shi\*

Department of Neurology, Affiliated Nanjing Brain Hospital, Nanjing Medical University, Nanjing, China

**Objective:** To provide a rigorous comparison between patients with mild cognitive impairment due to Alzheimer's disease (MCI-AD) and healthy elderly, as well as to assess the value of electroencephalography (EEG) in terms of early diagnosis, we conducted a neutral image recognition memory task involving individuals with positive biomarkers including  $\beta$  amyloid deposition, pathologic tau or neurodegeneration.

**Methods:** The task involving study and test blocks was designed to evaluate participants' recognition memory. Electroencephalogram was recorded synchronously to elicit event-related potentials in patients with MCI-AD and healthy control subjects. We further analyzed differences between groups or conditions in terms of behavioral performance, time domain, and time-frequency domain.

**Results:** The MCI-AD cohort showed a slower response time to old/new images and had low accuracy regarding behavioral performance. The amplitude of the late positive complex for the old/new effects was significantly suppressed in the MCI-AD cohort when compared with that in the HC cohort. The amplitude of the late old/new effects was correlated with the Auditory Verbal Learning Test recognition score in all participants. The time-frequency domain analysis revealed that correct recognition of old items elicited a decrease in beta power, mainly limited to the HC cohort. Moreover, the combination of behavioral (processing speed and accuracy) and electrophysiological (average amplitude and relative power of delta band) measures contributes to classifying patients with MCI-AD from healthy elderly people.

**Conclusion:** Changes of old/new effects, accuracy and response time are sensitive to the impairment of recognition memory in patients with MCI-AD and have moderate value in predicting the incipient stage of AD.

## KEYWORDS

event-related potential, electroencephalography, mild cognitive impairment, Alzheimer's disease, recognition memory

# 1. Introduction

According to the World Health Organization, more than 55 million people worldwide live with dementia, as reported in 2022, which has imposed a huge economic and healthcare burden (Jia et al., 2018). Alzheimer's disease (AD) is the major type of dementia, accounting for 60–70% of the total dementia cases (Ferreira et al., 2014). In the absence of a cure, risk reduction, timely diagnosis, and early intervention have become the mainstay of people's attention (Robinson et al., 2015). However, Alzheimer's Disease International has reported that 75% of people who live with dementia worldwide are not diagnosed clinically and that is not to mention about post-diagnosis support (Bamford et al., 2021).

Mild cognitive impairment due to AD (MCI-AD) is the symptomatic prodementia phase of AD, and such people may progress to AD-related dementia over time (Albert et al., 2011). However, people who receive effective interventions may have longer disability-free life expectancy. In AD, extracellular amyloid- $\beta$  (A $\beta$ ) aggregates and intracellular tau neurofibrillary tangles are typical pathological features that can persist for more than two decades before the onset of symptoms (Villemagne et al., 2018). These pathological changes can damage synapse structure and function, thereby promoting neurodegeneration and resulting in cognitive impairment (Sheng et al., 2012). Although various techniques enable accurate in-vivo assessment of AD biology through cerebrospinal fluid (CSF) analysis or amyloid positron emission tomography imaging, their application is slightly restricted for individuals with preclinical AD or for large-scale screening considering invasiveness, time, and cost concerns. Thus, newer tools or technology is required to improve the convenience and accuracy of early diagnosis.

Tools such as quantitative electroencephalography (qEEG) or event-related potentials (ERPs) are suitable not only for studying neurocognitive processes because they directly measure neural activity and may provide sensitive biomarkers for the early diagnosis of AD but also for assessing the effectiveness of novel interventions (Horvath et al., 2018). Given that cognitive, perceptual, linguistic, emotional, and motor processes are fast, EEG and related methods can capture cognitive dynamics within tens to hundreds of milliseconds. Characteristics of waveforms, spectral power, and event-related oscillatory responses can be useful for differentiating the cognitive status, and the differences have shown a relationship with the scores of common neuropsychological tests assessing cognitive functions, which make EEG and related methods ideal for quantifying cognitive decline (Yener and Başar, 2013; Horvath et al., 2018). Many studies have used qEEG or ERP indices as biomarkers of MCI or early AD. Generally, patients with MCI or early AD have decreased alpha and beta band power and increased theta band power of EEG when compared with those of healthy aging adults (Jelic et al., 2000; Horvath et al., 2018). Furthermore, ERPs are useful for studying specific cognitive processes including sensory, motor, or perceptual processes as well as cognitive operations. Visually elicited ERPs and auditory ERPs, containing components such as N200 or P300, may be useful for identifying older adults who are at high risk of developing MCI and AD (Morrison et al., 2018, 2019). Among various metrics, a reduction and slowing of the P300 response is relatively consistent (Jiang et al., 2015). However, this phenomenon can

also be observed in other types of dementia, for example, vascular dementia (Egerházi et al., 2008).

Impairment in episodic memory is commonly seen in patients with MCI-AD, reflecting a declining ability to learn and remember new information. In this regard, more attention should be paid to ERP components related to long-term memory, with a specific focus on episodic memory retrieval (Kappenman and Steven, 2011). ERPs are acquired and tested during separate test phases of a verbal or image recognition memory task (Dzulkifli et al., 2006; Waninger et al., 2018). Many studies have consistently reported retrieval-related effects, termed as “old/new effects,” that take the form of different ERPs for old (studied/previously seen) test items relative to new (non-studied/not seen) items. The ERPs show two effects. One effect is the early mid-frontal difference that occurs in the range of 300–500 ms after onset, which was first called “FN400” by Curran (1999). According to the dual-process theory (Mickes et al., 2009), the FN400 effect is related to familiarity, a sense reflecting the assessment of the experimental familiarity of a test item (Curran and Hancock, 2007). Some studies have hypothesized that this effect is related to an implicit form of memory called “conceptual fluency,” which is the subjective experience of ease or difficulty when processing information (Voss and Paller, 2006; Oppenheimer, 2008; Lucas et al., 2012). The other effect is the late positive potential (LPP) that is evoked in the range of 400–800 ms with a left parietal topography (Curran, 2000). The LPP is linked to the action of retrieving specific information.

Recent studies have shown that individuals with MCI have a reduction in the old/new effects that are generally observed in healthy control (HC) subjects (Yang et al., 2015; Waninger et al., 2018) and the reduction were consistent with neuropsychological assessments. Based on the above information, ERPs could be a suitable alternative owing to their sensitivity, low cost, and accessibility during the prescreening procedure to identify individuals with MCI.

In the present study, we performed an image recognition memory task together with response time measures and compared the outcomes between a cohort of patients diagnosed with MCI-AD and age-matched HC subjects. We adopted stricter inclusion criteria for the MCI-AD cohort by combining core clinical standards and CSF biomarkers, thus extending the results to early stage AD more precisely. Additionally, given that pictures with different emotional messages influence old/new responses (Weiss et al., 2008), we used neutral images collected from the International Affective Picture System (IAPS) to avoid any bias. The present study aimed to discover potential features during the retrieval of episodic memory to validate the ERP tasks as sensitive biomarkers for early stage AD. We hypothesized that patients with MCI-AD will have suppressed old/new effects in the image recognition memory task and that the ERP measurements may correlate with cognitive function evaluation.

## 2. Materials and methods

### 2.1. Participants

A total of 24 patients with MCI-AD and 31 HC subjects were enrolled in this study from the Department of Neurology at Nanjing

Brain Hospital between October 2020 and May 2022. A diagnosis of MCI-AD was made only when core clinical criteria and a positive biomarker reflecting A $\beta$  deposition, as proposed by the National Institute on Aging and Alzheimer's Association (NIA-AA) Working Group, were satisfied simultaneously (Albert et al., 2011).

The inclusion criteria of patients were as follows: right-handed adults aged 50–79 years old; no obvious visual or hearing impairment; at least primary school education (6 years of education); chief complaint of memory impairment and objective evidence of impairment, with Mini-Mental State Examination (MMSE) scores being greater than 20; preserved independent ability in activities of daily living; and disease meeting the definition for Alzheimer's continuum in accordance with the 2018 NIA-AA research framework (Jack et al., 2018). Subjects with any other systemic or brain diseases due to vascular, traumatic, and medical causes, such as hypothyroidism, cerebrovascular disease and brain trauma, that may have contributed to the cognitive decline were not included.

As control subjects, healthy elderly adults who were relatives of patients or community volunteers and had no evidence of a dementing or other neuropsychological disorder were recruited. The present study received approval from the Medical Research Ethics Committee of the Brain Hospital Affiliated to Nanjing Medical University. All participants enrolled in this study signed the informed consent before study initiation.

## 2.2. Clinical and neuropsychological assessments

The participants in both cohorts underwent comprehensive and standard clinical and neuropsychological assessments. Neuropsychological tests included the MMSE (Tombaugh and McIntyre, 1992), Montreal Cognitive Assessment (MoCA) (Horton et al., 2015), Hasegawa's Dementia Scale (HDS) (Gao, 1991), Clinical Dementia Rating (CDR) (Morris, 1993), Auditory Verbal Learning Test (AVLT) (Vakil and Blachstein, 1993), Hamilton Anxiety Scale (HAMA), and Hamilton Depression Scale (HAMD) (Bagby et al., 2004). Using these neuropsychological scales, experienced neuropsychologists evaluated participants' general cognitive function, episodic memory, and emotional state.

## 2.3. Cerebrospinal fluid biomarkers

All 24 patients underwent a lumbar puncture to confirm the CSF profile of AD pathology including A $\beta$ 1-42 and A $\beta$ 40 concentrations, A $\beta$ 42/A $\beta$ 40 ratio, and phosphorylated tau and total tau levels. These biomarkers were detected using INNO-BIA AlzBio3 immunoassay kit-based reagents (Innotest, Fujirebio, Ghent, Belgium). The cutoff values were set based on the patient groups studied and laboratory experience summarized by Mulder et al. (2010).

## 2.4. Design of the image recognition task

The image recognition task involving a study block and a test block was designed to evaluate the memory encoding and retrieval

processes. All 40 images, which could be seen frequently in daily life and had no positive or negative emotional bias, were selected carefully from the IAPS.

In the study block, the participants were presented with eight different pictures on the screen for maximum 1.0 s, with a 1.5 s interstimulus interval. These images were shown five times randomly on the left or right side of the cross-point “+,” and the participants were instructed to memorize each image to the best of their ability. The participants were then required to judge the position (right/left) of the pictures by pressing a button using their thumb (right/left thumb, respectively). When the participants entered the response within 1.0 s, the picture would disappear directly.

In the test block, a total of 64 trials comprising old pictures and 32 new pictures were shown on the center of the screen pseudo-randomly. Next, the participants were asked to judge whether they had already seen the picture in the study block. When the participants thought that they had seen the picture previously, they were asked to press the left button; otherwise, they were asked to press the right button. Even if the participants were unable to remember, they were asked to make a choice as soon as possible. Stimuli were generated and controlled using MATLAB and the Psychophysics Toolbox (Brainard, 1997). Example images are shown in Figure 1.

## 2.5. Behavioral data derived from the cognitive task

During the cognitive task, the participants were asked to finish the “right/left” or “old/new” judgment test. Accuracy was calculated as the percentage of correct trials per condition, including correct responses to old pictures (“Hits”) and correct rejections. Response time (RT) was defined as the time taken to press the button relative to the onset of trials, and the values were averaged separately for each condition, in a similar manner. Trials with incorrect responses or RT of < 200 or > 2,500 ms were excluded in response time analysis (Kappenman et al., 2014).

## 2.6. EEG recordings and preprocessing

The EEG signals were recorded at a sampling rate of 1,000 Hz using 64 electrodes in a BrainCap and amplified using BrainAmp DC (actiCHamp Plus, Brain Products GmbH, Gilching, Germany). The signal was low-pass filtered (100 Hz) online with a common reference between the Cz and Fz electrodes. Vertical electrooculography (EOG) was recorded from below the left eye, and horizontal EOG was recorded from the external right ocular canthus to detect blinks and eye movements. Electrode impedances were maintained below 10 k $\Omega$ . The recordings were preprocessed and analyzed offline using MATLAB (MathWorks Inc., Natick, MA, USA), EEGLAB software (MathWorks Inc., Natick, MA, USA), and FieldTrip toolbox. First, EOG channels were excluded, and then, raw EEG signals were re-referenced offline to global cerebral average reference, after which they were band-pass filtered offline at 0.1–40 Hz and down-sampled to 250 Hz. For continuous EEG data, independent component analysis was performed using EEGLAB

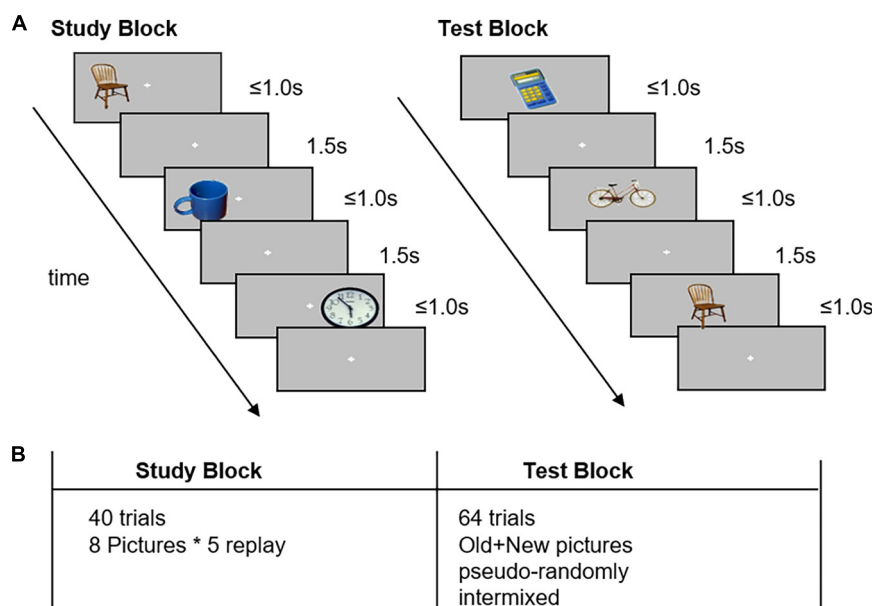


FIGURE 1

Task design in the image recognition memory task. Panel (A): The experiment comprised a study block and a test block. In the study block, participants memorized the pictures and identified the relative location of the pictures to the fixation cross. In the test block, the participants were asked to identify previously seen items and press the button with their left thumb; if they were unable to recognize, they pressed the button with their right thumb. Panel (B): The study consisted of 40 trials of neutral pictures. The test block consisted of 64 trials of studied (old) and non-studied (new) pictures, which were pseudo-randomly interleaved.

software. EEG artifacts (e.g., blinks and eye movements as well as electrical and sensor noise) were isolated and removed using BESA Research automatic artifact correction (Berg and Scherg, 1994).

## 2.7. Analysis of event-related potentials (ERPs)

The continuous EEG data were epoched from 0.5 s before until 1.5 s after stimulus onset. Baseline was removed using data from 500 ms before stimulus onset. Trials with gross artifacts, for example, large physical movement artifacts, were excluded by visual inspection. The remaining trials in the recognition condition were used for ERP and time-frequency analyses. For each participant and each electrode, grand average ERP from cross trials of two event types was calculated and compared between groups and old/new conditions. Furthermore, we constructed difference waveforms by subtracting the ERP of new stimuli from that of old stimuli to isolate specific ERP components.

## 2.8. Time-frequency analysis

Time-frequency analysis using continuous wavelet transform was performed using FieldTrip toolbox. For each group and condition, power was computed by averaging across trials at each electrode location using a Morlet wavelet (width = 7) for a conservatively large frequency range of 4–20 Hz, with an analysis window being centered from −0.2 to 1.5 s, sliding in steps of 0.01 s. Time-frequency data were  $\log_{10}$  transformed to normalize frequency distribution.

## 2.9. Statistical analysis

We used chi-square tests or independent-samples *t*-tests to evaluate group differences in gender distribution, age, education level, and cognitive function after testing normality and variance consistency. Data analysis was performed using IBM SPSS 26.0 software (SPSS Inc., Chicago, IL, USA). A repeated-measures analysis of variance (ANOVA) corrected using the Greenhouse–Geisser method and Scheirer-Ray-Hare test were applied to assess behavioral performance between different groups and conditions. Average amplitude values of difference waveforms across all electrodes, which were calculated from all groups, were calculated using independent-samples two-tailed *t*-test with the non-parametric cluster-based Monte Carlo permutation test (1,000 repetitions) to correct for multiple comparisons. Similarly, we compared power across all electrodes between groups using the cluster-based Monte Carlo permutation test (5,000 repetitions). Overall, statistical significance was assessed at a threshold of  $p = 0.025$  at each tail.

We used Spearman's Rho correlations to examine the relationship between behavioral or neural measures with neuropsychological performance. Finally, a receiver operator characteristic curve (ROC) was calculated to quantify the discriminatory power of each significantly altered biomarker between MCI-AD and HC groups. Multivariate binary logistic regression analysis was then conducted by combining the risk factors identified above. The predicted value of the model was calculated, and its discriminatory power was quantified by using ROC. The calibration was tested with the Hosmer–Lemeshow test for goodness of fit.  $P < 0.05$  was considered statistically significant.

TABLE 1 Demographics of subjects and neuropsychological test scores.

Characteristics	MCI-AD (Mean $\pm$ SD)	HC (Mean $\pm$ SD)	Test statistic	P-value
Sample size (male)	24 (13)	31 (14)	$\chi^2 = 0.439$	0.508
Age (years)	64.75 $\pm$ 9.377	65.06 $\pm$ 6.899	$T = 0.143$	0.887
Education (years)	12.25 $\pm$ 3.529	12.94 $\pm$ 3.326	$T = 0.738$	0.464
MMSE score	25.50 $\pm$ 2.571	28.06 $\pm$ 1.590	$T = 4.292$	<0.001
MOCA score	20.25 $\pm$ 3.859	26.35 $\pm$ 2.058	$T = 7.016$	<0.001
HDS score	27.44 $\pm$ 3.146	30.63 $\pm$ 1.565	$T = 4.553$	<0.001
AVLT delayed recall	1.58 $\pm$ 2.339	5.29 $\pm$ 2.479	$T = 5.635$	<0.001
AVLT recognition	16.29 $\pm$ 6.464	22.29 $\pm$ 1.637	$T = 4.438$	<0.001
ADL	21.38 $\pm$ 1.789	20.03 $\pm$ 0.180	$T = -3.662$	<0.001
HAMA	5.00 $\pm$ 2.964	2.84 $\pm$ 2.099	$T = -3.032$	0.004
HAMD	3.67 $\pm$ 2.792	2.00 $\pm$ 2.113	$T = -2.521$	0.015
CSF biomarkers				
A $\beta$ 42 $\downarrow$ (%)	23 (95.83)	–	–	–
A $\beta$ 42/A $\beta$ 40 ratio $\downarrow$ (%)	15 (62.50)	–	–	–
t-Tau $\uparrow$ (%)	14 (58.33)	–	–	–
p-Tau $\uparrow$ (%)	12 (50.00)	–	–	–

MCI-AD, mild cognitive impairment due to Alzheimer's disease; HC, healthy control; MMSE, Mini Mental State Examination; MoCA, Montreal Cognitive Assessment; ADL, activities of daily living; HDS, Hasegawa Dementia Scale; AVLT, Auditory Verbal Learning Test; CSF, cerebrospinal fluid; A $\beta$ 42, amyloid- $\beta$  (1-42); A $\beta$ 40, amyloid- $\beta$  (1-40); t-Tau, total tau; p-Tau, tau phosphorylated at threonine 181.

## 3. Results

### 3.1. Clinical characteristics

Table 1 lists the demographics and neuropsychological assessments for the MCI-AD and HC cohorts, wherein data are presented as mean values ( $\pm$  standard deviation). No significant differences were observed between the MCI-AD and HC groups regarding gender, education level, and age. The scores of general cognitive functions (MMSE, MoCA, and HDS scores) and episodic memory (AVLT: delayed recall and recognition) were lower in the MCI-AD group than in the HC group ( $p < 0.05$ ). Overall, although all participants in the MCI-AD group were non-demented with a CDR score of less than 1, the MCI-AD group had higher activities of daily living and CDR scores than the HC group ( $p < 0.05$ ). Moreover, patients who had evident anxiety and depression were excluded, but their HAMA and HAMD scores still tended to be higher than those of HC subjects ( $p < 0.05$ ). All patients had positive results for CSF biomarkers, together with a decreased A $\beta$ 42 level or a reduced A $\beta$ 42/A $\beta$ 40 ratio. Some participants also had an elevated tau protein concentration.

### 3.2. Behavioral results

To assess participants' behavioral performance during the task, we performed a  $2 \times 2$  repeated-measures ANOVA with factors of condition (old or new pictures) and group (MCI-AD or HC group). The results presented in Figure 2 showed significant differences in the main effects of conditions [ $F(1,53) = 17.610$ ,  $p < 0.001$ ,  $\eta_p^2 = 0.249$ ] and groups [ $F(1,53) = 12.691$ ,  $p = 0.001$ ,  $\eta_p^2 = 0.03$ ], but

no significant differences in the interaction of condition  $\times$  group [ $F(1,53) = 0.809$ ,  $p = 0.372$ ,  $\eta_p^2 = 0.015$ ], driven by a shorter RT in the old picture condition and the HC group. Given that the accuracy data didn't meet the assumptions of normality and homogeneity of variance, we performed Scheirer-Ray-Hare test. We also found significant differences in the main effects of group ( $H = 9.3612$ ,  $p = 0.002$ ) but not in the effects of condition ( $H = 0.1448$ ,  $p = 0.704$ ) or interaction ( $H = 0.8839$ ,  $p = 0.347$ ) when we set accuracy as the dependent variable, indicating that accuracy was mainly affected by cognitive state, not by event type.  $\eta_p^2$  indicates the partial eta-squared, a measure of effect size used in ANOVA.

### 3.3. ERP analysis results

We assessed whether old and new pictures elicited different patterns of brain activity in the all participants. For this assessment, the grand average ERP time-locked to stimulus onset of the IAPS images over left parietal electrodes (CP1, CP3, P1, and P3) was calculated for both conditions, which are presented in Figure 3. The LPP around 550 ms over the left parietal region could be seen in both groups.

Then, we constructed difference waveforms to compare the difference in the old/new effects (old-new) between the two groups (Figure 4A). The difference waveforms between groups were analyzed using a cluster-based Monte Carlo permutation test. The analysis revealed a significant cluster that showed that a higher positive amplitude of difference waveforms in the HC group, which lasted for 470–570 ms after stimulus onset and occurred at the left parietal electrodes on the scalp. To assess the variation in the old or new ERP effects between groups, we calculated the average ERP

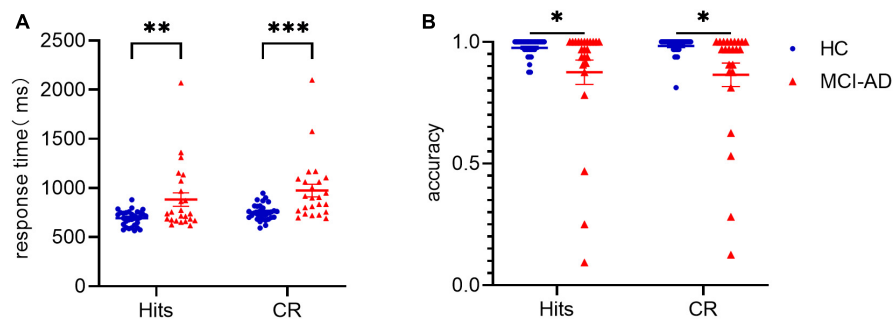


FIGURE 2

Data of behavioral performance in the HC and MCI-AD groups. Panel (A): Average response time to old pictures ("Hits") and new pictures (correct rejection) between the two groups. Panel (B): Average accuracy over the two conditions and two groups. \* indicates  $p < 0.05$ . \*\* indicates  $p < 0.01$ . \*\*\* indicates  $p < 0.0001$ . Error bars represent standard error of the mean.

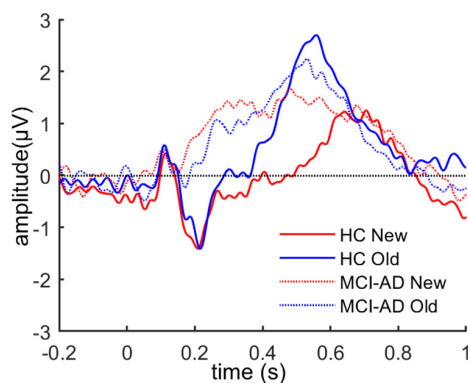


FIGURE 3

The grand average ERP waveforms over left parietal electrodes for both old and new images across the two groups.

activity at a represent electrode (i.e., P3) and performed repeated-measures ANOVA on condition (old and new images) and group (HC and MCI-AD groups; Figure 4B). However, the main effects of group [ $F(1,53) = 2.778$ ,  $p = 0.101$ ,  $\eta_p^2 = 0.050$ ] and condition [ $F(1,53) < 0.001$ ,  $p = 0.989$ ,  $\eta_p^2 < 0.001$ ] were not marked, and the interaction effect [ $F(1,53) = 3.889$ ,  $p = 0.054$ ,  $\eta_p^2 = 0.068$ ] was marginally significant. Furthermore, the simple effect analysis indicated that the simple effect of group was sharply different in the "old image" condition [ $F(1,53) = 4.714$ ,  $p = 0.034$ ,  $\eta_p^2 = 0.082$ ]. No significant simple effect of condition was observed.

### 3.4. Time-frequency analysis results

We found a significant group-by-condition interaction effect [ $F(1,54) = 115.02$ ,  $p < 0.001$ ], indicating the effect of condition differs between groups. The cluster-based non-parametric test revealed differences in the neural oscillatory response to old or new images in the HC cohort along the temporal  $\times$  frequency dimensions over the left parietal electrodes. The results revealed a significant cluster initiating at 600 ms from stimulus onset, comprising relatively high-frequency activity in the beta band (13–30 Hz; Figure 5A). No significant cluster was found in the MCI-AD

cohort between conditions (Figure 5B). We could not analyze the spectrum over low frequency such as the delta and theta bands precisely because the trial length was too short ( $< 1$  s). We could merely observe the old responses accompanied by a decrease in beta power, and this effect was seen over the left parietal region of the scalp, limited to the HC cohort. Furthermore, we tried to accumulate more information about the decrease in spectral power over time elicited by old or new stimuli between the groups. The results showed that the spectral power changes over time were different between the groups in the old image condition but not in the new image condition (threshold of  $p = 0.05$ ; Figure 5C). To make up for the lost information of the delta and theta bands, we simply extracted data of relative power through the Morlet wavelet power spectrum analysis. The relative power of the delta band showed noticeable difference between the groups ( $p = 0.004$ ), while no significant difference was found in the theta band ( $p = 0.10$ ).

### 3.5. Correlation of behavioral or neural measures with neuropsychological performance

A significant and negative correlation was observed between behavioral performance and MMSE score (Spearman  $r = -0.271$ ,  $p = 0.047$ ; Figure 6A). Participants with a higher score tended to make a faster response to old images. The old/new effect measured as the average amplitude values of difference waveforms at the P3 electrode showed significant correlation with AVLT recognition scores (Spearman  $r = 0.298$ ,  $p = 0.049$ ; Figure 6B). A substantial correlation was not observed between behavioral performance and old/new effect measures or between MMSE scores and old/new effect measures (all  $p > 0.05$ ).

### 3.6. Classifying patients with MCI-AD based on neural image and behavioral recognition memory performance

Patients with MCI-AD could be discriminated from healthy elderly adults in the HC cohort using the predicted value of binary logistic regression model combining the characters of the

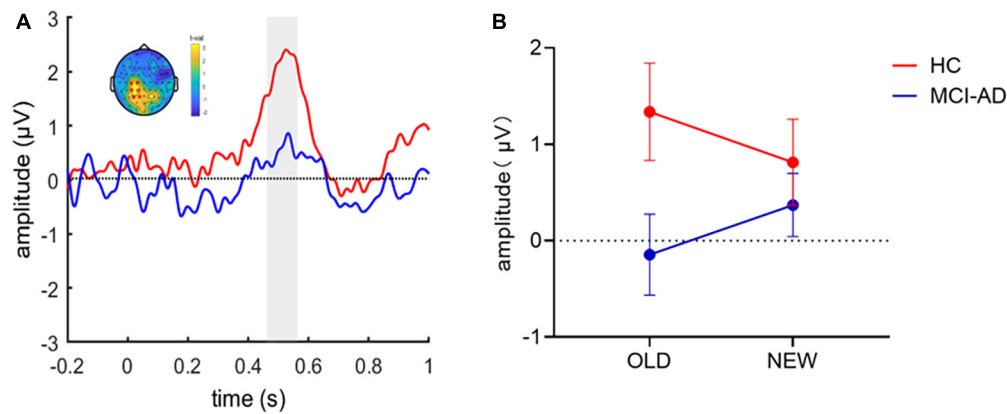


FIGURE 4

ERP old/new effect in the image recognition memory task. Panel (A): Old-new difference waveforms between the two groups. A cluster-based permutation analysis between the two conditions revealed that the HC group had greater old/new difference waveform amplitude than the MCI-AD group over the left parietal regions. The shadow indicates the temporal window of significance ( $p < 0.05$ , corrected). Panel (B): Average amplitude of ERPs at a present electrode (i.e., P3) for each group and condition. (Error bars represent standard error of the mean).

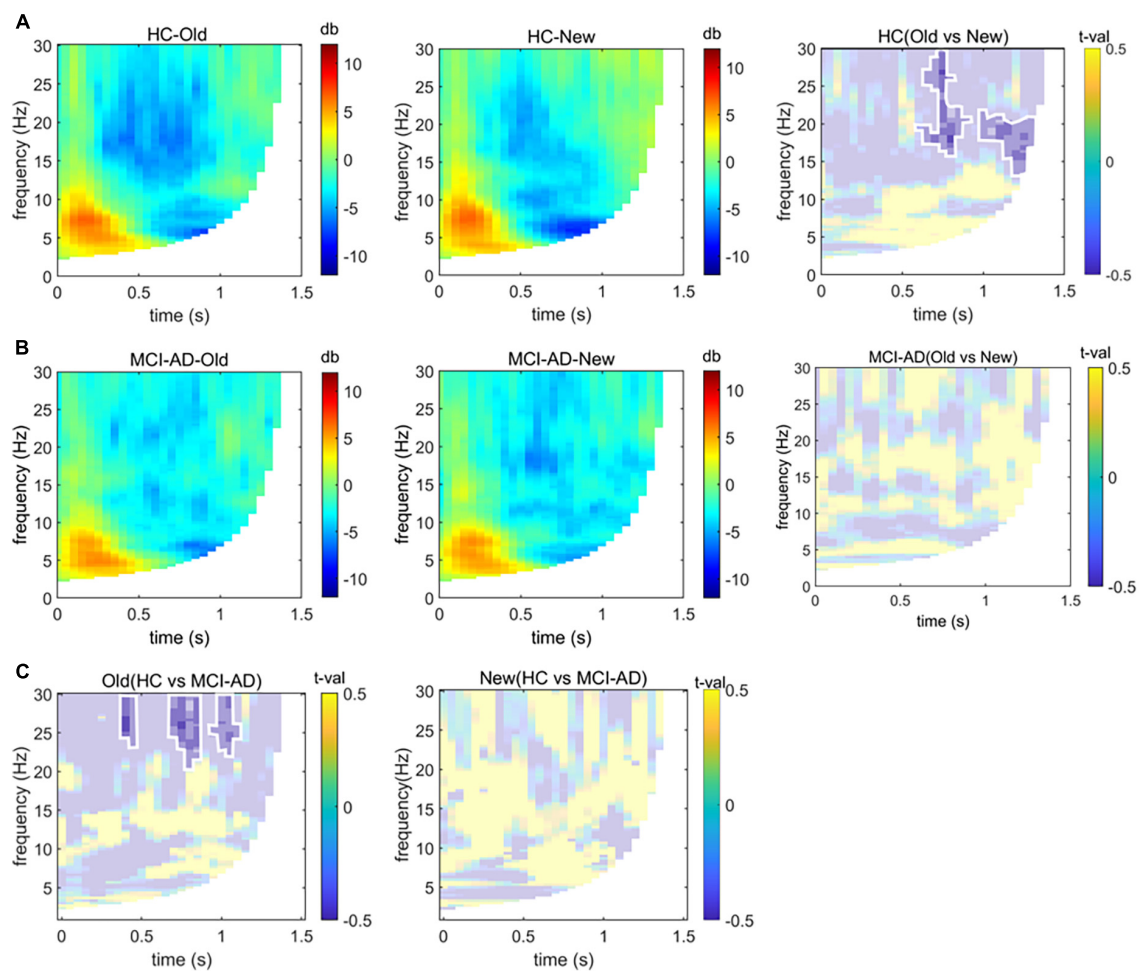


FIGURE 5

Time-frequency analysis. Panels (A,B): Group-based average changes in spectral power over the left parietal electrodes induced by old or new images in the HC and MCI-AD groups. The difference between old image and new image conditions is also displayed based on the significant cluster ( $p < 0.05$ ), marked with opaque color patches and circled by white lines. Panel (C): Differences in spectral power over time elicited by old or new image stimuli between groups ( $p < 0.05$ , non-parametric cluster-based Monte Carlo permutation test).

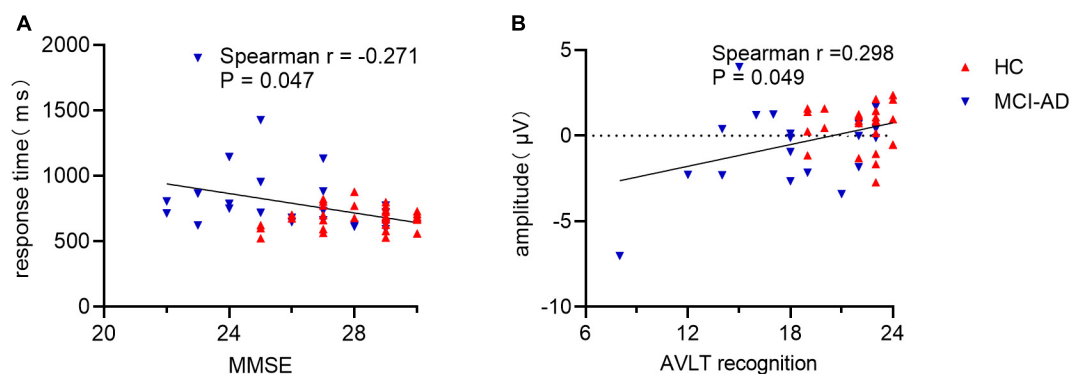


FIGURE 6

Correlation of behavioral response or old/new effect with cognitive assessment. Panel (A): Correlation between response time and MMSE scores in all participants. Panel (B): Correlation between mean amplitude of late old/new difference waveform and AVLT recognition scores. MMSE, Mini Mental State Examination; AVLT, Auditory Verbal Learning Test.

average amplitude, relative power and behavioral measure (area under the receiver operating characteristic curve (AUC) = 0.80, 95% confidence interval (CI): 0.69–0.92,  $p < 0.001$ ; Figure 7). Discrimination performance was moderate using single character such as the average amplitude (AUC = 0.66, 95% CI: 0.51–0.80), the relative power (AUC = 0.73, 95% CI: 0.60–0.87) and the behavioral measure (AUC = 0.67, 95% CI: 0.52–0.82). The amplitude was measured by values of difference waveforms at the P3 electrode in the recognition condition. Relative power of the delta band providing frequency information was selected, and the behavioral measure was calculated by combining measures of processing speed and accuracy, namely, equal to the product of mean RT and accuracy divided by the sum of them.

## 4. Discussion

The current study examined the different behavioral and ERP measures in the image recognition memory task between the MCI-AD and HC cohorts. To summarize, the MCI-AD cohort had a significantly longer response time to the pictures and lower accuracy, regardless of the old or new pictures. All participants responded faster in the old picture condition. Meanwhile, the MCI-AD cohort had significant differences in the electrophysiological measures during the image recognition task. Differences in the LPP components between the old and new image conditions existed in the HC cohort but not in the MCI-AD cohort, predominantly over the left parietal regions. We observed no significant differences between responses to old and new pictures in both groups along the temporal  $\times$  frequency  $\times$  spatial (scalp sensors) dimensions.

The most striking difference between the MCI-AD and HC cohorts was observed when comparing the amplitude of the old–new difference waveforms during the test block. In the present study, the amplitude of difference waveform was significantly suppressed in the MCI-AD cohort, when compared with the HC cohort, over the left parietal regions around 470–570 ms after stimulus onset according to the statistical analysis results. Patients in the MCI-AD cohort had a smaller recollection effect, which could be the result of poor retrieval in discrimination between the studied and non-studied pictures. This finding is consistent with

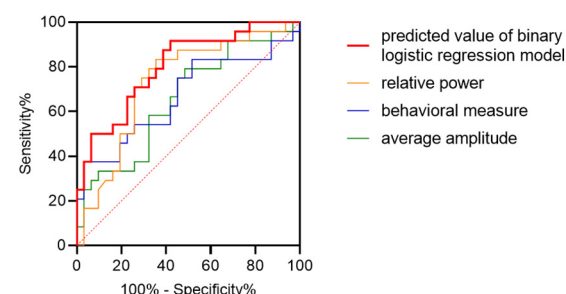


FIGURE 7

Classification of patients with MCI-AD from HC adults. Receiver operator characteristics (ROC) plots indicating the classification accuracy of MCI-AD versus HC using separate features and combined feature. Taking diagonal as the reference line, ROC curve above the line has classification significance.

that of other studies showing a relationship between late parietal old/new effects (400–800 ms) (Curran, 2000) and the ability to recollect specific pictures (Curran and Cleary, 2003). However, we did not find any notable difference in the FN400 old/new effect between groups, although a negative waveform did exist in both groups at 300–500 ms after stimulus onset. The FN400 old/new effect appears to be related to familiarity reflecting the ability of the cognitive process to differentiate old (studied) from new (non-studied) pictures and its inability to differentiate similar from studied pictures. Given this situation, all participants tended to share a similar sense of familiarity to studied and non-studied pictures. This may be because all pictures we selected for the test are commonly seen in daily life, such as chair, bicycle, and so on. Yet, retrieval of real-world events also elicited a high proportion of familiarity (Nicolás et al., 2021). Consequently, despite losing the difference of the FN400 old/new effect between groups, the results influenced by pre-experimental fluency were compatible with those of previous studies generally acknowledged (Curran and Hancock, 2007; Leynes et al., 2017; Andrew Leynes and Upadhyay, 2022). The LPP old/new effects still showed significant variation, wherein the MCI-AD cohort performed poorly in terms of retrieving episodic memory related to accurate source judgments

of episodic context (Addante et al., 2012), while the HC cohort performed better in identifying old pictures that appeared in the study block of the experiment. Importantly, although the cluster-based permutation test of difference waveforms between groups showed significant differences, the separate repeated-measures ANOVA results for ERPs specific to old and new images between groups revealed that none of them showed a significant main effect, but, instead, they showed a significant trend in the interaction effect of group  $\times$  condition, indicating that we may need more subjects.

Unexpectedly, correct recognition of old pictures elicited a decrease in beta power but not in theta or alpha power over the left parietal electrodes in the HC cohort, but this effect disappeared in the MCI-AD cohort. EEG theta oscillations are usually associated with retrieval of contextual information (Guderian and Düzel, 2005; Herweg et al., 2016), and alpha rhythms may be related to the retrieval of memories (Martín-Buro et al., 2019) or subjects' emotional states (Siqi-Liu et al., 2018). The task conducted in the current study was partly responsible for uncovering the theta oscillations because of the transient presentation of a single trial, while wavelet transform resulted in lower time resolution in the low-frequency band. Modulation of beta oscillations in human EEG was observed mainly during tasks that combined the cognition and execution processes, for example, the decision-making task (Zabielska-Mendyk et al., 2018), which is consistent with the current experimental design.

The MCI-AD cohort differed from the HC cohort in the performance evaluated using response time and accuracy during the image recognition task. However, it was difficult to distinguish whether the ability of memory or sustained attention was responsible for this outcome (Smid et al., 2006). As expected, response time to new pictures was slower in both groups, partly because of familiarity-based processing, but the accuracy did not differ between conditions. Accuracy showed group difference but not condition difference or interaction effect which might be related to ceiling effect and relatively few stimuli to some degree. However, it's challenging to balance the need for a sufficient number of trials for the ERP analysis with the need to keep the total duration of the experiment manageable to prevent attentional decline. It is also worthwhile to mention that sometimes longer RTs could be associated with better memory if they are driven by recollection rather than familiarity. RT condition differences may scale overall with mean RT so that we will consider it in our future analyses. Grand average response time was related to the scores of general cognitive functions, showing a significant and negative correlation and demonstrating that subjects lost the ability to receive and process new information gradually as the cognitive impairment increased. Meanwhile, electrophysiology measurements showed a significant and positive correlation with AVLT scores but not with MMSE scores, RT, or accuracy. The finding emphasized that the late old/new effect was consistent with the neuropsychological performance, especially in the retrieval of episodic memory. Fortunately, we collected the testing results of CSF for patients with MCI-AD. However, amyloid deposition showed no significant correlation with cognitive assessment or electrophysiological measurements. Finally, receiver operating characteristic curve analysis showed that the late old/new effect did have a moderate potential to indicate cognitive impairment on an individual basis and serve as a biomarker for detecting MCI-AD. The current amount of data was not enough for model validation and the classification effect of EEG features itself was still

unsatisfactory. We will keep on paying attention and further verify it in future research.

The current study had several limitations, which should be mentioned. First, differences in the merely old/new effects were compared between groups while other self-generated or other-generated sources such as visual and lingual ones and concentration remained unknown. Second, old images were presented multiple times during the test phase. This design could potentially allow participants to determine whether an item was old based on whether it was recently repeated, rather than whether they remembered it from the study phase. Considering of the cognitive state of our participants with cognitive impairment, the number of old images they can learn during the study phase is limited. In future studies, we will consider strategies to increase the number of trials and reduce the repetition of stimuli, while still accommodating the cognitive and attentional limitations of our participants. Additionally, the data used in the present study are not sufficient to set standards, and longitudinal follow-up of the HC and MCI-AD cohorts is meaningful to explore the association of the loss of old/new effect with conversion to AD-related dementia.

## 5. Conclusion

Collectively, these data suggest impaired recognition memory in patients with MCI-AD from the perspective of ERPs. This damage is manifested by the loss of late old/new effects, decreased accuracy, lower response time to stimuli, and abnormal late beta rhythm. Even though these changes show no significant correlation with A $\beta$  or tau levels in CSF, they provide a method for the assessment of cognition in dementia and, to a certain extent, contribute to the development of early diagnosis tools.

## Data availability statement

The raw data supporting the conclusions of this article will be made available by the authors, without undue reservation.

## Ethics statement

The studies involving human participants were reviewed and approved by the Medical Research Ethics Committee of the Brain Hospital Affiliated to Nanjing Medical University. The patients/participants provided their written informed consent to participate in this study.

## Author contributions

YW was mainly responsible for the research design, data collection, data analysis, and manuscript writing of this study. XY was mainly responsible for research design, data analysis, review, and editing. BS was mainly responsible for data collection and document retrieval. YY and WM was mainly responsible for data collection. JS was mainly responsible for conceptualization, resources, and project

administration. All authors contributed to the article and approved the submitted version.

## Funding

This work was supported by the Nanjing Medical Science and Technology Development key project (No. ZKX21034).

## Acknowledgments

We would like to thank all the subjects who participated in the experiment and the review, as well as MogoEditor ([www.mogoedit.com](http://www.mogoedit.com)) for providing English editing services during the preparation of this manuscript.

## References

- Addante, R. J., Ranganath, C., and Yonelinas, A. P. (2012). Examining ERP correlates of recognition memory: Evidence of accurate source recognition without recollection. *Neuroimage* 62, 439–450. doi: 10.1016/j.neuroimage.2012.04.031
- Albert, M. S., Dekosky, S. T., Dickson, D., Dubois, B., Feldman, H. H., Fox, N. C., et al. (2011). The diagnosis of mild cognitive impairment due to Alzheimer's disease: Recommendations from the National Institute on Aging-Alzheimer's Association workgroups on diagnostic guidelines for Alzheimer's disease. *Alzheimers Dement.* 7, 270–279. doi: 10.1016/j.jalz.2011.03.008
- Andrew Leynes, P., and Upadhyay, T. (2022). Context dissociations of the FN400 and N400 are evidence for recognition based on relative or absolute familiarity. *Brain Cogn.* 162:105903. doi: 10.1016/j.bandc.2022.105903
- Bagby, R. M., Ryder, A. G., Schuller, D. R., and Marshall, M. B. (2004). The Hamilton Depression Rating Scale: Has the gold standard become a lead weight? *Am. J. Psychiatry* 161, 2163–2177. doi: 10.1176/appi.ajp.161.12.2163
- Bamford, C., Wheatley, A., Brunskill, G., Booi, L., Allan, L., Banerjee, S., et al. (2021). Key components of post-diagnostic support for people with dementia and their carers: A qualitative study. *PLoS One* 16:e0260506. doi: 10.1371/journal.pone.0260506
- Berg, P., and Scherg, M. (1994). A multiple source approach to the correction of eye artifacts. *Electroencephalogr. Clin. Neurophysiol.* 90, 229–241. doi: 10.1016/0013-4694(94)90094-9
- Brainard, D. H. (1997). The psychophysics toolbox. *Spat. Vis.* 10, 433–436. doi: 10.1163/156856897X00357
- Curran, T. (1999). The electrophysiology of incidental and intentional retrieval: ERP old/new effects in lexical decision and recognition memory. *Neuropsychologia* 37, 771–785. doi: 10.1016/S0028-3932(98)00133-X
- Curran, T. (2000). Brain potentials of recollection and familiarity. *Mem. Cogn.* 28, 923–938. doi: 10.3758/BF03209340
- Curran, T., and Cleary, A. M. (2003). Using ERPs to dissociate recollection from familiarity in picture recognition. *Brain Res. Cogn. Brain Res.* 15, 191–205. doi: 10.1016/S0926-6410(02)00192-1
- Curran, T., and Hancock, J. (2007). The FN400 indexes familiarity-based recognition of faces. *Neuroimage* 36, 464–471. doi: 10.1016/j.neuroimage.2006.12.016
- Dzulkifli, M. A., Herron, J. E., and Wilding, E. L. (2006). Memory retrieval processing: Neural indices of processes supporting episodic retrieval. *Neuropsychologia* 44, 1120–1130. doi: 10.1016/j.neuropsychologia.2005.10.021
- Egerházi, A., Glaub, T., Balla, P., Berecz, R., and Degrell, I. (2008). [P300 in mild cognitive impairment and in dementia]. *Psychiatr. Hung* 23, 349–357.
- Ferreira, D., Perestelo-Pérez, L., Westman, E., Wahlund, L. O., Sarria, A., and Serrano-Aguilar, P. (2014). Meta-review of CSF core biomarkers in Alzheimer's disease: The state-of-the-art after the new revised diagnostic criteria. *Front. Aging Neurosci.* 6:47. doi: 10.3389/fnagi.2014.00047
- Gao, Z. (1991). [Assessment of Hasegawa's dementia scale for screening and diagnosis of dementia in the elderly]. *Zhonghua Shen Jing Jing Shen Ke Za Zhi* 24, 258–261, 316.
- Guderian, S., and Düzel, E. (2005). Induced theta oscillations mediate large-scale synchrony with mediotemporal areas during recollection in humans. *Hippocampus* 15, 901–912. doi: 10.1002/hipo.20125
- Herweg, N. A., Apitz, T., Leicht, G., Mulert, C., Fuentemilla, L., and Bunzeck, N. (2016). Theta-alpha oscillations bind the hippocampus, prefrontal cortex, and striatum during recollection: Evidence from simultaneous EEG-fMRI. *J. Neurosci.* 36, 3579–3587. doi: 10.1523/JNEUROSCI.3629-15.2016
- Horton, D. K., Hynan, L. S., Lacritz, L. H., Rossetti, H. C., Weiner, M. F., and Cullum, C. M. (2015). An abbreviated Montreal Cognitive Assessment (MoCA) for dementia screening. *Clin. Neuropsychol.* 29, 413–425. doi: 10.1080/13854046.2015.1043349
- Horvath, A., Szucs, A., Csukly, G., Sakovics, A., Stefanics, G., and Kamondi, A. (2018). EEG and ERP biomarkers of Alzheimer's disease: A critical review. *Front. Biosci. (Landmark Ed)* 23:183–220. doi: 10.2741/4587
- Jack, C. R. Jr., Bennett, D. A., Blennow, K., Carrillo, M. C., Dunn, B., Haeberlein, S. B., et al. (2018). NIA-AA research framework: Toward a biological definition of Alzheimer's disease. *Alzheimers Dement.* 14, 535–562. doi: 10.1016/j.jalz.2018.02.018
- Jelic, V., Johansson, S. E., Almkvist, O., Shigeta, M., Julin, P., Nordberg, A., et al. (2000). Quantitative electroencephalography in mild cognitive impairment: Longitudinal changes and possible prediction of Alzheimer's disease. *Neurobiol. Aging* 21, 533–540. doi: 10.1016/S0197-4580(00)00153-6
- Jia, J., Wei, C., Chen, S., Li, F., Tang, Y., Qin, W., et al. (2018). The cost of Alzheimer's disease in China and re-estimation of costs worldwide. *Alzheimers Dement.* 14, 483–491. doi: 10.1016/j.jalz.2017.12.006
- Jiang, S., Qu, C., Wang, F., Liu, Y., Qiao, Z., Qiu, X., et al. (2015). Using event-related potential P300 as an electrophysiological marker for differential diagnosis and to predict the progression of mild cognitive impairment: A meta-analysis. *Neurol. Sci.* 36, 1105–1112. doi: 10.1007/s10072-015-2099-z
- Kappenman, E. S., Farrens, J. L., Luck, S. J., and Proudfit, G. H. (2014). Behavioral and ERP measures of attentional bias to threat in the dot-probe task: Poor reliability and lack of correlation with anxiety. *Front. Psychol.* 5:1368. doi: 10.3389/fpsyg.2014.01368
- Kappenman, E., and Steven, J. (2011). *The oxford handbook of event-related potential components*. Oxford: Oxford University Press. doi: 10.1093/oxfordhb/9780195374148.001.0001
- Leynes, P. A., Bruett, H., Krizan, J., and Veloso, A. (2017). What psychological process is reflected in the FN400 event-related potential component? *Brain Cogn.* 113, 142–154. doi: 10.1016/j.bandc.2017.02.004
- Lucas, H. D., Paller, K. A., and Voss, J. L. (2012). On the pervasive influences of implicit memory. *Cogn. Neurosci.* 3, 219–226. doi: 10.1080/17588928.2012.697454
- Martin-Buro, M. C., Wimber, M., Henson, R. N., and Staresina, B. P. (2019). Alpha rhythms reveal when, where and how memories are retrieved. *bioRxiv* [Preprint]. bioRxiv 708602. doi: 10.1101/708602
- Mickes, L., Wais, P. E., and Wixted, J. T. (2009). Recollection is a continuous process: Implications for dual-process theories of recognition memory. *Psychol. Sci.* 20, 509–515. doi: 10.1111/j.1467-9280.2009.02324.x
- Morris, J. C. (1993). The Clinical Dementia Rating (CDR): Current version and scoring rules. *Neurology* 43, 2412–2414. doi: 10.1212/WNL.43.11.2412-a

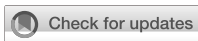
## Conflict of interest

The authors declare that the research was conducted in the absence of any commercial or financial relationships that could be construed as a potential conflict of interest.

## Publisher's note

All claims expressed in this article are solely those of the authors and do not necessarily represent those of their affiliated organizations, or those of the publisher, the editors and the reviewers. Any product that may be evaluated in this article, or claim that may be made by its manufacturer, is not guaranteed or endorsed by the publisher.

- Morrison, C., Rabipour, S., Knoefel, F., Sheppard, C., and Taler, V. (2018). Auditory event-related potentials in mild cognitive impairment and Alzheimer's disease. *Curr. Alzheimer Res.* 15, 702–715. doi: 10.2174/1567205015666180123123209
- Morrison, C., Rabipour, S., Taler, V., Sheppard, C., and Knoefel, F. (2019). Visual Event-related potentials in mild cognitive impairment and Alzheimer's disease: A literature review. *Curr. Alzheimer Res.* 16, 67–89. doi: 10.2174/1567205015666181022101036
- Mulder, C., Verwey, N. A., van der Flier, W., Bouwman, F. H., Kok, A., Van Elk, E., et al. (2010). Amyloid-beta(1-42), total tau, and phosphorylated tau as cerebrospinal fluid biomarkers for the diagnosis of Alzheimer disease. *Clin. Chem.* 56, 248–253. doi: 10.1373/clinchem.2009.130518
- Nicolás, B., Wu, X., García-Arch, J., Dimiccoli, M., Sierpowska, J., Saiz-Masvidal, C., et al. (2021). Behavioural and neurophysiological signatures in the retrieval of individual memories of recent and remote real-life routine episodic events. *Cortex* 141, 128–143. doi: 10.1016/j.cortex.2021.04.006
- Oppenheimer, D. M. (2008). The secret life of fluency. *Trends Cogn. Sci.* 12, 237–241. doi: 10.1016/j.tics.2008.02.014
- Robinson, L., Tang, E., and Taylor, J. P. (2015). Dementia: Timely diagnosis and early intervention. *BMJ* 350, h3029. doi: 10.1136/bmj.h3029
- Sheng, M., Sabatini, B. L., and Südhof, T. C. (2012). Synapses and Alzheimer's disease. *Cold Spring Harb. Perspect. Biol.* 4:a005777. doi: 10.1101/cshperspect.a005777
- Siqi-Liu, A., Harris, A. M., Atkinson, A. P., and Reed, C. L. (2018). Dissociable processing of emotional and neutral body movements revealed by  $\mu$ -alpha and beta rhythms. *Soc. Cogn. Affect. Neurosci.* 13, 1269–1279. doi: 10.1093/scan/nsy094
- Smid, H. G., de Witte, M. R., Homminga, I., and van den Bosch, R. J. (2006). Sustained and transient attention in the continuous performance task. *J. Clin. Exp. Neuropsychol.* 28, 859–883. doi: 10.1080/13803390591001025
- Tombaugh, T. N., and McIntyre, N. J. (1992). The mini-mental state examination: A comprehensive review. *J. Am. Geriatr. Soc.* 40, 922–935. doi: 10.1111/j.1532-5415.1992.tb01992.x
- Vakil, E., and Blachstein, H. (1993). Rey auditory-verbal learning test: Structure analysis. *J. Clin. Psychol.* 49, 883–890. doi: 10.1002/1097-4679(199311)49:6<883::AID-JCLP2270490616>3.0.CO;2-6
- Villemagne, V. L., Doré, V., Burnham, S. C., Masters, C. L., and Rowe, C. C. (2018). Imaging tau and amyloid- $\beta$  proteinopathies in Alzheimer disease and other conditions. *Nat. Rev. Neurol.* 14, 225–236. doi: 10.1038/nrneurol.2018.9
- Voss, J. L., and Paller, K. A. (2006). Fluent conceptual processing and explicit memory for faces are electrophysiologically distinct. *J. Neurosci.* 26, 926–933. doi: 10.1523/JNEUROSCI.3931-05.2006
- Waninger, S., Berka, C., Meghdadi, A., Karic, M. S., Stevens, K., Agüero, C., et al. (2018). Event-related potentials during sustained attention and memory tasks: Utility as biomarkers for mild cognitive impairment. *Alzheimers Dement. (Amst)* 10, 452–460. doi: 10.1016/j.dadm.2018.05.007
- Weiss, E. M., Kohler, C. G., Vonbank, J., Stadelmann, E., Kemmler, G., Hinterhuber, H., et al. (2008). Impairment in emotion recognition abilities in patients with mild cognitive impairment, early and moderate Alzheimer disease compared with healthy comparison subjects. *Am. J. Geriatr. Psychiatry* 16, 974–980. doi: 10.1097/JGP.0b013e318186bd53
- Yang, L., Zhao, X., Wang, L., Yu, L., Song, M., and Wang, X. (2015). Emotional face recognition deficit in amnesic patients with mild cognitive impairment: Behavioral and electrophysiological evidence. *Neuropsychiatr. Dis. Treat.* 11, 1973–1987. doi: 10.2147/NDT.S85169
- Yener, G. G., and Başar, E. (2013). Biomarkers in Alzheimer's disease with a special emphasis on event-related oscillatory responses. *Suppl. Clin. Neurophysiol.* 62, 237–273. doi: 10.1016/B978-0-7020-5307-8.00020-X
- Zabielska-Mendyk, E., Francuz, P., Jaśkiewicz, M., and Augustynowicz, P. (2018). The effects of motor expertise on sensorimotor rhythm desynchronization during execution and imagery of sequential movements. *Neuroscience* 384, 101–110. doi: 10.1016/j.neuroscience.2018.05.028



## OPEN ACCESS

## EDITED BY

Eduard Rodriguez-Farre,  
Institute of Biomedical Research of Barcelona,  
Spanish National Research Council (CSIC),  
Spain

## REVIEWED BY

Hao Chen,  
The Affiliated Hospital of Xuzhou Medical  
University, China  
Masaru Tanaka,  
University of Szeged (ELKH-SZTE), Hungary

## \*CORRESPONDENCE

Zhigang Liang  
✉ zgliang@hotmail.com

<sup>†</sup>These authors have contributed equally to this work and share first authorship

RECEIVED 26 June 2023

ACCEPTED 31 July 2023

PUBLISHED 10 August 2023

## CITATION

Xu L, Zhang H, Yuan H, Xie L, Zhang J and Liang Z (2023) Not your usual neurodegenerative disease: a case report of neuronal intranuclear inclusion disease with unconventional imaging patterns. *Front. Neurosci.* 17:1247403. doi: 10.3389/fnins.2023.1247403

## COPYRIGHT

© 2023 Xu, Zhang, Yuan, Xie, Zhang and Liang. This is an open-access article distributed under the terms of the [Creative Commons Attribution License \(CC BY\)](https://creativecommons.org/licenses/by/4.0/). The use, distribution or reproduction in other forums is permitted, provided the original author(s) and the copyright owner(s) are credited and that the original publication in this journal is cited, in accordance with accepted academic practice. No use, distribution or reproduction is permitted which does not comply with these terms.

# Not your usual neurodegenerative disease: a case report of neuronal intranuclear inclusion disease with unconventional imaging patterns

Luyao Xu<sup>†</sup>, Hongxia Zhang<sup>†</sup>, Hanyue Yuan, Liwen Xie, Junliang Zhang and Zhigang Liang\*

Department of Neurology, Yantai Yuhuangding Hospital Affiliated to Qingdao University, Yantai, China

**Background:** Neuronal intranuclear inclusion disease (NIID) is a rare neurodegenerative illness with characteristic brain magnetic resonance imaging (MRI) manifestations: diffuse symmetric white-matter hyperintensities in lateral cerebral ventricle areas in fluid-attenuated inversion recovery (FLAIR) and high-intensity signals along the corticomedullary junction of the frontal–parietal–temporal lobes in diffusion weighted imaging (DWI). Here, we report a case of adult-onset NIID who was misdiagnosed with Susac syndrome (SS) due to unusual corpus callosum imaging findings.

**Case presentation:** A 39-year-old man presented with chronic headache, blurred vision, tinnitus, and numbness in the hands as initial symptoms, accompanied by cognitive slowing and decreased memory. Brain MRI revealed round hypointense lesions on T1-weighted imaging (T1WI) and hyperintense lesions on T2WI/FLAIR/DWI in the genu and splenium of the corpus callosum. An initial diagnosis of SS was made based on the presence of the SS-typical symptoms and SS-characteristic radiology changes. Furthermore, the patient's symptoms improved upon completion of a combined pharmacotherapy plan. However, no significant changes were evident 18 months after the brain MRI scan. Eventually, the patient was then diagnosed with NIID based on a skin biopsy and detection of expanded GGC (guanine, guanine, cytosine) repeats in the NOTCH2NLC gene.

**Conclusion:** The present NIID case in which there was simultaneous onset of altered nervous and visual system functioning and atypical imaging findings, the atypical imaging findings may reflect an initial change of NIID leukoencephalopathy.

## KEYWORDS

neuronal intranuclear inclusion disease, Susac syndrome, skin biopsy, genetic testing, diffusion weighted imaging, characteristic imaging features

## Introduction

Neuronal intranuclear inclusion disease (NIID) is a slowly progressive neurodegenerative condition that is characterized by eosinophilic hyaline intranuclear inclusions in the central and peripheral nervous system, as well as in the visceral organs (Takahashi-Fujigasaki, 2003; Sone et al., 2016). The etiology and pathogenesis of NIID have not been clarified. Immunohistochemically, intranuclear inclusions are positive for ubiquitin and ubiquitin related proteins, including p62, SUMO1, FUS, MYO6, and OPTN-C, suggesting the

ubiquitin-proteasome pathway in the nucleus plays an important role in NIID (Kimber et al., 1998; Pountney et al., 2003; Mori et al., 2011, 2012; Nakamura et al., 2014). Recently, the GGC repeat expansions in the 5'UTR of the NOTCH2NLC gene have been identified as the pathogenic mutation of adult- and juvenile-onset NIID (Fiddes et al., 2018; Suzuki et al., 2018; Deng et al., 2019; Sone et al., 2019).

The onset of the disease varies from infancy to approximately between the ages of 60–70 years (Takahashi-Fujigasaki et al., 2016) and can be classified into three categories: infantile, juvenile, and adult NIID (Takumida et al., 2017). However, current knowledge of the clinical features of adult-onset NIID is lacking. The clinical characteristics of adult-onset NIID have been reported as follows: pyramidal and extrapyramidal symptoms, cerebellar ataxia, dementia, convulsions, neuropathy, sensory disturbance, and autonomic dysfunction (Sone et al., 2016; Liu et al., 2019). It is difficult to make a conclusive early diagnosis of NIID due to the disease's highly variable clinical symptoms, signs, and onset age. As a result, NIID is often misdiagnosed. In recent years, brain changes indicated by MRI, combined with skin biopsy pathological results and genetic testing [fragile X mental retardation 1 (FMR1) or Notch 2 N-terminal-like C (NOTCH2NLC) testing] can contribute to the accurate diagnosis of NIID.

Here, we report an adult-onset case of NIID in which the patient's nervous and visual systems were affected simultaneously at onset and the patient had atypical imaging findings of lesions in the corpus callosum. Susac syndrome (SS) was diagnosed initially due to symptom characteristics at disease onset resembling the SS-typical symptom triad and the observation of SS-characteristic radiology changes. An absence of radiology changes for 18 months after the diagnosis of SS had been made led to further investigation, which yielded a corrected diagnosis of NIID based on the identification of a NIID-associated NOTCH2NLC gene variant and the findings of skin biopsy.

## Case description

The case included in the current study was that of a 39-year-old man with no family history of NIID or any other neurodegenerative disease. He was admitted to the hospital in May 2020 after primarily complaining of headache (sharp pain), paroxysmal blurred vision (no abnormalities were found in visual acuity or color vision), tinnitus, and numbness of the hands over the preceding 6 months. Upon admission to the hospital, cognitive slowing and impaired memory function were detected by neurological examination; no abnormalities were found in other physical examinations. The following relevant scales were completed: the Mini-Mental State Examination scale (score, 27/30), the Montreal Cognitive Assessment scale (score, 27/30), and Barthel Index measure of activities of daily living (score, 100).

The results of blood biochemistry, routine blood panel, anti-endothelial cell antibody, anticardiolipin antibody, anti-cyclic citrullinated peptide antibody, antikeratin antibody, antiperinuclear factor, and routine and biochemical cerebrospinal fluid tests were all normal.

An MRI scan of the head revealed multiple round hypointense lesions on T1-weighted imaging (T1WI) (Figure 1A) and hyperintense lesions on T2WI/fluid-attenuated inversion recovery (FLAIR) analysis

(Figures 1B,C,F) in the genu and splenium of the corpus callosum. On diffusion-weighted imaging (DWI) (Figure 1D), multiple round hyperintense lesions were found to be located in the genu and splenium of the corpus callosum. Contrast-enhanced MRI revealed multiple round hypointense lesions on T1WI and hyperintense lesions on T2WI in the genu and splenium of the corpus callosum; no lesion enhancements were found (Figure 1E). The patient's electroencephalogram demonstrated paroxysmal short-range (5–7 Hz) slow waves in the eye-closed resting state. Fundus fluorescein angiography (FFA) of the (left and right) eyes (Figures 1G,H) demonstrated the presence of a dilated macular capillary and fluorescein leakage from dilated blood vessels. The patient had not experienced any hearing loss and there were no abnormal otolaryngological findings.

Anamnesis suggested that the patient's nervous, visual, and auditory systems were likely to have been affected simultaneously, an onset of disease symptoms similar to that seen with SS. Moreover, the symptoms themselves resembled the typical SS symptom triad (encephalopathy, visual disturbances, and hearing loss) (Lim et al., 2004), and SS-characteristic radiology changes (Egan, 2019) were observed. Notably, multiple round hyperintense lesions in the corpus callosum were evident on DWI, a finding that is an important indicator for SS diagnosis (Egan, 2019). The patient's neurological symptoms improved upon completion of a combined pharmacotherapy plan consisting of high-dose intravenous methylprednisolone (80 mg/d for 5 d), oral aspirin (an anti-platelet agent, 100 mg/d for 14 d), and oral idebenone tablets (a synthetic analogue of the antioxidant ubiquinone used for neuroprotection and cognitive enhancement, 90 mg/d for 3 months). Subsequently, the patient was given a maintenance prescription of oral methylprednisolone (1 mg/kg bodyweight with slow tapering) and idebenone tablets (90 mg/d). After 2 weeks, the patient's headache and blurred vision symptoms gradually improved, and he was discharged from the hospital.

One month after being discharged, a brain MRI showed multiple round hypointense lesions on T1WI (Figure 1I) and hyperintense lesions on T2WI/FLAIR/DWI (Figures 1J–L) in the genu and splenium of the corpus callosum; no significant changes were observed in the lesions, and the patient had fully recovered, except for a slightly impaired memory. Treatment was continued with oral methylprednisolone, and the dosage was gradually decreased. Three months after the patient's discharge from the hospital, his brain MRI findings remained unchanged relative to the diagnostic MRI findings (Figures 1M–P), but the patient had no disease symptoms or signs at this time.

The patient was readmitted to the hospital in April 2021 after complaining of a paroxysmal visual field defect, headache (sharp pain), and hypoesthesia of the right hand. Cognitive slowing and reduced tendon reflex responses were found by neurological examination; no abnormalities were observed during other neurological examinations. The findings of his brain MRI (Figures 1Q–T) and contrast-enhanced MRI remained unchanged from his initial admittance. His electroencephalogram showed paroxysmal short-range (4–7 Hz) slow waves in the eyes-closed resting state; following hyperventilation, slow waves with a slower rhythm and sharp slow waves (epileptic waves) appeared. His nerve conduction velocity revealed no peripheral nerve damage, but F-wave latencies were prolonged in both lower limbs.

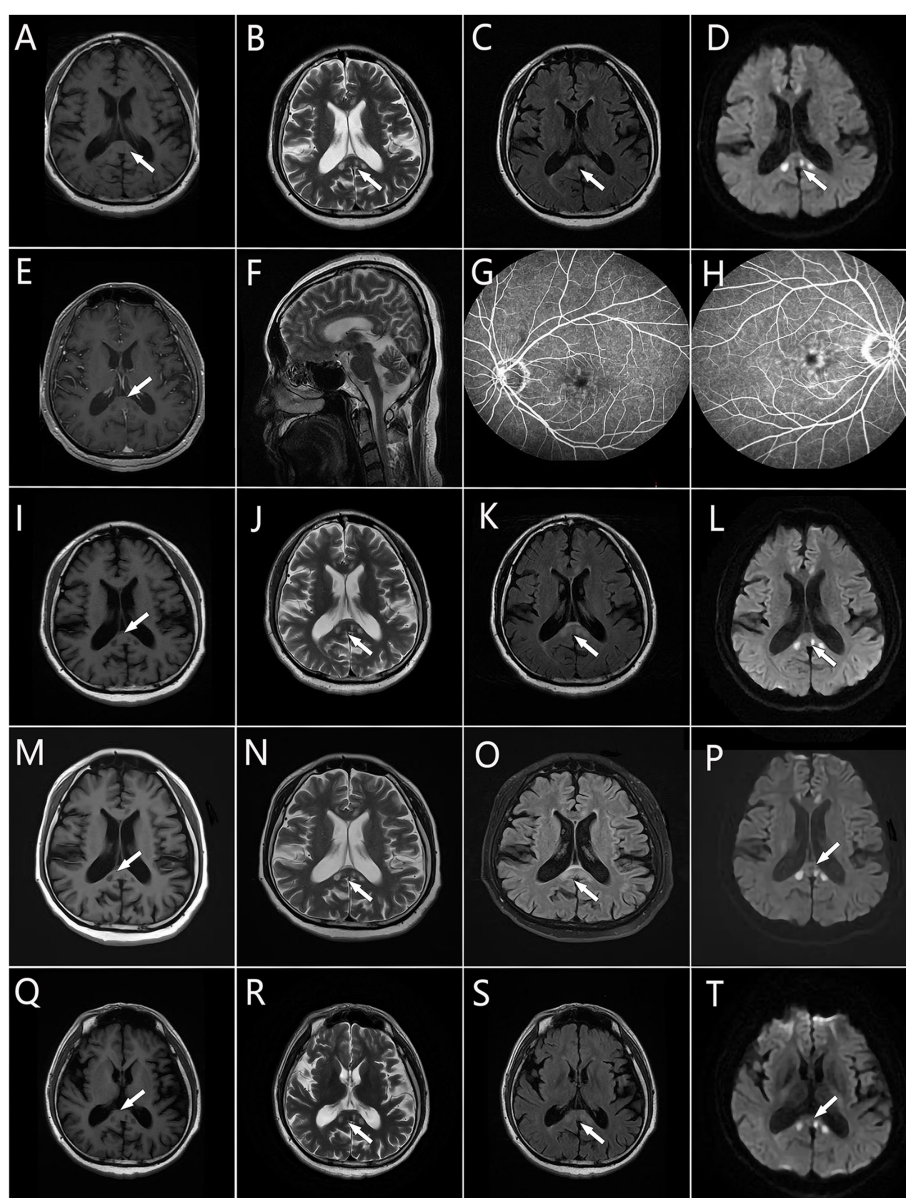


FIGURE 1

Brain MRI. (A,I,M,Q) Multiple round hypointense lesions on T1 in the corpus callosum. (B,F,J,N,R) Multiple round hyperintense lesions on T2 in the corpus callosum. (C,K,O,S) Multiple round hyperintense lesions on FLAIR located in the corpus callosum. (D,L,P,T) Multiple hyperintense lesions on DWI located in the corpus callosum. (E) Multiple hyperintense lesions on contrast-enhanced MR located in the corpus callosum. (G,H) The macular capillary was dilated and there is fluorescein leaking from the dilated blood vessels. Areas of hyperintensity or hypointensity are denoted by the white arrows.

Electromyography showed no signs of neurogenic injury or of myogenic lesion.

Genetic testing was conducted with repeat-primed polymerase chain reaction (RP-PCR) and guanine–cytosine-rich PCR (GC-PCR). We observed a 101 GGC (guanine, guanine, cytosine) repeat in the 5′-untranslated (5′UTR) region of the NOTCH2NLC gene [normal range <40 (Tian et al., 2019)] [Figures 2B(c)]. A skin biopsy was performed via light microscopy (3DHitech) on samples obtained above the patient's ankle and thigh; hematoxylin and eosin staining revealed eosinophilic spherical inclusion bodies within some sweat gland epithelial cell nuclei (Supplementary Figure S1). However, the

patient refused to undergo immunohistochemical staining (p62 and ubiquitin staining) due to reasons of its own. Based on these findings, the patient was given a revised diagnosis of NIID. He was then prescribed symptomatic treatment, including oral analgesics (sibelum, 10 mg/d for 14 days) and oral idebenone tablets (90 mg/d for 3 months). Over the subsequent months, the patient reported a gradual relief of his symptoms. Follow-up by telephone 18 months after the patient was discharged revealed that the patient no longer had a paroxysmal visual field defect or hypoesthesia of the hands and that he suffered from only occasional headaches.

The timeline of the patient's disease course is shown in Figure 3.

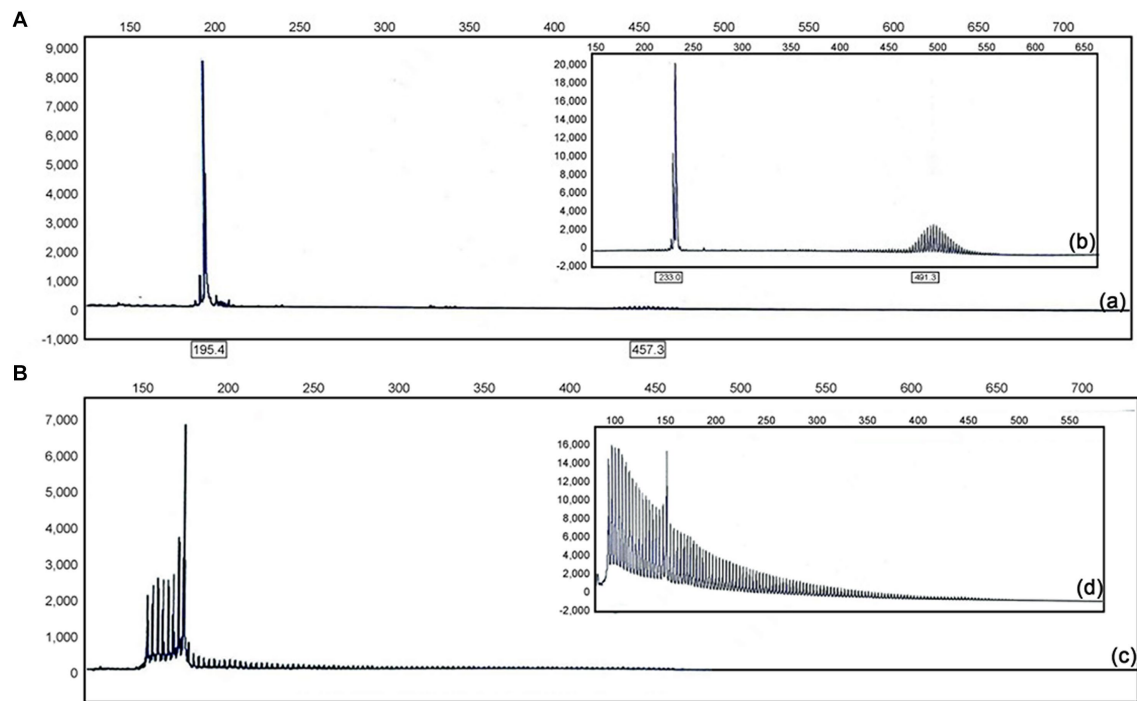


**FIGURE 2** (A) Electropherograms showing GC-rich regions using PCR and repeat-primed PCR assays in affected individuals (a) and positive control subjects (b). (B) GC-rich PCR showed the patient had 101 GGC repeats in the 5' UTR of NOTCH2NLC (c); GC-rich PCR showed the GGC repeats in the 5' UTR of NOTCH2NLC in positive control subjects (d).

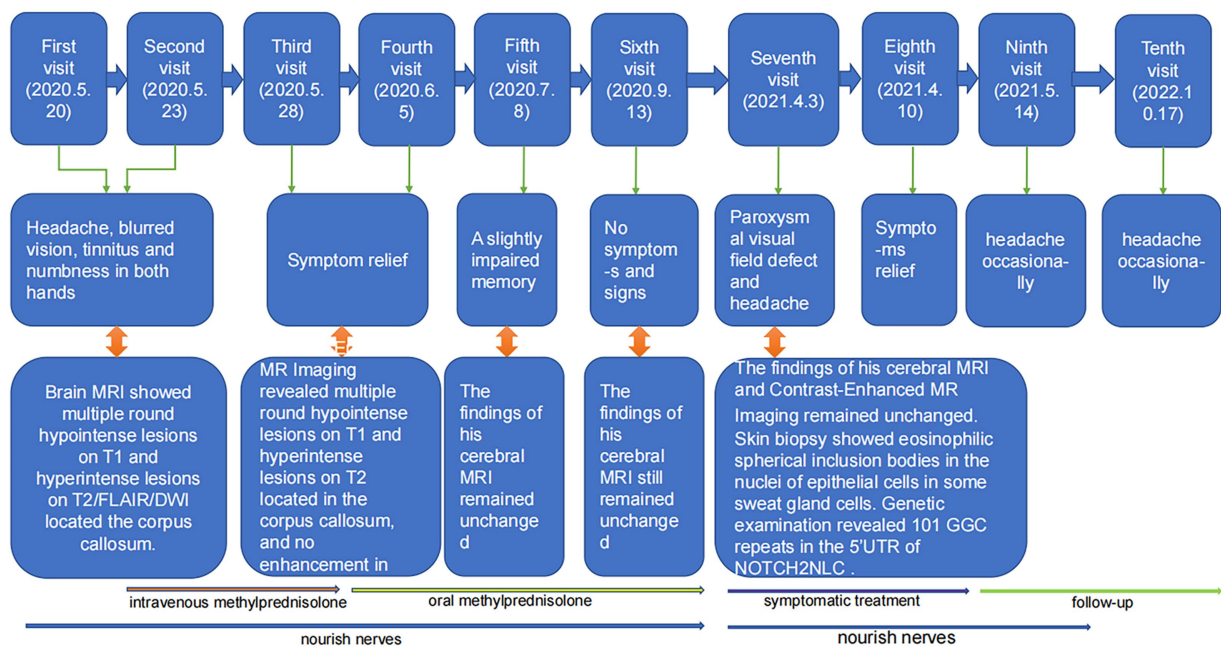


**FIGURE 3** The timeline of the patient's course of disease.

Discussion

NIID is a clinically heterogeneous illness with a range of clinical manifestations. For adult-onset NIID, dementia was the most

prominent initial symptom, followed by ataxia and unconsciousness (Sone et al., 2016). Affected patients may present with central nervous system impairments, including dementia (Munoz-Garcia and Ludwin, 1986; Araki et al., 2016), cerebellar ataxia (Patel et al., 1985), epilepsy

(Shindo et al., 2019), paroxysmal disturbances in consciousness (Zhang et al., 2022), Parkinsonism (Liu et al., 2008; López-Blanco et al., 2019) and abnormal mental behavior (Chi et al., 2020). Adult NIID may also present with peripheral nerve damage (Sone et al., 2005), including limb weakness and sensory disturbances. Other symptoms of autonomic nervous system involvement may include bladder dysfunction, miosis, syncope, and vomiting (Sone et al., 2005; Nakamura et al., 2018). According to published case reports, some patients have presented with subacute progressive encephalitis (Huang et al., 2021), stroke-like symptoms (Lin et al., 2020), mental abnormalities (Chi et al., 2020), and dopa-responsive dystonia (Paviour et al., 2005). The present report presents a case of adult-onset NIID in which the patient presented with the symptoms of headache, blurred vision, and tinnitus as initial symptoms, accompanied by numbness in the hands, cognitive slowing, and impaired memory.

Previously, brain MRI in patients with NIID has revealed diffuse symmetric white-matter hyperintensities in lateral cerebral ventricle areas in FLAIR images (Sone et al., 2014; Yu et al., 2019) and high-intensity signals along the corticomedullary junction of the frontal-parietal-temporal lobes in DWI (Sone et al., 2016; Yu et al., 2019). These findings, which are considered to be characteristic imaging manifestations of NIID, are known as the cortical linear sign and the subcortical lace sign, respectively. It has been suggested that the high-intensity DWI signal may be continuous across the corticomedullary junction in NIID patients, with lesions being confined mostly to the frontal lobe in early-stage NIID (Abe and Fujita, 2017). With progression of the disease, the high-intensity DWI signal may develop gradually without extending into the deep white matter (Nakamura et al., 2018; Omoto et al., 2018). However, high-intensity signal in the corticomedullary junction has been reported to disappear a few years after being observed (Kawarabayashi et al., 2018). Thus DWI findings may be dynamic across NIID phases. As such, it is vital that follow-up procedures be conducted in patients whose MRI scans indicate changes. The presently described patient's brain MRI revealed multiple small round hypointense lesions on T1WI and hyperintense lesions on T2WI/FLAIR/DWI located in the genu and splenium of the corpus callosum, and no significant changes were found after 18 months of follow-up. Some patients with NIID have shown high-intensity signal in the splenium of the corpus callosum only during an early disease stage (Yu et al., 2019; Wang et al., 2020b; Li et al., 2022), with subsequent gradual development of signal in the region of the corticomedullary junction as the disease progressed (Wang et al., 2020a). Therefore, we speculate that the atypical imaging manifestations of our patient may be attributed to his young age at which diffuse white matter lesions have not yet become evident. If so, then the small asymmetric round lesions observed could reflect an initial change of NIID leukoencephalopathy. What's more, compared with the patients with typical MRI findings, the presently described patient's symptoms are mild. Therefore, the atypical imaging findings have the potential to guide early diagnosis, so as to take early intervention to delay the progression of NIID.

Skin biopsy is feasible and helpful for the diagnosis of NIID. The pathological hallmarks are eosinophilic hyaline intranuclear inclusions in neuronal and non-neuronal central nervous system cells, in autonomic nervous system peripheral cells, as well as in visceral organs and skin (Sone et al., 2011, 2014). Intranuclear inclusions are round substances with a perinuclear diameter of 1.5–10  $\mu\text{m}$ . They are ubiquitin- and p62-positive, consisting of fibrous materials lacking

membranous structures when viewed under electron microscopy (Bitto et al., 2014; Sone et al., 2014). Currently, the identification of the GGC repeat expansion at the 5' end of NOTCH2NLC as the genetic cause of NIID will help in identifying the molecular pathogenesis in NIID. In NIID, the GGC repeat ranges from 66 to over 500; healthy people have fewer than 43 repeats. To date, there is no association between the GGC repeat size and the severity or the age of onset of the disease (Ishiura et al., 2019; Sone et al., 2019; Tian et al., 2019). In this case, genetic testing revealing a NOTCH2NLC allele with a GGC repeat expansion in the 5'UTR region, and the concomitant observation of eosinophilic inclusion bodies in sweat gland cells, both of them affirmed a diagnosis of NIID together.

Furthermore, in this case, FFA of the eyes showed dilated macular capillary and fluorescein leakage from dilated blood vessels. Dilation of macular capillaries leads to an expansion of intercellular space and increased vessel permeability, thereby enabling fluorescein leakage from dilated capillaries. This phenomenon may lead to retinal abnormalities over time. Retinal abnormalities, including dilated macular capillary, may be a very early retinal change in NIID (Liu et al., 2022; Sone et al., 2023).

There is, in addition, one further point to make. For NIID with corpus callosum lesions, it is mainly differentiated from Reversible splenial lesion syndrome (RESLES) and Marchiafava Bignami disease (MBD). In this case, the patient was initially misdiagnosed as SS due to the presence of the SS-typical symptoms and SS-characteristic radiology change. However, in the subsequent progression of SS, branch retinal artery occlusions and sensorineural hearing loss can also be seen, which is not available in NIID, which will help to distinguish the two.

There is not yet a standard treatment for NIID. Symptomatic treatment may improve a patient's quality of life and delay the progress of some symptoms. Analgesics have been reported to be typically effective in relieving the occurrence of NIID headache/migraine (Wang et al., 2020a). Steroid hormones have been used in the treatment of paroxysmal encephalopathy, but there is no clear evidence indicating that the drug can improve prognosis (Sone et al., 2016). In some cases, the treatment of intravenous methylprednisolone may improve the symptoms of dementia in patients with acute disease onset (Yadav et al., 2019). In the treatment of NIID with encephalitis-like symptoms, dehydration therapy can reduce brain edema and relieve symptoms. For infantile NIID or juvenile NIID with extrapyramidal disorder, there have been reported cases of dopamine treatment, but there is no clear efficacy (Paviour et al., 2005; Lai et al., 2010; Yoshimoto et al., 2017).

## Conclusion

This paper presents a NIID case in which the nervous and visual systems were affected simultaneously in early phase of the disease. The brain MRI showed multiple round hypointense lesions in T1WI analysis and hyperintense lesions in T2WI/FLAIR/DWI analysis in the corpus callosum. And the FFA of the eyes showed dilated macular capillary and fluorescein leakage from dilated blood vessels. Referring to previous literature, we consider the small asymmetric round lesions observed could reflect an initial change of NIID leukoencephalopathy, and the dilated macular capillary may be a very early retinal change in NIID. All in all, this report on a case of NIID may be conducive to

enriching clinicians' understanding of the disease based on its particular clinical manifestations and imaging characteristics.

## Data availability statement

The original contributions presented in the study are included in the article/[Supplementary material](#), further inquiries can be directed to the corresponding author.

## Ethics statement

The studies involving humans were approved by the Ethics Committee of Yuhuangding Hospital. The studies were conducted in accordance with the local legislation and institutional requirements. The participants provided their written informed consent to participate in this study. Written informed consent was obtained from the individual(s) for the publication of any potentially identifiable images or data included in this article.

## Author contributions

LY drafted and revised the manuscript. HZ collected patient information and revised the manuscript. ZL collected and analyzed patient information. HY, LW, and JZ interpreted the data and edited the manuscript. All authors contributed to the article and approved the submitted version.

## References

- Abe, K., and Fujita, M. (2017). Over 10 years MRI observation of a patient with neuronal intranuclear inclusion disease. *BMJ Case Rep.* 2017:bcr2016218790. doi: 10.1136/bcr-2016-218790
- Araki, K., Sone, J., Fujioka, Y., Masuda, M., Ohdake, R., Tanaka, Y., et al. (2016). Memory loss and frontal cognitive dysfunction in a patient with adult-onset neuronal intranuclear inclusion disease. *Intern. Med.* 55, 2281–2284. doi: 10.2169/internalmedicine.55.5544
- Bitto, A., Lerner, C. A., Nacarelli, T., Crowe, E., Torres, C., and Sell, C. (2014). P62/Sqstm1 at the Interface of aging, autophagy, and disease. *Age (Dordr.)* 36:9626. doi: 10.1007/s11357-014-9626-3
- Chi, X., Li, M., Huang, T., Tong, K., Xing, H., and Chen, J. (2020). Neuronal intranuclear inclusion disease with mental abnormality: a case report. *BMC Neurol.* 20:356. doi: 10.1186/s12883-020-01933-8
- Deng, J., Gu, M., Miao, Y., Yao, S., Zhu, M., Fang, P., et al. (2019). Long-read sequencing identified repeat expansions in the 5'utr of the Notch2ncl gene from Chinese patients with neuronal intranuclear inclusion disease. *J. Med. Genet.* 56, 758–764. doi: 10.1136/jmedgenet-2019-106268
- Egan, R. A. (2019). Diagnostic criteria and treatment algorithm for Susac syndrome. *J. Neuroophthalmol.* 39, 60–67. doi: 10.1097/WNO.0000000000000677
- Fiddes, I. T., Lodewijk, G. A., Mooring, M., Bosworth, C. M., Ewing, A. D., Mantalas, G. L., et al. (2018). Human-specific Notch2ncl genes affect notch signaling and cortical neurogenesis. *Cells* 173, 1356–1369.E22. doi: 10.1016/j.cell.2018.03.051
- Huang, Y., Jin, G., Zhan, Q. L., Tian, Y., and Shen, L. (2021). Adult-onset neuronal intranuclear inclusion disease, with both stroke-like onset and encephalitic attacks: a case report. *BMC Neurol.* 21:142. doi: 10.1186/s12883-021-02164-1
- Ishiura, H., Shibata, S., Yoshimura, J., Suzuki, Y., Qu, W., Doi, K., et al. (2019). Noncoding Cgg repeat expansions in neuronal intranuclear inclusion disease, oculopharyngodistal myopathy and an overlapping disease. *Nat. Genet.* 51, 1222–1232. doi: 10.1038/s41588-019-0458-z
- Kawarabayashi, T., Nakamura, T., Seino, Y., Hirohata, M., Mori, F., Wakabayashi, K., et al. (2018). Disappearance of MRI imaging signals in a patient with neuronal intranuclear inclusion disease. *J. Neurol. Sci.* 388, 1–3. doi: 10.1016/j.jns.2018.02.038

## Funding

This work was partially supported by grants from the Yantai Science and Technology Plan Project (2021YD033 and 2018SFGY092).

## Conflict of interest

The authors declare that the research was conducted in the absence of any commercial or financial relationships that could be construed as a potential conflict of interest.

## Publisher's note

All claims expressed in this article are solely those of the authors and do not necessarily represent those of their affiliated organizations, or those of the publisher, the editors and the reviewers. Any product that may be evaluated in this article, or claim that may be made by its manufacturer, is not guaranteed or endorsed by the publisher.

## Supplementary material

The Supplementary material for this article can be found online at: <https://www.frontiersin.org/articles/10.3389/fnins.2023.1247403/full#supplementary-material>

- Kimber, T. E., Blumbergs, P. C., Rice, J. P., Hallpike, J. F., Edis, R., Thompson, P. D., et al. (1998). Familial neuronal intranuclear inclusion disease with ubiquitin positive inclusions. *J. Neurol. Sci.* 160, 33–40. doi: 10.1016/S0022-510X(98)00169-5
- Lai, S. C., Jung, S. M., Grattan-Smith, P., Sugo, E., Lin, Y. W., Chen, R. S., et al. (2010). Neuronal intranuclear inclusion disease: two cases of dopa-responsive juvenile Parkinsonism with drug-induced dyskinesia. *Mov. Disord.* 25, 1274–1279. doi: 10.1002/mds.22876
- Li, F., Wang, Q., Zhu, Y., Xiao, J., Gu, M., Yu, J., et al. (2022). Unraveling rare form of adult-onset NIID by characteristic brain MRI features: a single-center retrospective review. *Front. Neurol.* 13:1085283. doi: 10.3389/fneur.2022.1085283
- Lim, C. C., Tan, C. B., and Umapathi, T. (2004). MRI findings in Susac's syndrome. *Neurology* 63:761. doi: 10.1212/wnl.63.4.761
- Lin, P., Jin, H., Yi, K. C., He, X. S., Lin, S. F., Wu, G., et al. (2020). A case report of sporadic adult neuronal intranuclear inclusion disease (NIID) with stroke-like onset. *Front. Neurol.* 11:530. doi: 10.3389/fneur.2020.00530
- Liu, Y., Lu, J., Li, K., Zhao, H., Feng, Y., Zhang, Z., et al. (2019). Correction to: a multimodal imaging features of the brain in adult-onset neuronal intranuclear inclusion disease. *Neurol. Sci.* 40:905. doi: 10.1007/s10072-019-03787-6
- Liu, C., Luan, X., Liu, X., Wang, X., Cai, X., Li, T., et al. (2022). Characteristics of ocular findings of patients with neuronal intranuclear inclusion disease. *Neurol. Sci.* 43, 3231–3237. doi: 10.1007/s10072-021-05748-4
- Liu, Y., Mimuro, M., Yoshida, M., Hashizume, Y., Niwa, H., Miyao, S., et al. (2008). Inclusion-positive cell types in adult-onset intranuclear inclusion body disease: implications for clinical diagnosis. *Acta Neuropathol.* 116, 615–623. doi: 10.1007/s00401-008-0442-7
- López-Blanco, R., Uriarte-Pérez De Urabayen, D., and Méndez-Guerrero, A. (2019). Reader response: neuronal intranuclear inclusion disease showing intranuclear inclusions in renal biopsy 12 years earlier. *Neurology* 93:414. doi: 10.1212/WNL.0000000000008020
- Mori, F., Miki, Y., Tanji, K., Ogura, E., Yagihashi, N., Jensen, P. H., et al. (2011). Incipient intranuclear inclusion body disease in a 78-year-old woman. *Neuropathology* 31, 188–193. doi: 10.1111/j.1440-1789.2010.01150.x

- Mori, F., Tanji, K., Kon, T., Odagiri, S., Hattori, M., Hoshikawa, Y., et al. (2012). FUS immunoreactivity of neuronal and glial intranuclear inclusions in intranuclear inclusion body disease. *Neuropathol. Appl. Neurobiol.* 38, 322–328. doi: 10.1111/j.1365-2990.2011.01217.x
- Munoz-Garcia, D., and Ludwin, S. K. (1986). Adult-onset neuronal intranuclear hyaline inclusion disease. *Neurology* 36, 785–790. doi: 10.1212/WNL.36.6.785
- Nakamura, M., Murray, M. E., Lin, W. L., Kusaka, H., and Dickson, D. W. (2014). Optineurin immunoreactivity in neuronal and glial intranuclear inclusions in adult-onset neuronal intranuclear inclusion disease. *Am. J. Neurodegener. Dis.* 3, 93–102.
- Nakamura, M., Ueki, S., Kubo, M., Yagi, H., Sasaki, R., Okada, Y., et al. (2018). Two cases of sporadic adult-onset neuronal intranuclear inclusion disease preceded by urinary disturbance for many years. *J. Neurol. Sci.* 392, 89–93. doi: 10.1016/j.jns.2018.07.012
- Omoto, S., Hayashi, T., Matsuno, H., Higa, H., Kameya, S., Sengoku, R., et al. (2018). Neuronal intranuclear hyaline inclusion disease presenting with childhood-onset night blindness associated with progressive retinal dystrophy. *J. Neurol. Sci.* 388, 84–86. doi: 10.1016/j.jns.2018.03.010
- Patel, H., Norman, M. G., Perry, T. L., and Berry, K. E. (1985). Multiple system atrophy with neuronal intranuclear hyaline inclusions. Report of a case and review of the literature. *J. Neurol. Sci.* 67, 57–65. doi: 10.1016/0022-510X(85)90022-X
- Paviour, D. C., Revesz, T., Holton, J. L., Evans, A., Olsson, J. E., and Lees, A. J. (2005). Neuronal intranuclear inclusion disease: report on a case originally diagnosed as dopa-responsive dystonia with Lewy bodies. *Mov. Disord.* 20, 1345–1349. doi: 10.1002/mds.20559
- Pountney, D. L., Huang, Y., Burns, R. J., Haan, E., Thompson, P. D., Blumbergs, P. C., et al. (2003). Sumo-1 Marks the nuclear inclusions in familial neuronal intranuclear inclusion disease. *Exp. Neurol.* 184, 436–446. doi: 10.1016/j.expneurol.2003.07.004
- Shindo, K., Tsuchiya, M., Hata, T., Ichinose, Y., Koh, K., Sone, J., et al. (2019). Non-convulsive status epilepticus associated with neuronal intranuclear inclusion disease: a case report and literature review. *Epilepsy Behav. Case Rep.* 11, 103–106. doi: 10.1016/j.ebcr.2019.01.007
- Sone, J., Hishikawa, N., Koike, H., Hattori, N., Hirayama, M., Nagamatsu, M., et al. (2005). Neuronal intranuclear hyaline inclusion disease showing motor-sensory and autonomic neuropathy. *Neurology* 65, 1538–1543. doi: 10.1212/01.wnl.0000184490.22527.90
- Sone, J., Kitagawa, N., Sugawara, E., Iguchi, M., Nakamura, R., Koike, H., et al. (2014). Neuronal intranuclear inclusion disease cases with leukoencephalopathy diagnosed via skin biopsy. *J. Neurol. Neurosurg. Psychiatry* 85, 354–356. doi: 10.1136/jnnp-2013-306084
- Sone, J., Mitsushashi, S., Fujita, A., Mizuguchi, T., Hamanaka, K., Mori, K., et al. (2019). Long-read sequencing identifies GGC repeat expansions in NOTCH2NL associated with neuronal intranuclear inclusion disease. *Nat. Genet.* 51, 1215–1221. doi: 10.1038/s41588-019-0459-y
- Sone, J., Mori, K., Inagaki, T., Katsumata, R., Takagi, S., Yokoi, S., et al. (2016). Clinicopathological features of adult-onset neuronal intranuclear inclusion disease. *Brain* 139, 3170–3186. doi: 10.1093/brain/aww249
- Sone, J., Tanaka, F., Koike, H., Inukai, A., Katsuno, M., Yoshida, M., et al. (2011). Skin biopsy is useful for the antemortem diagnosis of neuronal intranuclear inclusion disease. *Neurology* 76, 1372–1376. doi: 10.1212/WNL.0b013e3182166e13
- Sone, J., Ueno, S., Akagi, A., Miyahara, H., Tamai, C., Riku, Y., et al. (2023). NOTCH2NL GGC repeat expansion causes retinal pathology with intranuclear inclusions throughout the retina and causes visual impairment. *Acta Neuropathol. Commun.* 11:71. doi: 10.1186/s40478-023-01564-3
- Suzuki, I. K., Gacquer, D., Van Heurck, R., Kumar, D., Wojno, M., Bilheu, A., et al. (2018). Human-specific NOTCH2NL genes expand cortical neurogenesis through Delta/Notch regulation. *Cells* 173, 1370–1384.E16. doi: 10.1016/j.cell.2018.03.067
- Takahashi-Fujigasaki, J. (2003). Neuronal intranuclear hyaline inclusion disease. *Neuropathology* 23, 351–359. doi: 10.1046/j.1440-1789.2003.00524.x
- Takahashi-Fujigasaki, J., Nakano, Y., Uchino, A., and Murayama, S. (2016). Adult-onset neuronal intranuclear hyaline inclusion disease is not rare in older adults. *Geriatr Gerontol Int* 16, 51–56. doi: 10.1111/ggi.12725
- Takumida, H., Yakabe, M., Mori, H., Shibasaki, K., Umeda-Kameyama, Y., Urano, T., et al. (2017). Case of a 78-year-old woman with a neuronal intranuclear inclusion disease. *Geriatr Gerontol Int* 17, 2623–2625. doi: 10.1111/ggi.13174
- Tian, Y., Wang, J. L., Huang, W., Zeng, S., Jiao, B., Liu, Z., et al. (2019). Expansion of human-specific GGC repeat in neuronal intranuclear inclusion disease-related disorders. *Am. J. Hum. Genet.* 105, 166–176. doi: 10.1016/j.ajhg.2019.05.013
- Wang, R., Nie, X., Xu, S., Zhang, M., Dong, Z., and Yu, S. (2020a). Interrelated pathogenesis? Neuronal intranuclear inclusion disease combining with hemiplegic migraine. *Headache* 60, 382–395. doi: 10.1111/head.13687
- Wang, Y., Wang, B., Wang, L., Yao, S., Zhao, J., Zhong, S., et al. (2020b). Diagnostic indicators for adult-onset neuronal intranuclear inclusion disease. *Clin. Neuropathol.* 39, 7–18. doi: 10.5414/NP301203
- Yadav, N., Raja, P., Shetty, S. S., Jitender, S., Prasad, C., Kamble, N. L., et al. (2019). Neuronal intranuclear inclusion disease: a rare etiology for rapidly progressive dementia. *Alzheimer Dis. Assoc. Disord.* 33, 359–361. doi: 10.1097/WAD.0000000000000312
- Yoshimoto, T., Takamatsu, K., Kurashige, T., Sone, J., Sobue, G., and Kuriyama, M. (2017). Adult-onset neuronal intranuclear inclusion disease in two female siblings. *Brain Nerve* 69, 267–274. doi: 10.11477/mf.1416200737
- Yu, W. Y., Xu, Z., Lee, H. Y., Tokumaru, A., Tan, J. M. M., Ng, A., et al. (2019). Identifying patients with neuronal intranuclear inclusion disease in Singapore using characteristic diffusion-weighted MR images. *Neuroradiology* 61, 1281–1290. doi: 10.1007/s00234-019-02257-2
- Zhang, S., Shen, L., and Jiao, B. (2022). Cognitive dysfunction in repeat expansion diseases: a review. *Front. Aging Neurosci.* 14:841711. doi: 10.3389/fnagi.2022.1120252



## OPEN ACCESS

## EDITED BY

Jingming Hou,  
Army Medical University, China

## REVIEWED BY

Masaru Tanaka,  
University of Szeged (ELKH-SZTE), Hungary  
Simone Battaglia,  
University of Bologna, Italy

## \*CORRESPONDENCE

Hua Xue  
✉ xueh1895@163.com

RECEIVED 02 June 2023

ACCEPTED 26 July 2023

PUBLISHED 10 August 2023

## CITATION

Xue H, Zeng L and Liu S (2023) Unraveling the link: exploring the causal relationship between diabetes, multiple sclerosis, migraine, and Alzheimer's disease through Mendelian randomization.  
*Front. Neurosci.* 17:1233601.  
doi: 10.3389/fnins.2023.1233601

## COPYRIGHT

© 2023 Xue, Zeng and Liu. This is an open-access article distributed under the terms of the [Creative Commons Attribution License \(CC BY\)](#). The use, distribution or reproduction in other forums is permitted, provided the original author(s) and the copyright owner(s) are credited and that the original publication in this journal is cited, in accordance with accepted academic practice. No use, distribution or reproduction is permitted which does not comply with these terms.

# Unraveling the link: exploring the causal relationship between diabetes, multiple sclerosis, migraine, and Alzheimer's disease through Mendelian randomization

Hua Xue<sup>1\*</sup>, Li Zeng<sup>2</sup> and Shuangjuan Liu<sup>3</sup>

<sup>1</sup>Department of Neurology, Sichuan Taikang Hospital, Chengdu, Sichuan, China, <sup>2</sup>Department of Respiratory, Affiliated Hospital of Youjiang Medical University for Nationalities, Baise, Guangxi, China,

<sup>3</sup>Department of Neurology, Qionglai People's Hospital, Chengdu, Sichuan, China

**Introduction:** Observational studies suggested that diabetes mellitus [type 1 diabetes mellitus (T1DM), type 2 diabetes mellitus (T2DM)], multiple sclerosis (MS), and migraine are associated with Alzheimer's disease (AD). However, the causal link has not been fully elucidated. Thus, we aim to assess the causal link between T1DM, T2DM, MS, and migraine with the risk of AD using a two-sample Mendelian randomization (MR) study.

**Methods:** Genetic instruments were identified for AD, T1DM, T2DM, MS, and migraine respectively from genome-wide association study. MR analysis was conducted mainly using the inverse-variance weighted (IVW) method.

**Results:** The result of IVW method demonstrated that T2DM is causally associated with risk of AD (OR: 1.237, 95% CI: 1.099–1.391, P: 0.0003). According to the IVW method, there is no causal association between T1DM, MS, migraine, and the risk of AD (all *p* value > 0.05). Here we show, there is a causal link between T2DM and the risk of AD.

**Conclusion:** These findings highlight the significance of active monitoring and prevention of AD in T2DM patients. Further studies are required to actively search for the risk factors of T2DM combined with AD, explore the markers that can predict T2DM combined with AD, and intervene and treat early.

## KEYWORDS

diabetes mellitus, multiple sclerosis, migraine, Alzheimer's disease, Mendelian randomization, genome-wide association study

## 1. Introduction

Diabetes mellitus (DM) is one of the most common chronic metabolic disorders affecting multiple systems (Kashyap et al., 2018; Sempere-Bigorra et al., 2021). Multiple sclerosis (MS), migraine, and Alzheimer's disease (AD) are common neurological disorders, which cause a lot of inconvenience to the lives of patients and cause a heavy social and economic burden (Oh et al., 2018; Burch, 2019; Sheppard and Coleman, 2020). AD is a degenerative disease of the central nervous system characterized by progressive cognitive dysfunction and behavioral impairment that occurs in the elderly and pre-elderly (Zhang et al., 2021). Clinically, it is manifested as memory impairment, aphasia, apraxia, agnosia, visual-spatial ability impairment, abstract thinking and computing power impairment, and personality and behavior changes (Wang et al., 2020; Zhang et al., 2021). Previous epidemiological studies have observed an

increased risk of AD in patients with diabetes, migraine, or multiple sclerosis (Morton et al., 2019; Silva et al., 2019; Benedict et al., 2020). However, the strength and significance of the observed associations of DM, migraine, and MS with AD remain controversial.

Diabetes mellitus is a prevalent chronic disease characterized by chronic hyperglycemia resulting from various causes of defective insulin secretion or defective insulin action that leads to abnormal metabolism of glucose, protein, and fat (Lin et al., 2021; Cloete, 2022). Type 1 diabetes mellitus (T1DM) and type 2 diabetes mellitus (T2DM) are common types of DM. T1DM mostly occurs in adolescents, with acute onset, obvious and severe symptoms, and ketoacidosis as the first symptom, while T2DM mostly occurs in adults over 40 years old and the elderly, mostly obese, with hidden onset and not-so-obvious early symptoms (Gillani et al., 2021; Wu and Liang, 2022). It is widely acknowledged that the complications of DM are numerous and complex, not only affecting retinal arteries and leading to kidney damage but also a risk factor for cardiovascular and cerebrovascular diseases (Demir et al., 2021). In recent years, the associations between DM and AD drawn from epidemiological studies have attracted much attention (Silva et al., 2019; Zhang et al., 2021). Animal experiments have found that dementia is closely related to central insulin resistance (IR) in patients with DM (Rojas et al., 2021). The activities of  $\beta$ -secretase and  $\gamma$ -secretase were enhanced after central IR, and amyloid- $\beta$  (A $\beta$ ) was increased. A large number of A $\beta$  degrading enzymes were combined with insulin, which reduced the degradation of A $\beta$ , and the production, clearance, and aggregation of peptides were unbalanced, resulting in A $\beta$  deposition in the brain (Biessels and Despa, 2018). Alasia et al. cultured cerebellar granule cells *in vitro* and confirmed that A $\beta$  deposition is the direct cause of brain cell apoptosis. At the same time, A $\beta$  deposition also produces senile plaques and induces cognitive impairment in the body (Alasia et al., 2012). Disturbances in glucose metabolism have been shown to impact mitochondrial homeostasis in the brain (Cabezas-Opazo et al., 2015). Studies have found that patients with DM exhibit reduced brain glucose metabolism, which is accompanied by altered expression and decreased activity of mitochondrial energy-related proteins (Solanki et al., 2017). Interestingly, similar symptoms have also been observed in fibroblasts and brain tissues of patients with AD (Solanki et al., 2017). Additionally, a clinical study found that C-peptide was associated with poorer executive function in diabetic patients and insulin resistance may worsen prefrontal cortex function (Lesiewska et al., 2022).

Multiple sclerosis (MS) is an immune-mediated chronic inflammatory demyelinating disease of the central nervous system involving the periventricular, proximal cortex, optic nerve, spinal cord, brainstem, and cerebellum, with spatially multiple and temporally multiple lesions (Baecher-Allan et al., 2018). MS is characterized by a wide variety of clinical symptoms. In addition to the common motor, sensory, visual, and autonomic deficits, cognitive impairment is also a common symptom. The prevalence of cognitive impairment in patients with MS varies by age and may be difficult to distinguish from other causes (e.g., AD) in older patients (Luczynski et al., 2019; Benedict et al., 2020). A cohort study testing MS-related cognitive impairment found greater differences between MS patients ( $n=66$ ) and healthy controls ( $n=22$ ) (Taranu et al., 2022). Although the exact pathogenesis of MS with cognitive impairment is still unclear, it is thought to be primarily related to pathological changes in lesioned and normal-appearing white matter, specific neural gray matter structures, and immunological changes, especially to synaptic transmission and plasticity impact (Portaccio and Amato, 2022). The pathological features of MS include

white matter lesions characterized by demyelination and inflammation, resulting in axonal injury and progressive degeneration. Demyelination can cause a reduction in the speed and reliability of axonal transmission. Specifically, it leads to a decrease in conduction speed and information processing speed, leading to cognitive impairment (Conti et al., 2021). Furthermore, a study suggested that abnormalities in the Tryptophan-Kynurenine metabolic system were observed in patients with MS and that the Kynurenine metabolite profile may serve as a biomarker for progressive MS (Polyák et al., 2023). However, the Tryptophan-Kynurenine metabolic pathway was considered to be an important pathway of neuronal damage in neurodegenerative diseases and severe brain injuries (Schwarcz et al., 2012; Battaglia et al., 2023).

Migraine is a highly prevalent and disabling neurological disorder that affects approximately 14.4% of the global population (Zhao et al., 2023). Migraine can cause different levels and types of outcomes, including stroke, subclinical cerebrovascular lesions, hypertension, psychiatric disorders (depression, anxiety, bipolar disorder, panic disorder, and suicide), obesity, and restless legs syndrome. A prospective cohort study involving 679 patients, which followed community-dwelling older adults for 5 years, found that migraines were a significant risk factor for AD and all-cause dementia (Morton et al., 2019). More and more studies have concluded that there is a certain degree of cognitive impairment in patients with migraine, and the degree of cognitive impairment is related to the intensity of headaches, the frequency of attacks, and the duration of attacks in patients (Karami et al., 2019; Klan et al., 2019). The pathological mechanism may be a decrease in the basal metabolic rate of the limbic system composed of the hippocampus, cingulate gyrus, hippocampal gyrus, and amygdala in patients with migraine, affecting the cognitive function of the patients (Guo et al., 2022). A study from China found that serum 5-hydroxytryptamine (5-HT) levels increased in patients with migraine, which may be due to impaired oxidative balance and excessive neuronal excitation (Smith and Ebrahim, 2003). 5-HT is released into the blood, which may further damage the blood-brain barrier and affect cognitive function (Lawlor et al., 2008).

In light of the abovementioned studies, we hypothesized that diabetes, multiple sclerosis, and migraine may be potential factors for AD. However, traditional observational studies are susceptible to potential confounders and reverse causality bias, making the inference of causality difficult. Therefore, the potential causal relationship between appellate disease and AD is unclear. Mendelian randomization (MR) is a new epidemiological technique based on whole genome-wide association studies (GWAS). It uses single nucleotide polymorphisms (SNPs) as instrumental variables (IVs) to reveal causal relationships (Li et al., 2022). Compared with cohort studies and other types of studies, MR can effectively reduce bias; genetic variation is randomly transmitted to offspring and remains unchanged after conception, making it less prone to reverse causality and confounding factors (Grover and Sharma, 2022). Hence, we aimed to explore the causal individual links between AD and diabetes, multiple sclerosis, and migraine through MR studies.

## 2. Materials and methods

Mendelian randomization (MR), proposed by the famous statistician Fisher, is a method of causal inference based on genetic variation and is based on the principle of using the effect of randomly assigned genotypes on phenotypes in nature to infer the effect of

biological factors on disease (Nikpay et al., 2015). In MR study, researchers analyze genome-wide association studies (GWAS) to find single nucleotide polymorphisms (SNPs) as instrumental variables (IVs), which are associated with biological factors, and then use these IVs to infer the effects of biological factors on disease (Davey Smith and Hemani, 2014). Since genes are randomly assigned and are not affected by confounding factors, the use of genetic variation to study causality can avoid the influence of confounding factors on the results and improve the reliability of causality inference (Chen et al., 2022).

## 2.1. Study design

At present, GWAS has found that hundreds of thousands or even millions of genetic variants are associated with disease outcomes, and these data are the basis of MR analysis (Pierce et al., 2011). In general, MR is based on three conditional assumptions (Figure 1). The first assumption is that the genetic variants chosen as IVs are only associated with exposure (T1DM, T2DM, MS, and migraine) to ensure the relevance of the IVs. Second, selected IVs are uncorrelated with known or unknown confounding factors to ensure the independence of IVs. A final assumption is that genetic variation affects outcomes (AD) only through exposure and not elsewhere to ensure the exclusivity of IVs (Mahajan et al., 2018). Only by satisfying the above three assumptions can the selected IVs make the results as reliable as possible.

## 2.2. Instrument variables selection

We selected SNPs strongly correlated with exposure from GWAS ( $p$  value  $< 5 \times 10^{-8}$ ) as IVs at first. The strength of IVs was assessed using the  $F$ -statistic. The threshold of  $F$ -statistic  $> 10$  indicated that the genetic

variant has a strong estimation effect, in order to effectively avoid the bias caused by IVs (International Multiple Sclerosis Genetics Consortium, 2019). The second step was to remove the SNP linkage disequilibrium (set the parameter as  $r^2 = 0.001$ ,  $kb = 10,000$ ). Finally, if the selected SNPs were associated with confounder factors that significantly correlated ( $p$  value  $< 5 \times 10^{-8}$ ), it was removed from the list of selected SNPs (Hautakangas et al., 2022).

## 2.3. Exposure and outcome GWAS dataset

In this study, the T1DM GWAS summary dataset was derived from a large multigenic T1DM genome-wide association meta-analysis that includes 9,266 T1DM cases and 15,575 normal controls (24,840 in total), all from European ancestry (Forgetta et al., 2020). Summary statistics for T2DM have been acquired from the large multigenic T2DM genome-wide association meta-analysis that includes 81,412 T2DM cases and 15,575 normal controls (452,244 participants in total) all from European ancestry (Wang et al., 2022). For MS, summary data were extracted from a multiple sclerosis genomic map that involved 47,429 cases (68,374 controls) from the International Multiple Sclerosis Genetics Consortium, 2019; (Park et al., 2023). The summary-level data on migraine was obtained from the largest available genome-wide meta-analysis, comprising 102,084 migraine cases and 771,257 controls, all from European ancestry (Nazarzadeh et al., 2020).

The AD GWAS summary data was downloaded from a large genome-wide analysis involving 21,982 cases (41,944 controls) from the Alzheimer Disease Genetics Consortium (ADGC), which conducted a large-scale meta-analysis in 2019 [Alzheimer Disease Genetics Consortium (ADGC) et al., 2019]. The information on all the genetic datasets used in the current study is displayed in Table 1.

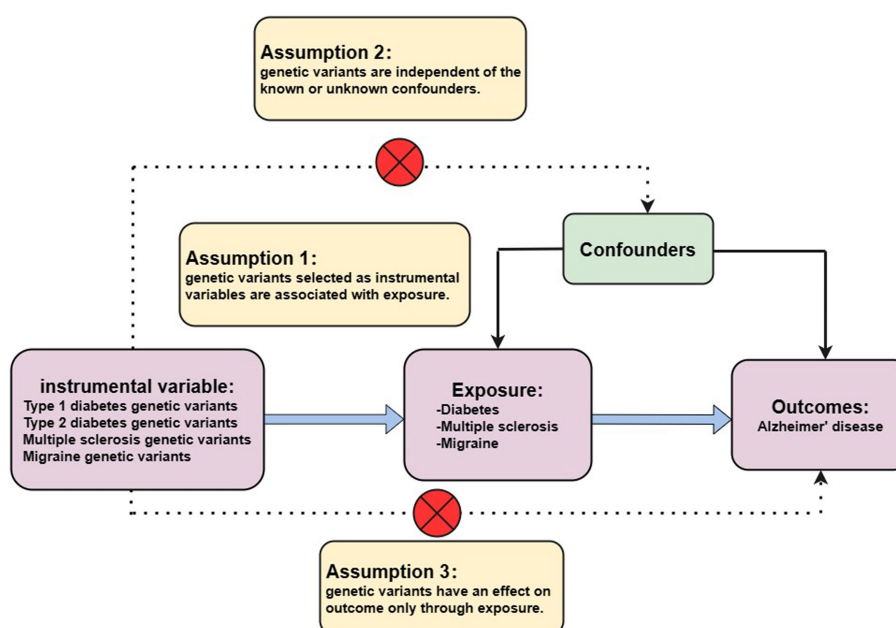


FIGURE 1

Three assumptions for MR analysis. First, the genetic variants, which are selected as the instrumental variables, are associated with exposure (type 1 diabetes, type 2 diabetes, multiple sclerosis, and migraine). Second, genetic variants are not related to known or unknown confounder factors. Third, genetic variants would have an influence on the outcome (Alzheimer's disease) only through exposure, not through other pathways.

TABLE 1 Detailed information on the studies and datasets used for Mendelian randomization analyses.

Phenotype	Consortium	Ethnicity	Sample size	Cases	Year	PubMed ID
Alzheimer's disease	PCG	European	63,976	21,982	2019	30820047
Type 1 diabetes	NA	European	24,840	9,266	2020	33830302
Type 2 diabetes	NA	European	452,244	81,412	2018	29632382
Multiple sclerosis	IMSGC	European	115,803	47,429	2019	31604244
Migraine	Neale Lab	European	873,341	102,084	2022	35115687

## 2.4. Statistical analysis

We performed a two-sample MR analysis of the collected GWAS data, using an inverse variance weighting (IVW) approach that combined the Wald ratio as the primary analysis to assess the individual causal association between exposure (T1DM, T2DM, MS, or migraine) and outcome (AD) (Jayaraj et al., 2020). If there was no heterogeneity in the MR results, the fixed effect IVW calculation was used, otherwise, the random effect was performed. IVW is a method for MR to perform a meta-summary on the effect of multiple sites when analyzing multiple SNPs. The premise of the IVW application is that all SNPs are effective IVs and are completely independent of each other (Shen et al., 2022). As a result, the results calculated by the IVW method are more robust and reliable. We first identified genome-wide significant (value of  $p < 5 \times 10^{-8}$ ) and independent ( $r^2 < 0.001$ , kb = 10,000) SNPs from the exposure dataset as genetic IVs of exposure. The exposure-associated SNPs obtained from the AD dataset were then correlated with the genetics of AD. In addition, additional MR analyses, including MR-Egger regression, weighted median regression (WMR), and Mendelian randomized multivariate residuals and outliers (MR-PRESSO) methods, complement the IVW as these methods can provide more robust estimates in a wider range of scenarios (Jayaraj et al., 2020). MR-Egger regression can provide tests for unbalanced pleiotropy and considerable heterogeneity, whereas larger sample sizes are required for the same underexposed variants. WMR is the median of the distribution function obtained by sorting all individual SNP effect values according to weights. When at least 50% of the information comes from valid IVs, WMR can obtain robust estimates (Tzoporis et al., 2020). In addition, strict instrumental value of  $p$  thresholds and recalculations were used if results from different MR analyses were inconsistent.

To assess the robustness of the results, we performed a series of sensitivity analyses using Cochran's Q test, MR-Egger intercept test, and MR-PRESSO global test. All value of  $p$  of the MR-Egger intercept tests were  $> 0.05$ , indicating that no horizontal pleiotropy existed.

All the aforementioned statistical analyses were conducted in "TwoSample MR" (version 0.5.6) and "Mendelian Randomization" (version 0.5.2) packages in the statistical program R (version 4.1.1). Statistical significance was defined as a value of  $p < 0.05$ .

## 3. Results

We obtained 69 SNPs as IVs of T1DM from the GWAS. The F-statistics of 69 SNPs were above the threshold of 10, which indicated that they strongly predicted T1DM in the MR analysis. We obtained 53 genetic variants associated with T2DM as IVs. As for MS, we analyzed 92 genetic variants highly associated with MS as IVs. As for migraine, there were 12 genetic variants associated with migraine

as IVs. Detailed information on IVs is shown in [Supplementary Tables S1–S4](#).

In the IVW analyses, no evidence was found for the causal associations between T1DM and the risk of AD (OR: 1.005, 95% CI: 0.983–1.026,  $P = 0.641$ ). The results of the IVW analyses demonstrated that there is a causal association between T2DM and the risk of AD (OR: 1.237, 95% CI: 1.099–1.391,  $P = 0.0003$ ). No evidence was found for the causal associations between MS and the risk of AD in the IVW method (OR: 0.984, 95% CI: 0.950–1.019,  $P = 0.381$ ). There was no association between migraine and AD in the IVW method (OR: 20.264, 95% CI: 0.124–3287.978,  $P = 0.246$ ). The detailed information of MR estimates for the exposures on AD risk is described in [Table 2](#). Scatter plots and funnel plots from genetically predicted exposure on AD are shown in [Figures 2–5](#).

In order to evaluate the robustness of the abovementioned results, we conducted a sensitivity analysis, including Cochran's Q test, MR-Egger intercept test, and MR-PRESSO global test. In the sensitivity analysis, the association patterns of most statistical models maintained directional consistency ([Table 3](#)). The leave-one-out analysis is shown in [Supplementary Figures S1–S4](#).

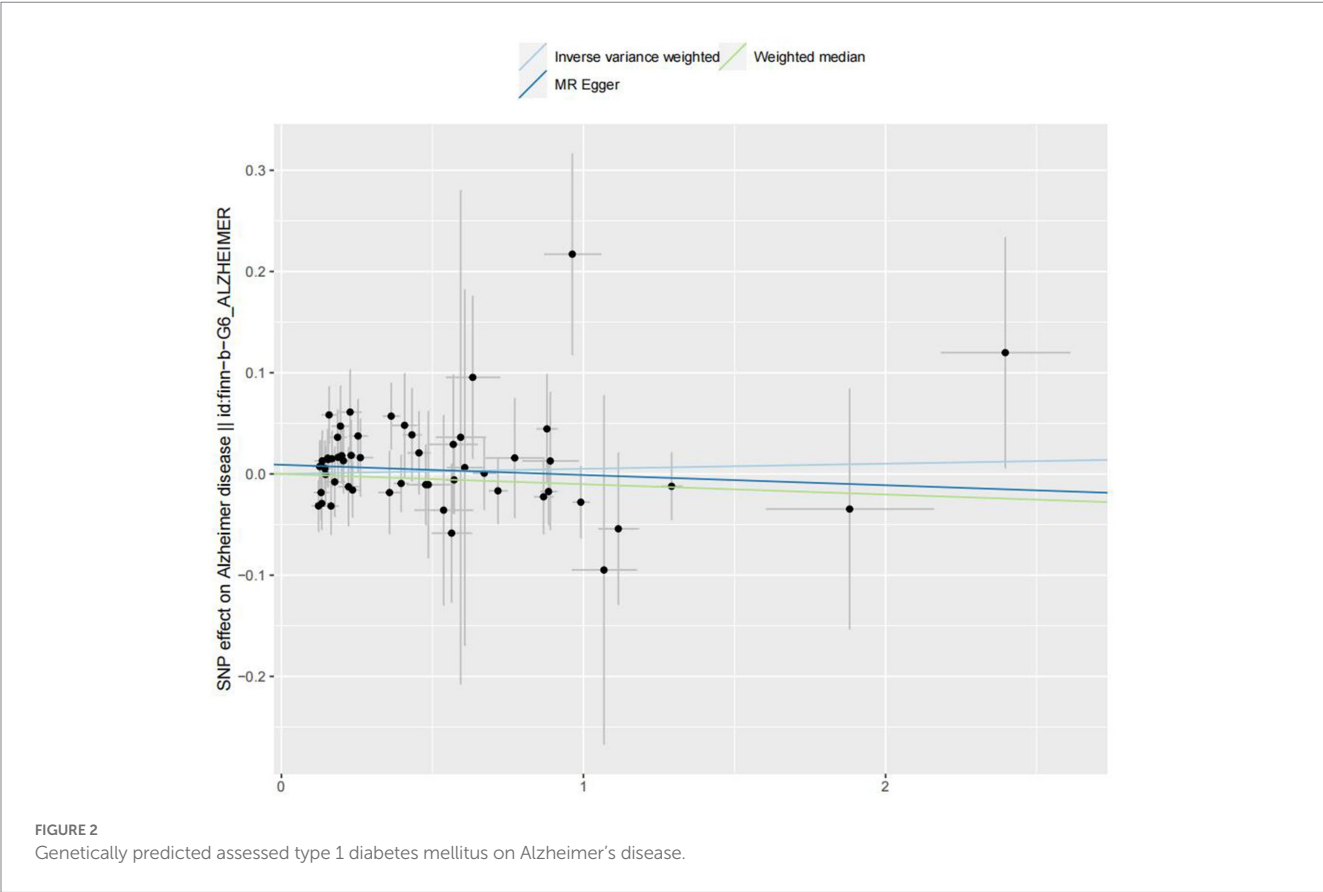
## 4. Discussion

In this study, we performed several MR analyses from large consortia and genetic studies to individually investigate the causal relationship between T1DM, T2DM, MS, migraine, and AD. The result suggested that T2DM was causally associated with AD (OR: 1.237, 95% CI: 1.099–1.391,  $P = 0.0003$  for IVW method; OR: 1.248, 95% CI: 1.019–1.529,  $P = 0.031$  for WMR method). In addition, there was no causal link between T1DM, MS, migraine, and AD according to our results, which means that these chronic diseases would not be significantly associated with the development of AD. Perhaps, T1DM, MS, migraine, and AD are complicated diseases, and their development and progression would be caused by other factors.

Both T2DM and AD are common chronic diseases in the elderly, and there is a close relationship between them. Clinical studies have confirmed that T2DM increases the risk of cerebrovascular disease, impairs cognitive function, and may even lead to the development of AD. It has been reported that the prevalence of T2DM combined with AD is increasing, and the risk of AD in patients with T2DM is much higher than in patients without T2DM (Jia et al., 2020; Lorente et al., 2022; Cao et al., 2023). With the aging of the world population, the number of T2DM and AD patients in the world is increasing, and the prevention and treatment of T2DM and AD have become a global public health problem. Our two-sample MR study demonstrated a

TABLE 2 MR estimates for the exposures on AD risk.

Exposure	Methods	Odds ratio	95% CI	<i>p</i>
Type 1 diabetes	IVW	1.005	0.983–1.026	0.641
	WMR	0.989	0.960–1.019	0.506
	MR Egger	0.989	0.958–1.021	0.536
Type 2 diabetes	IVW	1.237	1.099–1.391	0.0003
	WMR	1.248	1.019–1.529	0.031
	MR Egger	1.304	0.973–1.746	0.081
Multiple sclerosis	IVW	0.984	0.950–1.019	0.381
	WMR	0.991	0.941–1.045	0.761
	MR Egger	0.843	0.939–1.052	0.994
Migraine	IVW	20.264	0.124–3287.978	0.246
	WMR	19.243	0.234–15824.467	0.387
	MR Egger	14.034	0.135–288.882	0.156



causal link between T2DM and AD risk, which is consistent with previous observational studies.

At present, exploring the high-risk molecular mechanism and new treatment methods for T2DM combined with AD is a hot spot of clinical research. Serum soluble apoptosis factor (sFas) and sFas ligand (sFasL) may be high-risk molecules for predicting T2DM combined with AD (Chi et al., 2022; Zheng et al., 2023). A Chinese study on T2DM combined with AD showed that the area under the curve (AUC) of serum sFas and sFasL in the diagnosis of T2DM combined with AD were 0.760 and 0.774, respectively, which suggested that both

sFas and sFasL have certain diagnostic value for T2DM combined with AD. The AUC of serum sFas and sFasL in the combined diagnosis of T2DM combined with AD was 0.836, which indicated that the value of the combined diagnosis was higher (Damanik and Yunir, 2021). Therefore, it is necessary to closely monitor the serum sFas and sFasL levels of patients with T2DM for early AD prevention. Previous studies demonstrated that sFas and sFasL are not only related to apoptosis but also related to insulin resistance (Zheng et al., 2023). The occurrence of various central nervous system diseases is closely related to apoptosis, and sFas and sFasL play an important role in mediating

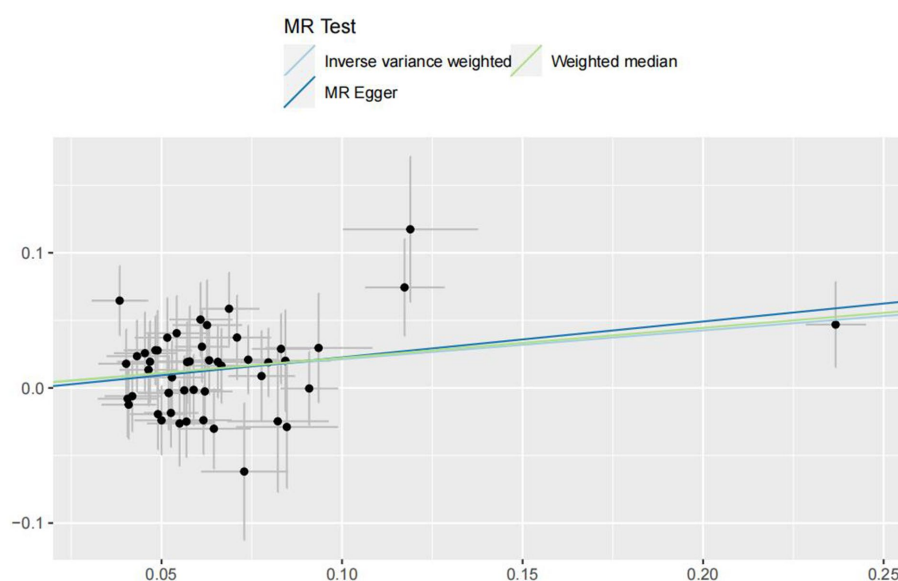


FIGURE 3  
Genetically predicted assessed type 2 diabetes mellitus on Alzheimer's disease.

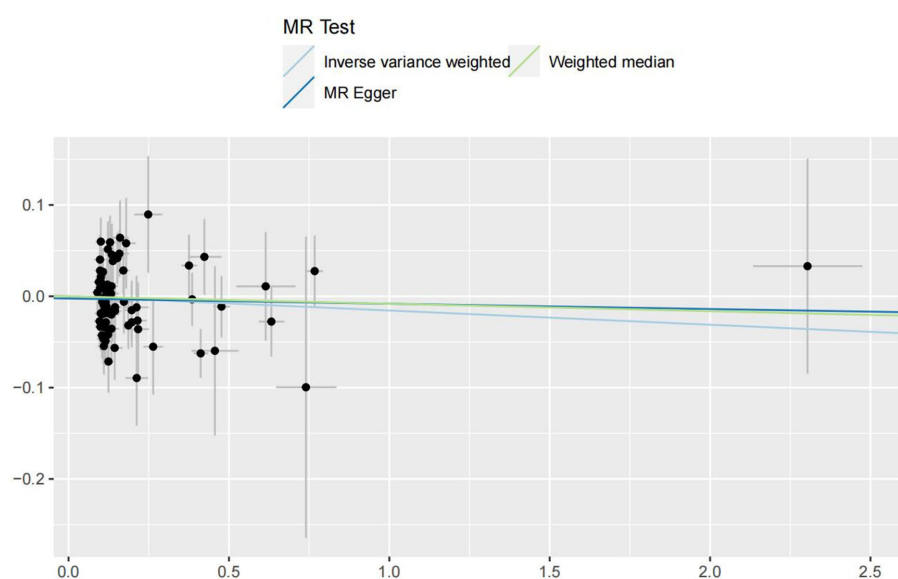


FIGURE 4  
Genetically predicted assessed multiple sclerosis on Alzheimer's disease.

apoptosis (Nortley et al., 2019). The reason for the increased serum sFas and sFasL levels in patients with T2DM combined with AD may be that hyperglycemia produces a variety of cytokines, which activate the sFas and sFasL systems, leading to increased expression of sFas and sFasL on the surface of the cells, causing apoptosis of central nervous system cells, and then altering cognitive functions (Nortley et al., 2019). Moreover, neuron-specific enolase (NSE) and phosphorylated tau (P-tau) in serum exosomes have also been considered indicators of cognitive impairment secondary to T2DM (Dove et al., 2021). Clinical studies involving 114 patients with T2DM

suggested that the combination of NSE and P-tau in serum exosomes, which predicts the AUC of cognitive impairment in patients with T2DM, was 0.827 (Domínguez et al., 2014).

Several underlying mechanisms have been proposed to explain the increased risk of AD in patients with T2DM. First, the hyperglycemic state causes mitochondrial dysfunction, which eventually turns into neuronal apoptosis (Wang et al., 2022). Mitochondria, as an important organelle for cells to generate energy through aerobic respiration, play an important role in maintaining brain homeostasis and meeting the energy needs of neurons

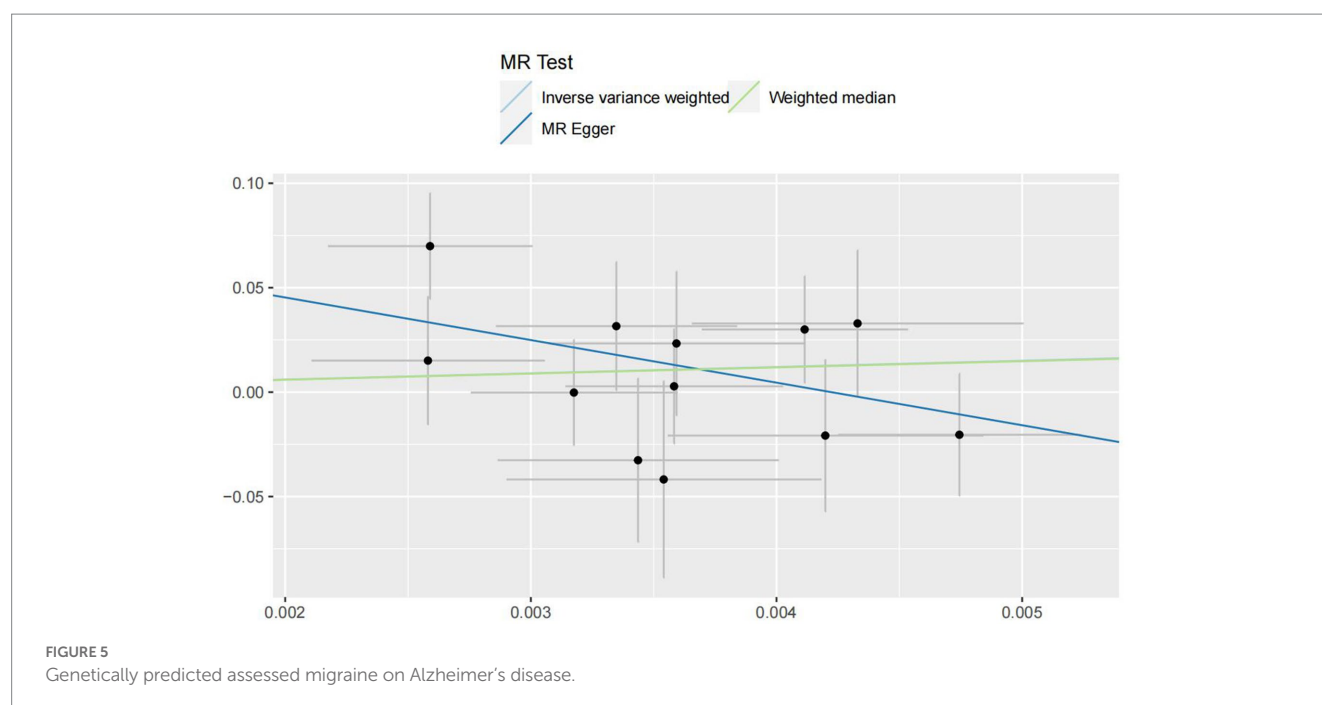


TABLE 3 Sensitivity analysis of the causal association between exposure and the risk of AD.

Exposure	Cochran's Q test		MR-Egger		MR-PRESSO value of $p$
	Q value	$p$	Intercept	$p$	
Type 1 diabetes	35.701	0.973	0.009	0.214	0.523
Type 2 diabetes	40.140	0.782	0.005	0.956	0.795
Multiple sclerosis	101.963	0.264	88.368	0.244	0.264
Migraine	12.367	0.336	0.086	0.103	0.392

(Cabezas-Opazo et al., 2015). Hyperglycemia interferes with the balance of mitochondrial fusion and fission, affecting the number, shape, and function of mitochondria (Solanki et al., 2017; Wang et al., 2022). Abnormal mitochondrial function can generate a large amount of reactive oxygen species and enhance oxidative stress response (Zhang et al., 2022). Accumulating evidence suggests that mitochondria may be damaged to varying degrees in morphology, mitochondrial dynamics, and bioenergetics in the pathogenesis of AD, accelerating AD lesions in the brain (Cabezas-Opazo et al., 2015). Oxidative stress to mitochondria in neurons was increased in a study of a streptozotocin-induced diabetic mice model, and oxidative damage to brain mitochondria further led to impaired motor and memory behavioral functions (Solanki et al., 2017). Second, diabetic cerebrovascular damage could also explain the increased risk of AD in patients with T2DM. In the brains of patients with AD, about 8.1% of the cerebral blood vessels contracted due to A $\beta$  deposition, resulting in a reduction of about 50% of the blood flow in the brain and a reduced energy supply. In patients with AD, the blood flow of gray matter decreased by approximately 42% (Kellar and Craft, 2020). Third, abnormal cholesterol in the state of type 2 diabetes can cause AD through the increase of A $\beta$ . According to a perspective study, cholesterol plays a crucial role in the process of A $\beta$  generation and aggregation. Another perspective study claimed that cholesterol can be changed

by A $\beta$  during neuronal dynamics, thereby promoting the subsequent development of cognitive impairment (Hanyu, 2019). Fourth, the central insulin signaling pathway is disrupted in patients with T2DM, and the impairment of insulin signaling can easily lead to a decrease in energy metabolism, specifically manifested in the decrease in ATP and glucose intake, the permeability and stability of nerve cells, and the negative impact of glucose metabolism disorders (Tamura et al., 2020). Finally, insulin resistance plays an important role in the overall occurrence and subsequent development of cognitive impairment in patients with T2DM. Patients with T2DM have insulin resistance both centrally and peripherally, and the insulin that breaks through the blood-brain barrier and is transported to the brain tissue is also greatly reduced, which ultimately damages energy, a stable form of glucose metabolism, and white matter fiber structure and function (Hanyu, 2019; Kellar and Craft, 2020; Tamura et al., 2020).

There was a causal link between T2DM and AD according to our MR analysis. Therefore, early identification and prediction of T2DM combined with AD is particularly important. In clinical practice, a few studies have discovered serum markers that can early predict the development of T2DM with cognitive impairment, such as sFas, sFasL, and P-tau (Dove et al., 2021; Chi et al., 2022; Zheng et al., 2023). We hope that, in the future, more scholars will pay attention to the study of T2DM combined with AD, actively search for the risk factors

of T2DM combined with AD and explore the markers that can predict T2DM combined with AD, leading to early intervention and treatment of the disease.

This study includes several notable strengths. First, MR analysis, which can largely reduce the impact of environmental confounding factors and reverse causality, was used for the first time to explore the causal relationship between T1DM, T2DM, MS, and migraine and AD. Second, the selected SNPs accounted for a higher proportion of T1DM, T2DM, MS, and migraine. Furthermore, the large sample size of each MR analysis and the robust estimation effect of each instrumental variable guaranteed the statistical power of our study. Finally, the consistency of causality was confirmed by sensitivity analyses such as weighted median analysis, MR-Egger regression, MR-PRESSO, and leave-one-out analysis. However, several limitations should be considered when interpreting our findings. First, the participants in this study were all of European ancestry, which may limit the generalizability of our findings to other populations. Further studies are needed to validate our findings in populations of non-European ancestry. Second, the causal associations between AD and migraine subtypes (e.g., migraine with or without aura) were not further explored due to a lack of available GWAS with enough power for MR analysis. Third, we tried to figure out several confounder factors of AD, but there may be additional confounder factors that we did not figure out.

## 5. Conclusion

In conclusion, this two-sample MR study showed genetic evidence for the causal link between T2DM and AD. These findings highlight the significance of active monitoring and prevention of AD in patients with T2DM. We hope more scholars will pay attention to the study of T2DM combined with AD in the future, actively search for the risk factors of T2DM combined with AD and explore the markers that can predict T2DM combined with AD, leading to early intervention and treatment of the disease.

## References

- Alasia, S., Aimar, P., Merighi, A., and Lossi, L. (2012). Context-dependent toxicity of amyloid- $\beta$  peptides on mouse cerebellar cells. *J. Alzheimers Dis.* 30, 41–51. doi: 10.3233/jad-2012-120043
- Alzheimer Disease Genetics Consortium (ADGC), The European Alzheimer's Disease Initiative (EADI), Cohorts for Heart and Aging Research in Genomic Epidemiology Consortium (CHARGE), Genetic and Environmental Risk in AD/Defining Genetic, Polygenic and Environmental Risk for Alzheimer's Disease Consortium (GERAD/PERADES), Kunkle, B. W., Grenier-Boley, B., et al. (2019). Genetic meta-analysis of diagnosed Alzheimer's disease identifies new risk loci and implicates A $\beta$ , tau, immunity and lipid processing. *Nat. Genet.* 51, 414–430. doi: 10.1038/s41588-019-0358-2
- Baecher-Allan, C., Kaskow, B. J., and Weiner, H. L. (2018). Multiple sclerosis: mechanisms and immunotherapy. *Neuron* 97, 742–768. doi: 10.1016/j.neuron.2018.01.021
- Battaglia, S., Nazzi, C., and Thayer, J. F. (2023). Fear-induced bradycardia in mental disorders: foundations, current advances, future perspectives. *Neurosci. Biobehav. Rev.* 149:105163. doi: 10.1016/j.neubiorev.2023.105163
- Benedict, R. H. B., Amato, M. P., DeLuca, J., and Geurts, J. J. G. (2020). Cognitive impairment in multiple sclerosis: clinical management, MRI, and therapeutic avenues. *Lancet Neurol.* 19, 860–871. doi: 10.1016/s1474-4422(20)30277-5
- Biessels, G. J., and Despa, F. (2018). Cognitive decline and dementia in diabetes mellitus: mechanisms and clinical implications. *Nat. Rev. Endocrinol.* 14, 591–604. doi: 10.1038/s41574-018-0048-7
- Burch, R. (2019). Migraine and tension-type headache: diagnosis and treatment. *Med. Clin. North Am.* 103, 215–233. doi: 10.1016/j.mcna.2018.10.003
- Cabezas-Opazo, F. A., Vergara-Pulgar, K., Pérez, M. J., Jara, C., Osorio-Fuentealba, C., and Quintanilla, R. A. (2015). Mitochondrial dysfunction contributes to the pathogenesis of Alzheimer's disease. *Oxidative Med. Cell. Longev.* 2015:509654. doi: 10.1155/2015/509654
- Cao, L., Ke, J., Xia, S. S., and Yu, X. X. (2023). Expression and clinical significance of serum sFas and sFasL in patients with diabetes mellitus and Alzheimer. *Chinese J. Cardio. Cerebrovas. Dis. Elder.* 25, 171–174. doi: 10.3969/ji.ssn.1009-0126.2023.02.015
- Chen, X., Hong, X., Gao, W., Luo, S., Cai, J., Liu, G., et al. (2022). Causal relationship between physical activity, leisure sedentary behaviors and COVID-19 risk: a Mendelian randomization study. *J. Transl. Med.* 20:216. doi: 10.1186/s12967-022-03407-6
- Chi, H., Yao, R., Sun, C., Leng, B., Shen, T., Wang, T., et al. (2022). Blood Neuroexosomal mitochondrial proteins predict Alzheimer disease in diabetes. *Diabetes* 71, 1313–1323. doi: 10.2337/db21-0969
- Cloete, L. (2022). Diabetes mellitus: an overview of the types, symptoms, complications and management. *Nurs. Stand.* 37, 61–66. doi: 10.7748/ns.2021.e11709
- Conti, L., Preziosa, P., Meani, A., Pagani, E., Valsasina, P., Marchesi, O., et al. (2021). Unraveling the substrates of cognitive impairment in multiple sclerosis: a multiparametric structural and functional magnetic resonance imaging study. *Eur. J. Neurol.* 28, 3749–3759. doi: 10.1111/ene.15023

## Data availability statement

The original contributions presented in the study are included in the article/[Supplementary material](#), further inquiries can be directed to the corresponding author.

## Author contributions

HX: conceptualization, resources, data curation, and writing – original draft. HX and LZ: methodology and formal analysis. HX and SL: software and investigation. HX: writing – review and editing. All authors contributed to the article and approved the submitted version.

## Conflict of interest

The authors declare that the research was conducted in the absence of any commercial or financial relationships that could be construed as a potential conflict of interest.

## Publisher's note

All claims expressed in this article are solely those of the authors and do not necessarily represent those of their affiliated organizations, or those of the publisher, the editors and the reviewers. Any product that may be evaluated in this article, or claim that may be made by its manufacturer, is not guaranteed or endorsed by the publisher.

## Supplementary material

The Supplementary material for this article can be found online at: <https://www.frontiersin.org/articles/10.3389/fnins.2023.1233601/full#supplementary-material>

- Damanik, J., and Yunir, E. (2021). Type 2 diabetes mellitus and cognitive impairment. *Acta Med. Indones.* 53, 213–220.
- Davey Smith, G., and Hemani, G. (2014). Mendelian randomization: genetic anchors for causal inference in epidemiological studies. *Hum. Mol. Genet.* 23, R89–R98. doi: 10.1093/hmg/ddu328
- Demir, S., Nawroth, P. P., Herzig, S., and Ekim Üstünel, B. (2021). Emerging targets in type 2 diabetes and diabetic complications. *Adv. Sci.* 8:e2100275:2100275. doi: 10.1002/advs.202100275
- Domínguez, R. O., Pagano, M. A., Marschoff, E. R., González, S. E., Repetto, M. G., and Serra, J. A. (2014). Alzheimer disease and cognitive impairment associated with diabetes mellitus type 2: associations and a hypothesis. *Neurologia* 29, 567–572. doi: 10.1016/j.nrl.2013.05.006
- Dove, A., Shang, Y., Xu, W., Grande, G., Laukka, E. J., Fratiglioni, L., et al. (2021). The impact of diabetes on cognitive impairment and its progression to dementia. *Alzheimers Dement.* 17, 1769–1778. doi: 10.1002/alz.12482
- Forgetta, V., Manousaki, D., Istomine, R., Ross, S., Tessier, M. C., Marchand, L., et al. (2020). Rare genetic variants of large effect influence risk of type 1 diabetes. *Diabetes* 69, 784–795. doi: 10.2337/db19-0831
- Gillani, S. M. R., Raghavan, R., and Singh, B. M. (2021). A 5-year assessment of the epidemiology and natural history of possible diabetes in remission. *Prim. Care Diabetes* 15, 688–692. doi: 10.1016/j.pcd.2021.04.007
- Grover, S., and Sharma, M. (2022). Sleep, pain, and neurodegeneration: a Mendelian randomization study. *Front. Neurol.* 13:765321. doi: 10.3389/fneur.2022.765321
- Guo, Y. J., Zhang, M., Yan, Z. H. and Ji, H. (2022). Relationship between serum 8-hydroxydeoxyguanylic acid, manganese superoxide dismutase levels and cognitive dysfunction in elderly patients with migraine. *Cardio-Cerebrovasc. Dis. Prev. Treat* 22, 47–50. doi: 10.3969/j.issn.1009-816x.2022.01.013
- Hanyu, H. (2019). Diabetes-related dementia. *Adv. Exp. Med. Biol.* 1128, 147–160. doi: 10.1007/978-981-13-3540-2\_8
- Hautakangas, H., Winsvold, B. S., Ruotsalainen, S. E., Björnsdóttir, G., Harder, A. V. E., Kogelman, L. J. A., et al. (2022). Genome-wide analysis of 102,084 migraine cases identifies 123 risk loci and subtype-specific risk alleles. *Nat. Genet.* 54, 152–160. doi: 10.1038/s41588-021-00990-0
- International Multiple Sclerosis Genetics Consortium (2019). Multiple sclerosis genomic map implicates peripheral immune cells and microglia in susceptibility. *Science* 365:eaav7188. doi: 10.1126/science.aav7188
- Jayaraj, R. L., Azimullah, S., and Beiram, R. (2020). Diabetes as a risk factor for Alzheimer's disease in the Middle East and its shared pathological mediators. *Saudi J. Biol. Sci.* 27, 736–750. doi: 10.1016/j.sjbs.2019.12.028
- Jia, L., Quan, M., Fu, Y., Zhao, T., Li, Y., Wei, C., et al. (2020). Dementia in China: epidemiology, clinical management, and research advances. *Lancet Neurol.* 19, 81–92. doi: 10.1016/s1474-4422(19)30290-x
- Karami, A., Khodarahimi, S., and Mazaheri, M. (2019). Cognitive and perceptual functions in patients with occipital lobe epilepsy, patients with migraine, and healthy controls. *Epilepsy Behav.* 97, 265–268. doi: 10.1016/j.yebch.2019.04.005
- Kashyap, M. P., Roberts, C., Waseem, M., and Tyagi, P. (2018). Drug targets in Neurotrophin signaling in the central and peripheral nervous system. *Mol. Neurobiol.* 55, 6939–6955. doi: 10.1007/s12035-018-0885-3
- Kellar, D., and Craft, S. (2020). Brain insulin resistance in Alzheimer's disease and related disorders: mechanisms and therapeutic approaches. *Lancet Neurol.* 19, 758–766. doi: 10.1016/s1474-4422(20)30231-3
- Klan, T., Liesering-Latta, E., Gaul, C., Martin, P. R., and Witthöft, M. (2019). An integrative cognitive behavioral therapy program for adults with migraine: a feasibility study. *Headache* 59, 741–755. doi: 10.1111/head.13532
- Lawlor, D. A., Harbord, R. M., Sterne, J. A., Timpson, N., and Davey Smith, G. (2008). Mendelian randomization: using genes as instruments for making causal inferences in epidemiology. *Stat. Med.* 27, 1133–1163. doi: 10.1002/sim.3034
- Lesiewska, N., Borkowska, A., Junik, R., Kamińska, A., Jaracz, K., and Bieliński, M. (2022). Consequences of diabetes and pre-diabetes and the role of biochemical parameters of carbohydrate metabolism for the functioning of the prefrontal cortex in obese patients. *Front. Biosci.* 27:076. doi: 10.31083/j.fbl2703076
- Li, C., Liu, J., Lin, J., and Shang, H. (2022). COVID-19 and risk of neurodegenerative disorders: a Mendelian randomization study. *Transl. Psychiatry* 12:283. doi: 10.1038/s41398-022-02052-3
- Lin, R., Brown, F., James, S., Jones, J., and Ekinici, E. (2021). Continuous glucose monitoring: a review of the evidence in type 1 and 2 diabetes mellitus. *Diabet. Med.* 38:e14528. doi: 10.1111/dme.14528
- Lorente, L., Martín, M. M., Pérez-Cejas, A., González-Rivero, A. F., Ramos-Gómez, L., Solé-Violán, J., et al. (2022). Mortality prediction of patients with spontaneous intracerebral hemorrhage by serum soluble Fas ligand concentrations. *Expert. Rev. Mol. Diagn.* 22, 233–238. doi: 10.1080/14737159.2022.2017775
- Luczynski, P., Laule, C., Hsiung, G. R., Moore, G. R. W., and Tremlett, H. (2019). Coexistence of multiple sclerosis and Alzheimer's disease: a review. *Mult. Scler. Relat. Disord.* 27, 232–238. doi: 10.1016/j.msard.2018.10.109
- Mahajan, A., Wessel, J., Willems, S. M., Zhao, W., Robertson, N. R., Chu, A. Y., et al. (2018). Refining the accuracy of validated target identification through coding variant fine-mapping in type 2 diabetes. *Nat. Genet.* 50, 559–571. doi: 10.1038/s41588-018-0084-1
- Morton, R. E., St John, P. D., and Tyas, S. L. (2019). Migraine and the risk of all-cause dementia, Alzheimer's disease, and vascular dementia: a prospective cohort study in community-dwelling older adults. *Int. J. Geriatr. Psychiatry* 34, 1667–1676. doi: 10.1002/gps.5180
- Nazarzadeh, M., Pinho-Gomes, A. C., Bidel, Z., Dehghan, A., Canoy, D., Hassaine, A., et al. (2020). Plasma lipids and risk of aortic valve stenosis: a Mendelian randomization study. *Eur. Heart J.* 41, 3913–3920. doi: 10.1093/eurheartj/ehaa070
- Nikpay, M., Goel, A., Won, H. H., Hall, L. M., Willenborg, C., Kanoni, S., et al. (2015). A comprehensive 1,000 genomes-based genome-wide association meta-analysis of coronary artery disease. *Nat. Genet.* 47, 1121–1130. doi: 10.1038/ng.3396
- Nortley, R., Korte, N., Izquierdo, P., Hirunpattarasilp, C., Mishra, A., Jaunmuktane, Z., et al. (2019). Amyloid  $\beta$  oligomers constrict human capillaries in Alzheimer's disease via signaling to pericytes. *Science* 365:eaav9518. doi: 10.1126/science.aav9518
- Oh, J., Vidal-Jordana, A., and Montalban, X. (2018). Multiple sclerosis: clinical aspects. *Curr. Opin. Neurol.* 31, 752–759. doi: 10.1097/wco.0000000000000622
- Park, K. W., Hwang, Y. S., Lee, S. H., Jo, S., and Chung, S. J. (2023). The effect of blood lipids, type 2 diabetes, and body mass index on Parkinson's disease: a Korean Mendelian randomization study. *J. Mov. Disord.* 16, 79–85. doi: 10.14802/jmd.22175
- Pierce, B. L., Ahsan, H., and Vanderweele, T. J. (2011). Power and instrument strength requirements for Mendelian randomization studies using multiple genetic variants. *Int. J. Epidemiol.* 40, 740–752. doi: 10.1093/ije/dyq151
- Polyák, H., Galla, Z., Nánási, N., Cseh, E. K., Rajda, C., Veres, G., et al. (2023). The tryptophan-kynurenine metabolic system is suppressed in Cuprizone-induced model of demyelination simulating progressive multiple sclerosis. *Biomedicine* 11:945. doi: 10.3390/biomedicines11030945
- Portaccio, E., and Amato, M. P. (2022). Cognitive impairment in multiple sclerosis: an update on assessment and management. *Neuro Sci.* 3, 667–676. doi: 10.3390/neurosci3040048
- Rojas, M., Chávez-Castillo, M., Pirela, D., Parra, H., Nava, M., Chacín, M., et al. (2021). Metabolic syndrome: is it time to add the central nervous system? *Nutrients* 13:2254. doi: 10.3390/nu13072254
- Schwarcz, R., Bruno, J. P., Muchowski, P. J., and Wu, H. Q. (2012). Kynurenines in the mammalian brain: when physiology meets pathology. *Nat. Rev. Neurosci.* 13, 465–477. doi: 10.1038/nrn3257
- Sempere-Bigorra, M., Julián-Rochina, I., and Cauli, O. (2021). Differences and similarities in neuropathy in type 1 and 2 diabetes: a systematic review. *J. Pers. Med.* 11:230. doi: 10.3390/jpm11030230
- Shen, J., Yu, H., Li, K., Ding, B., Xiao, R., and Ma, W. (2022). The association between plasma fatty acid and cognitive function mediated by inflammation in patients with type 2 diabetes mellitus. *Diabetes Metab. Syndr. Obes.* 15, 1423–1436. doi: 10.2147/dms0.S353449
- Sheppard, O., and Coleman, M. (2020). "Alzheimer's disease: Etiology, neuropathology and pathogenesis" in *Alzheimer's disease: drug discovery*. ed. X. Huang (Brisbane: Exon)
- Silva, M. V. F., Loures, C. M. G., Alves, L. C. V., de Souza, L. C., Borges, K. B. G., and Carvalho, M. G. (2019). Alzheimer's disease: risk factors and potentially protective measures. *J. Biomed. Sci.* 26:33. doi: 10.1186/s12929-019-0524-y
- Smith, G. D., and Ebrahim, S. (2003). 'Mendelian randomization': can genetic epidemiology contribute to understanding environmental determinants of disease? *Int. J. Epidemiol.* 32, 1–22. doi: 10.1093/ije/dyg070
- Solanki, I., Parihar, P., Shetty, R., and Parihar, M. S. (2017). Synaptosomal and mitochondrial oxidative damage followed by behavioral impairments in streptozotocin induced diabetes mellitus: restoration by *Malvastrum tricuspidatum*. *Cell. Mol. Biol.* 63, 94–101. doi: 10.14715/cmb/2017.63.7.16
- Tamura, Y., Omura, T., Toyoshima, K., and Araki, A. (2020). Nutrition Management in Older Adults with diabetes: a review on the importance of shifting prevention strategies from metabolic syndrome to frailty. *Nutrients* 12:3367. doi: 10.3390/nu12113367
- Taranu, D., Tuman, H., Holbrook, J., Tuman, V., Uttner, I., and Fissler, P. (2022). The TRACK-MS test battery: a very brief tool to Track multiple sclerosis-related cognitive impairment. *Biomedicine* 10:2975. doi: 10.3390/biomedicines10112975
- Tsoporis, J. N., Hatzigelaki, E., Gupta, S., Izhar, S., Salpeas, V., Tsiavou, A., et al. (2020). Circulating ligands of the receptor for advanced glycation end products and the soluble form of the receptor modulate cardiovascular cell apoptosis in diabetes. *Molecules* 25:5235. doi: 10.3390/molecules25225235
- Wang, Z., Chen, M., Wei, Y. Z., Zhuo, C. G., Xu, H. F., Li, W. D., et al. (2022). The causal relationship between sleep traits and the risk of schizophrenia: a two-sample bidirectional Mendelian randomization study. *BMC Psychiatry* 22:399. doi: 10.1186/s12888-022-03946-8
- Wang, J., Li, L., Zhang, Z., Zhang, X., Zhu, Y., Zhang, C., et al. (2022). Extracellular vesicles mediate the communication of adipose tissue with brain and promote cognitive impairment associated with insulin resistance. *Cell Metab.* 34, 1264–1279.e8. doi: 10.1016/j.cmet.2022.08.004

- Wang, T., Ni, Q. B., Wang, K., Han, Z., and Sun, B. L. (2020). Stroke and Alzheimer's disease: a Mendelian randomization study. *Front. Genet.* 11:581. doi: 10.3389/fgene.2020.00581
- Wu, F., and Liang, P. (2022). Application of metabolomics in various types of diabetes. *Diabetes Metab. Syndr. Obes.* 15, 2051–2059. doi: 10.2147/dmso.S370158
- Zhang, X. X., Tian, Y., Wang, Z. T., Ma, Y. H., Tan, L., and Yu, J. T. (2021). The epidemiology of Alzheimer's disease modifiable risk factors and prevention. *J. Prev. Alzheimers Dis.* 8, 1–9. doi: 10.14283/jpad.2021.15
- Zhang, S., Zhao, J., Quan, Z., Li, H., and Qing, H. (2022). Mitochondria and other organelles in neural development and their potential as therapeutic targets in neurodegenerative diseases. *Front. Neurosci.* 16:853911. doi: 10.3389/fnins.2022.853911
- Zhao, L., Zhao, W., International Headache Genetics Consortium (IHGC) Anttila, V., Artto, V., Belin, A. C., et al. (2023). Causal relationships between migraine and microstructural white matter: a Mendelian randomization study. *J. Headache Pain* 24:10. doi: 10.1186/s10194-023-01550-z
- Zheng, T. L., Liu, C., and Peng, F. (2023). Expression of neuron-specific enolase and phosphorylated tau in serum-derived exosomes and its correlation with secondary mild cognitive impairment in elderly patients with type 2 diabetes mellitus. *Chin. J. Mult. Organ. Dis. Elderly* 22, 433–438. doi: 10.11915/j.issn.1671-5403.2023.06.090



## OPEN ACCESS

## EDITED BY

Nicolas Casadei,  
University of Tübingen, Germany

## REVIEWED BY

David James Brooks,  
Newcastle University, United Kingdom  
Anandan Balakrishnan,  
University of Madras, India

## \*CORRESPONDENCE

Seong Lin Teoh  
✉ teohseonglin@uukm.edu.my

RECEIVED 07 June 2023

ACCEPTED 07 August 2023

PUBLISHED 25 August 2023

## CITATION

Omar NA, Kumar J and Teoh SL (2023)  
Parkinson's disease model in zebrafish using  
intraperitoneal MPTP injection.  
*Front. Neurosci.* 17:1236049.  
doi: 10.3389/fnins.2023.1236049

## COPYRIGHT

© 2023 Omar, Kumar and Teoh. This is an open-access article distributed under the terms of the [Creative Commons Attribution License \(CC BY\)](#). The use, distribution or reproduction in other forums is permitted, provided the original author(s) and the copyright owner(s) are credited and that the original publication in this journal is cited, in accordance with accepted academic practice. No use, distribution or reproduction is permitted which does not comply with these terms.

# Parkinson's disease model in zebrafish using intraperitoneal MPTP injection

Noor Azzizah Omar<sup>1,2</sup>, Jaya Kumar<sup>3</sup> and Seong Lin Teoh<sup>1\*</sup>

<sup>1</sup>Department of Anatomy, Faculty of Medicine, Universiti Kebangsaan Malaysia, Kuala Lumpur, Malaysia,

<sup>2</sup>Department of Medical Sciences, Faculty of Medicine and Health Sciences, Universiti Sains Islam Malaysia, Bandar Baru Nilai, Malaysia, <sup>3</sup>Department of Physiology, Faculty of Medicine, Universiti Kebangsaan Malaysia, Kuala Lumpur, Malaysia

**Introduction:** Parkinson's disease (PD) is the second most common neurodegenerative disease that severely affects the quality of life of patients and their family members. Exposure to 1-Methyl-4-phenyl-1,2,3,6-tetrahydropyridine (MPTP) has been shown to reflect behavioral, molecular, and proteomic features of PD. This study aimed to assess the protocol for inducing PD following MPTP injection in adult zebrafish.

**Methods:** Fish were injected with 100 µg/g of MPTP intraperitoneally once or twice and then assessed on days 1 to 30 post-injection.

**Results:** Between one-time and two-time injections, there was no significant difference in most locomotor parameters, expressions of *tyrosine hydroxylase-2* (*th2*) and *dopamine transporter* (*dat*) genes, and dopaminergic neurons (tyrosine hydroxylase positive, TH+ cells) counts. However, caspase-3 levels significantly differed between one- and two-time injections on the day 1 assessment.

**Discussion:** Over a 30-day period, the parameters showed significant differences in swimming speed, total distance traveled, *tyrosine hydroxylase-1* (*th1*) and *dat* gene expressions, caspase-3 and glutathione protein levels, and TH+ cell counts. Days 3 and 5 showed the most changes compared to the control. In conclusion, a one-time injection of MPTP with delayed assessment on days 3 to 5 is a good PD model for animal studies.

## KEYWORDS

neurodegenerative disease, *Danio rerio*, tyrosine hydroxylase, dopaminergic neuron, neurotoxin

## 1. Introduction

Parkinson's disease (PD) is the second most common neurodegenerative disease, characterized by a spectrum of motor rigidity, bradykinesia, tremor, rigidity, and postural instability (Tysnes and Storstein, 2017). This occurs as a result of the formation of Lewy bodies, which eventually leads to the loss of dopaminergic neurons in the substantia nigra pars compacta (Kalia and Lang, 2015). It has been established that the prevalence of PD peaked in the older age group (Pringsheim et al., 2014; Williams-Gray and Worth, 2016). In this aging population era, PD significantly impacts the healthcare system due to its chronic pattern of illness and its psychosocial impact on caregivers (García-Ramos et al., 2016). In view of the fact that there is still no cure, the current treatment regime faces challenges involving drug tolerance and other side effects. Studies have been vastly designed to find the pathogenesis and potential cure of this disease. Animal studies have been one of the methods widely used over the decades, where

animals are used to mimic PD for further investigation. The two primary methods for inducing PD in animal models include either neurotoxin chemical induction or a transgenic gene modification approach. Neurotoxins such as 6-hydroxydopamine (6-OHDA), 1-methyl-4-phenyl-1,2,3,6-tetrahydropyridine (MPTP), rotenone, paraquat, maneb, and trichloroethylene have been widely used in animal models (Vijayanathan et al., 2017; Liu et al., 2018; Zeng et al., 2018; Cao et al., 2019).

Zebrafish (*Danio rerio*) is a freshwater fish belonging to the Cyprinidae of the order Cypriniformes. Their natural habitat is in Southeast Asian streams, rivers, or well-vegetated pools (Spence et al., 2008). There have been a growing number of studies using zebrafish as an animal model due to its high fecundability, ease of maintenance, and similarity to the human genome. Its females can spawn every 2–3 days, with a short generation time of 3–4 months (Kimmel et al., 1995). Their external fertilization results in relatively large transparent eggs, making them accessible for manipulation and monitoring through all developmental stages (Kimmel et al., 1995). The development stage starts from the embryonic pre-hatching phase at 0–72 h post fertilization (hpf); larvae stage at 1 to 29 days post fertilization (dpf); juvenile fish 90 dpf to 2 years; and the aging phase from 2 to 5 years (Kalueff et al., 2014). Their development is rather rapid, with the precursors to all major organs developing within 5 dpf (Kimmel et al., 1995). It has been reported that 70% of human genes have at least one zebrafish orthologue. Mutations in these genes will result in pathologies similar to those in humans (Howe et al., 2013). In the early phase of zebrafish, studies have shown a variety of human disease conditions were able to be replicated in a zebrafish model (Barut and Zon, 2000). Henceforth, the swift adoption of zebrafish as an animal model for the past three decades was assisted by technological advances including late targeted mutagenesis (Burton, 2015). This has been reflected in many diseases, including neurological diseases. Although there are differences in complexity between zebrafish and the human nervous system, there is evidence of the conservation of critical structures and molecular components that shows its potential as a suitable animal model to study the basic pathogenesis of neurological diseases (Burton, 2015). However, there is still relatively little data on the use of neurotoxins to induce PD (Razali et al., 2021). The challenges faced in handling the zebrafish model include the alteration of dose from other animal models, the delivery method, and the timing of assessment before the regenerative capability of their nervous system (Bhattarai et al., 2016, 2020; Vijayanathan et al., 2017).

MPTP is a type of meperidine analog formed as a by-product of the synthesis of 1-methyl-4-phenyl-4-propionoxypiperidine (MPP), synthetic heroin that is 5–10 times more potent than morphine (Ziering and Lee, 1947; Langston, 2017). The earliest case of Parkinsonism induced by a meperidine analog was reported by Davis et al. (1979), where they found a Parkinsonism feature in a young man who is an avid drug user of various drugs, including a home-synthesized unknown meperidine analog. It was not until 1983 that MPTP was discovered and linked to Parkinsonism feature. A group of neurologists and scientists has found a series of patients that develop Parkinsonism features as early as 4 days following intravenous injection of the “new synthetic heroin,” which was later found to be MPTP (Langston et al., 1983). Following that, an eruption of studies evolved to understand and analyze this chemical and its role in causing Parkinsonism.

MPTP readily crosses the blood–brain barrier, and induces Parkinson-like behavioral, molecular, and proteomic features in

various animal models, including zebrafish (Sarath Babu et al., 2016; Beaudry and Huot, 2020; Mustapha and Mat Taib, 2021; Sun et al., 2022). However, most studies involving zebrafish have induced PD using MPTP in the embryonic or larval stage (Lam et al., 2005; McKinley et al., 2005; Ustundag et al., 2020; Zhao et al., 2020; Cansiz et al., 2021). There is a sparse study on using MPTP for the PD model in adult zebrafish. To the best of our knowledge, there have only been five studies on MPTP in adult zebrafish with different dosing, administration routes, and assessment periods (Anichtchik et al., 2004; Sarath Babu et al., 2016; Saszik and Smith, 2018; Selvaraj et al., 2019; Kalyn and Ekker, 2021; Table 1). These studies have shown promising results in terms of locomotor analysis, dopaminergic gene dysregulation, dopamine (DA) protein depletion, and significant changes in tissue section analysis. However, questions arise about the suitable dose, the need for multiple doses, or the timing of assessment post-injection. Hence, this study aims to design a structured protocol for the PD zebrafish model using MPTP and to assess the effectiveness of this method via an assessment of the locomotor effects, dopaminergic gene expression, protein analysis, and tissue section analysis.

## 2. Materials and methods

### 2.1. The animals

Adult zebrafish aged 4–6 months were housed in 6 L freshwater aquaria at a density of 3–5 fish per L (Cachat et al., 2010) with the temperature kept at  $27 \pm 0.5^\circ\text{C}$  and a controlled normal photo regimen (14 h light and 10 h dark). The fish were fed adult zebrafish food twice daily. Experiments were conducted after 2 weeks of acclimatizing to laboratory conditions (Howe et al., 2013; Teoh et al., 2015). The sample size was calculated using Power and Sample size calculation (PPS) version 3.1.6, October 2018 by William D. Dupont and Walton D Plummer, Jr. with  $\alpha$  score of 0.05, power of 0.8, and a m score of 1, based on the study conducted on the assessment of zebrafish as a PD model (Sarath Babu et al., 2016; Vijayanathan et al., 2017). The sample size for locomotor behavior was found to be  $n=4$  fish per group, and for gene expression is  $n=6$  per group. On the objectives that had no previous study, such as each of the protein level markers and dopaminergic neuron cell counts, a pilot study with a sample size of 6 per group per test was conducted, adapting the Markov Chain Monte Carlo approach (Allgoewer and Mayer, 2017). To provide a standardized representation, each group and each test were kept at  $n=6$  of fish as the numbers provided in the PPS calculator are within this number. The fish were grouped into Control, Vehicle, and MPTP groups. The control group was not injected with any solution, and the vehicle group was injected with saline (10  $\mu\text{L/g}$  weight) intraperitoneally to mimic the volume injected in the treatment group. MPTP groups were divided into one- and two-time injection groups with assessment intervals (Figure 1).

### 2.2. PD model induction

Before the procedure, fish were fasted for 24 h by withholding feeding and placing 3 layers of marbles at the base of the fish tank to ensure they were on an empty stomach. MPTP solution (Cat#M0896, Sigma, United States) was diluted in saline to make a 10  $\mu\text{g}/\mu\text{L}$  solution (Selvaraj et al., 2019; Mustapha and Mat Taib, 2021). Each

TABLE 1 Summary of previous studies that used MPTP as a neurotoxin in the adult zebrafish PD model.

Study	MPTP dose	Route of administration	Frequency of administration	Time of assessment	Findings that mimic PD				Other findings
					Locomotor	Gene dysregulation	Proteomic analysis	Tissue changes	
Sarath Babu et al. (2016)	50 µg/fish	Intraperitoneal	One-time injection and two-time injection	24 h after injection	Increased freezing bouts and distance traveled in two-times injection group	13 significant dysregulation of gene markers in 2-time injection and 8 genes in 1-time injection	TH protein showed no significant changes in both groups, PARK8 protein significant in both group	Overexpression of synuclein in the optic tectum, significant down-regulation of TH+ cell in 2x injection group	A dose above 75 µg/fish resulted in casualty. Two-dose does not affect casualty. MPTP-injected fish showed erratic swimming patterns.
Anichtchik et al. (2004)	20 µg/g	Intramuscular	One	24, 72, 144, 216 h after injection	Total distance and speed reduced from day 1 after injection and slowly recovered by day 9 after injection	–	Maximum reduction in DA level observed 2 days after MPTP injection No changes in TH level, caspase 3	No significant changes in TH+ neuron counts and caspase-3 stains No significant change in DNA fragmentation TUNEL staining	–
Selvaraj et al. (2019)	100 µg/g	Intraperitoneal	One	24 h after injection	Reduced locomotion, distance traveled, and speed with longer freezing duration	Down-regulation of <i>dat</i> gene in the MPTP group	Significant decrease in DA level in HPLC analysis		–
Saszik and Smith (2018)	2 mmol/L for 2 min in 300 mL beaker	Water immersion	One	Following MPTP exposure	No significant changes in total distance and speed of swimming	–	–	–	A low dose of MPTP altered social shoaling swim behavior
Kalyn and Ekker (2021)	25 mM for 4 consecutive days	Cerebroventricular microinjection	Four	Following 4 <sup>th</sup> injection	Reduced total distance in swimming and speed, increase in freezing activity following 3 <sup>rd</sup> and 4 <sup>th</sup> injection	<i>dat</i> and <i>th1</i> gene down-regulated in the MPTP group	–	Dopaminergic neurons were affected in optic bulb, telencephalon, and periventricular pretectal nucleus. Significant increase in fragmented mitochondria in the MPTP group	The concentration of 35 mM and higher resulted in casualties in fish <i>sox2</i> and <i>nestin</i> gene expression up-regulated after day 4 suggesting immediate regenerative activation All swimming patterns and histological changes return to normal within 2 weeks

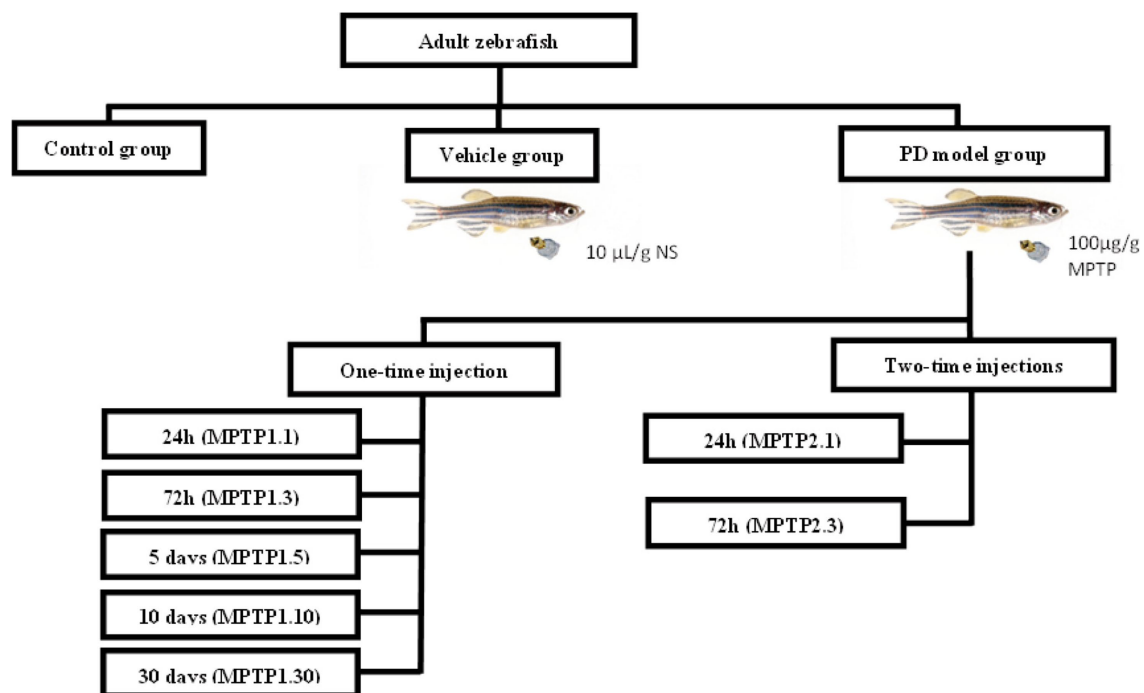


FIGURE 1

Grouping of experimental animals. Fish were divided into control, vehicle, and MPTP groups. The MPTP1 group received one injection and was further divided based on assessment day, namely 24 h post-injection (MPTP1.1), 72 h post-injection (MPTP1.3), day 5 assessment (MPTP1.5), day 10 assessment (MPTP1.10) and day 30 assessment (MPTP1.30). MPTP2 group received the second dose 24 h after the first dose and was assessed either at 24 h post-second injection (MPTP2.1) or 72 h post-second injection (MPTP2.3). Assessment on all intervals includes a neuro-behavioral assessment from locomotor activity, gene expression, protein level, and histochemical analysis.

fish was weighed individually by transferring the fish to a beaker filled with 1/3rd of the system water. The dose of MPTP was calculated at 100 µg/g per fish. The fish's weight ranged from 0.440 to 0.760 g. The volume of the solution was kept at 10 µL/g (Turner et al., 2011a,b; Al Shoyaib et al., 2019). Following dose measurement, the fish were transferred one at a time to a beaker with 0.0035% benzocaine for the anesthetizing process. Upon reaching anesthesia stage 3 (Coyle et al., 2004), the fish was transferred to a slitted surgical bed, belly up. The desired dose of MPTP was administered intraperitoneally using a 30G needle with a Hamilton syringe into the midline between the pelvic fins (Kinkel et al., 2010). Once MPTP was administered, the fish was placed in a beaker with 1/3rd of the system water for recovery, and then transferred to the fish tank according to the groups.

In the first part of the study, we assessed the differences between one- and two-time injections of MPTP. The MPTP1 group received only one injection and was further divided into two groups, assessed 24 h (MPTP1.1) and 72 h post-injection (MPTP1.3). The MPTP2 group received the second dose 24 h after the first dose and was assessed either at 24 h (MPTP2.1) or 72 h post-second injection (MPTP2.3). In the second part of the study, we have extended the assessment up to 30 days post-injection in light of the study conducted by Anichtchik et al. (2004) and Kalyn and Ekker (2021) where they found reversibility of MPTP in zebrafish on the second week post-injection. Based on the preliminary data between the one- and two-time injection groups, we have concluded to focus on the reversibility effect of the one-time injection group only. Hence,

the assessments were extended at intervals of 5 (MPTP1.5), 10 (MPTP1.10), and 30 days post-injection (MPTP1.30) for the one-time injection group. On the day of assessment, the fish were assessed for their locomotor behavior, dopaminergic gene expression, protein level, and immunohistochemistry analysis.

## 2.3. Locomotor assessment

The locomotor assessment was conducted by placing the fish in a 2.5 L system water in a tank. Video recording of the fish swimming pattern was performed by c992 pro stream webcam LogiCapture and analyzed using the SMART tracking device Smart 3.0.02, Panlab Harvard Apparatus®. The fish were assessed individually by placing one fish at a time in the locomotor tank. The fish were allowed to acclimatize to the new tank for 5 min before the recording, followed by an assessment of their total swimming distance, speed of swimming, time spent on the top half of the tank, and latency to reach the top half of the tank for 5 min (Cachat et al., 2010).

## 2.4. Gene expression analysis

The sequence of the zebrafish gene was retrieved from the National Centre for Biotechnology Information Database. Chromosomal gene location was identified using UCSC Genome

TABLE 2 Oligo sequence for real-time PCR.

Gene		Oligo sequence (5'→3')	Product size	Accession number
<i>th1</i>	Forward	TGGATCAGGATCACCCAGGA	149 bp	NM_131149.1
	Reverse	GTAGACCTCCCGCCATGTTC		
<i>th2</i>	Forward	GAATGCCACATGGGAGGTTT	129 bp	NM_001001829.1
	Reverse	AGCTGAGGGATCTGGTCTTCT		
<i>dat</i>	Forward	GAGTCGGGTTTGGTGTGCTA	71 bp	NM_131755.1
	Reverse	GGCGTCTCTGTAGCAGTTGT		
<i>actb1</i>	Forward	GCCTTCCTTCCTGGGTATGG	78 bp	NM_131031.1
	Reverse	ATGTCCACGTCGCACTTCAT		

Browser,<sup>1</sup> and Ensembl Genome Browser.<sup>2</sup> The dopaminergic genes that were assessed are namely tyrosine hydroxylase (*th1*, *th2*), and DA transporter (*dat*) (Table 2). The fish were euthanized using ice water immersion kept at 0 to 2°C. Their brains were dissected and homogenized using 400 µL of TRIZOL reagent, and RNA was extracted as per the manufacturer's protocol. Following that, the 500 ng RNA sample was converted to cDNA in a 20 µL reaction volume using the reverse transcriptase kit (Protoscript® First Strand DNA Synthesis Kit) following the manufacturer's protocol. The cDNA samples were mixed with the desired primers (Table 2) and proceeded with real-time PCR (Luna® Universal qPCR Master Mix). The  $\beta$  actin1 (*actb1*) gene was used as a reference gene, and data analysis was based on the relative expression of genes using the formula  $2^{-\Delta\Delta Cq}$ .

## 2.5. Protein expression analysis

The expression of DA, glutathione S Transferase (GST), and caspase-3 (CASP3) enzymes and brain-derived neurotrophic factor (BDNF) were assessed using a zebrafish enzyme-linked immunosorbent assay kit (ELK Biotechnology). Brain samples (0.006–0.007 g each) were homogenized using cold Phosphate Buffered Solution (PBS) in a 1:9 (weight: volume) dilution. The homogenates were centrifuged for 5 min at 10,000 g at 4°C. Around 50–100 µL supernatant was collected to be used on each well as per the manufacturer's protocol. In each run, the samples were processed with a set of freshly prepared standard solutions to develop the standard curve for analysis. The samples and standard were processed in pre-coated wells with biotinylated antibodies, streptavidin-horseradish peroxidase (HRP), and 3,3',5,5'-Tetramethylbenzidine (TMB) solution, with a series of washings with washing buffer in between. Following the administration of the stop reagent after incubation of the TMB solution, the photometric assessment was conducted as soon as possible at 450 nm and 540 nm wavelength. The optical density (OD) reading of 450 nm was deducted from a 540 nm reading to minimize error. Following that, the OD of all the wells was deducted from the mean OD of the blank. The ODs of the standard solution were plotted on a graph with a linear equation. The results of the samples were analyzed based on the plotted graph.

<sup>1</sup> <http://www.genome.ucsc.edu/>

<sup>2</sup> <http://www.ensembl.org>

## 2.6. Immunohistochemistry tissue section

Fresh brain tissues were fixed in 4% PFA for 6 h and kept in a 20% sucrose solution overnight for cryoprotection. The tissue samples were frozen in Tissue-Tek® Optimal Cutting Temperature compound and cryosectioned at –20°C at 14 µm thickness. The tissue slides were stored at –80°C before the staining protocol. Tissue sections were processed using avidin-biotin and peroxidase methodologies using a Peroxidase kit for Mouse Primary Antibody (Dako ARK™, Cat#K3954, Agilent, United States). This was conducted by labeling the primary antibody, anti-TH mouse monoclonal antibody (1:500, Cat#22941, Immunostar, United States) with biotinylated anti-mouse immunoglobulin in Tris HCl buffer for 20 min followed by the addition of normal mouse serum as the blocking reagent to bind to the residual unbound biotinylated antibody. Upon antibody incubation, the tissue was incubated with streptavidin-peroxidase, followed by a reaction with diaminobenzidine (DAB)/hydrogen peroxidase reaction as the substrate-chromogen as per manufacturer protocol. Stained tissue was mounted with coverslips and viewed under light microscopy. The TH positive (TH+) cells were analyzed based on overall positive cell groups that have been reported previously (Rink and Wullmann, 2002; Wullmann and Rink, 2002; Filippi et al., 2010; Yamamoto et al., 2010). Inter- and intra-rater validation of the microscopic evaluation of the chromogenic staining was conducted by an expert pathologist and an anatomist where the tissue sections were blinded, and positive cells were counted. The results were analyzed to confirm the cell count method used. The regions that were analyzed included the olfactory bulb (OB), subpallidum (SP), pretectum (PR), preoptic region (PO), ventral thalamus (VT), paraventricular organ (PVO), and periventricular nucleus of posterior tubercle (TPp) of the posterior tuberculum (PT).

## 2.7. Statistical analysis

The data received was updated in the Statistical Package for the Social Sciences version 20 software (SPSS Inc., United States). All data were expressed as mean  $\pm$  standard error of mean (SEM). The data were plotted to evaluate the normality based on a histogram plot, z value, and Shapiro–Wilk test. A suitable statistical analysis was chosen based on the normality plot and the aim of the study. Data for locomotor assessment, gene expression, and protein level. TH+ cell counts were normally

distributed. These data were expressed as mean  $\pm$  SEM and analyzed with One-Way Analysis of Variance (ANOVA) and *post hoc* Tukey's test. In view of multiple group comparisons, independent-sample *t*-test were used for paired comparisons between two specific groups. A *p* value of  $<0.05$  is considered statistically significant.

## 3. Results

### 3.1. Locomotor assessment

The mean swimming speed was affected from day 1 post-MPTP injection, where there was a 16 and 12% reduction in MPTP1.1 ( $4.56 \pm 0.20$ ;  $p = 0.026$ ) and MPTP2.1 ( $4.78 \pm 0.36$ ;  $p = 0.151$ ) groups, respectively. However, only one-time injection reached statistical significance. Similarly, there were 27 and 20% reductions in mean speed in day 3 assessment for one- and two-time injection groups, respectively, with MPTP1.3 ( $3.95 \pm 0.24$ ;  $p < 0.001$ ) and MPTP2.3 ( $4.35 \pm 0.40$ ;  $p = 0.015$ ). There was no significant difference in the mean speed between the groups on the same assessment day, but different injection frequencies. Subsequently, the mean speed was monitored for an extended period until day 30 post-injection. There was a 26% reduction in MPTP1.5 ( $4.02 \pm 0.21$ ;  $p < 0.001$ ) and a 29% reduction in MPTP1.10 ( $3.88 \pm 0.19$ ;  $p < 0.001$ ). However, the swimming velocity improved significantly with an increment in speed of 26% from the control in the MPTP1.30 group ( $7.01 \pm 0.31$ ;  $p < 0.001$ ) (Figure 2).

Coherently, the total distance swam followed a similar pattern with the speed. It was observed that total distance was affected from day one post-injection MPTP1.1 ( $1350.15 \pm 58.35$ ;  $p = 0.002$ ), where there was a 17% reduction in distance observed, and 12% reduction in MPTP2.1 ( $1422.96 \pm 109.78$ ;  $p = 0.126$ ), however, only one-time injection group reached statistical significance. The distance traveled was further affected on day 3, with a 28% reduction in the distance in MPTP1.3 ( $1175.32 \pm 72.64$ ;  $p < 0.001$ ) and a 20% reduction in the distance in MPTP2.3 ( $1305.04 \pm 90.78$ ;  $p = 0.015$ ). There was no significant difference in one- and two-times injection group findings on similar assessment days (Figure 2). The swimming distance plateaued from day 3 to day 10, where there was a 26% reduction in the distance in MPTP1.5 ( $1203.10 \pm 64.39$ ;  $p < 0.001$ ) and a 29% reduction in MPTP1.10 ( $1160.30 \pm 59.00$ ;  $p < 0.001$ ). There was no statistical significance difference among these three groups. On day 30, there was a significant boost in swimming distance, with a 27% increase in distance compared to control in the MPTP1.30 group ( $2064.57 \pm 38.51$ ;  $p = 0.001$ ) (Figure 2).

It was observed that the mean speed and total distance traveled from day 1 to day 30 were significantly different statistically ( $p < 0.001$ ). We have also assessed the swimming pattern to observe the explorative capabilities of the fish across the groups. Although there were some fluctuations in the readings for the percentage of time spent on the top tank and the latency to reach the top, the results were not statistically significant. This could be due to the high variability of the findings, which has affected the SEM reading. The findings of all locomotor parameters between the control and vehicle groups were statistically not significant (Supplementary Figure S1).

### 3.2. Gene expression

Gene expressions were measured relatively using quantitative real-time PCR against the *actb1* gene (Rassier et al., 2020). All gene markers that were tested showed no statistical difference between the control and the vehicle group. There has been significant dysregulation of the gene, especially the *th1* gene across the treatment group. In contrast to the locomotor findings, the gene dysregulation was not evident at day 1 post-injection for one-time MPTP injection, MPTP1.1 ( $0.78 \pm 0.10$ ;  $p = 0.30$ ), however, it was significantly down-regulated in the two-times injection group, MPTP2.1 ( $0.18 \pm 0.08$ ;  $p = 0.006$ ). On day three of the assessment, both one- and two-time injection groups showed down-regulation of the *th1* gene, MPTP1.3 ( $0.07 \pm 0.03$ ;  $p = 0.003$ ) and MPTP2.3 ( $0.07 \pm 0.01$ ;  $p = 0.001$ ) (Figure 3). The differences between one- and two-times injections on day 3 of the assessment were not statistically significant. *th1* gene expression was observed to incline afterward at day 5, albeit still down-regulated from the vehicle group, MPTP1.5 ( $0.28 \pm 0.10$ ;  $p = 0.029$ ). This continued on day 10, where the differences in expression were not statistically significant compared to the vehicle group, MPTP1.10 ( $0.57 \pm 0.20$ ;  $p = 0.276$ ). On day 30 of the assessment, the *th1* gene was significantly down-regulated compared to the vehicle group ( $0.25 \pm 0.02$ ;  $p = 0.007$ ). Comparing *th1* gene expression over the period of 30 days, the differences were significant ( $p < 0.001$ ) where there was a deepest dip in the *th1* expression during day 3 to 5, then slowly improving, however, to be down-regulated again at day 30. We could observe similar trends in *th2* and *dat* gene expression (Figure 3). However, none of the groups reached a statistically significant difference from the control or vehicle group and within the same injection frequency or assessment day, except for MPTP1.10 where the *th2* gene was significantly up-regulated ( $1.64 \pm 0.11$ ;  $p = 0.021$ ) (Table 3).

### 3.3. Protein level

Whole zebrafish brains were analyzed for four proteins, namely DA, CASP3, GST, and BDNF. CASP3 and GST were assessed in view of their vital roles in apoptosis and cellular protection in oxidative stress (Saleem et al., 2019; Silva et al., 2020; Omoruyi et al., 2021). CASP3 has been shown to significantly double its level in the MPTP1.1 and MPTP2.3 groups. MPTP2.1 ( $122.19 \pm 14.81$ ) has shown elevated CASP3, almost similar to the former two groups, but did not reach statistical significance. Interestingly, MPTP1.3 has a slightly lower CASP3 level compared to the control and vehicle groups, however, it was not statistically significant. Comparisons between one- and two-time injections were only significant at day 3 assessment with a *p*-value of 0.041 (Table 4). Subsequently, MPTP1.5 ( $302.40 \pm 11.00$ ) had a remarkable increment in CASP3 level of 4.2 times higher than the vehicle group significantly. This was then dropped again to the control level on day 10, only to double again on day 30 (Figure 4). These rather extreme changes over 30 days have been shown to be statistically significant with a *p*-value of  $<0.001$ .

In contrast to CASP3, the GST level has steadily risen following MPTP injection. One- and two-time injection groups did not reach statistically significant differences when compared with either vehicle group or within similar assessment date groups. Following that, the day 5 group almost doubled its GST level ( $1.99 \pm 0.37$ ) but did not reach statistical significance. It was not until day 10 that the differences

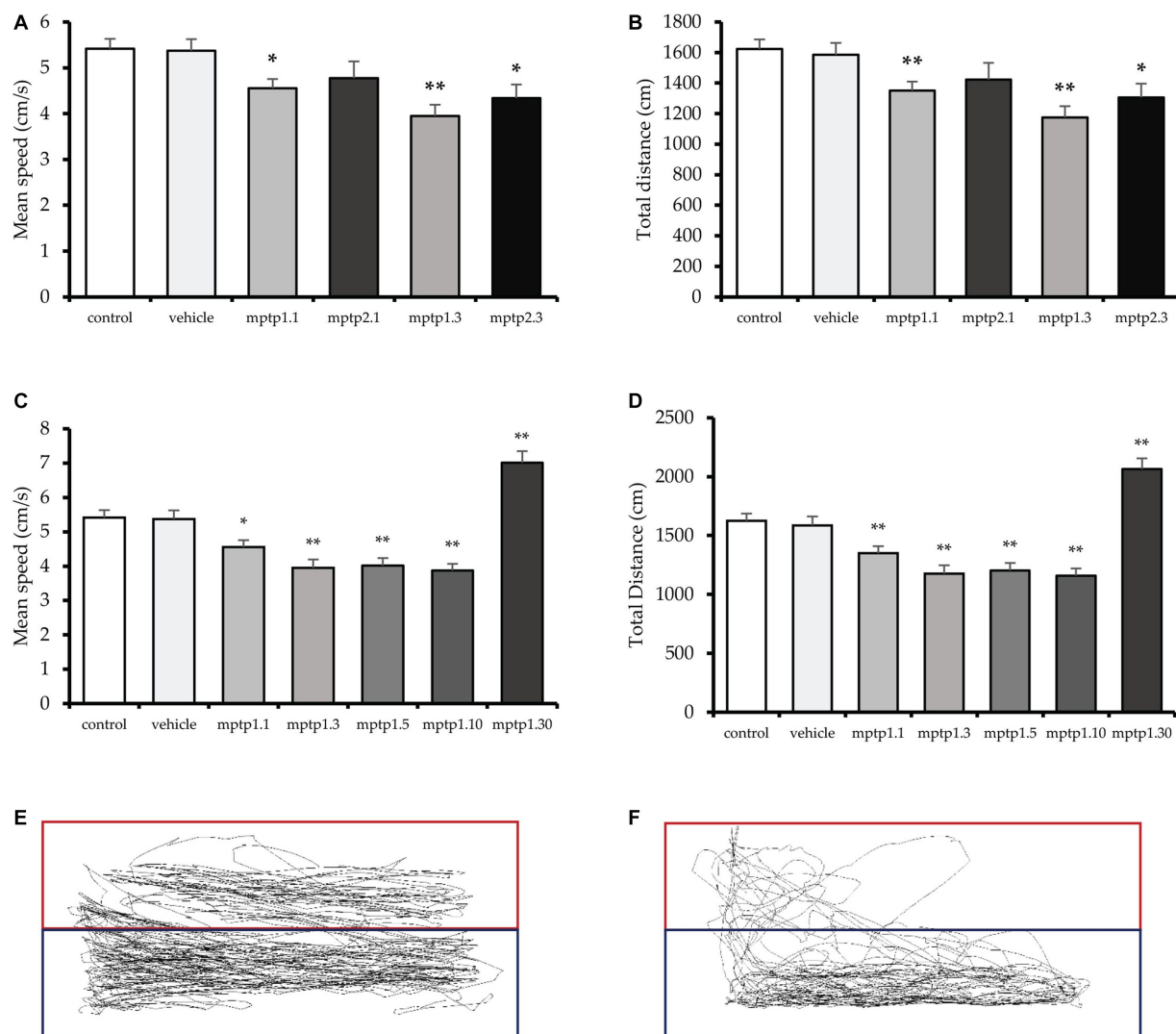


FIGURE 2

The locomotor assessment of the zebrafish models. (A,B) Total distance traveled and speed of the zebrafish between one- and two-times injection groups. (C,D) Total distance traveled and speed of one-time injection groups from day 1 to 30 post-MPTP injection. The deepest dip in speed and distance can be appreciated at day 3 post-injection, which is then plateaued until day 10. There is no difference in speed and distance traveled between day 3 to 10 groups. (E) Tracking of the swimming pattern in the control. (F) Tracking for group MPTP1.3. The exploration of the top tank is more substantial in the control group. Data are presented as mean  $\pm$  SEM. Asterisks (\*) indicate a significant difference between vehicle and treated fish at \* $p < 0.01$  or \*\* $p < 0.05$ .

in GST levels reached statistically significant results, where MPTP1.10 had 2.5 times and MPTP1.30 had 3.2 times higher GST levels compared to the vehicle group. The steady rise of GST levels over the period of 30 days has been shown to be statistically significant with a  $p$ -value of 0.002 (Figure 4).

DA levels of all groups were found to be equivocal except for MPTP2.1 ( $635.52 \pm 36.27$ ;  $p = 0.002$ ) and MPTP1.3 ( $489.61 \pm 38.72$ ;  $p = 0.043$ ) where the DA level was peculiarly increased by triple and double respectively, compared to the vehicle group level. The comparison of this group to the one-time injection group, MPTP1.1, was significantly different, with a  $p$ -value of 0.022. The extended observation days had equivocal results for the control and vehicle groups (Figure 4). Comparison of one-time injection over the period of 30 days was statistically insignificant in their DA level ( $p = 0.225$ ). BDNF was assessed as a protective neurotrophic factor that is involved

in neuronal regeneration and repair. In this study, the BDNF level showed an almost similar pattern to the DA level, where all groups had equivocal levels. Comparisons between one- and two-time injections and comparisons between days 1 to 30 were all statistically insignificant (Table 4; Supplementary Figure S2).

### 3.4. Immunohistochemistry assessment

The immunohistochemistry assessment using chromogenic stain against TH protein was based on TH+ cell counts in all regions known to express dopaminergic neurons, as previously described. There was no statistical difference in TH+ cell counts between the control and vehicle group tissue sections. VT has been shown to be one of the earliest regions to be affected by

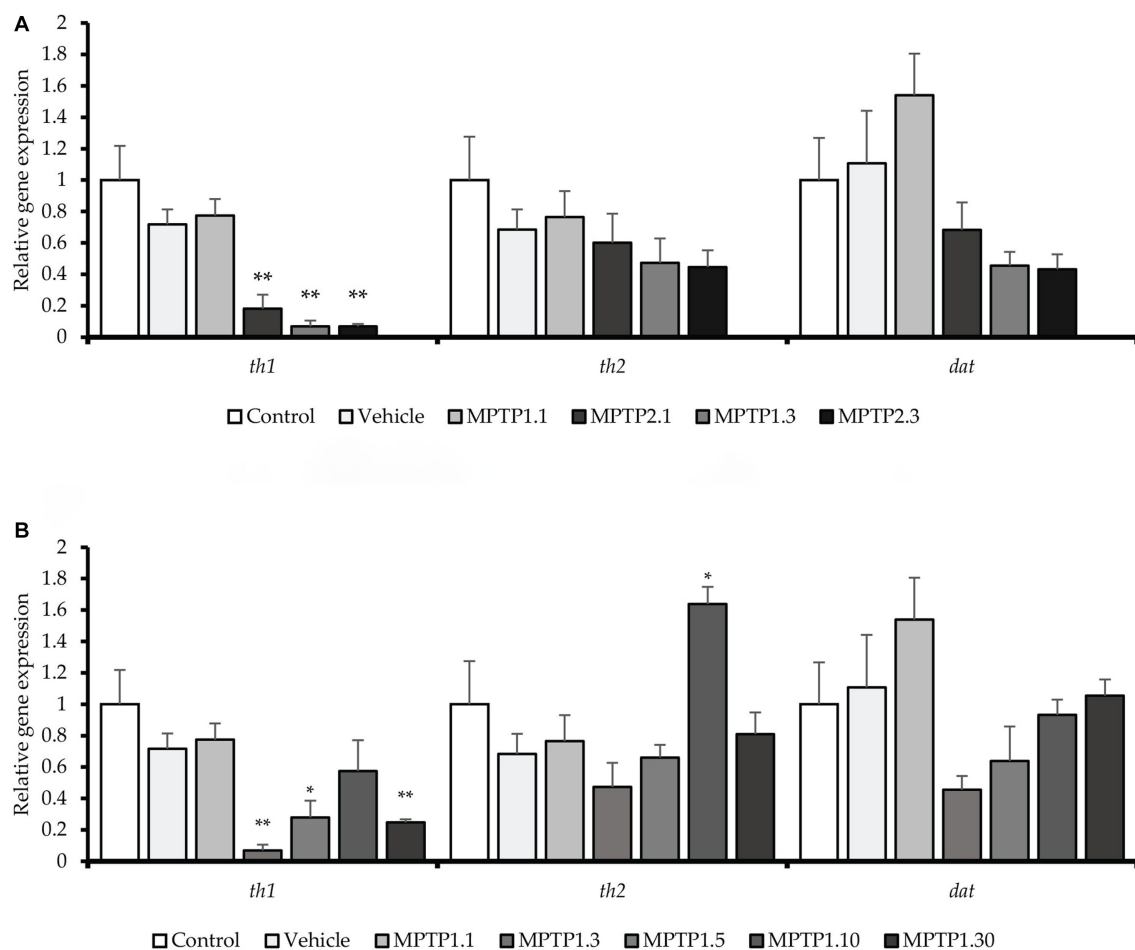


FIGURE 3

The relative gene expression in the zebrafish model across the group. *th1* gene was significantly down-regulated in MPTP1.3, MPTP1.5, MPTP2.1, and MPTP2.3. *th2* gene expression was down-regulated initially however was not statistically significant. However, at MPTP1.10, there is a spike in *th2* gene expression which eventually down-regulated in MPTP1.30. *dat* gene was down-regulated, especially in MPTP1.3 and MPTP2.3 then steadily increased afterward; however, these changes were not statistically significant. (A) The relative gene expression between one- and two-time injections. (B) The relative gene expression among MPTP days 1 to 30. Data are presented as mean  $\pm$  SEM. Asterisks (\*) indicate a significant difference between vehicle and treated fish at  $*p < 0.01$  or  $**p < 0.05$ .

TABLE 3 Mean relative gene expression in zebrafish whole brain.

Gene	Control	Vehicle	MPTP 1.1	MPTP 2.1	MPTP 1.3	MPTP 2.3	MPTP 1.5	MPTP 1.10	MPTP 1.30
<i>th1</i>	1.00 $\pm$ 0.22	0.72 $\pm$ 0.10	0.78 $\pm$ 0.10	0.18 $\pm$ 0.08*	0.07 $\pm$ 0.03**	0.07 $\pm$ 0.01**	0.28 $\pm$ 0.10*	0.57 $\pm$ 0.20	0.25 $\pm$ 0.02**
<i>th2</i>	1.00 $\pm$ 0.28	0.68 $\pm$ 0.12	0.77 $\pm$ 0.17	0.60 $\pm$ 0.18	0.47 $\pm$ 0.15	0.45 $\pm$ 0.11	0.66 $\pm$ 0.08	1.64 $\pm$ 0.11**	0.81 $\pm$ 0.14
<i>dat</i>	1.00 $\pm$ 0.27	1.10 $\pm$ 0.33	1.54 $\pm$ 0.27	0.68 $\pm$ 0.17	0.46 $\pm$ 0.09	0.43 $\pm$ 0.09	0.64 $\pm$ 0.22	0.93 $\pm$ 0.09	1.06 $\pm$ 0.10

*actb1* gene was used as the reference gene. Data are presented as mean  $\pm$  SEM. Asterisks (\*) indicate a significant difference between control and treated fish at  $*p < 0.05$  or  $**p < 0.01$ .

MPTP injection, where there is a drop of 11% and a significant drop of 41% of TH+ cells 1 day following one- and two-time injections of MPTP, respectively. The differences in TH+ cell counts on day one of assessment in these two groups were statistically significant. Which further dropped 63% from control during the day 3 assessment for both one- and two-time injection groups. Following that, the day 5 assessment showed a slight improvement in TH+ cell counts, where there was a 56% reduction of TH+ cells compared to the vehicle group. The recovery is more evident on day 10, where only 22% of TH+ dropped compared to the vehicle group. By day 30, the TH+ cell count had resumed,

similar to the control, and the counts were not statistically significant (Figures 5, 6).

Similarly, the PO region has shown a similar pattern to the VT cell count loss. There was a significant reduction of 45% and 69% in TH+ cell counts following 1 day of injection in the one- and two-time injection groups, respectively. Again, like in VT, the differences between these two groups were statistically significant. Day 3 assessment in one- and two-time injection showed a slight difference, where only one-time injection showed a significant drop of 56% of positive cell counts, while two-time injection cell counts only dropped 40%. However, the differences between these two groups did not reach

TABLE 4 Protein level from ELISA test.

Protein	Control	Vehicle	MPTP1.1	MPTP2.1	MPTP1.3	MPTP2.3	MPTP1.5	MPTP1.10	MPTP1.30
DA (pg/mL)	430.42 ± 40.60	279.88 ± 71.08	478.89 ± 45.53	635.52 ± 36.27**	489.61 ± 38.72*	372.23 ± 34.98	449.99 ± 44.18	446.74 ± 33.56	423.62 ± 50.14
CASP3 (pg/mL)	90.30 ± 19.88	72.01 ± 19.64	156.34 ± 13.01*	122.19 ± 14.81	66.47 ± 4.34	184.61 ± 39.61*	302.40 ± 11.00**	91.21 ± 27.19	170.64 ± 29.45*
GST (ng/mL)	1.09 ± 0.96	0.966 ± 0.23	0.96 ± 0.20	1.51 ± 0.54	1.38 ± 0.23	1.51 ± 0.25	1.99 ± 0.37	2.51 ± 0.33*	3.11 ± 0.56*
BNDF (pg/mL)	331.49 ± 23.64	369.654 ± 19.08	350.52 ± 14.17	301.56 ± 25.35	320.82 ± 35.85	319.56 ± 28.05	348.82 ± 44.51	335.27 ± 12.58	339.49 ± 26.43

Data are presented as mean ± SEM. Asterisks (\*) indicate a significant difference between vehicle and treated fish at \* $p < 0.05$  or \*\* $p < 0.01$ .

statistical significance. Following that, the recovery in this region has occurred swiftly compared to VT, where there was only a 23% reduction in positive cell counts in the MPTP 1.5 group compared to the vehicle group. Subsequently, the day 10 and 30 groups have shown to resume the TH+ cells similar to the control and vehicle groups.

In the PT region, TPp and PVO were assessed. In the TPp region, during day one of the assessment, although both groups showed a reduction in TH+ cell count, neither reached statistical significance when compared with the vehicle group. In addition, there was no significant difference in the cell counts between one- and two-time injections on day one of assessment. TH+ cell counts were drastically reduced by 60% compared to the vehicle group in the day 3 assessment for both one- and two-time injection groups, which plateaued during days 5 and 10 of the assessment. In contrast to VT and PO, day 30 of the assessment has not resumed TH+ cell count, where there is still a significant drop in TH+ cell counts by 25% compared to the vehicle group. Similarly, in PVO, during the day one assessment, only MPTP 2.1 had a significant reduction in TH+ cell count by as much as 10%. However, there is no significant difference between one- and two-time injections on day 1 assessment. Following that, there is a drastic drop in TH+ cell count at day 3 assessment in both one- and two-time injections, 61 and 40%, respectively. From thereon, the TH+ cell count steadily rose, with a significant 9% improvement in TH+ in MPTP 1.5 compared to MPTP 1.3. From day 10 onwards, the TH+ cell count continues to rise, and there is no significant difference in the TH+ cell count in MPTP 1.10 and MPTP 1.30 compared to the control and vehicle groups (Figures 5, 7).

The PR region has shown similar TH+ cell counts in all groups except MPTP 1.30, with a significant increment in the doubling of TH+ cell counts compared to the vehicle group. OB and SP have been shown to have equivocal TH+ cell counts in all MPTP groups, and there is no significant difference when comparing one- and two-time injections or between day one to day 30 of the assessment. Assessment of the groups from day one to 30 was significantly different selectively at VT, TPp, PVO, and PR (Table 5; Supplementary Figure S3).

## 4. Discussion

### 4.1. Frequency of injection and duration of induction

MPTP injection in animal models has been shown to mimic the PD phenotype. Our initial concern was to optimize the MPTP protocol specifically for a zebrafish animal model. This is because, despite having many benefits in terms of high fecundability and similarities with the human genome, its ability to regenerate its central nervous system makes it a face-to-face battle between choosing the right time of assessment following MPTP induction, as reported by (Sarath Babu et al., 2016) in their paper, where they induced PD in zebrafish with MPTP with either one- or two-time injections and were assessed 24h later. Their study has shown that two-time injected zebrafish have significant PD features on more positive markers than one-time injection. Based on this study, we have conducted the first part of our study. However, we reported a similar result between the one-time and two-time injection groups. We then extended the study to assess the zebrafish for another 2 days. This is when we saw significant changes, however, not between one- and two-time

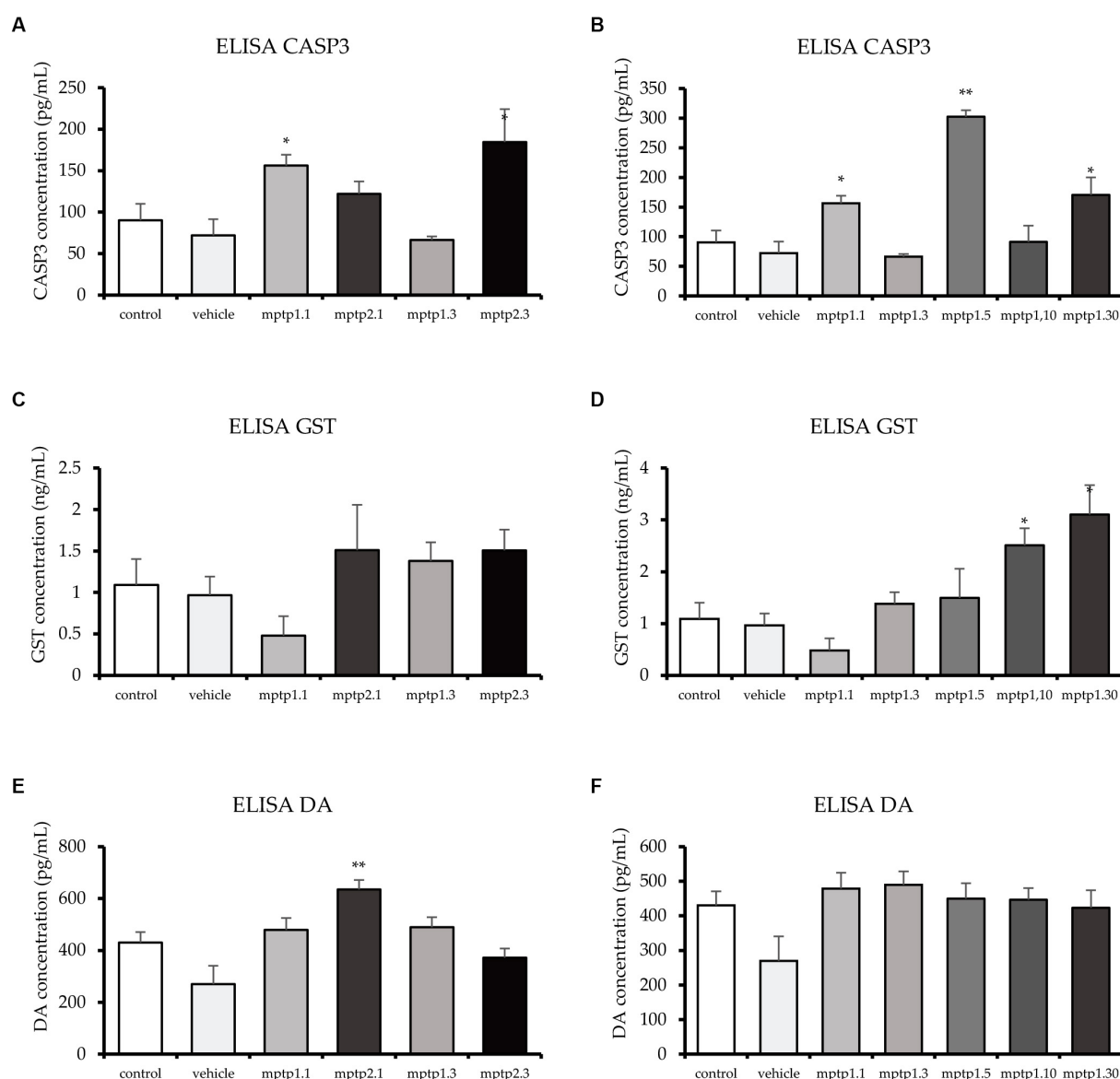


FIGURE 4

ELISA test for CASP3, GST and DA. CASP3 levels fluctuated across the group, with MPTP1.1 and MPTP1.5 significantly elevated. The GST protein was assessed and showed a sudden drop in MPTP1.1, albeit statistically insignificant. Henceforth, the level significantly increased in the day 10 and day 30 groups. DA levels were equivocal except for MPTP2.1 where it is significantly elevated. (A,C,E) ELISA results between one- and two-time injection. (B,D,F) Result between days of assessment from day 1 to 30. Data are presented as mean  $\pm$  SEM. Asterisks (\*) indicate a significant difference between vehicle and treated fish at  $*p < 0.01$  or  $**p < 0.05$ .

injections, but between the days of assessment, where day 3 post-MPTP injection has shown statistically significantly reduced swimming speed, a total distance of swimming, reduced *th1* and *dat* gene expression and reduced TH+ cells in immunohistochemistry, regardless of frequency of injection.

We then extended the assessment for up to 30 days to review the benefits of delaying the assessment. Hence, in the second part of the study, we analyzed the fish on days 5, 10, and 30 post-MPTP injections. From this assessment, it has been shown coherently for all markers, that the day 3 to day 5 group has shown the most statistically significant changes in locomotion, *th1* and *dat* gene expression, and TH+ neuronal degenerated cells. From that moment on, improvement in these parameters have been seen from day 10 onwards, and by day

30, the parameters are comparable to the control group. In the day 30 assessment, locomotor activity was higher than in the vehicle group, with significant recovery in TH+ cell counts, especially in the VT, PO, and PT regions. The *th1* gene was seen to be down-regulated compared to the vehicle group, but looking at the pattern, this happened following a peak in *th1* expression during day 10. The recovery features were more evident with the steady inclining of the GST level. Although the caspase-3 level was significantly higher than the vehicle group, looking at the fluctuating pattern of caspase-3, the increase is less pronounced following a dip on day 10. This is similar to a recent study that induced PD in an adult zebrafish group using CVMi injection using 6-OHDA, where they could see the recovery process of the parameter that they tested in the second week following

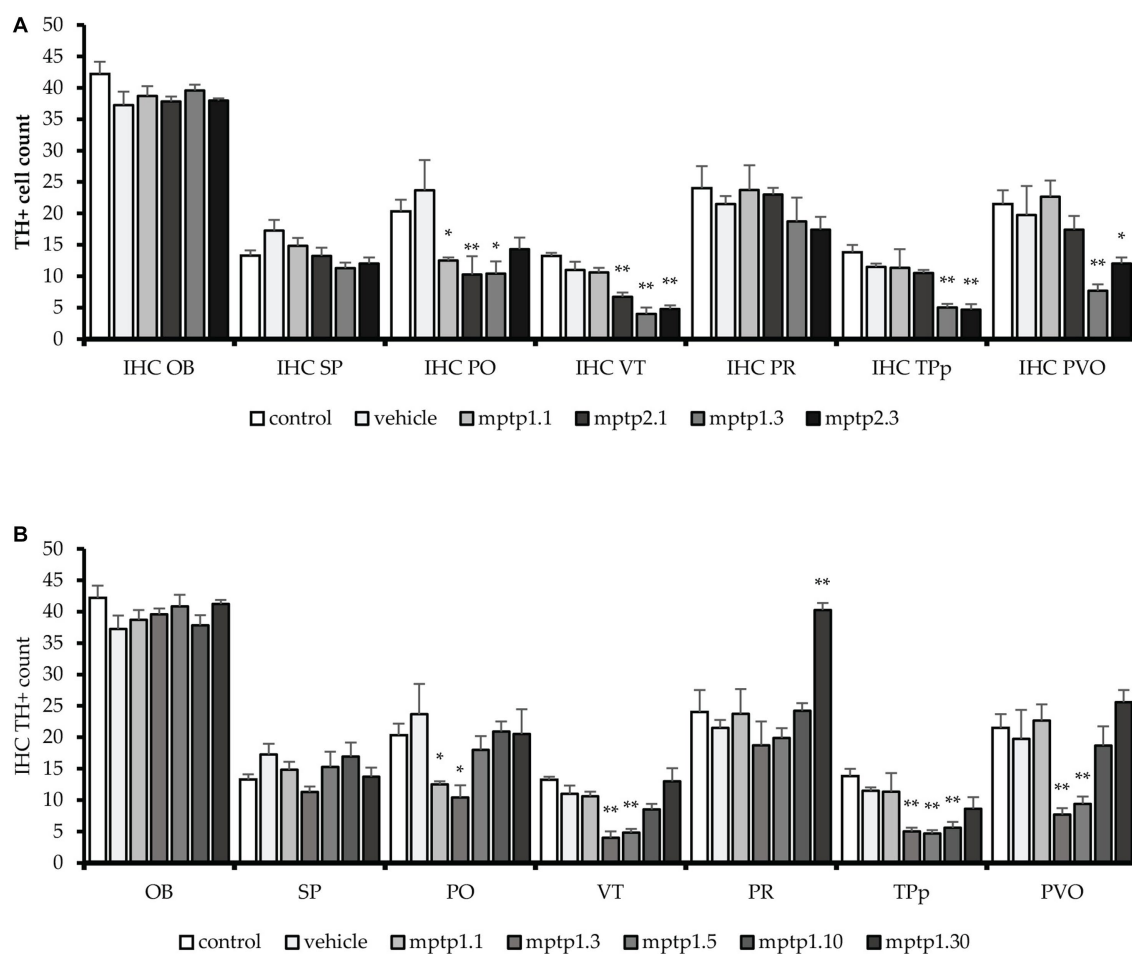


FIGURE 5

TH+ cells count in different regions of the brain. MPTP in this study has been shown to affect a few areas of dopaminergic neurons, sparing the OB, SP and PR areas. VT and PO area has been seen to be affected the earliest, as early as day 1. Subsequently, other areas were affected. The pattern is similar to other markers tested before, where the lowest counts were noted in MPTP1.3 and MPTP1.5. Day 10 assessment has shown recovery of the cell counts, which mostly return to the same counts as in control on day 10. Although cell counts did not reduce in pretectum following MPTP insult, it is noted that on day 30, the PR cell counts were significantly increased. (A) TH+ cell between one- and two-times injection. (B) TH+ cells between days of assessment from day 1 to 30. Data are presented as mean  $\pm$  SEM. Asterisks (\*) indicate a significant difference between vehicle and treated fish at \* $p < 0.01$  or \*\* $p < 0.05$ .

neurotoxin insult (Md Hamzah et al., 2021). In other words, the timing of PD model induction may be more related to the pharmacodynamics of the drugs in the zebrafish model than to the drug itself. This is particularly important as any form of PD treatment to be given post-MPTP induction should not exceed day 10, when the fish can repair and regenerate neuronal cells.

## 4.2. Swimming pattern, bradykinesia, and anxiety

We have analyzed the locomotor assessment based on the total distance of swimming within 5 min and the speed of the swim. These are pathognomonic features of PD where the clinical features of bradykinesia have been reflected in the swimming speed and distance. In this study, it has been shown that regardless of the day and frequency of injection, MPTP has successfully reflected the typical neurobehavioral feature in the PD zebrafish model, which is

bradykinesia (reduction in mean speed of swimming). There is a slight increment in mean speed and total swimming distance in the two-time injection group when compared to the one-time injection group. Although the differences did not reach statistical significance, it is rather peculiar to see an increment rather than a further drop in the two-time injection group. This could be the effect of multiple anesthesia that could induce stress or anxiety in this group. A study conducted on the effects of anesthesia on the serum cortisol level of teleost fish has found that the time of anesthesia corresponds 96% with the increment of the serum cortisol level (Wosnick et al., 2018). This in turn could be presented as an acute stress response in the zebrafish group. A review conducted looking at the fish response to acute and chronic stress has summarized that acute stress in fish could be presented as a higher swimming distance compared to control (Demin et al., 2021). However, we did not further explore the analysis as this was beyond the scope of the current study.

Apart from that, we have also analyzed the latency of the fish to reach the top half of the tank and the percentage of time spent in the

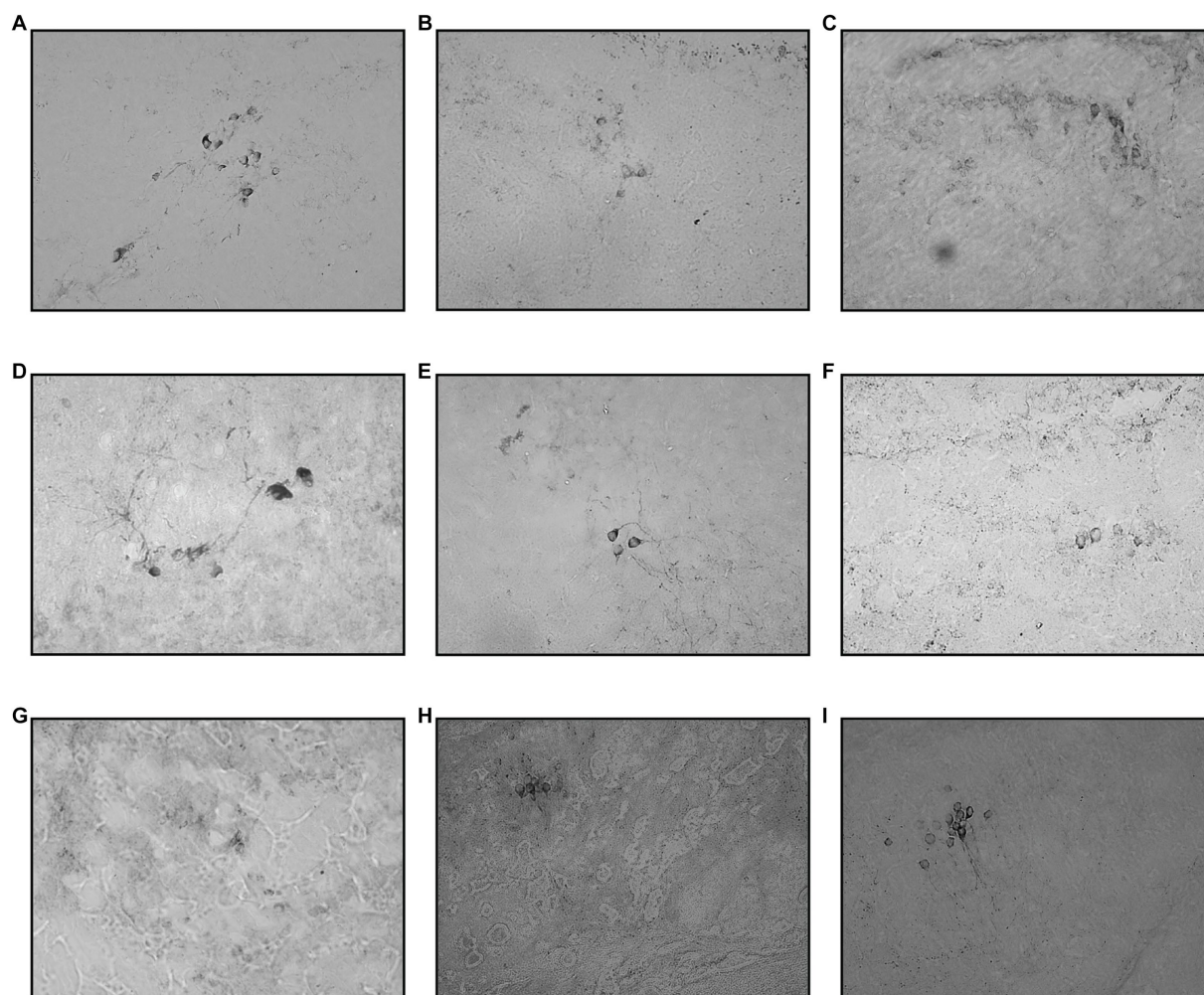


FIGURE 6

Coronal section of ventral thalamus. The TH+ cells were marked by a deep chromogenic stain. The cell number can be seen declining from day one and peaked around days 3 and 5. Day 10 and Day 30 sections showed re-emerging of positive TH+ cell stain. (A) Control, (B) Vehicle, (C) MPTP1.1, (D) MPTP2.1, (E) MPTP1.3, (F) MPTP2.3, (G) MPTP1.5, (H) MPTP1.10, (I) MPTP 1.30.

top half of the tank. These are markers to show the explorative abilities of the fish where anxiety could lead to less explorative capability of the fish, hence less time on the top half of the tank and longer time needed for them to explore the top half (latency to reach the top) (Robinson et al., 2013). In our study, MPTP1.3 to MPTP1.10 have shown some reduction in the percentage of time spent by the fish on the top half of the tank, and coherently, it takes a longer time for these groups for the first to start and explore the top half for the first time during the assessment. This is in accordance with a few studies showing non-motor PD behaviors in adult zebrafish following induction with neurotoxins (Wang et al., 2017; Selvaraj et al., 2019). However, the results were not statistically significant due to some variation in results within the same group that resulted in a higher SEM value. PD is associated with numerous non-motor symptoms, i.e., mental illness, cognitive dysfunction, and pain (Samat et al., 2017; Carapellotti et al., 2020). The anxiety symptoms in PD patients have also been well reported, with anxiety reported in 25.7% of PD patients (Broen et al., 2016b). The fact that the pattern of anxiety features in zebrafish and PD-specific features is similar may indicate the possibility that the neurochemical pathway

plays a bigger role in inducing anxiety in PD patients than previously thought (Broen et al., 2016a).

### 4.3. Gene expression in the PD model

As reported by Yamamoto et al., as a result of teleost whole genome duplication, there have been two *th* genes found in zebrafish species. It has been found that *th1* gene were more abundant in the brain and eye regions, while *th2* were more abundant in the liver, gills, heart and kidney of the zebrafish, with *th2*-expressing cells in the brains being more confined in the diencephalic region (Chen et al., 2009; Filippi et al., 2010). In the diencephalon, neurons expressing both these genes are dopaminergic neurons that were located either co-existing, like in the PT and PO, or in separate areas (Yamamoto et al., 2010). Whilst *dat* gene is responsible for the synthesis of DAT protein, which is vital for DA metabolism, uptake and release in the neuron (Vaughan and Foster, 2013). Our findings of selective *th1* and *dat* gene down-regulation sparing the *th2* gene were similar to a previous study that induced PD in a zebrafish model using paraquat

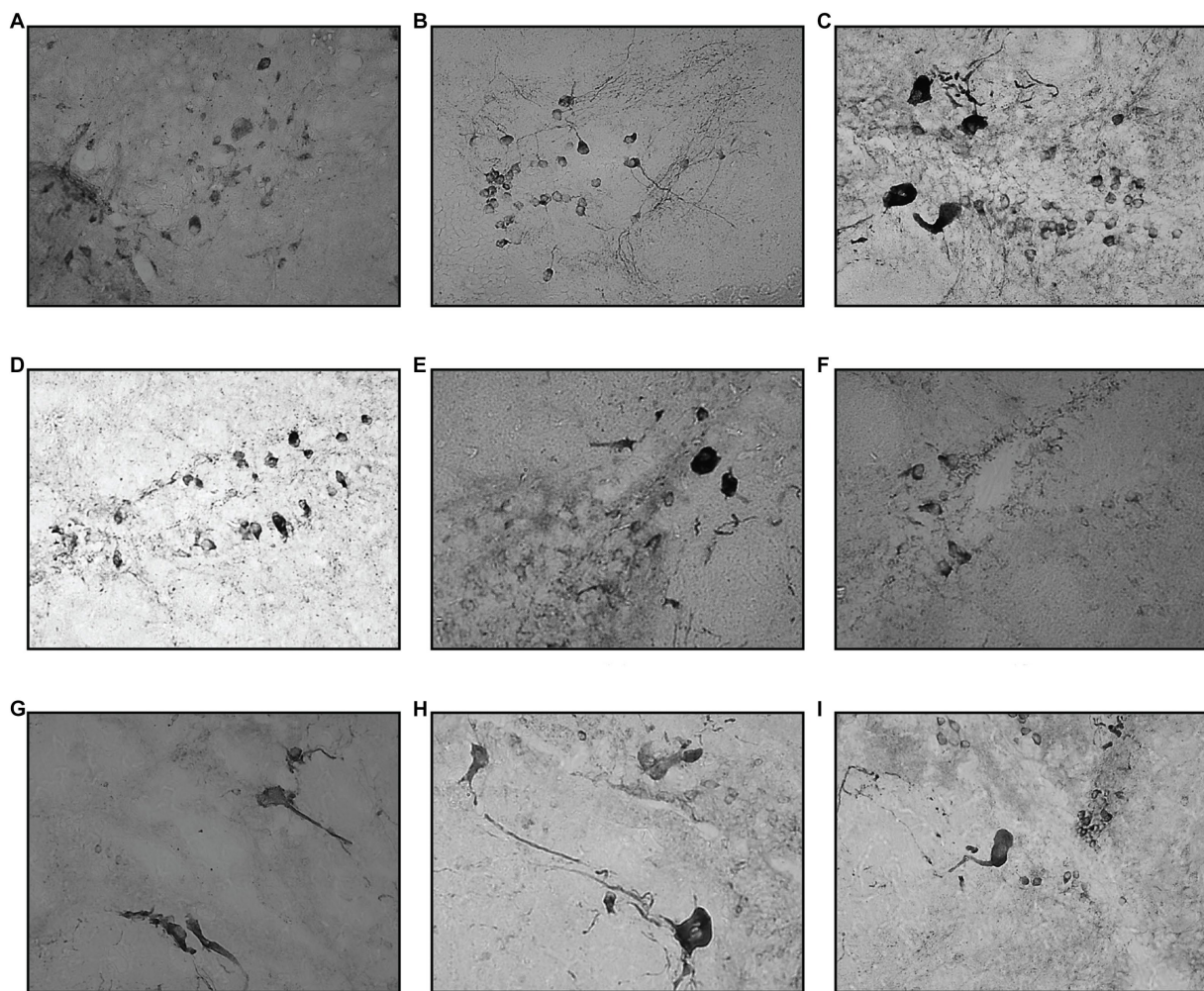


FIGURE 7

Coronal section of Tpp and PVO. Compared to VT, the drop in TH+ cell counts were more evident starting from day 3, for both one- and two-time MPTP injections. This finding persisted on day 5 of the assessment. Day 10 tissue section showed a slight improvement in TH+ cell count, which progressed eventually during the day 30 assessment. (A) Control, (B) Vehicle, (C) MPTP1.1, (D) MPTP2.1, (E) MPTP1.3, (F) MPTP2.3, (G) MPTP1.5; (H) MPTP1.10, (I) MPTP1.30.

TABLE 5 TH+ cell count in different regions of the zebrafish brain.

Region	Control	Vehicle	MPTP1.1	MPTP2.1	MPTP1.3	MPTP2.3	MPTP1.5	MPTP1.10	MPTP1.30
OB	42.20 ± 1.93	37.25 ± 2.12	38.71 ± 1.56	37.84 ± 0.74	39.60 ± 0.92	38.00 ± 0.32	40.87 ± 1.80	37.82 ± 1.61	41.25 ± 0.63
SP	13.30 ± 0.82	17.25 ± 1.70	14.81 ± 1.26	13.22 ± 1.31	11.29 ± 0.86	12.00 ± 0.98	15.27 ± 2.41	16.91 ± 2.23	13.71 ± 1.46
PO	20.33 ± 1.86	23.67 ± 4.84	12.50 ± 0.50*	7.33 ± 0.33**	10.42 ± 1.92*	14.29 ± 1.86	18.00 ± 2.16	20.89 ± 1.62	20.50 ± 3.96
VT	13.25 ± 0.47	12 ± 1.30	10.60 ± 0.74	6.71 ± 0.68*	4.00 ± 1.00**	4.75 ± 0.63**	4.80 ± 0.58**	8.50 ± 0.87	13.00 ± 2.08
PR	24.00 ± 3.53	21.5 ± 1.25	23.75 ± 3.90	23.00 ± 1.08	18.71 ± 3.82	17.40 ± 2.09	19.90 ± 1.56	24.20 ± 1.24	40.25 ± 1.10**
Tpp	13.80 ± 1.20	11.5 ± 0.5	11.33 ± 1.20	10.50 ± 0.50	5.00 ± 0.58**	4.67 ± 0.89**	4.67 ± 0.56**	5.60 ± 0.91**	8.60 ± 1.86*
PVO	21.50 ± 2.18	19.75 ± 4.58	22.67 ± 2.56	17.40 ± 2.18	7.67 ± 1.04**	12.00 ± 1.00*	9.40 ± 1.16**	18.67 ± 3.07	25.60 ± 1.94

Data are presented as mean ± SEM. Asterisks (\*) indicate a significant difference between vehicle and treated fish at \* $p < 0.05$  or \*\* $p < 0.01$ .

(Mohamad Najib et al., 2021). It is also important to note that, in PD, only certain regions of dopaminergic neurons are affected, hence these locations are essential to understanding why only certain *th1* genes are affected by the neurotoxin. It was mentioned in previous studies that the location of *th2* cells is more abundant in the caudal hypothalamic region (Filippi et al., 2010; Yamamoto et al., 2010; Semenova et al.,

2014), which is not directly related to the regions affected in the zebrafish PD model. It could also be due to the slightly different function of *th1* compared to *th2*-expressing neurons. Studies have linked *th2* with stress-related studies, which showed the up-regulation of *th2* genes and staining in response to stress in zebrafish (Pavlidis et al., 2011; Semenova et al., 2014).

Looking at the pattern of gene expression throughout the 30 days post-injection period, the gene expression follows a similar pattern whereby the least down-regulation was seen on day 3, and following that, gene expression has been seen to increase the most by day 10. Following that, the gene expression has either returned to similar levels to control or been slightly down-regulated. On day 10, the *th2* gene expression was markedly up-regulated and was the only day where *th2* expression was significantly different from the control and vehicle groups. Similarly, the *th1* gene was up-regulated the most on a similar day following MPTP injection. This could be part of the neuroregeneration effort by the zebrafish to recover from the neurotoxic effects of the MPTP. This is consistent with a study conducted by Yamamoto et al., where they established that both TH1 and TH2-containing cells are responsible for synthesizing DA. It is also worth noting that, albeit not abundantly, there are regions in the brain, especially in the paraventricular region, where TH1- and TH2-expressing cells coexist (Filippi et al., 2010; Yamamoto et al., 2010).

#### 4.4. Protein expression in the PD model

We also conducted ELISA assessments measuring the level of protein in the zebrafish brain for all the groups. The first protein examined is DA, which is one of the catecholamine neurotransmitters, aside from noradrenergic and adrenergic (Bhat and Ganesh, 2017). DA is the activated protein processed from tyrosine by the enzyme TH. It has been shown that DA levels change in conditions like PD and anxiety in zebrafish. In our study, DA levels were measured from the whole zebrafish brain, which has shown no significant difference compared to the control group. There could be a few reasons for this, for instance, it is worth noting that dopaminergic neurons have a specific function in a specific region of the brain. Hence, the result may vary depending on whether the assessment is done as a whole brain or in a specific brain region. Another reason could be that the anxiety features that have been shown in locomotor assessment could be reflected as elevated DA levels (Kacprzak et al., 2017; Liu et al., 2020) in the hypothalamus of the zebrafish brain (Filippi et al., 2010; Yamamoto et al., 2010; Semenova et al., 2014) (which were not measured in this study), that have been reflected as equivocal DA level during the assessment of the whole brain. MPTP used in the study has also been known for its selective degenerative effects in PD dopaminergic clusters, which may not reflect on the total DA level in the whole zebrafish brain (Pollard et al., 1996; Storch et al., 2004; Langston, 2017).

CASP3 is one of the cysteine proteases that play an essential role in the apoptotic signaling pathway and is known as the primary executioner of cell death (Valencia et al., 2007; Brentnall et al., 2013). It has been found that CASP3 is responsible for the proapoptotic cascade in both intrinsic and extrinsic pathways (Pyati et al., 2007). Studies have proven the role of CASP3-induced cell apoptosis following MPTP injection in their *in vivo* studies (Turmel et al., 2001; Yamada et al., 2010; Spead et al., 2018). In our study, the CASP3 level from ELISA peaked significantly on day 1 post-injection and subsequently fluctuated as the day progressed. Towards day 30, the level remained higher than in the vehicle group. The increment of CASP3 following MPTP injection had a similar result in a recent study, which showed a significant increment of CASP3 in their

colorimetric or western blotting assessment of the protein (Liang et al., 2019; Haque et al., 2021). The last protein that was assessed was GST. This intracellular thiol compound can be found in the cytosol and mitochondria and plays a crucial role in defense against respiration-induced reactive oxygen species (ROS) (Ribas et al., 2014). The vital redox agent for ROS is generated mainly in complexes 1 and 3 of the electron transport chain (Ribas et al., 2014). The GST level showed a sudden drop in the day 1 assessment, which followed the pattern of the peak in CASP3 on the same day, however, this level did not reach statistical significance. Following that, there is a steady rise in GST level, significantly from day 10 onwards. The steady increment in GST with fluctuating CASP3 levels could be a sign of non-apoptotic CASP3 activity that could be activated following the regenerative and healing process in the zebrafish brain (Imbriani et al., 2019; Eskandari and Eaves, 2022).

Immunohistochemistry assessments of the zebrafish brain were conducted using chromogenic TH stain. It is vital to note that TH enzymes are located in the cytosol and cell membrane of the cells. Hence, negative TH+ could be a sign of cell degeneration in the regions that are expected to be positive. Among all the regions assessed, the areas affected were specific to VT, PO, Tpp, and PVO, while sparing other regions, namely OB, SP, and PR. Locus coeruleus was not analyzed in this study as this TH+ region is the regional expression of noradrenergic catecholamines, which is beyond the scope of the study. The results were coherent with the previous study which has shown that neurotoxin agent causes dopaminergic neurodegeneration specifically in the VT, PO, PVO, and PT while sparing other areas (Caldwell et al., 2019). PT (Tpp and PVO) has been reported to represent the dopaminergic neuron in the substantia nigra pars compacta (Matsui, 2017a,b; Matsui and Sugie, 2017; Matsui and Takahashi, 2018). Brown et al. (2021) have also reported the vulnerability of dopaminergic neurons in this region, which is age dependent and was significantly affected following the PINK1 gene knockout-PD model. The VT is one of the first regions to be affected even as early as day one of this study. The pattern of TH+ cell reduction is similar to the previously described parameters, where day 3 has been shown the most marked reduction compared to other groups. The day 30 group has been shown to have a TH+ cell count similar to the control group in all the regions previously affected on earlier days. The peculiar increase in TH+ cell counts in the PR region on day 30 of assessment, where there was a doubling of TH+ cell counts compared to the control or vehicle groups intrigued us for further exploration. The increment could be due to part of the regenerative capacity of the zebrafish itself, where the PR region is one of the regenerative loci that could regenerate TH+ cells that will further migrate centrifugally to the desired locus to replace the degenerated neurons (Grandel et al., 2006). However, we are still unclear on why the other unaffected regenerative loci did not have the same effect, such as in the OB and SP. This could be due to the non-retinorecipient connection of PR to other regions such as the cerebellum and hypothalamus that may have effects on motor function in the zebrafish in order to compensate for the neuronal loss in the PT region which was lower than the control group on the same assessment day (Yanez et al., 2018; Barrios et al., 2020). This is crucial information that needs to be addressed before planning methodologies for treatment research in the PD model.

Most studies have been carried out using MPTP to induce PD in the larval stage of zebrafish, which exhibits reduced dopaminergic

neurons and locomotor activity (Najib et al., 2020). Additionally, the larval model is preferred probably because of its small size, which enables high-throughput screening; its transparent body, which is preferred for imaging; similar inflammatory response as in adults; and the exponential phenotypic features induced by small brain alteration (Sallinen et al., 2009; Zanandrea et al., 2020). In this study, we exposed MPTP to adult zebrafish, considering the brain's ability for regeneration has peaked and the effects of neurotoxins may be observed more closely corresponding to humans. This allows adult zebrafish to provide a more accurate comparison with mammals than their larval counterparts. In contrast, pro-regenerative signals and cell types are known to exist in zebrafish larvae between the larval and adult phases (Alper and Dorsky, 2022).

## 5. Conclusion

Intraperitoneal injection of MPTP has successfully induced PD in an adult zebrafish model. One-time injection with delayed assessment on days 3 to 5 is sufficient to show significant PD features in the zebrafish. The regeneration time shown from day 10 onwards is important to address, especially for studies involving treatment trials for neurodegenerative diseases. Nevertheless, inducing neuroregeneration may serve as a potential therapeutic strategy to treat PD.

## Data availability statement

The original contributions presented in the study are included in the article/Supplementary materials, further inquiries can be directed to the corresponding author.

## Ethics statement

The animal study was approved by Universiti Kebangsaan Malaysia Animal Ethics Committee. The study was conducted in accordance with the local legislation and institutional requirements.

## Author contributions

JK and ST: conceptualization and supervision. ST and NO: methodology. NO, JK, and ST: validation and writing—review and

editing. NO: formal analysis, data curation, and writing—original draft preparation. ST: funding acquisition. All authors contributed to the article and approved the submitted version.

## Funding

This research was funded by the Universiti Kebangsaan Malaysia through the Faculty of Medicine Fundamental Grant (grant number FF-2021-177) and the Ministry of Higher Education (MOHE), Malaysia through the Fundamental Research Grant Scheme (grant number FRGS/1/2018/SKK08/UKM/03/5).

## Acknowledgments

We would like to express our immense gratitude to Nur Aqilah Kamaruddin, Shaiful Ridzwan Sapri, and Natasya Nadia Sahrudin for their assistance in conducting the study. We would also like to thank the Department of Pathology and Physiology of Universiti Kebangsaan Malaysia for its instruments' services during the study period.

## Conflict of interest

The authors declare that the research was conducted in the absence of any commercial or financial relationships that could be construed as a potential conflict of interest.

## Publisher's note

All claims expressed in this article are solely those of the authors and do not necessarily represent those of their affiliated organizations, or those of the publisher, the editors and the reviewers. Any product that may be evaluated in this article, or claim that may be made by its manufacturer, is not guaranteed or endorsed by the publisher.

## Supplementary material

The Supplementary material for this article can be found online at: <https://www.frontiersin.org/articles/10.3389/fnins.2023.1236049/full#supplementary-material>

## References

- Al Shoyaib, A., Archie, S. R., and Karamyan, V. T. (2019). Intraperitoneal route of drug administration: Should it be used in experimental animal studies? *Pharm. Res.* 37:12. doi: 10.1007/s11095-019-2745-x
- Allgoewer, A., and Mayer, B. (2017). Sample size estimation for pilot animal experiments by using a Markov Chain Monte Carlo approach. *Altern. Lab. Anim* 45, 83–90. doi: 10.1177/026119291704500201
- Alper, S. R., and Dorsky, R. I. (2022). Unique advantages of zebrafish larvae as a model for spinal cord regeneration. *Front. Mol. Neurosci.* 15:983336. doi: 10.3389/fnmol.2022.983336
- Anichtchik, O. V., Kaslin, J., Peitsaro, N., Scheinin, M., and Panula, P. (2004). Neurochemical and behavioural changes in zebrafish *Danio rerio* after systemic administration of 6-hydroxydopamine and 1-methyl-4-phenyl-1,2,3,6-tetrahydropyridine. *J. Neurochem.* 88, 443–453. doi: 10.1111/j.1471-4159.2004.02190.x
- Barrios, J. P., Wang, W. C., England, R., Reifenberg, E., and Douglass, A. D. (2020). Hypothalamic dopamine neurons control sensorimotor behavior by modulating brainstem premotor nuclei in zebrafish. *Curr. Biol.* 30, 4606–4618.e4. doi: 10.1016/j.cub.2020.09.002
- Barut, B. A., and Zon, L. I. (2000). Realizing the potential of zebrafish as a model for human disease. *Physiol. Genomics* 2, 49–51. doi: 10.1152/physiolgenomics.2000.2.2.49
- Beaudry, F., and Huot, P. (2020). The MPTP-lesioned marmoset model of Parkinson's disease: proposed efficacy thresholds that may potentially predict successful clinical trial results. *J. Neural Transm.* 127, 1343–1358. doi: 10.1007/s00702-020-02247-2

- Bhat, S. K., and Ganesh, C. B. (2017). Distribution of tyrosine hydroxylase-immunoreactive neurons in the brain of the viviparous fish *Gambusia affinis*. *J. Chem. Neuroanat.* 85, 1–12. doi: 10.1016/j.jchemneu.2017.05.004
- Bhattarai, P., Cosacak, M. I., Mashkaryan, V., Demir, S., Popova, S. D., Govindarajan, N., et al. (2020). Neuron-glia interaction through serotonin-BDNF-NGFR axis enables regenerative neurogenesis in Alzheimer's model of adult zebrafish brain. *PLoS Biol.* 18:e3000585. doi: 10.1371/journal.pbio.3000585
- Bhattarai, P., Thomas, A. K., Cosacak, M. I., Papadimitriou, C., Mashkaryan, V., Froc, C., et al. (2016). IL4/STAT6 signaling activates neural stem cell proliferation and neurogenesis upon amyloid- $\beta$ 2 aggregation in adult zebrafish brain. *Cell Rep.* 17, 941–948. doi: 10.1016/j.celrep.2016.09.075
- Brentnall, M., Rodriguez-Menocal, L., De Guevara, R. L., Cepero, E., and Boise, L. H. (2013). Caspase-9, caspase-3 and caspase-7 have distinct roles during intrinsic apoptosis. *BMC Cell Biol.* 14:32. doi: 10.1186/1471-2121-14-32
- Broen, M. P., Köhler, S., Moonen, A. J., Kuijff, M. L., Dujardin, K., Marsh, L., et al. (2016a). Modeling anxiety in Parkinson's disease. *Mov. Disord.* 31, 310–316. doi: 10.1002/mds.26461
- Broen, M. P., Narayan, N. E., Kuijff, M. L., Dissanayaka, N. N., and Leentjens, A. F. (2016b). Prevalence of anxiety in Parkinson's disease: a systematic review and meta-analysis. *Mov. Disord.* 31, 1125–1133. doi: 10.1002/mds.26643
- Brown, S. J., Boussaad, I., Jarazo, J., Fitzgerald, J. C., Antony, P., Keatinge, M., et al. (2021). PINK1 deficiency impairs adult neurogenesis of dopaminergic neurons. *Sci. Rep.* 11:6617. doi: 10.1038/s41598-021-84278-7
- Burton, E. A. (2015). "Zebrafish" in *Movement disorders*. ed. M. S. LeDoux (Amsterdam: Academic Press), 117–138.
- Cachat, J., Stewart, A., Grossman, L., Gaikwad, S., Kadri, F., Chung, K. M., et al. (2010). Measuring behavioral and endocrine responses to novelty stress in adult zebrafish. *Nat. Protoc.* 5, 1786–1799. doi: 10.1038/nprot.2010.140
- Caldwell, L. J., Davies, N. O., Cavone, L., Mysiak, K. S., Semenova, S. A., Panula, P., et al. (2019). Regeneration of dopaminergic neurons in adult zebrafish depends on immune system activation and differs for distinct populations. *J. Neurosci.* 39, 4694–4713. doi: 10.1523/JNEUROSCI.2706-18.2019
- Cansiz, D., Ustundag, U. V., Unal, I., Alturfan, A. A., and Emekli-Alturfan, E. (2021). Morphine attenuates neurotoxic effects of MPTP in zebrafish embryos by regulating oxidant/antioxidant balance and acetylcholinesterase activity. *Drug Chem. Toxicol.* 45, 2439–2447. doi: 10.1080/01480545.2021.1957558
- Cao, F., Souders, C. L. 2nd, Li, P., Pang, S., Liang, X., Qiu, L., et al. (2019). Developmental neurotoxicity of maneb: notochord defects, mitochondrial dysfunction and hypoactivity in zebrafish (*Danio rerio*) embryos and larvae. *Ecotoxicol. Environ. Saf.* 170, 227–237. doi: 10.1016/j.ecoenv.2018.11.110
- Carapellotti, A. M., Stevenson, R., and Doumas, M. (2020). The efficacy of dance for improving motor impairments, non-motor symptoms, and quality of life in Parkinson's disease: a systematic review and meta-analysis. *PLoS One* 15:e0236820. doi: 10.1371/journal.pone.0236820
- Chen, Y. C., Priyadarshini, M., and Panula, P. (2009). Complementary developmental expression of the two tyrosine hydroxylase transcripts in zebrafish. *Histochem. Cell Biol.* 132, 375–381. doi: 10.1007/s00418-009-0619-8
- Coyle, S., Durborow, R., and Tidwell, J. H. (2004). Anesthetics in aquaculture. Southern Regional Aquaculture Centre 3900, 1–6. Available at: <https://fisheries.tamu.edu/files/2013/09/SRAC-Publication-No.-3900-Anesthetics-in-Aquaculture.pdf>.
- Davis, G. C., Williams, A. C., Markey, S. P., Ebert, M. H., Caine, E. D., Reichert, C. M., et al. (1979). Chronic Parkinsonism secondary to intravenous injection of meperidine analogues. *Psychiatry Res.* 1, 249–254. doi: 10.1016/0165-1781(79)90006-4
- Demin, K. A., Taranov, A. S., Ilyin, N. P., Lakstygla, A. M., Volgin, A. D., de Abreu, M. S., et al. (2021). Understanding neurobehavioral effects of acute and chronic stress in zebrafish. *Stress* 24, 1–18. doi: 10.1080/10253890.2020.1724948
- Eskandari, E., and Eaves, C. J. (2022). Paradoxical roles of caspase-3 in regulating cell survival, proliferation, and tumorigenesis. *J. Cell Biol.* 221:e202201159. doi: 10.1083/jcb.202201159
- Filippi, A., Mahler, J., Schweitzer, J., and Driever, W. (2010). Expression of the paralogous tyrosine hydroxylase encoding genes *th1* and *th2* reveals the full complement of dopaminergic and noradrenergic neurons in zebrafish larval and juvenile brain. *J. Comp. Neurol.* 518, 423–438. doi: 10.1002/cne.22213
- García-Ramos, R., López Valdés, E., Ballesteros, L., Jesús, S., and Mir, P. (2016). The social impact of Parkinson's disease in Spain: report by the Spanish Foundation for the brain. *Neurologia* 31, 401–413. doi: 10.1016/j.nrleng.2013.04.008
- Grandel, H., Kaslin, J., Ganz, J., Wenzel, I., and Brand, M. (2006). Neural stem cells and neurogenesis in the adult zebrafish brain: origin, proliferation dynamics, migration and cell fate. *Dev. Biol.* 295, 263–277. doi: 10.1016/j.ydbio.2006.03.040
- Haque, M. E., Azam, S., Akther, M., Cho, D. Y., Kim, I. S., and Choi, D. K. (2021). The neuroprotective effects of GPR4 inhibition through the attenuation of caspase mediated apoptotic cell death in an MPTP induced mouse model of Parkinson's disease. *Int. J. Mol. Sci.* 22:4674. doi: 10.3390/ijms22094674
- Howe, K., Clark, M. D., Torroja, C. F., Torrance, J., Berthelot, C., Muffato, M., et al. (2013). The zebrafish reference genome sequence and its relationship to the human genome. *Nature* 496, 498–503. doi: 10.1038/nature12111
- Imbriani, P., Tassone, A., Meringolo, M., Ponterio, G., Madeo, G., Pisani, A., et al. (2019). Loss of non-apoptotic role of caspase-3 in the PINK1 mouse model of Parkinson's disease. *Int. J. Mol. Sci.* 20:3407. doi: 10.3390/ijms20143407
- Kacprzak, V., Patel, N. A., Riley, E., Yu, L., Yeh, J. J., and Zhdanova, I. V. (2017). Dopaminergic control of anxiety in young and aged zebrafish. *Pharmacol. Biochem. Behav.* 157, 1–8. doi: 10.1016/j.pbb.2017.01.005
- Kalia, L. V., and Lang, A. E. (2015). Parkinson's disease. *Lancet* 386, 896–912. doi: 10.1016/s0140-6736(14)61393-3
- Kalueff, A. V., Stewart, A. M., and Gerlai, R. (2014). Zebrafish as an emerging model for studying complex brain disorders. *Trends Pharmacol. Sci.* 35, 63–75. doi: 10.1016/j.tips.2013.12.002
- Kalyn, M., and Ekker, M. (2021). Cerebroventricular microinjections of MPTP on adult zebrafish induces dopaminergic neuronal death, mitochondrial fragmentation, and sensorimotor impairments. *Front. Neurosci.* 15:718244. doi: 10.3389/fnins.2021.718244
- Kimmel, C. B., Ballard, W. W., Kimmel, S. R., Ullmann, B., and Schilling, T. F. (1995). Stages of embryonic development of the zebrafish. *Dev. Dyn.* 203, 253–310. doi: 10.1002/aja.1002030302
- Kinkel, M. D., Eames, S. C., Philipson, L. H., and Prince, V. E. (2010). Intraperitoneal injection into adult zebrafish. *J. Vis. Exp.* 42:e2126. doi: 10.3791/2126
- Lam, C. S., Korzh, V., and Strahle, U. (2005). Zebrafish embryos are susceptible to the dopaminergic neurotoxin MPTP. *Eur. J. Neurosci.* 21, 1758–1762. doi: 10.1111/j.1460-9568.2005.03988.x
- Langston, J. W. (2017). The MPTP story. *J. Parkinsons Dis.* 7, S11–S19. doi: 10.3233/JPD-179006
- Langston, J. W., Ballard, P., Tetrad, J. W., and Irwin, I. (1983). Chronic Parkinsonism in humans due to a product of meperidine-analog synthesis. *Science* 219, 979–980. doi: 10.1126/science.6823561
- Liang, Y., Chen, C., Xia, B., Wu, W., Tang, J., Chen, Q., et al. (2019). Neuroprotective effect of echinacoside in subacute mouse model of Parkinson's disease. *Biomed. Res. Int.* 2019:4379639. doi: 10.1155/2019/4379639
- Liu, M., Shin, E. J., Dang, D. K., Jin, C. H., Lee, P. H., Jeong, J. H., et al. (2018). Trichloroethylene and Parkinson's disease: risk assessment. *Mol. Neurobiol.* 55, 6201–6214. doi: 10.1007/s12035-017-0830-x
- Liu, S., Yu, M., Xie, X., Ru, Y., and Ru, S. (2020). Carbofuran induces increased anxiety-like behaviors in female zebrafish (*Danio rerio*) through disturbing dopaminergic/norepinephrine system. *Chemosphere* 253:126635. doi: 10.1016/j.chemosphere.2020.126635
- Matsui, H. (2017a). Dopamine system, cerebellum, and nucleus ruber in fish and mammals. *Develop. Growth Differ.* 59, 219–227. doi: 10.1111/dgd.12357
- Matsui, H. (2017b). The use of fish models to study human neurological disorders. *Neurosci. Res.* 120, 1–7. doi: 10.1016/j.neures.2017.02.004
- Matsui, H., and Sugie, A. (2017). An optimized method for counting dopaminergic neurons in zebrafish. *PLoS One* 12:e0184363. doi: 10.1371/journal.pone.0184363
- Matsui, H., and Takahashi, R. (2018). Parkinson's disease pathogenesis from the viewpoint of small fish models. *J. Neural Transm.* 125, 25–33. doi: 10.1007/s00702-017-1772-1
- McKinley, E. T., Baranowski, T. C., Blavo, D. O., Cato, C., Doan, T. N., and Rubinstein, A. L. (2005). Neuroprotection of MPTP-induced toxicity in zebrafish dopaminergic neurons. *Brain Res. Mol. Brain Res.* 141, 128–137. doi: 10.1016/j.molbrainres.2005.08.014
- Md Hamzah, N., Lim, S. M., Vijayanathan, Y., Lim, F. T., Abdul Majeed, A. B., Tan, M. P., et al. (2021). Locomotor assessment of 6-hydroxydopamine-induced adult zebrafish-based Parkinson's disease model. *J. Vis. Exp.* 178:e63355. doi: 10.3791/63355
- Mohamad Najib, N. H., Yahaya, M. F., Das, S., and Teoh, S. L. (2021). The effects of metallothionein in paraquat-induced Parkinson disease model of zebrafish. *Int. J. Neurosci.* 133, 822–883. doi: 10.1080/00207454.2021.1990916
- Mustapha, M., and Mat Taib, C. N. (2021). MPTP-induced mouse model of Parkinson's disease: a promising direction of therapeutic strategies. *Bosn. J. Basic Med. Sci.* 21, 422–433. doi: 10.17305/bjbm.2020.5181
- Najib, N. H. M., Nies, Y. H., Abd Halim, S. A. S., Yahaya, M. F., Das, S., Lim, W. L., et al. (2020). Modeling Parkinson's disease in zebrafish. *CNS Neurol. Disord. Drug Targets* 19, 386–399. doi: 10.2174/1871527319666200708124117
- Omoruyi, S. I., Ibrakaw, A. S., Ekpo, O. E., Boatwright, J. S., Cupido, C. N., and Hussein, A. A. (2021). Neuroprotective activities of *Crossyne flava* bulbs and amaryllidaceae alkaloids: implications for Parkinson's disease. *Molecules* 26:3990. doi: 10.3390/molecules26133990
- Pavlidis, M., Sundvik, M., Chen, Y. C., and Panula, P. (2011). Adaptive changes in zebrafish brain in dominant-subordinate behavioral context. *Behav. Brain Res.* 225, 529–537. doi: 10.1016/j.bbr.2011.08.022
- Pollard, H. B., Kuijpers, G. A., Adeyemo, O. M., Youdim, M. B., and Goping, G. (1996). The MPTP-induced parkinsonian syndrome in the goldfish is associated with major cell destruction in the forebrain and subtle changes in the optic tectum. *Exp. Neurol.* 142, 170–178. doi: 10.1006/exnr.1996.0188

- Pringsheim, T., Jette, N., Frolkis, A., and Steeves, T. D. (2014). The prevalence of Parkinson's disease: a systematic review and meta-analysis. *Mov. Disord.* 29, 1583–1590. doi: 10.1002/mds.25945
- Piyat, U. J., Look, A. T., and Hammerschmidt, M. (2007). Zebrafish as a powerful vertebrate model system for *in vivo* studies of cell death. *Semin. Cancer Biol.* 17, 154–165. doi: 10.1016/j.semcancer.2006.11.007
- Rassier, G. T., Silveira, T. L. R., Remiao, M. H., Daneluz, L. O., Martins, A. W. S., Dellagostin, E. N., et al. (2020). Evaluation of qPCR reference genes in GH-overexpressing transgenic zebrafish (*Danio rerio*). *Sci. Rep.* 10:12692. doi: 10.1038/s41598-020-69423-y
- Razali, K., Othman, N., Mohd Nasir, M. H., Doolaanea, A. A., Kumar, J., Ibrahim, W. N., et al. (2021). The promise of the zebrafish model for Parkinson's disease: today's science and tomorrow's treatment. *Front. Genet.* 12:655550. doi: 10.3389/fgene.2021.655550
- Ribas, V., Garcia-Ruiz, C., and Fernandez-Checa, J. C. (2014). Glutathione and mitochondria. *Front. Pharmacol.* 5:151. doi: 10.3389/fphar.2014.00151
- Rink, E., and Wullmann, M. F. (2002). Development of the catecholaminergic system in the early zebrafish brain: an immunohistochemical study. *Dev. Brain Res.* 137, 89–100. doi: 10.1016/s0165-3806(02)00354-1
- Robinson, K. S., Stewart, A. M., Cachat, J., Landsman, S., Gebhardt, M., and Kalueff, A. V. (2013). Psychopharmacological effects of acute exposure to kynurenic acid (KYNA) in zebrafish. *Pharmacol. Biochem. Behav.* 108, 54–60. doi: 10.1016/j.pbb.2013.04.002
- Saleem, U., Raza, Z., Anwar, F., Ahmad, B., Hira, S., and Ali, T. (2019). Experimental and computational studies to characterize and evaluate the therapeutic effect of *Albizia lebbek* (L.) seeds in Alzheimer's disease. *Medicina* 55:184. doi: 10.3390/medicina55050184
- Sallinen, V., Torkko, V., Sundvik, M., Reenila, I., Khrestalyov, D., Kaslin, J., et al. (2009). MPTP and MPP+ target specific aminergic cell populations in larval zebrafish. *J. Neurochem.* 108, 719–731. doi: 10.1111/j.1471-4159.2008.05793.x
- Samat, N. A., Abdul Murad, N. A., Mohamad, K., Abdul Razak, M. R., and Mohamed Ibrahim, N. (2017). Apolipoprotein Eε4: a biomarker for executive dysfunction among Parkinson's disease patients with mild cognitive impairment. *Front. Neurosci.* 11:712. doi: 10.3389/fnins.2017.00712
- Sarath Babu, N., Murthy, C. L., Kakara, S., Sharma, R., Brahmendra Swamy, C. V., and Idris, M. M. (2016). 1-Methyl-4-phenyl-1,2,3,6-tetrahydropyridine induced Parkinson's disease in zebrafish. *Proteomics* 16, 1407–1420. doi: 10.1002/pmic.201500291
- Sasiz, S. M., and Smith, C. M. (2018). The impact of stress on social behavior in adult zebrafish (*Danio rerio*). *Behav. Pharmacol.* 29, 53–59. doi: 10.1097/FBP.0000000000000338
- Selvaraj, V., Venkatasubramanian, H., Ilango, K., and Santhakumar, K. (2019). A simple method to study motor and non-motor behaviors in adult zebrafish. *J. Neurosci. Methods* 320, 16–25. doi: 10.1016/j.jneumeth.2019.03.008
- Semenova, S. A., Chen, Y. C., Zhao, X., Rauvala, H., and Panula, P. (2014). The tyrosine hydroxylase 2 (TH2) system in zebrafish brain and stress activation of hypothalamic cells. *Histochem. Cell Biol.* 142, 619–633. doi: 10.1007/s00418-014-1240-z
- Silva, J., Alves, C., Pinteus, S., Mendes, S., and Pedrosa, R. (2020). Seaweeds' neuroprotective potential set in vitro on a human cellular stress model. *Mol. Cell. Biochem.* 473, 229–238. doi: 10.1007/s11010-020-03824-5
- Spad, O., Verreet, T., Donelson, C. J., and Poulain, F. E. (2018). Characterization of the caspase family in zebrafish. *PLoS One* 13:e0197966. doi: 10.1371/journal.pone.0197966
- Spence, R., Gerlach, G., Lawrence, C., and Smith, C. (2008). The behaviour and ecology of the zebrafish, *Danio rerio*. *Biol. Rev. Camb. Philos. Soc.* 83, 13–34. doi: 10.1111/j.1469-185X.2007.00030.x
- Storch, A., Ludolph, A. C., and Schwarz, J. (2004). Dopamine transporter: involvement in selective dopaminergic neurotoxicity and degeneration. *J. Neural Transm.* 111, 1267–1286. doi: 10.1007/s00702-004-0203-2
- Sun, C. P., Zhou, J. J., Yu, Z. L., Huo, X. K., Zhang, J., Morisseau, C., et al. (2022). Kurarinone alleviated Parkinson's disease via stabilization of epoxyeicosatrienoic acids in animal model. *Proc. Natl. Acad. Sci. U. S. A.* 119:e2118818119. doi: 10.1073/pnas.2118818119
- Teoh, S. L., Ogawa, S., and Parhar, I. S. (2015). Localization of genes encoding metallothionein-like protein (mt2 and smtb) in the brain of zebrafish. *J. Chem. Neuroanat.* 70, 20–32. doi: 10.1016/j.jchemneu.2015.10.004
- Turmel, H., Hartmann, A., Parain, K., Douhou, A., Srinivasan, A., Agid, Y., et al. (2001). Caspase-3 activation in 1-methyl-4-phenyl-1,2,3,6-tetrahydropyridine (MPTP)-treated mice. *Mov. Disord.* 16, 185–189. doi: 10.1002/mds.1037
- Turner, P. V., Brabb, T., Pekow, C., and Vasbinder, M. A. (2011a). Administration of substances to laboratory animals: routes of administration and factors to consider. *J. Am. Assoc. Lab. Anim. Sci.* 50, 600–613.
- Turner, P. V., Pekow, C., Vasbinder, M. A., and Brabb, T. (2011b). Administration of substances to laboratory animals: equipment considerations, vehicle selection, and solute preparation. *J. Am. Assoc. Lab. Anim. Sci.* 50, 614–627.
- Tysnes, O. B., and Storstein, A. (2017). Epidemiology of Parkinson's disease. *J. Neural Transm.* 124, 901–905. doi: 10.1007/s00702-017-1686-y
- Ustundag, F. D., Unal, I., Cansiz, D., Ustundag, U. V., Subasat, H. K., Alturfan, A. A., et al. (2020). 3-Pyridinylboronic acid normalizes the effects of 1-Methyl-4-phenyl-1,2,3,6-tetrahydropyridine exposure in zebrafish embryos. *Drug Chem. Toxicol.* 45, 947–954. doi: 10.1080/01480545.2020.1795189
- Valencia, C. A., Bailey, C., and Liu, R. (2007). Novel zebrafish caspase-3 substrates. *Biochem. Biophys. Res. Commun.* 361, 311–316. doi: 10.1016/j.bbrc.2007.06.173
- Vaughan, R. A., and Foster, J. D. (2013). Mechanisms of dopamine transporter regulation in normal and disease states. *Trends Pharmacol. Sci.* 34, 489–496. doi: 10.1016/j.tips.2013.07.005
- Vijayanathan, Y., Lim, F. T., Lim, S. M., Long, C. M., Tan, M. P., Majeed, A. B. A., et al. (2017). 6-OHDA-lesioned adult zebrafish as a useful Parkinson's disease model for dopaminergic neuroregeneration. *Neurotox. Res.* 32, 496–508. doi: 10.1007/s12640-017-9778-x
- Wang, Y., Liu, W., Yang, J., Wang, F., Sima, Y., Zhong, Z. M., et al. (2017). Parkinson's disease-like motor and non-motor symptoms in rotenone-treated zebrafish. *Neurotoxicology* 58, 103–109. doi: 10.1016/j.neuro.2016.11.006
- Williams-Gray, C. H., and Worth, P. F. (2016). Parkinson's disease. *Medicine (Baltimore)* 44, 542–546. doi: 10.1016/j.mpmed.2016.06.001
- Wosnick, N., Bendhack, F., Leite, R. D., Morais, R. N., and Freire, C. A. (2018). Benzocaine-induced stress in the euryhaline teleost, *Centropomus parallelus* and its implications for anesthesia protocols. *Comp. Biochem. Physiol. A Mol. Integr. Physiol.* 226, 32–37. doi: 10.1016/j.cbpa.2018.07.021
- Wullmann, M. F., and Rink, E. (2002). The teleostean forebrain: a comparative and developmental view based on early proliferation, Pax6 activity and catecholaminergic organization. *Brain Res. Bull.* 57, 363–370. doi: 10.1016/s0361-9230(01)00666-9
- Yamada, M., Kida, K., Amutuhare, W., Ichinose, F., and Kaneki, M. (2010). Gene disruption of caspase-3 prevents MPTP-induced Parkinson's disease in mice. *Biochem. Biophys. Res. Commun.* 402, 312–318. doi: 10.1016/j.bbrc.2010.10.023
- Yamamoto, K., Ruuskanen, J. O., Wullmann, M. F., and Vernier, P. (2010). Two tyrosine hydroxylase genes in vertebrates new dopaminergic territories revealed in the zebrafish brain. *Mol. Cell. Neurosci.* 43, 394–402. doi: 10.1016/j.mcn.2010.01.006
- Yanez, J., Suarez, T., Quelle, A., Folguez, M., and Anadon, R. (2018). Neural connections of the pretectum in zebrafish (*Danio rerio*). *J. Comp. Neurol.* 526, 1017–1040. doi: 10.1002/cne.24388
- Zanandrea, R., Bonan, C. D., and Campos, M. M. (2020). Zebrafish as a model for inflammation and drug discovery. *Drug Discov. Today* 25, 2201–2211. doi: 10.1016/j.drudis.2020.09.036
- Zeng, X. S., Geng, W. S., and Jia, J. J. (2018). Neurotoxin-induced animal models of Parkinson disease: pathogenic mechanism and assessment. *ASN Neuro* 10:1759091418777438. doi: 10.1177/1759091418777438
- Zhao, Y., Han, Y., Wang, Z., Chen, T., Qian, H., He, J., et al. (2020). Rosmarinic acid protects against 1-methyl-4-phenyl-1,2,3,6-tetrahydropyridine-induced dopaminergic neurotoxicity in zebrafish embryos. *Toxicol. in Vitro* 65:104823. doi: 10.1016/j.tiv.2020.104823
- Ziering, A., and Lee, J. (1947). Piperidine derivatives; 1,3-dialkyl-4-aryl-4-acyloxy piperidines. *J. Org. Chem.* 12, 911–914. doi: 10.1021/jo01170a024



## OPEN ACCESS

## EDITED BY

Sudhanshu P. Raikwar,  
Barrow Neurological Institute (BNI),  
United States

## REVIEWED BY

Yarreiphang Haorei,  
National Institute of Mental Health and  
Neurosciences (NIMHANS), India  
Maria Teresa Colomina,  
University of Rovira i Virgili, Spain  
Silvestre Alavez,  
Autonomous Metropolitan University, Mexico

## \*CORRESPONDENCE

Eduard Rodríguez-Farré  
✉ [eduardo.rodriquez.farre@csic.es](mailto:eduardo.rodriquez.farre@csic.es)

RECEIVED 27 June 2023

ACCEPTED 18 December 2023

PUBLISHED 08 January 2024

## CITATION

Sanfeliu C, Bartra C, Suñol C and  
Rodríguez-Farré E (2024) New insights in  
animal models of neurotoxicity-induced  
neurodegeneration.  
*Front. Neurosci.* 17:1248727.  
doi: 10.3389/fnins.2023.1248727

## COPYRIGHT

© 2024 Sanfeliu, Bartra, Suñol and  
Rodríguez-Farré. This is an open-access  
article distributed under the terms of the  
[Creative Commons Attribution License  
\(CC BY\)](https://creativecommons.org/licenses/by/4.0/). The use, distribution or reproduction  
in other forums is permitted, provided the  
original author(s) and the copyright owner(s)  
are credited and that the original publication  
in this journal is cited, in accordance with  
accepted academic practice. No use,  
distribution or reproduction is permitted  
which does not comply with these terms.

# New insights in animal models of neurotoxicity-induced neurodegeneration

Coral Sanfeliu<sup>1</sup>, Clara Bartra<sup>1,2</sup>, Cristina Suñol<sup>1</sup> and  
Eduard Rodríguez-Farré<sup>1\*</sup>

<sup>1</sup>Institut d'Investigacions Biomèdiques de Barcelona (IIBB), Consejo Superior de Investigaciones Científicas (CSIC), and Institut d'Investigacions Biomèdiques August Pi i Sunyer (IDIBAPS), Barcelona, Spain, <sup>2</sup>PhD Program in Biotechnology, Facultat de Farmàcia i Ciències de l'Alimentació, Universitat de Barcelona, Barcelona, Spain

The high prevalence of neurodegenerative diseases is an unintended consequence of the high longevity of the population, together with the lack of effective preventive and therapeutic options. There is great pressure on preclinical research, and both old and new models of neurodegenerative diseases are required to increase the pipeline of new drugs for clinical testing. We review here the main models of neurotoxicity-based animal models leading to central neurodegeneration. Our main focus was on studying how changes in neurotransmission and neuroinflammation, mainly in rodent models, contribute to harmful processes linked to neurodegeneration. The majority of the models currently in use mimic Parkinson's disease (PD) and Alzheimer's disease (AD), which are the most common neurodegenerative conditions in older adults. AD is the most common age-related dementia, whereas PD is the most common movement disorder with also cases of dementia. Several natural toxins and xenobiotic agents induce dopaminergic neurodegeneration and can reproduce neuropathological traits of PD. The literature analysis of MPTP, 6-OH-dopamine, and rotenone models suggested the latter as a useful model when specific doses of rotenone were administrated systemically to C57BL/6 mice. Cholinergic neurodegeneration is mainly modelled with the toxin scopolamine, which is a useful rodent model for the screening of protective drugs against cognitive decline and AD. Several agents have been used to model neuroinflammation-based neurodegeneration and dementia in AD, including lipopolysaccharide (LPS), streptozotocin, and monomeric C-reactive protein. The bacterial agent LPS makes a useful rodent model for testing anti-inflammatory therapies to halt the development and severity of AD. However, neurotoxin models might be more useful than genetic models for drug discovery in PD but that is not the case in AD where they cannot beat the new developments in transgenic mouse models. Overall, we should work using all available models, either *in vivo*, *in vitro*, or *in silico*, considering the seriousness of the moment and urgency of developing effective drugs.

## KEYWORDS

neurodegeneration, experimental models, neurotoxic agents, neurotransmission, neuroinflammation, Parkinson's disease, Alzheimer's disease

# 1 Introduction

A wide spectrum of disease animal models has been used in preclinical research of neurodegenerative diseases for decades. However, all too often positive results with new drugs are not replicated in the clinical setting, thus contributing to raise opposition against animal experimentation. Therefore, it is time to reassess the models we use and look for experimental models of neurodegeneration that are more faithful to human neuropathological processes. At present, genetic models are widely used. These models refer to an organism, often a laboratory animal such as a mouse, that has been genetically modified to carry specific genes or mutations associated with a human trait, disease, or condition. However, pathologies driven by specific mutations would only mimic a minority of human neurodegenerative processes. That problem is exacerbated when we consider age-related diseases that make up the bulk of neurodegenerative cases in our increasingly old population (Azam et al., 2021). An option is to use classic and new neurotoxicity-based animal models that mimic external and internal environmental insults received throughout lifetime but mainly during the aging process. These models rely on the functional or structural alterations of the central nervous system (CNS) induced by natural toxins and xenobiotics that ultimately cause neurodegeneration (Shaw and Höglinger, 2008).

Small rodents, such as mice and rats, can be treated with specific neurotoxic agents to induce neurodegeneration and test the neuroprotection of drugs, allowing comprehensive studies from the molecular level to complex behavior. Although other rodents or primates are also suggested for specific purposes, such as gerbils for ischemic neurodegeneration or aged primates for AD (Shin et al., 2019; Trouche et al., 2023), the advantages of mice and rats are undeniable. These advantages include similarities in brain anatomy, short lifespan, rapid breeding, small size, cost-effectiveness and ease of maintenance, behavioral testing capabilities, genetic manipulation, and disease modeling (Bryda, 2013). Furthermore, animal experimentation remains essential in the preclinical studies of many diseases, as *in silico*, *ex vivo*, and *in vitro* testing cannot reproduce the complexity of the body–brain interaction and the neuropsychological processes. It should be added the need to address differential sex neurodegenerative processes (Bianco et al., 2023) and responses to drugs (Buoncervello et al., 2017) that can be fulfilled by using male and female rodents.

Here, we critically analyze known and new neurotoxic agent-mediated models of neurodegeneration as reliable models that may complement gene-mediated approaches and contribute to demonstrate druggable targets in neurodegenerative disease. We focus on rodent models of neurotoxic agents that cause pathological changes in neurotransmission and neuroinflammation mechanisms. We propose these alterations as relevant early factors in the progressive loss of structure or function of neurons ultimately leading to cognitive loss and dementia in neurodegenerative diseases. Several models of neurotoxicity-induced cholinergic alteration or neuroinflammation are used to test new drugs for Alzheimer's disease (AD), the most common age-related dementia. CNS neurodegeneration can lead to motor diseases such as Parkinson's disease (PD), the most common movement disorder that also shows an increased risk of dementia. Specifically, neurotoxin models of PD are successful in reproducing

the main aspects of the disease, and we address dopaminergic neurodegeneration models more broadly.

## 2 Validated and new experimental models of neurodegeneration

### 2.1 Models based on dopaminergic neurodegeneration

In the CNS, there exist four main dopaminergic systems: nigrostriatal and ventral tegmental, mesocortical, mesolimbic, and tuberoinfundibular area. The progressive, lengthy, relatively selective, extensive, and irreversible loss of dopaminergic neurons in the substantia nigra (SN) pars compacta and their projections in the corpus striatum (caudate nucleus and putamen) constitute the main pathological manifestation of the neurodegenerative disorder present in PD. A second hallmark of PD is the presence in the nigrostriatal dopaminergic neurons of characteristic cytoplasmic inclusions known as Lewy bodies, which contain fibrils of misfolded  $\alpha$ -synuclein protein. The clinical features of the striatal loss of dopamine in PD are resting tremor, postural and gait dysfunction, bradykinesia, muscular rigidity, etc. (Braak and Del Tredici, 2008). In addition, PD encompasses in its evolution non-motor manifestations (e.g., depression, sleep alteration, declining memory, and psychoses) which involve the other dopaminergic systems and CNS structures.

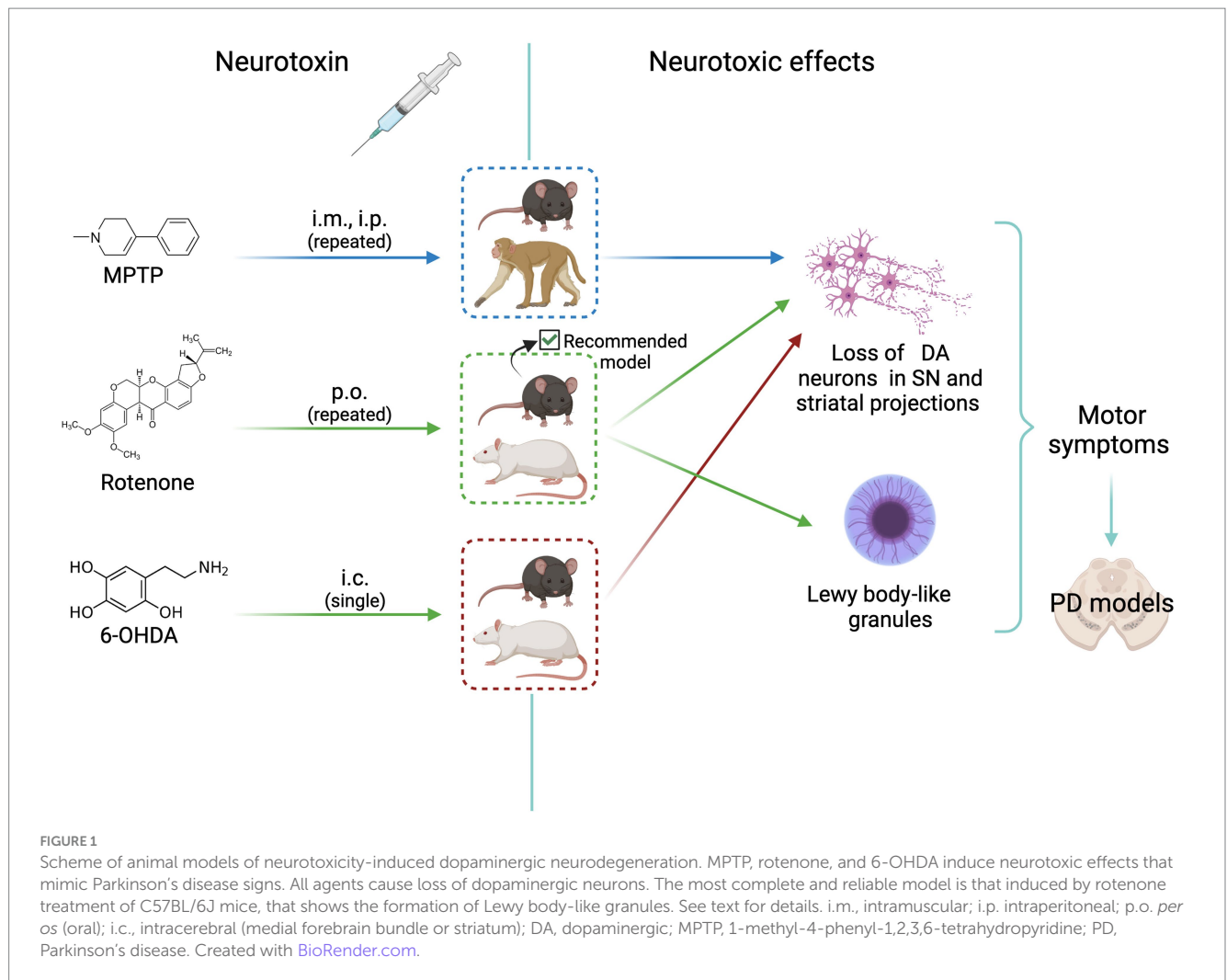
PD is expressed in two forms: familial, with approximately 5% of cases, and sporadic or idiopathic with 95%. Sporadic PD represents the second most frequent neurodegenerative disease, only after AD, affecting approximately 1% of the elderly population (Ray Dorsey et al., 2018; Ou et al., 2021), thus implying a high burden for affected people and for public health. Epidemiological studies have reported an association between exposure to environmental chemicals, particularly pesticides, and increased risk of PD (Kuopio et al., 1999; Pedro-Cuesta Jd et al., 2009; Goldman, 2014).

In recent years, the above classical definition of PD is becoming to be considered a systemic or multicentric and staging pathology, involving the entire nervous system, i.e., the CNS, the peripheral (PNS), and the enteric nervous system (ENS) (Braak and Del Tredici, 2008; Braak and Del Tredici, 2017). In this concept, PD is viewed as a gut–brain neurodegenerative process in which the central pathology is an  $\alpha$ -synucleinopathy (Natale et al., 2010; McCann et al., 2014; Li et al., 2023).

The goal of experimental models for sporadic PD is to reproduce as close as possible the pathological and clinical manifestations of human disease (there are no spontaneous PD observed in animals). Three models are currently used to investigate the pathophysiology and the pharmacology of PD. Figure 1 shows the scheme of the treatment route, the animal species used, and the neurotoxic effects elicited in these models, as detailed below.

#### 2.1.1 1-methyl-4-phenyl-1,2,3,6-tetrahydropyridine model of PD

Forty years ago, Langston et al. (1983) reported that several young adults in California developed a marked and irreversible parkinsonism shortly after using intravenously a new synthetic illicit drug (Nonnekes et al., 2018). This heroin-like drug resulted to become meperidine, which contained 1-methyl-4-phenyl-1,2,3,6-tetrahydropyridine



(MPTP) as a contaminant. The toxicity of MPTP in non-human primates (NHP) displayed clinical signs and nigrostriatal neuropathology similar to the human sporadic PD, henceforth providing an experimental tool for investigating parkinsonism (Burns et al., 1983; Langston et al., 1983).

MPTP as a model of xenobiotic-induced parkinsonism has been studied extensively for many years and constituted the gold standard for experimental PD research. It appeared as a selective neurotoxic xenobiotic inducing dopaminergic nigrostriatal neurodegeneration. As a lipophilic compound, MPTP crosses easily the blood–brain-barrier (BBB) to reach the CNS but it has no toxicity. There it is taken up by astrocytes where MPTP is swiftly oxidized in two steps by monoamine oxidase B (MAO-B) to the neuroactive metabolite 1-methyl-4-phenylpyridinium (MPP<sup>+</sup>). Pharmacological inhibition of MAO-B protects against MPTP toxicity, while MPP<sup>+</sup> systemic administration does not cross the BBB and is only neurotoxic by intracerebral injection. MPP<sup>+</sup> released from astrocytes is captured into dopaminergic neurons by the dopamine transporter (DAT) located in the neuronal membrane. This dopamine carrier has a greater expression in neurons of the SN than in other areas and shows a high affinity for MPP<sup>+</sup>. The final step of MPP<sup>+</sup> neurotoxicity consists of the inhibition of complex I activity in mitochondria, resulting in dopamine oxidation to form quinones and reactive oxygen

species (ROS) which cause cell death. Due to the high expression of DAT and its high affinity for MPP<sup>+</sup> neuronal death is nearly circumscribed to SN and ventral tegmental area, a neuropathology mimicking that of PD (Blesa and Przedborski, 2014).

Different animal species have been and are used to model PD by means of MPTP. Despite its limited use (cost, adequate facilities, technical skills, and ethical issues), NHPs are considered for their close physiology and brain structure with humans the best standard for studies of MPTP-induced parkinsonism (Emborg, 2017; Masilamoni and Smith, 2018; Khan et al., 2023). The NHP model provides the various species of MPTP-treated monkey's motor, behavioral, and neuropathological features observed in PD patients. However, there are divergences in certain pathophysiological pictures described. The different regimes of treatment may account for the diverse results observed. Thus, NHP treated with acute high doses of MPTP (e.g., 1–4 mg/kg/day, i.p., for 5 days) develop in a short time acute and long-term effects with signs of motor parkinsonism and a clear nigrostriatal loss of dopaminergic neurons and their synaptic terminals in striatum (Waters et al., 1987; Masilamoni and Smith, 2018). In front of this classical treatment, it has been observed that chronic treatment with low doses of MPTP (e.g., 0.2–0.5 mg/kg i.m. once a week) after approximately 21 weeks, and the NHP displayed motor signs non-motor manifestations of PD (Masilamoni et al., 2011). In this

chronic study, besides the important nigrostriatal dopaminergic loss, MPTP also caused the loss of non-nigrostriatal dopaminergic neurons and noradrenergic neurons in the locus coeruleus (Oertel et al., 2019), a characteristic pathological feature observed in PD patients. In other experiments, a NHP loss of serotonergic neurons in the dorsal raphe has also been observed (Duperrier et al., 2022).

When comparing the features of MPTP-induced parkinsonism with the neuropathology of patients, the most striking difference is the absence of Lewy bodies and Lewy neurites in the model animals, be NHP or mice.

The most widely used animal model for MPTP-induced parkinsonism is the pigmented C57BL/6 mice. This is the rodent model of choice because rats do not respond to MPTP toxicity and different strains of mice have variable and erratic effects to its exposure (Tello et al., 2022; Khan et al., 2023). The neurotoxic action of MPTP on C57BL/6 mice follows the same pattern as described above for NHP. Here again, the rodent model shows certain variability according to the dose level and the time span of treatment (Merghani et al., 2021; Khan et al., 2023). In this way, mice MPTP-treated with 30 mg/kg/day i.p. for 6 days (a dose much greater than those used with NHP) developed degeneration of the nigrostriatal pathway in both the SN and the striatum, as shown by loss of dopaminergic neurons immunostained for tyrosine hydroxylase (TH), depletion of striatal dopamine, activation of glial cells in the nigrostriatal pathway, and impairment in behavioral tests (Bhurtel et al., 2019). It has been proposed that oxidation of dopamine plays a role in the loss of dopaminergic neurons in SN. However, pharmacological depletion of dopamine does not protect against nigrostriatal degeneration in MPTP-treated C57BL/6 mice (Hasbani et al., 2005).

In humans, sex differences have been reported for PD, especially a higher incidence in men than in women (Miller and Cronin-Golomb, 2010). The MPTP model in NHP has been carried out in female (Waters et al., 1987; Masilamoni et al., 2011) and male (Burns et al., 1983; Masilamoni and Smith, 2018), but to the best of our knowledge, no sex differences were studied. Most research using C57BL/6 mice includes only male subjects; nevertheless, comparison of male and female mice treated with small, chronic doses of MPTP revealed selective motor impairment only in male subjects (Antzoulatos et al., 2010).

### 2.1.2 The rotenone model of PD

Rotenone is a toxic isoflavone present in certain plants of the genera *Derris* and *Lonchocarpus*. It has been used as a broad-spectrum ichthyotoxin, insecticide, and pesticide. The epidemiological observation that chronic exposure to systemic pesticides such as rotenone is associated with an increased risk of PD led to investigate whether rotenone produces in experimental animal manifestations of PD (Betarbet et al., 2000). The positive results of that research established the rotenone model, since then, one of the most employed in PD studies.

Rotenone as a lipophilic compound crosses the biological membranes, including the BBB and, in contrast with MPTP, acts directly in the cell inhibiting the electron transport chain of the mitochondrial complex I (NADH: ubiquinone oxidoreductase). This effect reduces ATP formation and can produce ROS and lead to cell death. In contrast with MPTP, there is no selective toxicity. Rotenone acts as a toxin on all cells of the organism, and the CNS manifestations are related to the greater vulnerability of certain systems. The chronic inhibition of

mitochondrial complex I by rotenone determines a highly selective nigrostriatal dopaminergic degeneration associated with motor signs (hypokinesia and rigidity). A specific mark of the rotenone-treated rats is that nigral neurons accumulate fibrillary cytoplasmic inclusions containing  $\alpha$ -synuclein and ubiquitin, morphologically similar to Lewy bodies (Johnson and Bobrovskaya, 2015).

The original rotenone model, briefly seen above, established an optimal dose for producing the PD pathology: 2–3 mg/kg/day administered by osmotic pump in Lewis rats for periods of 7 days to 5 weeks of continuous administration. Motor and behavioral tests, biochemistry, and neuropathology defined the model. Nonetheless, a great number of variants in animal species, dosage, via and span of administration, and methods of evaluation have appeared over time. Numerous articles testing drugs or biologicals use a quick behavioral or motor test in a short-term, high-dose pseudorotenone model. It is well known that high doses of rotenone, up to 100 mg/kg, for a short period produced systemic toxicity and unspecific lesions in the brain such as necrosis in the striatum. The ability of the different rotenone model variants to reproduce the clinical features of PD has been analyzed in various reports (Johnson and Bobrovskaya, 2015; Tello et al., 2022; Khan et al., 2023).

A question concerning the usefulness of the MPTP and rotenone models in inducing the clinical neurological signs and neuropathology of sporadic PD is still open. Two recent studies have addressed the issue by comparing experimentally both models. Bhurtel et al. (2019) treated groups of four C57BL/6 mice with MPTP 30 mg/kg/day i.p. or with rotenone 2.5 mg/kg/day i.p. for 6 days and compared the neurotoxicity of both compounds. A battery of behavioral tests, neurochemical analysis, and immunohistochemical staining were applied to both treated groups. It was determined that MPTP induces dopaminergic nigrostriatal lesions with neuronal loss and behavioral impairment as it has been seen above, but not rotenone (at least at the dosing level administered). The rotenone group only displayed neurodegeneration and glial activation in the hippocampus. The authors propose that MPTP is more specific than rotenone to produce dopaminergic neurodegeneration.

In contrast, in a comprehensive study, Zhang et al. (2022) dosed groups of 30 C57BL/6 mice with MPTP 20 mg/kg i.p. twice a week over 6 consecutive weeks, or with rotenone 30 mg/kg by gavage following the same schedule. To compare the effects of both neurotoxic agents, neurobehavior, neuropathology, neurochemistry, and mitochondrial function were assessed in treated and control groups by means of a large and complete battery of adequate techniques. Locomotor activity and coordination and exploratory behavior were significantly lower in both treated groups compared with controls. The MPTP-treated group showed the typical loss of dopaminergic neurons in SN pars compacta and the reduction of TH content in SN and striatum that were more significant than in the rotenone group. Remarkably, oxygen consumption in mitochondrial complex I in the SN was significantly reduced in the rotenone group compared with the MPTP group. As expected, Lewy bodies were only present in SN neurons in the rotenone group.

The striking difference in the rotenone effects observed in these studies may belong to the low dose of rotenone, via administration used, and duration of treatment. After pondering the different procedures described in the literature for the rotenone model, it appears as more reproducible and consistent those described by Betarbet et al. (2000) and Zhang et al. (2022).

The rotenone model has also provided an experimental approach to the hypothesis considering sporadic PD as a staging disease that can start in the ENS and progress through the nervous system until reaching the brain (Braak and Del Tredici, 2008; Braak and Del Tredici, 2017). In relation to that concept, the administration of rotenone intragastrically to C57BL/6J mice 5 mg/kg 5 days a week for 1.5–3 months induced  $\alpha$ -synuclein accumulation in all the nervous system structures considered for the progression of PD. Namely, it starts in the ENS and follows the dorsal motor nucleus of the vagus, the intermediolateral nucleus of the spinal cord and the SN.  $\alpha$ -synuclein phosphorylation in the ENS and other nervous structures was also observed. The alterations are sequential appearing only in synaptically connected structures. The rotenone model, then, may be apt for studying the  $\alpha$ -synucleinopathies (Pan-Montojo et al., 2010).

The rotenone model has been commonly studied in male rats and mice. Related to sex, one study reported that rotenone-treated male rats show a decrease in testosterone levels in blood plasma (Alam and Schmidt, 2004). This decrease is one of the comorbidity signs found in male PD patients (Okun et al., 2002) and is probably linked to the more severe motor deficits in male rodents (Antzoulatos et al., 2010). Furthermore, sex differences have been shown in female rats that display a decreased sensitivity to rotenone-induced neurodegeneration (De Miranda et al., 2019). These female subjects showed less inflammation and less accumulation of  $\alpha$ -synuclein than matched males. Sex differences in sensitivity may reflect the higher male ratio in human PD.

### 2.1.3 6-hydroxydopamine model of PD

6-Hydroxydopamine (6-OHDA) is a neurotoxic xenobiotic analogue to the catecholaminergic transmitters. Its systemic administration produces a long-lasting depletion of noradrenaline and dopamine in peripheral nerve terminals but not in the CNS as it does not traverse the BBB. Injecting intracerebrally 6-OHDA in experimental animals is the oldest method of modelling PD (Ungerstedt, 1968). Although with many refinements added over time, 6-OHDA continues to be used to investigate the pathophysiology of PD as well as the preclinical aspects of putative neuroprotective or therapeutic drugs (Simola et al., 2007; Hernandez-Baltazar et al., 2017). By means of stereotaxic surgery, 6-OHDA is injected into the medial forebrain bundle that destroys the dopamine neurons projecting from the midbrain to the striatum. To increase the selectivity of 6-OHDA for dopaminergic neurons, animals must be treated previously with a blocker of the noradrenaline transporter, usually with desipramine. Stereotaxic administration of 6-OHDA is also done in the striatum, causing a more progressive and less severe lesion. Most studies on the motor deficits of PD use the ipsilateral injection of 6-OHDA in the right medial forebrain bundle or in the right mid-striatum to obtain the model of contralateral rotational behavior. This model works satisfactorily in many species (monkeys, rats, and mice). An application of interest is the use of the mouse model of rotation for tissue transplantation in the damaged zone, an area of stem cell research (Bagga et al., 2015; Guimarães et al., 2021). The 6-OHDA model in its rotational version is also employed in transgenic mice to search for very specific aspects of dyskinesias (Castela et al., 2023).

The mechanisms of neurotoxicity and usefulness of the 6-OHDA model are to a great extent similar to those of MPTP although in several aspects 6-OHDA can provide more precise and detailed neuropathological information. Both models do not express

$\alpha$ -synuclein, but in a recent study (Cui et al., 2023), 6-OHDA injected in the rat medial forebrain bundle did not induce expression of  $\alpha$ -synuclein in the brain, but at 5 weeks, post-lesion were detected as having increased levels of phosphorylated  $\alpha$ -synuclein in ileum and colon. That finding may be related to the multistage theory seen above on the axis gut–brain for sporadic PD.

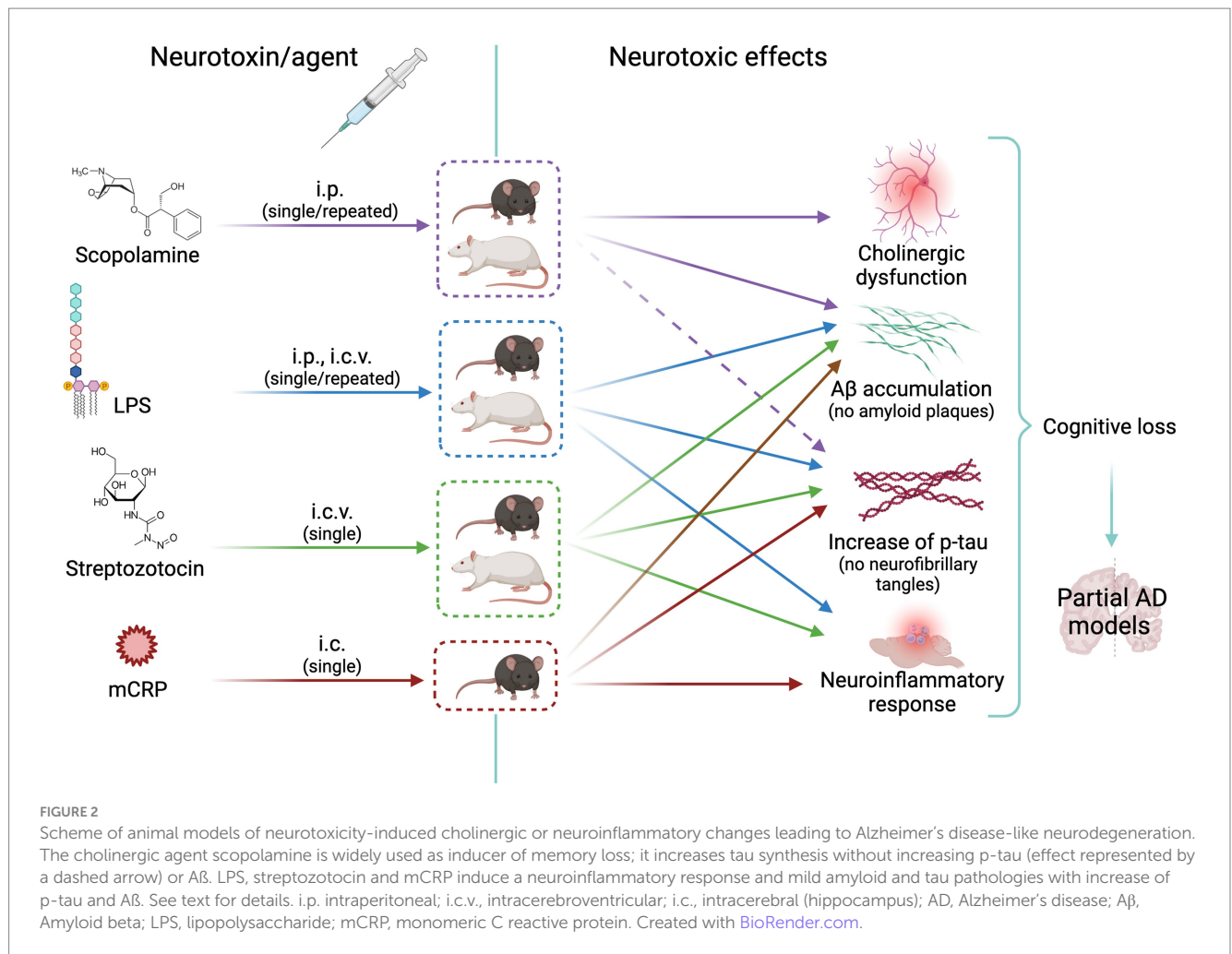
Male rats and mice are the customary animals used in the 6-OHDA model. A study of bilateral partial lesions with 6-OHDA in rats of both sexes observed a reduction of locomotor activity in aged male subjects but not in female subjects (Cass et al., 2005). Moreover, it has been shown that the effects of 6-OHDA striatal lesions on spatial cognition are sex-specific in rats and testosterone-dependent in male subjects (Betancourt et al., 2017).

## 2.2 Models based on cholinergic neurodegeneration

Cholinergic neurotransmission plays an important role in encoding new memories and other high brain functions. This fact together with the cholinergic atrophy paralleling cognitive decline in aging and AD led to the early cholinergic hypothesis of AD. It is known that neurofibrillary degeneration and death of forebrain cholinergic neurons cause presynaptic cholinergic denervation in AD (Hampel et al., 2018). Cholinergic neurotransmission enhancers acting through acetylcholinesterase (AChE) inhibition (donepezil, rivastigmine, and galantamine) have been used for decades to temporarily slow AD progression. AChE is increased around amyloid plaques and neurofibrillary tangles, the two main neuropathological hallmarks in the AD brain, suggesting a vicious cycle between AChE and amyloid and tau dysregulation (García-Ayllón et al., 2011). Preclinical and clinical research of new drugs moved soon to anti-amyloid and anti-tau therapies according to the amyloid and tau hypotheses of AD [see the history of AD hypotheses in Liu et al. (2019)]. It is estimated that less than 1% of cases are caused by autosomal dominant mutations and the majority is the sporadic form of AD. The prevalence of this devastating disease is approximately 10% in the population aged 65 years and older (Alzheimer's Association Report, 2022; Manly et al., 2022). However, only recent developments in anti-amyloid immunotherapy opened the path to disease-modifying drugs with current hope in the monoclonal antibody lecanemab (Van et al., 2023) and others in development. Rat and mouse models of cholinergic neurodegeneration are still widely used for screening pro-cognitive and anti-dementia drugs, including those addressed to AD. The first row of Figure 2 shows the scheme of the treatment route, the animal species used, and the neurotoxic effects elicited with scopolamine, as detailed below.

### 2.2.1 Scopolamine model of AD

Scopolamine is a tropane alkaloid found in several plants. It is a cholinergic neurotoxin due to its properties as a competitive antagonist of the muscarinic receptors. At the right dose, it is used as anti-emetic drug. Scopolamine is lipophilic and easily crosses the BBB causing a powerful effect in the CNS. Single or repeated i.p. administration of scopolamine in mice and rats induces cholinergic dysfunction and increase of AChE that further cleaves acetylcholine at the synapses leading to amnesia and cognitive loss. Doses administered range from 0.4 mg/kg to 3 mg/kg i.p., with longer-lasting memory impairment after repeated daily administration for one or



more weeks than a single injection (Rahimzadegan and Soodi, 2018; Chen and Yeong, 2020; Kose et al., 2023). This model is mainly used for behavioral studies, but some authors report that scopolamine induces an imbalance of the amyloid-beta precursor protein (APP) processing to the amyloidogenic pathway causing intraneuronal accumulation of amyloid-beta (Aβ) and also increased tau synthesis (Chen and Yeong, 2020; Kose et al., 2023). Noticeably, the scopolamine model in mice and, to a minor extent, in rats, was found the most widely used *in vivo* model for multitarget anti-AD drug discovery in a bibliometric analysis of the last 3 decades (Sampietro et al., 2022). Male and female rats experience a similar increase in AChE and memory loss in response to scopolamine (Ali and Arafa, 2011) although sex differences in fine cholinergic responses cannot be discarded.

### 2.3 Models based on neuroinflammation-induced neurodegeneration

Neuroinflammation, that is, the inflammatory response within the CNS, is a double-edged sword depending on its triggering cause, its duration until it resolves, and the stage of frailty of the organism (Disabato et al., 2016). The innate immune cells of the nervous system

will fight against infectious agents or local injuries, but if their response is deregulated, they can contribute to further injury and either initiate or worsen neurodegeneration. This is the case of the pathological reactive phenotype of microglia, the first-line innate immune brain cells in AD and other neurodegenerative diseases (Hammond et al., 2019). Systemic inflammation may also contribute to brain neurodegeneration (Chouhan et al., 2022). That interaction is highly relevant in old age when sustained low-grade inflammation in several organs and tissues is a key driver of age-related diseases including neurodegenerative diseases (McGeer and McGeer, 2004). Therefore, drug protection against neuroinflammation will halt brain inflammation and decrease the risk of late-onset neurodegeneration.

The relevance of neuroinflammatory mechanisms on the triggering and progression of AD promoted the use of various models of neuroinflammation in AD. The second, third, and fourth rows of Figure 2 show the scheme of the treatment route, the animal species used, and the neurotoxic effects in the three selected AD models described below.

Mixed proinflammatory and dopaminergic toxin models were developed for PD. Other neurodegenerative disease such as Huntington's disease or amyotrophic lateral sclerosis also show neuroinflammation, but this is not an early mechanism and specific animal models of neuroinflammation were not established (Vinther-Jensen et al., 2016; Chakraborty and Diwan, 2022).

### 2.3.1 Lipopolysaccharide model of AD

Lipopolysaccharide (LPS), the major component of the outer membrane of Gram-negative bacteria, is widely used to induce neuroinflammation in rats and mice. There are a variety of protocols using different LPS serotypes and doses ranging from 0.3 mg/kg to 10 mg/kg i.p. and 0.25 µg to 50 µg i.c.v., with single or repeated administration over one or more days (Nava Catorce and Gevorkian, 2016; Zakaria et al., 2017). The systemic treatment through i.p. injection in mice is very convenient for testing protective anti-inflammatory agents (Nava Catorce and Gevorkian, 2016). The sickness behavior response of mice to LPS peripheral infection parallels the release of proinflammatory cytokines in the brain and blood (Molina-Martínez et al., 2021). The mechanisms of microglia activation by LPS have been fully characterized either after peripheral (i.p.) or central (i.c.v.) administration in mice and rats. LPS elicits a robust neuroinflammatory response followed by cognitive loss and neurodegeneration although the response and the brain areas affected may differ according to the administration regimen and the age of the animal (Nazem et al., 2015; Zakaria et al., 2017; Decandia et al., 2023). Furthermore, some clinical evidence supports an involvement of LPS from Gram-negative bacteria resident in the gastrointestinal tract as a potential contributor to the onset of AD (Zhao et al., 2017). Rodents dosed peripherally with LPS make a reliable model of AD neuroinflammation. In addition, LPS may promote increased brain Aβ levels and tau pathology although the wide diversity in the treatment design and the LPS serotypes used do not yield clear conclusions (Batista et al., 2019). Male and female rodents are used with good results (Nava Catorce and Gevorkian, 2016). However, there are sex differences in the pattern of immune responses to LPS treatment that should be taken into account when evaluating proinflammatory biomarkers (Sharma et al., 2018).

### 2.3.2 Streptozotocin model of AD

Streptozotocin (STZ) is a naturally occurring glucosamine-nitrosourea compound identified in a *Streptomyces* bacteria strain. The first use of this toxin is to model diabetes in rodents as peripheral injection of STZ damages pancreatic β-cells. Impaired insulin sensitivity is indeed a risk factor for AD development. In the brain, both i.p. and i.c.v. injections of STZ cause neuroinflammation and cognitive deficits in mice and rats (Nazem et al., 2015). Interestingly, bilateral i.c.v. injections of STZ in mice elicit chronic neuroinflammation and increased levels of Aβ and hyperphosphorylated tau (p-tau) in the hippocampus (Fan et al., 2022). Therefore, centrally administered STZ, at doses 1 or 3 mg/Kg i.c.v., is considered a better model of sporadic AD than peripherally administered STZ (Nazem et al., 2015; Fan et al., 2022). A sex-difference study reported that female rats respond less than male subjects to i.c.v. STZ (Bao et al., 2017), and thus, female subjects might not be suitable as the STZ model of AD.

### 2.3.3 mCRP model of AD

Monomeric C-reactive protein (mCRP) is a proinflammatory molecule yielded by activation and disaggregation of the pentameric CRP. Clinically, it has been associated with the triggering and progression of AD through its deposition in stroke-damaged areas (Slevin et al., 2015, 2020). A recently developed mouse model of dementia by intrahippocampal injection of mCRP may be a new tool to study AD and neuroprotective agents (García-Lara et al., 2021).

C57BL/6J mice injected bilaterally with a dose of 3.5 µg of mCRP show a long-lasting loss of learning and memory. Remarkably, cognitive loss was protected by the oral administration of an anti-inflammatory drug (García-Lara et al., 2021). The mCRP dementia model shows a marked increase in p-tau levels in the hippocampus area (Slevin et al., 2015; García-Lara et al., 2021), whereas a slight increase in Aβ was detected by immunostaining (Slevin et al., 2015). Sex differences have not yet been analyzed in this new model.

### 2.3.4 Other AD models of neuroinflammation

The rodent models generated with the marine toxin okadaic acid and the neurotoxic metal aluminum are less characterized regarding neuroinflammation. Okadaic acid inhibits selective protein phosphatases. It would induce neuroinflammation and associated memory impairment after i.c.v. injection, but it is mainly used as a model of tau hyperphosphorylation in rats and mice (Nazem et al., 2015). No clear sex differences in susceptibility to okadaic acid have been reported.

Furthermore, administration of aluminum chloride in rats induces brain damage and cognitive impairment, but the underlying mechanisms are not clarified and may involve activation of tau phosphorylation enzymes (Sanajou et al., 2023). Despite suggestions of gender bias in the effect of aluminum in humans, no sex differences have been reported in rodent models.

Finally, neuroinflammation induced by a high-fat diet (HFD) in rodents is also a model of AD neurodegeneration, where neuroinflammation and oxidative stress trigger tau and amyloid pathology and cause cognitive impairment (Sharma, 2021). Several studies have analyzed the effects of antiinflammatory treatments against HFD (Zameer et al., 2020; Sarroca et al., 2021). HFD induces higher neuroinflammation and metabolic impairment in male subjects than female subjects, and this dimorphism likely causes a sex bias as a model of AD (see Sharma, 2021).

### 2.3.5 Neuroinflammation models of PD

Neuroinflammation plays a role in PD although it may be less decisive for the neurodegeneration triggering and development than in AD. Studies in animal models suggest that neuroinflammation exacerbates the outcome of neurotoxicity induced by specific dopaminergic toxins (Ramsey and Tansey, 2014). Animal models based on the combination of central and peripheral inflammatory challenges show microglial activation and death of dopaminergic neurons after treatment with proinflammatory agents, such as LPS, paired with neurotoxic agents as paraquat and rotenone (García-Revilla et al., 2022).

## 3 Discussion

Most of the experimental rodent models of neurotoxicity-induced neurodegeneration reviewed here have been widely used for pharmacological screening or for studying specific mechanisms of neurodegeneration. They were developed following human findings such as the neurotoxicity of MPTP or rotenone, the amnesia induced by scopolamine, and mental dysfunction associated with sickness behavior by LPS from bacterial infection. Despite its expected translational profile, no model to date reproduces all the features of the corresponding human neurodegenerative disease. We must keep

in mind that the crucial factors in the etiology and physiopathology of diseases such as PD and AD are still unclear. On the other hand, rodent models bearing mutations of familial cases of neurodegenerative disease have gained a lot of prominence in recent years, but they cannot reproduce the whole pathology either. In addition, the bulk of neurodegenerative human cases are age-related, with lengthy processes and not driven by the inheritance of autosomal dominant mutations.

Over the years, considerable progress has been made in understanding PD mechanisms, developing experimental models and testing potential therapeutics. We consider here the latest developments, challenges, and gaps in neurodegeneration models of PD. Animal models have been the primary tool for studying PD due to their genetic and neuroanatomical similarity to humans. Rodent models, such as MPTP and 6-OHDA models, have provided valuable insights into disease pathogenesis. However, their limitations include inadequate modelling of non-motor signs and the lack of  $\alpha$ -synuclein aggregation, a hallmark of PD, and the limitation of the MPTP model to a specific mouse strain, as described above. The most recent and advantageous model to date for drug development in sporadic PD is the rotenone model, which can be established in most rodent species and produces  $\alpha$ -synuclein aggregates, in the form of Lewy body-like aggregates, in addition to motor and non-motor signs. Nonetheless, the dosage range is critical and near to general toxicity in contrast with the former models that act directly on the CNS. NHP models, particularly macaques, are still instrumental in investigating PD motor symptoms and  $\alpha$ -synuclein pathology. Nevertheless, ethical concerns, high costs, and limited availability hinder the widespread utilization of this model.

There exist numerous challenges in the development of improved PD animal models. Among them is the variability in clinical phenotypes: PD exhibits substantial heterogeneity in its clinical presentation, disease progression, sex differences, and response to treatments. Reproducing this diversity in animal models remains a significant challenge. Another challenge is the lack of comprehensive non-motor phenotyping, as non-motor signs, including cognitive impairment and psychiatric disturbances, significantly impact patients' quality of life. However, these aspects are often overlooked in animal models, limiting our understanding of PD full spectrum. Future developed models should mimic  $\alpha$ -synuclein pathology, a major shortcoming in MPTP and 6-OHDA rodent models. Furthermore, there are several lacunae in the current research with PD models. An important omission is the limited longitudinal studies. These studies are essential for understanding disease progression and evaluating potential therapies. Similarly, long-term animal models could offer insights into the chronic nature of PD and its interaction with age-related changes and genetic background. PD is a multifactorial disorder with both genetic and environmental contributions. Current models often focus on either genetic or toxin-induced approaches, neglecting the intricate interplay between genetics and environmental factors.

Animal models of AD based on the wild-type mouse and rat cannot show the overt amyloid pathology of AD transgenic mice (TgAD) because rodent A $\beta$  is not prone to form fibrillary deposits as that of human or non-human primates and other animals (Ueno et al., 2014). Fibrillary tangles are not generated either. AD models of cholinergic dysfunction and neuroinflammation do not recapitulate the proteinopathy linked to the human disorder although they may induce some imbalances in the synthesis or processing of APP and

tau, as described above. The absence of these pathological hallmarks of AD is a major limitation of these models because they do not mimic other underlying mechanisms in AD caused by either A $\beta$  aggregation or other factors (Iliyasu et al., 2023; Ratan et al., 2023). However, they model neurodegenerative mechanisms of broad implication in AD and other neurodegenerative diseases. For instance, scopolamine is also used to model cholinergic dysfunction in PD and Lewy body dementia (Zhang et al., 2019) although its main application is in AD. The scopolamine model is useful as a first step for testing compounds against learning and memory loss in AD. Although there is more interest in the development of disease-modifying anti-amyloid or anti-tau drugs, as noted above, cholinesterase inhibitors are still considered valid drugs in the current scenario of AD treatments (Molchan and Fugh-Berman, 2023). The feasibility of peripherally injected scopolamine in mice to produce cognitive loss that can be rescued with cholinergic drugs makes it an advantageous model in many laboratories. However, it is recommended that TgAD mice be used as a next step to more fully characterize the anti-AD mechanisms of selected drugs (Sampietro et al., 2022). Similarly, peripheral injection of the proinflammatory endotoxin LPS in mice is a convenient and useful model for drug development and research in AD and other dementia cursing with neuroinflammation (Nava Catorce and Gevorkian, 2016). However, selected AD anti-inflammatory drugs would also require further testing in a more reliable background such as TgAD mice. STZ has an additional limitation in the requirement of its i.c.v. administration for modeling an AD mouse (Chen et al., 2013). mCRP also requires intracerebral injection, but this model is suitable for a second round of anti-inflammatory drug testing or specific studies of AD dementia associated with cerebrovascular damage. Okadaic acid is also limited by its i.c.v. administration. Aluminum chloride is poorly characterized as the AD model. HFD neuroinflammation is induced by metabolic disorders associated with AD risk, with the consequent limitation for comprehensive testing of protective drugs.

The first challenge is to develop assays of LPS, STZ, and other neurotoxic agents in mice with a humanized APP gene that would yield A $\beta$  prone to form amyloid plaques. These engineered mice have been an important breakthrough in the recent development of the second and third generation of TgAD mice, namely, mice with humanized APP gene bearing either familial AD mutations in this gene or in both APP and PS1 genes, respectively (Sasaguri et al., 2022). There is also a need for standardized protocols of treatment and phenotype characterization, including translational non-invasive biomarkers. The main gaps in the reviewed AD models here are the consideration of the response to the neurotoxic agent with the age and sex of the animals and the agent interaction with alleles of genetic risk. Another gap is the concomitant study of systemic comorbidities.

In addition to their possible utility for pharmacological testing as discussed above for each model, wild-type animal models of neurotoxicity-induced neurodegeneration may contribute to uncovering the role of environmental neurotoxic agents as etiological factors in neurodegenerative diseases.

While there was no enough improvement in finding suitable drugs and therapies against neurodegenerative disease, we should take advantage of all available tools (Drummond and Wisniewski, 2017; Khan et al., 2023). Non-transgenic and transgenic rodents and other animals can be used for specific purposes. Animal experimentation cannot be avoided in drug development in the near future. Where

convenient, there is also a range of CNS cell culture models for *in vitro* assays. Furthermore, new advances such as cultures from human-induced pluripotent stem cells obtained from patients, brain organoids, or computational brain modelling will hopefully contribute to therapies that lead to maintaining brain health into old age.

## Author contributions

ER-F contributed to conception and design of the review. CSa, CSu, and ER-F wrote sections of the first draft of the manuscript. CB searched for and organized the references and drew the figures. All authors contributed to manuscript revision, read, and approved the submitted version.

## Funding

This research was funded by the Spanish Ministerio de Ciencia e Innovación and the Agencia Estatal de Investigación (MCIN/

AEI/10.13039/501100011033, grants PID2019-106285RB and PDC2021-121096) and by the European Union “NextGenerationEU”/PRTR; CERCA program/Generalitat de Catalunya; and 2021-SGR-00357 from AGAUR.

## Conflict of interest

The authors declare that the research was conducted in the absence of any commercial or financial relationships that could be construed as a potential conflict of interest.

## Publisher's note

All claims expressed in this article are solely those of the authors and do not necessarily represent those of their affiliated organizations, or those of the publisher, the editors and the reviewers. Any product that may be evaluated in this article, or claim that may be made by its manufacturer, is not guaranteed or endorsed by the publisher.

## References

- Alam, M., and Schmidt, W. J. (2004). Mitochondrial complex I inhibition depletes plasma testosterone in the rotenone model of Parkinson's disease. *Physiol. Behav.* 83, 395–400. doi: 10.1016/j.physbeh.2004.08.010
- Ali, E. H. A., and Arafat, N. M. S. (2011). Comparative protective action of curcumin, memantine and diclofenac against scopolamine-induced memory dysfunction. *Fitoerapia* 82, 601–608. doi: 10.1016/J.FITOTE.2011.01.016
- Alzheimer's Association Report (2022). 2022 Alzheimer's disease facts and figures. *Alzheimer's and Dementia* 18, 700–789. doi: 10.1002/alz.12638
- Antzoulatos, E., Jakowec, M. W., Petzinger, G. M., and Wood, R. I. (2010). Sex differences in motor behavior in the MPTP mouse model of Parkinson's disease. *Pharmacol. Biochem. Behav.* 95, 466–472. doi: 10.1016/J.PBB.2010.03.009
- Azam, S., Haque, M. E., Balakrishnan, R., Kim, I. S., and Choi, D. K. (2021). The ageing brain: molecular and cellular basis of neurodegeneration. *Front. Cell Dev. Biol.* 9:684359. doi: 10.3389/FCELL.2021.684359
- Bagga, V., Dunnett, S. B., and Fricker, R. A. (2015). The 6-OHDA mouse model of Parkinson's disease - terminal striatal lesions provide a superior measure of neuronal loss and replacement than median forebrain bundle lesions. *Behav. Brain Res.* 288, 107–117. doi: 10.1016/j.bbr.2015.03.058
- Bao, J., YAR, M., Liu, R., Wang, J. Z., Zhang, Z., Zhang, B., et al. (2017). Sex differences in the cognitive and hippocampal effects of streptozotocin in an animal model of sporadic AD. *Front. Aging Neurosci.* 9:347. doi: 10.3389/FNAGI.2017.00347/FULL
- Batista, C. R. A., Gomes, G. F., Candelario-Jalil, E., Fiebich, B. L., and de Oliveira, A. C. P. (2019). Lipopolysaccharide-induced neuroinflammation as a bridge to understand neurodegeneration. *Int. J. Mol. Sci.* 20:2293. doi: 10.3390/IJMS20092293
- Betancourt, E., Wachtel, J., Michaelos, M., Haggerty, M., Conforti, J., and Kritzer, M. F. (2017). The impact of biological sex and sex hormones on cognition in a rat model of early, pre-motor Parkinson's disease. *Neuroscience* 345, 297–314. doi: 10.1016/j.neuroscience.2016.05.041
- Betarbet, R., Sherer, T. B., MacKenzie, G., Garcia-Osuna, M., Panov, A. V., and Greenamyre, J. T. (2000). Chronic systemic pesticide exposure reproduces features of Parkinson's disease. *Nat. Neurosci.* 3, 1301–1306. doi: 10.1038/81834
- Bhurlert, S., Katila, N., Srivastav, S., Neupane, S., and Choi, D. Y. (2019). Mechanistic comparison between MPTP and rotenone neurotoxicity in mice. *Neurotoxicology* 71, 113–121. doi: 10.1016/j.neuro.2018.12.009
- Bianco, A., Antonacci, Y., and Liguori, M. (2023). Sex and gender differences in neurodegenerative diseases: challenges for therapeutic opportunities. *Int. J. Mol. Sci.* 24:6354. doi: 10.3390/IJMS24076354
- Blesa, J., and Przedborski, S. (2014). Parkinson's disease: animal models and dopaminergic cell vulnerability. *Front. Neuroanat.* 8:155. doi: 10.3389/fnana.2014.00155
- Braak, H., and Del Tredici, K. (2008). Invited article: nervous system pathology in sporadic Parkinson disease. *Neurology* 70, 1916–1925. doi: 10.1212/01.wnl.0000312279.49272.9f
- Braak, H., and Del Tredici, K. (2017). Neuropathological staging of brain pathology in sporadic Parkinson's disease: separating the wheat from the chaff. *J. Parkinsons Dis.* 7, S71–S85. doi: 10.3233/JPD-179001
- Bryda, E. C. (2013). The mighty mouse: the impact of rodents on advances in biomedical research. *Mo. Med.* 110, 207–211.
- Buonocervello, M., Marconi, M., Carè, A., Piscopo, P., Malorni, W., and Matarrese, P. (2017). Preclinical models in the study of sex differences. *Clin. Sci.* 131, 449–469. doi: 10.1042/CS20160847
- Burns, R. S., Chiueh, C. C., Markey, S. P., Ebert, M. H., Jacobowitz, D. M., and Kopin, I. J. (1983). A primate model of parkinsonism: selective destruction of dopaminergic neurons in the pars compacta of the substantia nigra by N-methyl-4-phenyl-1,2,3,6-tetrahydropyridine. *Neurobiology* 80, 4546–4550. doi: 10.1073/pnas.80.14.4546
- Cass, W. A., Peters, L. E., and Smith, M. P. (2005). Reductions in spontaneous locomotor activity in aged male, but not female, rats in a model of early Parkinson's disease. *Brain Res.* 1034, 153–161. doi: 10.1016/j.brainres.2004.12.009
- Castela, I., Casado-Polanco, R., YVW, R., da Silva, J. A., Marquez, R., Pro, B., et al. (2023). Selective activation of striatal indirect pathway suppresses levodopa induced-dyskinesias. *Neurobiol. Dis.* 176:105930. doi: 10.1016/j.nbd.2022.105930
- Chakraborty, A., and Diwan, A. (2022). Biomarkers and molecular mechanisms of amyotrophic lateral sclerosis. *AIMS Neurosci.* 9, 423–443. doi: 10.3934/NEUROSCIENCE.2022023
- Chen, Y., Liang, Z., Blanchard, J., Dai, C. L., Sun, S., Lee, M. H., et al. (2013). A non-transgenic mouse model (icv-STZ mouse) of Alzheimer's disease: similarities to and differences from the transgenic model (3xTg-AD mouse). *Mol. Neurobiol.* 47, 711–725. doi: 10.1007/S12035-012-8375-5
- Chen, W. N., and Yeong, K. Y. (2020). Scopolamine, a toxin-induced experimental model, used for research in Alzheimer's disease. *CNS Neurol. Disord. Drug Targets* 19, 85–93. doi: 10.2174/1871527319666200214104331
- Chouhan, J. K., Püntener, U., Booth, S. G., and Teeling, J. L. (2022). Systemic inflammation accelerates changes in microglial and synaptic markers in an experimental model of chronic neurodegeneration. *Front. Neurosci.* 15:760721. doi: 10.3389/FNINS.2021.760721
- Cui, H., Elford, J. D., Alitalo, O., Perez-Pardo, P., Tampio, J., Huttunen, K. M., et al. (2023). Nigrostriatal 6-hydroxydopamine lesions increase alpha-synuclein levels and permeability in rat colon. *Neurobiol. Aging* 129, 62–71. doi: 10.1016/j.neurobiolaging.2023.05.007
- De Miranda, B. R., Fazzari, M., Rocha, E. M., Castro, S., and Greenamyre, J. T. (2019). Sex differences in rotenone sensitivity reflect the male-to-female ratio in human Parkinson's disease incidence. *Toxicol. Sci.* 170, 133–143. doi: 10.1093/toxsci/kfz082
- Decandia, D., Gelfo, F., Landolfo, E., Balsamo, F., Petrosini, L., and Cutuli, D. (2023). Dietary protection against cognitive impairment, Neuroinflammation and oxidative stress in Alzheimer's disease animal models of lipopolysaccharide-induced inflammation. *Int. J. Mol. Sci.* 24:5921. doi: 10.3390/IJMS24065921
- Disabato, D., Quan, N., and Godbout, J. P. (2016). Neuroinflammation: the devil is in the details. *J. Neurochem.* 139, 136–153. doi: 10.1111/jnc.13607
- Drummond, E., and Wisniewski, T. (2017). Alzheimer's disease: experimental models and reality. *Acta Neuropathol.* 133, 155–175. doi: 10.1007/S00401-016-1662-X

- Duperrier, S., Bortolozzi, A., and Sgambato, V. (2022). Increased expression of alpha-, Beta-, and gamma-Synucleins in brainstem regions of a non-human primate model of Parkinson's disease. *Int. J. Mol. Sci.* 23:8586. doi: 10.3390/ijms23158586
- Emborg, M. E. (2017). Nonhuman primate models of neurodegenerative disorders. *ILAR J.* 58, 190–201. doi: 10.1093/ilar/ilx021
- Fan, M., Liu, S., Sun, H. M., Ma, M. D., Gao, Y. J., Qi, C. C., et al. (2022). Bilateral intracerebroventricular injection of streptozotocin induces AD-like behavioral impairments and neuropathological features in mice: involved with the fundamental role of neuroinflammation. *Biomed. Pharmacother.* 153:113375. doi: 10.1016/j.biopha.2022.113375
- García-Ayllón, M. S., Small, D. H., Avila, J., and Sáez-Valero, J. (2011). Revisiting the role of acetylcholinesterase in Alzheimer's disease: cross-talk with P-tau and  $\beta$ -amyloid. *Front. Mol. Neurosci.* 4:22. doi: 10.3389/fnmol.2011.00022
- García-Lara, E., Aguirre, S., Clotet, N., Sawkyluc, X., Bartra, C., Almenara-Fuentes, L., et al. (2021). Antibody protection against long-term memory loss induced by monomeric c-reactive protein in a mouse model of dementia. *Biomedicine* 9:828. doi: 10.3390/biomedicines907828/S1
- García-Revilla, J., Herrera, A. J., De Pablos, R. M., and Venero, J. L. (2022). Inflammatory animal models of Parkinson's disease. *J. Parkinsons Dis.* 12, S165–S182. doi: 10.3233/JPD-213138
- Goldman, S. M. (2014). Environmental toxins and Parkinson's disease. *Annu. Rev. Pharmacol. Toxicol.* 54, 141–164. doi: 10.1146/annurev-pharmtox-011613-135937
- Guimarães, R. P., Ribeiro, D. L., Dos Santos, K. B., Godoy, L. D., Corrêa, M. R., and Padovan-Neto, F. E. (2021). The 6-hydroxydopamine rat model of Parkinson's disease. *J. Vis. Exp.*:176. doi: 10.3791/62923
- Hammond, T. R., Marsh, S. E., and Stevens, B. (2019). Immune Signaling in Neurodegeneration. *Immunity* 50, 955–974. doi: 10.1016/j.immuni.2019.03.016
- Hampel, H., Mesulam, M. M., Cuello, A. C., Farlow, M. R., Giacobini, E., Grossberg, G. T., et al. (2018). The cholinergic system in the pathophysiology and treatment of Alzheimer's disease. *Brain* 141, 1917–1933. doi: 10.1093/brain/aww132
- Hasbani, D. M., Perez, F. A., Palmiter, R. D., and O'Malley, K. L. (2005). Dopamine depletion does not protect against acute 1-methyl-4-phenyl-1,2,3,6-tetrahydropyridine toxicity in vivo. *J. Neurosci.* 25, 9428–9433. doi: 10.1523/JNEUROSCI.0130-05.2005
- Hernandez-Baltazar, D., Zavala-Flores, L. M., and Villanueva-Olivo, A. (2017). The 6-hydroxydopamine model and parkinsonian pathophysiology: novel findings in an older model. *Neurologia* 32, 533–539. doi: 10.1016/j.nrl.2015.06.011
- Ilyasu, M. O., Musa, S. A., Oladele, S. B., and Iliya, A. I. (2023). Amyloid-beta aggregation implicates multiple pathways in Alzheimer's disease: understanding the mechanisms. *Front. Neurosci.* 17:1081938. doi: 10.3389/fnins.2023.1081938
- Johnson, M. E., and Bobrovskaya, L. (2015). An update on the rotenone models of Parkinson's disease: their ability to reproduce the features of clinical disease and model gene-environment interactions. *Neurotoxicology* 46, 101–116. doi: 10.1016/j.neuro.2014.12.002
- Khan, E., Hasan, I., and Haque, M. E. (2023). Parkinson's disease: exploring different animal model systems. *Int. J. Mol. Sci.* 24:9088. doi: 10.3390/ijms24109088
- Kose, S., Kutlu, M. D., Kara, S., Polat, S., and Akkiloglu, K. (2023). Investigation of the protective effect of long-term exercise on molecular pathways and behaviours in scopolamine induced alzheimer's disease-like condition. *Brain Res.* 1814:148429. doi: 10.1016/j.brainres.2023.148429
- Kuopio, A. M., Marttila, R. J., Helenius, H., and Rinne, U. K. (1999). Environmental risk factors in Parkinson's disease. *Mov. Disord.* 14, 928–939. doi: 10.1002/1531-8257(199911)14:6<928::AID-MDS1004>3.0.CO;2-Z
- Langston, J. W., Ballard, P., Tetrad, J. W., and Irwin, I. (1983). Chronic parkinsonism in humans due to a product of meperidine-analog synthesis. *Science* 219, 979–980. doi: 10.1126/science.6823561
- Li, Q., Meng, L. B., Chen, L. J., Shi, X., Tu, L., Zhou, Q., et al. (2023). The role of the microbiota-gut-brain axis and intestinal microbiome dysregulation in Parkinson's disease. *Front. Neurol.* 14:1185375. doi: 10.3389/fneur.2023.1185375
- Liu, P. P., Xie, Y., Meng, X. Y., and Kang, J. S. (2019). History and progress of hypotheses and clinical trials for Alzheimer's disease. *Signal Transduct. Target. Ther.* 4:37. doi: 10.1038/S41392-019-0071-8
- Manly, J. J., Jones, R. N., Langa, K. M., Ryan, L. H., Levine, D. A., McCammon, R., et al. (2022). Estimating the prevalence of dementia and mild cognitive impairment in the US: the 2016 health and retirement study harmonized cognitive assessment protocol project. *JAMA Neurol.* 79, 1242–1249. doi: 10.1001/jamaneurol.2022.3543
- Masilamoni, G. J., Bogenpohl, J. W., Alagille, D., Delevich, K., Tamagnan, G., Votaw, J. R., et al. (2011). Metabotropic glutamate receptor 5 antagonist protects dopaminergic and noradrenergic neurons from degeneration in MPTP-treated monkeys. *Brain* 134, 2057–2073. doi: 10.1093/brain/awr137
- Masilamoni, G. J., and Smith, Y. (2018). Chronic MPTP administration regimen in monkeys: a model of dopaminergic and non-dopaminergic cell loss in Parkinson's disease. *J. Neural Transm.* 125, 337–363. doi: 10.1007/s00702-017-1774-z
- McCann, H., Stevens, C. H., Cartwright, H., and Halliday, G. M. (2014).  $\alpha$ -Synucleinopathy phenotypes. *Parkinsonism Relat. Disord.* 20, S62–S67. doi: 10.1016/S1353-8020(13)70017-8
- McGeer, P. L., and McGeer, E. G. (2004). Inflammation and the degenerative diseases of aging. *Ann. N. Y. Acad. Sci.* 1035, 104–116. doi: 10.1196/ANNALS.1332.007
- Merghani, M. M., Ardah, M. T., Al Shamsi, M., Kitada, T., and Haque, M. E. (2021). Dose-related biphasic effect of the Parkinson's disease neurotoxin MPTP, on the spread, accumulation, and toxicity of  $\alpha$ -synuclein. *Neurotoxicology* 84, 41–52. doi: 10.1016/j.neuro.2021.02.001
- Miller, I. N., and Cronin-Golomb, A. (2010). Gender differences in parkinson's disease: clinical characteristics and cognition. *Mov. Disord.* 25, 2695–2703. doi: 10.1002/MDS.23388
- Molchan, S., and Fugh-Berman, A. (2023). Are New Alzheimer Drugs Better Than Older Drugs? *JAMA Intern. Med.* 183:902. doi: 10.1001/JAMAINTERNMED.2023.3061
- Molina-Martínez, P., Corpas, R., García-Lara, E., Cosín-Tomás, M., Cristófol, R., Kaliman, P., et al. (2021). Microglial Hyperreactivity evolved to immunosuppression in the Hippocampus of a mouse model of accelerated aging and Alzheimer's disease traits. *Front. Aging Neurosci.* 12:622360. doi: 10.3389/fnagi.2020.622360
- Natale, G., Kastsiushenka, O., Fulceri, F., Ruggieri, S., Paparelli, A., and Fornai, F. (2010). MPTP-induced parkinsonism extends to a subclass of TH-positive neurons in the gut. *Brain Res.* 1355, 195–206. doi: 10.1016/j.brainres.2010.07.076
- Nava Catorce, M., and Gevorkian, G. (2016). LPS-induced murine neuroinflammation model: Main features and suitability for pre-clinical assessment of nutraceuticals. *Curr. Neuropharmacol.* 14, 155–164. doi: 10.2174/1570159X14666151204122017
- Nazem, A., Sankowski, R., Bacher, M., and Al-Abed, Y. (2015). Rodent models of neuroinflammation for Alzheimer's disease. *J. Neuroinflammation* 12:74. doi: 10.1186/S12974-015-0291-Y
- Nonnekes, J., Post, B., Tetrad, J. W., Langston, J. W., and Bloem, B. R. (2018). MPTP-induced parkinsonism: an historical case series. *Lancet Neurol.* 17, 300–301. doi: 10.1016/S1474-4422(18)30072-3
- Oertel, W. H., Henrich, M. T., Janzen, A., and Geibl, F. F. (2019). The locus coeruleus: another vulnerability target in Parkinson's disease. *Mov. Disord.* 34, 1423–1429. doi: 10.1002/mds.27785
- Okun, M. S., WM, M. D., and Delong, M. R. (2002). Refractory nonmotor symptoms in male patients with Parkinson disease due to testosterone deficiency: a common unrecognized comorbidity. *Arch. Neurol.* 59, 807–811. doi: 10.1001/ARCHNEUR.59.5.807
- Ou, Z., Pan, J., Tang, S., Duan, D., Yu, D., Nong, H., et al. (2021). Global trends in the incidence, prevalence, and years lived with disability of Parkinson's disease in 204 countries/territories from 1990 to 2019. *Front. Public Health* 9:776847. doi: 10.3389/fpubh.2021.776847
- Pan-Montojo, F., Anichtchik, O., Dening, Y., Knels, L., Pursche, S., Jung, R., et al. (2010). Progression of Parkinson's disease pathology is reproduced by intragastric administration of rotenone in mice. *PLoS One* 5:e8762. doi: 10.1371/journal.pone.0008762
- Pedro-Cuesta Jd, , Rodríguez-Farré, E., and Lopez-Abente, G. (2009). Spatial distribution of Parkinson's disease mortality in Spain, 1989–1998, as a guide for focused aetiological research or health-care intervention. *BMC Public Health* 9:445. doi: 10.1186/1471-2458-9-445
- Rahimzadegan, M., and Soodi, M. (2018). Comparison of memory impairment and oxidative stress following single or repeated doses administration of scopolamine in rat hippocampus. *Basic Clin Neurosci* 9, 5–14. doi: 10.29252/nirp.bcn.9.1.5
- Ramsey, C. P., and Tansey, M. G. (2014). A survey from 2012 of evidence for the role of neuroinflammation in neurotoxin animal models of Parkinson's disease and potential molecular targets. *Exp. Neurol.* 256, 126–132. doi: 10.1016/j.expneurol.2013.05.014
- Ratan, Y., Rajput, A., Maleysm, S., Pareek, A., Jain, V., Pareek, A., et al. (2023). An insight into cellular and molecular mechanisms underlying the pathogenesis of neurodegeneration in Alzheimer's disease. *Biomedicine* 11:1398. doi: 10.3390/biomedicines11051398
- Ray Dorsey, E., Elbaz, A., Nichols, E., Abd-Allah, F., Abdelalim, A., Adsuar, J. C., et al. (2018). Global, regional, and national burden of Parkinson's disease, 1990–2016: a systematic analysis for the global burden of disease study 2016. *Lancet Neurol.* 17, 939–953. doi: 10.1016/S1474-4422(18)30295-3
- Sampietro, A., Pérez-Areales, F. J., Martínez, P., Arce, E. M., Galdeano, C., and Muñoz-Torrero, D. (2022). Unveiling the multitarget anti-Alzheimer drug discovery landscape: a bibliometric analysis. *Pharmaceuticals (Basel)* 15:545. doi: 10.3390/PH15050545
- Sanajou, S., Erkekoğlu, P., Şahin, G., and Baydar, T. (2023). Role of aluminum exposure on Alzheimer's disease and related glycogen synthase kinase pathway. *Drug Chem. Toxicol.* 46, 510–522. doi: 10.1080/01480545.2022.2065291
- Sarroca, S., Gatiús, A., Rodríguez-Farré, E., Vilchez, D., Pallàs, M., Griñán-Ferré, C., et al. (2021). Resveratrol confers neuroprotection against high-fat diet in a mouse model of Alzheimer's disease via modulation of proteolytic mechanisms. *J. Nutr. Biochem.* 89:108569. doi: 10.1016/j.jnubio.2020.108569
- Sasaguri, H., Hashimoto, S., Watamura, N., Sato, K., Takamura, R., Nagata, K., et al. (2022). Recent advances in the modeling of Alzheimer's disease. *Front. Neurosci.* 16:807473. doi: 10.3389/fnins.2022.807473
- Sharma, S. (2021). High fat diet and its effects on cognitive health: alterations of neuronal and vascular components of brain. *Physiol. Behav.* 240:113528. doi: 10.1016/j.physbeh.2021.113528

- Sharma, R., Rooke, J., Kolmogorova, D., Melanson, B., Mallet, J. F., Matar, C., et al. (2018). Sex differences in the peripheral and central immune responses following lipopolysaccharide treatment in pubertal and adult CD-1 mice. *Int. J. Dev. Neurosci.* 71, 94–104. doi: 10.1016/j.ijdevneu.2018.07.012
- Shaw, C. A., and Höglinger, G. U. (2008). Neurodegenerative diseases: neurotoxins as sufficient etiologic agents? *NeuroMolecular Med.* 10, 1–9. doi: 10.1007/S12017-007-8016-8
- Shin, B. N., Kim, D. W., Kim, I. H., Park, J. H., Ahn, J. H., Kang, I. J., et al. (2019). Down-regulation of cyclin-dependent kinase 5 attenuates p53-dependent apoptosis of hippocampal CA1 pyramidal neurons following transient cerebral ischemia. *Sci. Rep.* 9:13032. doi: 10.1038/s41598-019-49623-x
- Simola, N., Morelli, M., and Carta, A. R. (2007). The 6-hydroxydopamine model of Parkinson's disease. *Neurotox. Res.* 11, 151–167. doi: 10.1007/BF03033565/METRICS
- Slevin, M., Garcia-Lara, E., Capitanescu, B., Sanfeliu, C., Zeinolabediny, Y., Albaradie, R., et al. (2020). Monomeric C-reactive protein aggravates secondary degeneration after intracerebral Haemorrhagic stroke and may function as a sensor for systemic inflammation. *J. Clin. Med.* 9, 1–12. doi: 10.3390/JCM9093053
- Slevin, M., Matou, S., Zeinolabediny, Y., Corpas, R., Weston, R., Liu, D., et al. (2015). Monomeric C-reactive protein--a key molecule driving development of Alzheimer's disease associated with brain ischaemia? *Sci. Rep.* 5:13281. doi: 10.1038/SREP13281
- Tello, J. A., Williams, H. E., Eppler, R. M., Steinhilb, M. L., and Khanna, M. (2022). Animal models of neurodegenerative disease: recent advances in Fly highlight innovative approaches to drug discovery. *Front. Mol. Neurosci.* 15:883358. doi: 10.3389/fnmol.2022.883358
- Trouche, S. G., Boutajangout, A., Asuni, A., Fontés, P., Sigurdsson, E. M., Verdier, J. M., et al. (2023). Amyloid- $\beta$  targeting immunisation in aged non-human primate (*Microcebus murinus*). *Brain Behav. Immun.* 109, 63–77. doi: 10.1016/j.bbi.2022.12.021
- Ueno, H., Yamaguchi, T., Fukunaga, S., Okada, Y., Yano, Y., Hoshino, M., et al. (2014). Comparison between the aggregation of human and rodent amyloid  $\beta$ -proteins in GM1 ganglioside clusters. *Biochemistry* 53, 7523–7530. doi: 10.1021/BI501239Q
- Ungerstedt, U. (1968). 6-hydroxy-dopamine induced degeneration of central monoamine neurons. *Eur. J. Pharmacol.* 5, 107–110. doi: 10.1016/0014-2999(68)90164-7
- Van, D. C. H., Swanson, C. J., Aisen, P., Bateman, R. J., Chen, C., Gee, M., et al. (2023). Lecanemab in early Alzheimer's disease. *N. Engl. J. Med.* 388, 9–21. doi: 10.1056/NEJMOA2212948
- Vinther-Jensen, T., Börnsen, L., Budtz-Jørgensen, E., Ammitzbøll, C., Larsen, I. U., Hjermind, L. E., et al. (2016). Selected CSF biomarkers indicate no evidence of early neuroinflammation in Huntington disease. *Neurol Neuroimmunol Neuroinflamm* 3:e287. doi: 10.1212/NXI.0000000000000287
- Waters, C. M., Hunt, S. P., Jenner, P., and Marsden, C. D. (1987). An immunohistochemical study of the acute and long-term effects of 1-Methyl-4-Phenyl-1,2,3,6-Tetrahydropyridine in the marmoset. *Neuroscience* 23, 1025–1039. doi: 10.1016/0306-4522(87)90178-3
- Zakaria, R., WMH, W. Y., Othman, Z., Long, I., Ahmad, A. H., and Al-Rahbi, B. (2017). Lipopolysaccharide-induced memory impairment in rats: a model of Alzheimer's disease. *Physiol. Res.* 66, 553–565. doi: 10.33549/PHYSIOLRES.933480
- Zameer, S., Alam, M., Hussain, S., Vohora, D., Ali, J., Najmi, A. K., et al. (2020). Neuroprotective role of alendronate against APP processing and neuroinflammation in mice fed a high fat diet. *Brain Res. Bull.* 161, 197–212. doi: 10.1016/J.BRAINRESBULL.2020.04.010
- Zhang, Q., Jung, D., Larson, T., Kim, Y., and Narayanan, N. S. (2019). Scopolamine and medial frontal stimulus-processing during interval timing. *Neuroscience* 414, 219–227. doi: 10.1016/J.NEUROSCIENCE.2019.07.004
- Zhang, J., Sun, B., Yang, J., Chen, Z., Li, Z., Zhang, N., et al. (2022). Comparison of the effect of rotenone and 1-methyl-4-phenyl-1,2,3,6-tetrahydropyridine on inducing chronic Parkinson's disease in mouse models. *Mol. Med. Rep.* 25:91. doi: 10.3892/mmr.2022.12607
- Zhao, Y., Jaber, V., and Lukiw, W. J. (2017). Secretory products of the human GI tract microbiome and their potential impact on Alzheimer's disease (AD): detection of lipopolysaccharide (LPS) in AD Hippocampus. *Front. Cell. Infect. Microbiol.* 7:318. doi: 10.3389/fcimb.2017.00318

# Frontiers in Neuroscience

Provides a holistic understanding of brain  
function from genes to behavior

Part of the most cited neuroscience journal series  
which explores the brain - from the new eras  
of causation and anatomical neurosciences to  
neuroeconomics and neuroenergetics.

## Discover the latest Research Topics

See more →

### Frontiers

Avenue du Tribunal-Fédéral 34  
1005 Lausanne, Switzerland  
[frontiersin.org](https://frontiersin.org)

### Contact us

+41 (0)21 510 17 00  
[frontiersin.org/about/contact](https://frontiersin.org/about/contact)

